EMBRY-RIDDLE
Aeronautical University™
SCHOLARLY COMMONS

Dissertations and Theses

11-2016

Automotive-Inspired Inceptors and Control Laws Designed for Simplified Piloted Flight

Kashif Ali

Follow this and additional works at: https://commons.erau.edu/edt

Part of the Aerospace Engineering Commons, and the Aviation Commons

AUTOMOTIVE-INSPIRED INCEPTORS AND CONTROL LAWS

DESIGNED FOR SIMPLIFIED PILOTED FLIGHT

A Thesis

Submitted to the Faculty

of

Embry-Riddle Aeronautical University

by

Kashif Ali

In Partial Fulfillment of the

Requirements for the Degree

of

Master of Science in Aerospace Engineering

November 2016

Embry-Riddle Aeronautical University

Daytona Beach, Florida

AUTOMOTIVE-INSPIRED INCEPTORS AND CONTROL LAWS
DESIGNED FOR SIMPLIFIED PILOTED FLIGHT

by

Kashif Ali

A Thesis prepared under the direction of the candidate's committee chairman, Dr. Richard P. Anderson, Department of Aerospace Engineering, and has been approved by the members of the thesis committee. It was submitted to the School of Graduate Studies and Research and was accepted in partial fulfillment of the requirements for the degree of Master of Science in Aerospace Engineering.
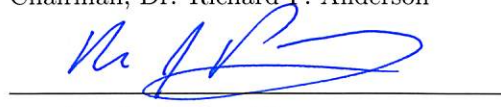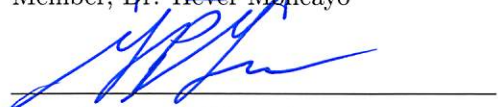
THESIS COMMITTEE

_____
Chairman, Dr. Richard P. Anderson

_____
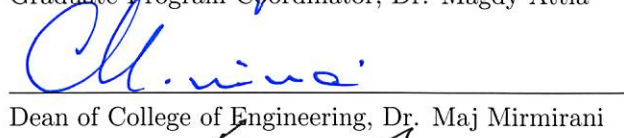Member, Dr. Richard Prazenica

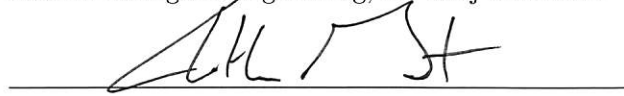_____
Member, Dr. Hever Moncayo

_____
Member, Prof. Glenn Greiner

_____
Graduate Program Coordinator, Dr. Magdy Attia

_____
Dean of College of Engineering, Dr. Maj Mirmirani

_____
Vice Chancellor, Academic Support, Dr. Christopher Grant

12.8.2016
_____
Date

12/8/16
_____
Date

12/8/16
_____
Date

ACKNOWLEDGMENTS

Foremost, I would like to express my sincere gratitude to my advisor Dr. Pat Anderson for his support, knowledge and patience. My association with EFRC began when he generously accepted my request to work part-time on the DA-42L flight test program as an undergraduate. That gesture continues to pay dividends.

I would also like to thank the rest of my committee: Prof. Glenn Greiner, Dr. Hever Moncayo, and Dr. Richard Prazenica for their time, encouragement and insightful comments. A special thank you to Dr. Borja Martos who sat alongside my committee and offered valuable insight in the area of my research and to Christopher Carvalho, for being a great colleague to work with on this project.

To Shirley Koelker, thank you for putting up with me and helping me get to the finish line. We students couldn't ask for a better support system than you. To the rest of the EFRC crew - you all know who you are. The time spent with you is the source of some of the best memories of my life. Also Chipotle.

I must express my very profound gratitude to my parents, Asif Ali and Kausar Ali and my brother, Ahmed Ali (Neepti) for their unfailing support and for simply lighting up my life. This accomplishment would not have been possible without you. Thank you.

Finally, to my wife, Aiysha, thank you for making my defense possible, thank you for proofreading an unnecessary number of drafts and thank you for the hot cocoa. Kram min jaan.

TABLE OF CONTENTS

LIST OF TABLES

LIST OF FIGURES

SYMBOLS

A coefficient matrix

a_z vertical load factor in the body-axis

B input weighting matrix

C state variable weighting matrix

C_D Coefficient of drag

C_{D_α} coefficient of drag with respect to angle-of-attack

C_L Coefficient of lift

C_{L_α} lift-curve slope

$C_{L_{\dot\alpha}}$ coefficient of lift with respect to the rate of change of angle-of-attack

C_{L_β} coefficient of rolling moment with respect to angle-of-sideslip (dihedral effect derivative)

$C_{L_{\delta_a}}$ coefficient of rolling moment with respect to aileron deflection (aileron control power derivative)

$C_{L_{\delta_e}}$ coefficient of lift with respect to elevator deflection

$C_{L_{\delta_r}}$ coefficient of rolling moment with respect to rudder deflection

$C_{L_{max}}$ coefficient of maximum lift

C_{L_p} coefficient of rolling moment with respect to roll rate (rolling damping derivative)

C_{L_q} coefficient of lift with respect to pitch rate

C_{L_r} coefficient of rolling moment with respect to yaw rate

C_{M_α} coefficient of static longitudinal stability

$C_{M_{\dot\alpha}}$ coefficient of pitching moment with respect to the rate of change of angle-of-attack

$C_{M_{\delta_e}}$ coefficient of pitching moment with respect to elevator deflection (elevator control power derivative)

C_{M_q} coefficient of pitching moment with respect to pitch rate (pitch-damping derivative)

C_{N_β} coefficient of yawing moment with respect to angle-of-sideslip (weather-vane stability derivative)

$C_{N_{\delta_a}}$ coefficient of yawing moment with respect to aileron deflection (adverse yaw derivative)

$C_{N_{\delta_r}}$ coefficient of yawing moment with respect to rudder deflection (rudder control power)

C_{N_p} coefficient of yawing moment with respect to roll rate

C_{N_r} coefficient of yawing moment with respect to yaw rate (yaw damping derivative)

C_{Y_β}	coefficient of side force with respect to angle-of-sideslip
$C_{Y_{\delta_r}}$	coefficient of side force with respect to rudder deflection
g	gravity
$\dot{h}$	rate-of-climb
$\dot{h}_{base}$	baseline rate-of-climb term
$\dot{h}_{cmd}$	commanded rate-of-climb
I	integral term in PID controller
K	control gain matrix
k_1, k_2	scaling terms to translate pedal inceptor deflections to rate-of-climb values
k_3, k_4	scaling terms to translate pedal inceptor deflections to flight-path angle values
$\dot{K}_h$	scaling term to convert altitude to a rate-of-climb term
K_q	scaling term to convert RoC to pitch rate
K_{roll}	scaling term to convert bank angle to a roll rate term
n_{pll}	positive load limit
P	solution to the Riccati equation or proportional term in PID controller
p	roll rate
P_{base}	baseline manifold air pressure setting
p_{cmd}	roll-rate command
p_e	error between roll-rate command and aircraft roll-rate
Q	state penalizing matrix
q	pitch rate
q_{cmd}	pitch-rate command
q_e	error between pitch-rate command and aircraft pitch-rate
R	control penalizing matrix
r	yaw rate
s	complex variable in frequency domain
S_w	reference wing area
u	linear x-component of velocity in the body-axis
v	linear y-component of velocity in the body-axis
V	True airspeed
V_{gnd}	ground speed
V_{rot}	takeoff rotation speed
W	weight
w	linear z-component of velocity in the body-axis
W_{max}	maximum weight
x	state vector
y	column vector of output variables
α	angle-of-attack
β	angle-of-sideslip
γ	vertical flight path angle

γ_{cmd}	commanded vertical flight path angle
γ_{ref}	reference vertical flight-path angle
δ	input vector
δ_a	aileron surface deflection
δ_e	elevator surface deflection
δ_g	gyro tilt angle
δ_{MAP}	regulated throttle position
δ_r	rudder surface deflection
δ_{+R}	right pedal inceptor deflection
δ_{-R}	left pedal inceptor deflection
δ_{RoT}	normalized deflection of Ω-inceptor
δ_s	normalized deflection of Ω-inceptor
δ_{th}	regulated throttle position
δ_{th}	throttle deflection
$\delta_{th_{cmd}}$	commanded throttle due to pilot input
$\delta_{th_{dem}}$	demanded throttle
θ	pitch angle
ρ	density
ϕ	bank angle
ϕ_{cmd}	bank angle command
ψ	heading angle
$\dot{\psi}$	heading rate
Ω	rate-of-turn
Ω_{max}	Maximum rate-of-turn

ABBREVIATIONS

ADS-B	Automatic Dependent Surveillance-Broadcast
AGARS	Advanced General Aviation Research Simulator
AGATE	Advanced General Aviation Transportation Experiments
Alt.	altitude
AoA	angle-of-attack
Avg.	average
bhp	brake horsepower
CAS	calibrated airspeed
CFIT	Controlled Flight Into Terrain
CLAW	Control Law
cmd or CMD	Commanded
CWS	Control Wheel Steering
deg	degrees
EoU	Ease of Use
FAA	Federal Aviation Authority
FBW	Fly-by-Wire
FCS	Flight Control System
FEP	Flight Envelope Protection
FFT	Fast-Fourier transform
FLC	Fuzzy-logic Controller
FRC	Flight Research Center
ft	feet
FTS	Fast-time Simulation
GA	General Aviation
GND	ground
GPS	Global Positioning System
HFCS	Haptic Flight Control System
HH	Heading-hold
HITS	Highway-in-the-Sky
H-metaphor	Horse-metaphor
H-Mode	Haptic Mode
Hz	Hertz
IFR	Instrument Flight Rules
ILS	Instrument Landing System
inHg	inches-of-mercury
KIAS	Knots Indicated airspeed
KOAK	Oakland Municipal Airport

KSFO	San Francisco International Airport
KSQL	San Carlos Airport
kts	knots
LaRC	Langley Research Center
Lat	latitude
lbf	pound-force
LCD	Liquid crystal display
LQR	Linear Quadratic Regulator
LTI	Linear Time-Invariant
m	meters
MAP	Manifold Air Pressure
max	maximum
min	minute
NACA	National Advisory Committee for Aeronautics
NASA	National Aeronautics and Space Administration
NFD	Naturalistic Flight Deck
NP	non-pilot
OTW	Out-the-Window
PAV	Personal Air Vehicle
PC	Personal Computer
PI	Proportional-integral
PID	Proportional-integral-derivative
rad	radians
RoC	Rate-of-climb
RoD	Rate-of-descent
RoT	Rate-of-turn
RMS	Root-mean square
RPM	Revolution per minute
s	second(s)
SAC	Safe Aircraft Competition
SAFAR	Small Aircraft Future Avionics Architecture
SATS	Small Aircraft Transportation System
SUS	System Usability Scale
TAS	True airspeed
TCVP	Terminal Configured Vehicle Program
T-O	takeoff
TRL	Technology Readiness Level
UDP	User Datagram Protocol
XP	pilot

ABSTRACT

Ali, Kashif MSAE, Embry-Riddle Aeronautical University, November 2016. Automotive-

Inspired Inceptors and Control Laws Designed for Simplified Piloted Flight.

This thesis details the development of a simulator-based experiment in automotive-inspired controls for aircraft. The goal is to fuse the ease of drivability of a car with the flight of an aircraft. A standard automotive control hardware setup coupled with fly-by-wire control laws will allow non-pilots to fly a plane using their familiarity with driving a car. A mathematical description of the control law logic and controller implementation is presented and the human subjects' performance is measured from data collected during experimental testing of the simulator. Preliminary results indicate that non-pilots improve their path-tracking performance and reduce control activity within a short span of time achieving results comparable to those achieved by trained pilots.

1. Introduction

This thesis details the development of a flight simulation model and control interface for the purpose of testing a new concept in the area of flight controls and the associated human-machine interface. It is a follow-up publication to my colleague Christopher Carvalho's thesis topic (Carvalho, 2013) on the same concept.

The concept submits a possible solution for certain obstacles that lie in the path of proliferating general aviation (GA) as an alternative means of transport to that afforded by the national highway system, or commercial hub-and-spoke airline operations.

In this chapter, a brief background is provided to illustrate the motivation behind this endeavor. A problem statement is defined which outlines a subset of challenges the proposed concept intends to address. A method is identified which lays the foundation for the mathematical description and results presented in Chapters 3 and 4, respectively.

A review of the literature on flight controls and the solutions proposed for simplifying pilot control tasks for GA aircraft is presented in Chapter 2.

Finally, in Chapter 5, impressions based on quantitative and qualitative results are submitted along with footnotes from the design process, and concluding remarks on future areas of investigation.

1.1 Background

Since the birth of aviation, people have sought to improve flight, permitting us faster travel and longer distances in increasingly safer and reliable vehicles. As a result, the aircraft of today are a testament to the spirit of innovation and progress in aeronautics. Looking ahead, the hope of many, including NASA, is to realize the dream of personal air vehicles. These aircraft will enable future commuters to travel distances greater than those within the reach of a three hour car ride and shorter than those that are currently serviced by the airline industry, introducing a paradigm shift in the nation's transportation infrastructure.

An affordable safe personal aircraft would offer an attractive alternative to the commuter requiring regular travel between distances of about 150 to 700 miles, and reignite an industry that suffered a sharp decline in the 1980s ("Affordable Alternative Transportation AGATE – Revitalizing General Aviation", 1996). Furthermore, in 1993, GA production numbers experienced an all-time low of 954 units versus the 18,000 units made in 1978 ("Affordable Alternative Transportation AGATE – Revitalizing General Aviation", 1996).

The vision of an expanded transportation system driven by a new generation of advanced general aviation (GA) aircraft is by no means a recent idea. Programs as early as the Advanced General Aviation Transport Experiments (AGATE) from the mid-90s ("Affordable Alternative Transportation AGATE – Revitalizing General Aviation", 1996) and the Small Aircraft Transportation System (SATS) beginning in

2001 were instituted to explore the expansion of the technological capabilities of GA aircraft. In doing so, this enabled them to become part of a new transportation system designed to alleviate the existing burden on conventional ground transportation networks.

The AGATE Consortium

If the goal of a new transportation system was to be realized, a multifaceted push forward, implementing lighter composite airframes, efficient powerplants, advanced flight decks and control systems, and other available technology was deemed necessary to pull the small GA industry out from the past. Under the leadership of Bruce Holmes of the NASA Langley Research Center (LaRC), the AGATE consortium successfully created a platform for the advancement of GA technology. The research activities supported by the program resulted in superior avionics, engines, airframes and flight training methods (Chambers, 2005).

The SATS Program

Similarly, in 2005, the follow-up SATS program demonstrated various retro-fitted integrated technologies to prove the safe operation of a personal-owner aircraft from small uncontrolled airports. Technologies such as the Global Positioning System (GPS) were an indispensable feature in making the SATS concept work (Chambers, 2005). The recently developed Automatic Dependent Surveillance-Broadcast (ADS-B) provided three-dimensional information regarding air traffic and the Highway-in-the-Sky concept was integrated with sensor information to provide enhanced single-pilot performance (Chambers, 2005). The SATS program met its objectives of demon-

strating that greater utility could be extracted from the nation's 5,000 or so small, public-use airports by equipping GA aircraft with appropriate flight deck and flight path technologies, whilst lifting the burden off of larger hub-and-spoke operations (Chambers, 2005).

Personal Air Vehicle (PAV) Research

Following the success of the SATS program, LaRC researchers took to exploring emerging technologies in order to develop long-term solutions to the PAV concept. The concept was to revolutionize the personal-owner aircraft - vehicles designed from the ground up to be safe, cost-effective ($100,000 in 2004 to acquire), fuel efficient, easy to operate and perhaps offer some degree of roadability, à la 'flying car' (Chambers, 2005). Perhaps the most ambitious goal was to develop an aircraft requiring only a tenth of the training time and cost; in about a week and a $1,000 (Chambers, 2005).

Central to the PAV concept achieving its Ease-of-Use (EoU) goals was the emergence of a new flight control system (FCS) termed the 'H-Mode' for Haptic-Mode, developed by Flemisch and Goodrich (Hahn, 2006). This full authority system offers the pilot full engagement and does not interfere until workload levels increase beyond his/her capability, or mistakes are made. The FCS is coupled with a Naturalistic Flight Deck (NFD) providing a one-stop avionics suite designed to present relevant information in an easy-to-assimilate fashion (Hahn, 2006). However, NASA has identified that such an advanced system could be prohibitively expensive to develop and the unit cost for a commuter-class aircraft equipped with such an FCS could

very well discourage production unless considerable transportation value is identified (Hahn, 2006).

A New 'Development Space'

Between NASA's initial and sophomoric contributions through the AGATE and SATS programs, and the futuristic, but distant H-Mode, lies the possibility of near-term solutions which combine the functionality afforded by AGATE and SATS with the control augmentation made possible via fly-by-wire (FBW) flight control laws (CLAW). In this 'development space' exists the opportunity to rethink the pilot-vehicle interface. The following section will expand this notion into a problem statement that defines the scope of the work presented.

1.2   Defining the Problem

The process of delineating the problem-space and finding a question to answer is structured as follows,

- What problems currently exist in the realm of the personal-owner aircraft and its operation?

- What has been done in the past to simplify flight? (from a flight controls standpoint)

- And, finally, define a problem that when solved, will contribute in closing the gap between where technology is and where technology needs to be.

The following sub-sections seek to answer these questions, and ultimately provide a problem statement.

1.2.1 Extant Problems

Several problems and challenges currently restrict the personal-owner aircraft from gaining popularity as a candidate to base an alternative transportation system.

At the forefront of GA's problems lie long-standing flight safety issues, with statistics suffering from controlled-flight-into-terrain (CFIT) scenarios - a situational awareness problem (FAA, 2003). Other types of incidents can be partially, or exclusively, a result of poor handling and adverse weather conditions.

The typical single-engine propeller aircraft of today has seen avionics upgrades in an additive manner, with instrument panels becoming increasingly cluttered. Such incremental-ism in cockpit design cannot fully accommodate human factors solutions which aim to unify the information display systems and navigation equipment. Furthermore, a niche industry supplying electronic flight bag type solutions and equipping the average pilot with tablet devices to serve as drop-in flight displays continues to grow and simplify flight. That said, new synergistic designs do exist with redesigned cockpits and unified systems such as that of the Cessna TT$^{\text{x}}$ and the Pipestrel Panthera. However, such aircraft still lack the implementation of full authority FBW systems commonly found in military and transport category aircraft (Martin, 1990).

Finally, the cost of obtaining a private pilot's license is high, requiring a considerable investment of time and money (Chambers, 2005; Hahn, 2006). As a result, the proliferation of personal-owner aircraft as a means of commuting is prohibited.

Although the problems described above are significant, they do not account for all the hurdles in realizing the SATS style transport infrastructure. However, for the sake of defining our problem, the issues mentioned thus far do help in defining a problem.

1.2.2   Past Attempts at Simplifying Flight

The philosophy of augmenting aircraft controllability and safety dates back to the 1920s where innovators pursued the familiar goal of simplifying flight by envisioning it as something best compared by the ease of driving a car (*Sixteenth Annual Report of the National Advisory Committee for Aeronautics*, 1930). This pursuit took shape in the form of several National Advisory Committee for Aeronautics (NACA) investigations in the first half of the 20th century (Campbell et al., 1952; W. H. Phillips et al., 1956) whereby existing personal-owner aircraft were retro-fitted with centering springs on their lateral control to prevent unintentional roll-off and reduce pilot workload.

Subsequent studies conducted by NASA in the mid-70s investigated control system and flight information display designs for small GA aircraft in an effort to further reduce pilot workload especially in turbulent conditions and bad weather. The studies comprised a survey of seven aircraft and their handling qualities with and without these improved systems. Pilot feedback indicated improvements in handling and EoU

with the inclusion of an attitude-command control system and flight director (Loschke et al., 1974).

With the AGATE consortium striving to reignite GA in the 90s, the University of Kansas Center for Research investigated the benefits of replacing the traditional yolk with a sidestick. With a reduced moment arm, stick forces went up and a geared tab was proposed to reduce forces to within Federal Aviation Regulations (FAR), enabling the pilots of the single-engine high wing GA aircraft to benefit from improved trajectory control and reduced fatigue (Martin, 1990).

Continuing in this vein, in 2002, the FAA's Office of Aerospace Medicine conducted simulation trials of a Piper Malibu using a four-axis side-arm controller implementing a fuzzy-logic controller (FLC) to allow the pilot to 'command higher-level performance goals (for example, rate of turn/bank; rate of climb/descent)' (Beringer, 2002). Test subjects also had a highway-in-the-sky visual representation available to guide themselves to their destination. The motivation behind this experiment was to explore the benefits of finding a compromise between automated maneuvering (as that afforded by a typical GA autopilot) and the inherent authority of manually guided maneuvering. Barring the cost of development and implementation, results demonstrated that the FLC system was a successful endeavor and the significant reduction in tracking error meant it could be a potential candidate for controlling the next-generation of GA aircraft (Beringer, 2002).

In 2010, the Small Aircraft Future Avionics Architecture (SAFAR) program set about to develop a low-cost FBW Diamond DA-42 to demonstrate the readiness of

technology to facilitate full-authority digital control systems in small GA aircraft (Falkena, 2012). The DA-42 control system was designed to operate without the need for a mechanical backup and ensuring a 10^{-9} failure probability. This technology platform delivered on its promises of improved handling, enhanced situational awareness, and envelope protection. However, the system was complex and required extensive training and experience (Falkena & Borst, 2010).

The cross-section of historical data presented above lends itself to posing a problem as will be seen in the following section.

1.2.3   Problem Statement

This brief survey of improving aircraft EoU over the past 90 years or so indicates the persistence of the goal to simplify flight and increase its accessibility in society. Some ideas, of course, are too antiquated to be of any real value but others, along with the H-Mode introduced under the LaRC's PAV studies, provide a foundation on which to pose a new problem -

> *To exploit the familiarity most people have with driving a car. To design automotive inspired inceptors which aim to fuse the ease of driving a car with the simplified control of flying an aircraft. To create a new pilot-vehicle interface wrapped around a desirable level of envelope protection. Furthermore, to decrease the required time to train a pilot such that the time spent driving a typical automobile may contribute to overall currency in the aircraft.*

Broadly speaking, the introduction of fly-by-wire technology holds the potential to drastically alter the personal aircraft. Combining said FBW technology with a cockpit control layout similar to a typical automobile may introduce the right mix of autonomy and manual control.

1.3   Method

To set about solving the defined problem, a flight simulation model was developed which included automotive inceptors as the primary control input devices. A set of six control modes was designed to cover the takeoff (Mode 1), climb (Mode 2), cruise (Mode 3 and dountfull, descend (Mode 5) and approach (Mode 6) legs of a given flight profile.

1.3.1   Experiment Design

Eighteen subjects, a mix of experienced pilots and student pilots, along with non-pilots, were tasked to fly three separate courses starting with takeoff and ending with a final-approach-to-land at another airport. All subjects were given the opportunity to study a 10-minute tutorial presentation on how to fly the simulator using the provided controls. Upon completion of the three scenarios, they were requested to complete a survey based on the system usability scale (SUS) (Bangor, Kortum, & Miller, 2009).

1.3.2 Equipment

The flight simulation model was developed in MATLAB® and Simulink®, and output to FlightGear (an open source flight simulation environment), to provide an out-the-window (OTW) view of the aircraft in flight. The out-the-window (OTW) visualization was modified to introduce a virtual highway-in-the-sky (HITS) graphical representation of the path all pilots were meant to fly through. A consumer-grade automotive control set served as the primary flight inceptors for piloted flight by the subjects.

The proposed control *inceptors*, a steering wheel, shifter module and two foot-pedals, are the only controls made available to the pilot to maneuver the aircraft. The desired aim is to provide the non-pilot safer and faster access to flight and its benefits as a viable mode of point-to-point transportation.

1.3.3 Control Hardware

The primary flight control inceptor hardware comprise of a steering wheel, a 7-position shifter module, and an accelerator and brake pedal (see Figures 1.1, 1.2 and 1.3, and 1.4). The third pedal (clutch pedal) was not used. Additionally, all other buttons and controls were programmed to be inoperative to constrain the final simulator with only typical automotive controls.

The controls were designated based on their function to the names listed in Table 1.1.

Figure 1.1: Logitech G27 automotive steering wheel

Figure 1.2: Logitech G27 automotive pedals

Figure 1.3: Logitech G27 manual shifter

Figure 1.4: Pilot control hardware

Table 1.1: Reassignment of control hardware to new functions.

Device	New Designation	Inceptor Function
Steering wheel	Rate-of-turn (Ω) inceptor	control of horizontal flight path at a commanded RoT
Accelerator pedal	Right pedal inceptor	↑ RoC/RoD for modes 2 & 5 ↑ MAP in cruise modes 3 & 4
Brake pedal	Left pedal inceptor	↓ RoC/RoD for modes 2 & 5 ↓ MAP in cruise modes 3 & 4

1.3.4 Operation
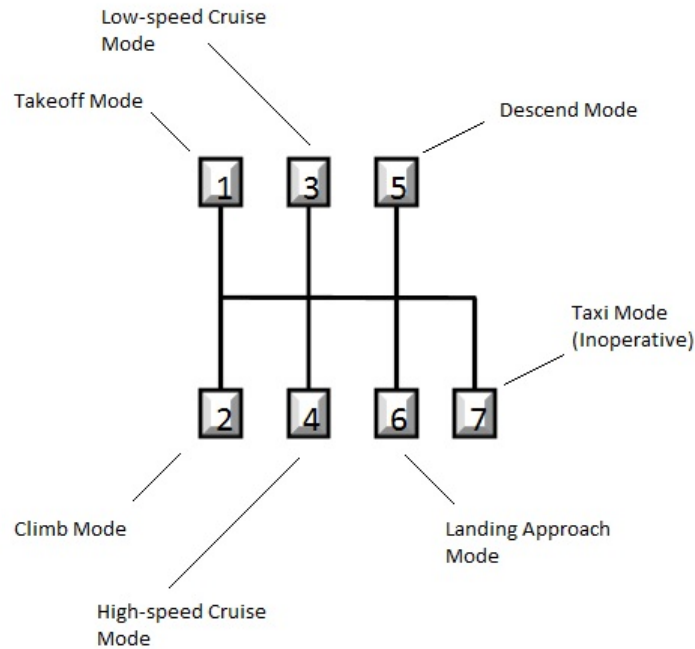
Figure 1.5: Modes developed for the shifter module

The steering wheel enables control of horizontal flight path while the shifter module was used to switch between six available flight modes (See Figure 1.5). Finally, depending on the selected mode, the two pedals allow the pilot to adjust rate of climb (or descent), cruising airspeed, or flight path angle.

The typical sequence of events would follow as the pilot attempted to fly within the confines of the highway-in-the-sky:

- Each subject was setup to begin a flight from takeoff. The aircraft's position was initialized at one end of the runway with the mode selector in 'takeoff' mode.

- The subject would then hold down the right pedal inceptor opening the throttle and speeding up to takeoff speed, at which point the aircraft would initiate rotation without pilot input.

- The subject would then switch to a climb mode and have the ability to increase or decrease the rate of climb (RoC) as needed. However, even without input the aircraft would maintain a baseline rate (applicable while in descend mode as well).

- Approaching the desired flight level, while still in climb mode, the pilot would be able to reduce the RoC to a minimum of 0 feet-per-minute by completely holding down the left pedal inceptor.

- At this point, one of two cruise modes (low or high speed) may be engaged and the left pedal inceptor can be released. The aircraft would now hold altitude.

- In cruise mode, the right and left pedal inceptors serve to increase or decrease power (while maintaining altitude), respectively.

- A descent or another climb could be initiated from the cruise mode by preemptively holding down the left pedal inceptor and switching modes. The action of holding down the inceptor ensures that the climb or descent mode is entered at

0 feet-per-minute. Relaxing pressure on the left pedal inceptor will allow the climb/descend mode to track to the desired rate.

- Throughout all flight modes the Ω-inceptor would allow the pilot to change horizontal flight path without any additional compensation to remain coordinated.

- Finally, upon rendezvousing and centering with the portion of the 'highway-in-the-sky' lined up with the destination runway, the pilot could engage the landing approach mode. The aircraft would maintain a 3 degree flight path angle, γ. The right and left pedal inceptors would allow the subject to increase or decrease flight path if overshooting or undershooting the runway.

The final setup had subjects tasked with flying three separate courses starting with takeoff, and ending with a final approach to land at another airport.

Figure 1.6 shows the projected display of the FlightGear environment with a virtual 'highway-in-the-sky'.

The following chapters shall detail the resulting flight model design, control algorithms, their performance and areas of further research.

1.3.5 Flight Data Model

Given the low Technology Readiness Level (TRL) of this investigation, it was deemed unnecessary to develop a non-linear aerodynamic database for high-fidelity representation of a specific aircraft. Instead, typical point values for the stability and control derivatives of a North American Aviation Navion were used in a six degree-
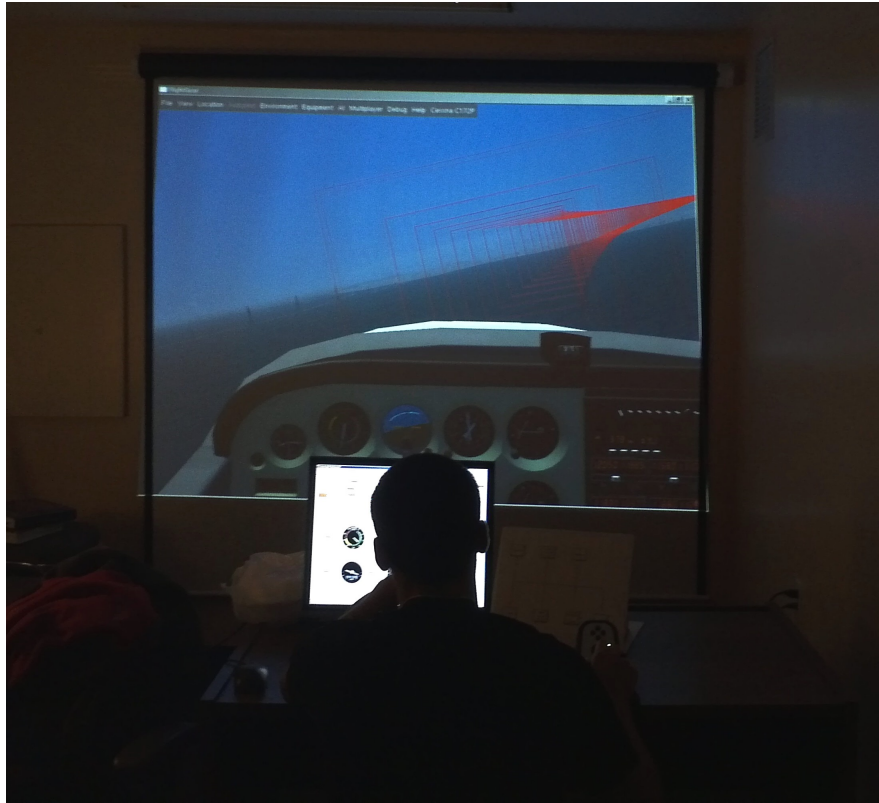
Figure 1.6: Test candidate flying simulator through a virtual 'highway'

of-freedom model. The Navion was a 4-seat single-engine GA aircraft designed in the 1940s and produced up to the mid-70s. Takeoff scenarios were facilitated by implementing a three-point ground reaction model.

With data readily available, a propulsion model of the Lycoming IO-360 reciprocating engine with an MTV-6-A-C-F/CF187-129 constant-speed propeller was incorporated to provide values for thrust based on appropriate revolutions per minute (RPM) and manifold air pressure (MAP) settings. It should be noted that the Navion does not use this specific engine or propeller; however, for the purposes of simulation, this change can be treated as negligible in affecting the overall validity of the model.

Table 1.2: Navion stability and control derivatives (per radian)

C_L	C_D	C_{L_α}	C_{D_α}	C_{M_α}	$C_{L_{\dot\alpha}}$	$C_{M_{\dot\alpha}}$	C_{L_q}
0.41	0.05	4.44	0.33	-0.683	0.0	-4.36	3.8

C_{M_q}	$C_{L_{\delta_e}}$	$C_{M_{\delta_e}}$	C_{Y_β}	C_{L_β}	C_{N_β}	C_{L_p}	C_{N_p}
-9.96	0.355	-0.923	-0.564	-0.074	0.071	-0.410	-0.0575

C_{L_r}	C_{N_r}	$C_{L_{\delta_a}}$	$C_{N_{\delta_a}}$	$C_{Y_{\delta_r}}$	$C_{L_{\delta_r}}$	$C_{N_{\delta_r}}$	-
0.107	-0.125	-0.134	-0.0035	0.157	0.107	-0.072	-

1.3.6 Visual Interface

To enable piloted flight of the simulation model, the FlightGear platform was modified to provide a virtual 'highway-in-the-sky'. A set of red glide slope tunnel-style boxes were generated to create a course for the test subjects to fly through.

The aircraft state variables along with additional flight and engine parameters computed in simulation, were sent via User Datagram Protocol (UDP) to a remote PC running the FlightGear environment. Table 1.3 lists the output variables sent to the remote PC.

This chapter identified the motivation, challenges and possible solutions associated with simplifying piloted flight for the personal-owner aircraft. It also presented the problem statement of this thesis, introducing a new concept with regard to the pilot-vehicle interface, and subsequently provided a top-level description of a solution that

Table 1.3: Required input parameters sent from model to FlightGear

Parameter	Description	Units
Latitude/longitude	-	radians (rad)
Altitude	-	meters (m)
ϕ,θ,ψ	Euler angles	radians (rad)
CAS	Calibrated airspeed	knots (kts)

was designed and tested. The following chapter revisits attempts in aeronautical history to simplify flight. This will enable the reader to appreciate the solution presented in Chapter 3 of this paper.

2. Literature Review

Given the close relationship between advances in technology and progress in flight control systems, this chapter is divided into two parts which chronologically review solutions proposed to augment and simplify flight. The first part provides a historical account of early attempts prior to digital flight control technology, whilst the second part introduces relevant research conducted from the late 1980s to present day.

2.1 Simplifying Flight Prior to Digital Control

Although primitive, the solutions presented in this section were motivated by a desire that is still relevant to the advancement of aviation today; that is, to simplify piloted flight for the purpose of safer aircraft operation in inclement weather, and to reduce pilot workload.

As a result, the inspiration for much of the work in this thesis on FBW-type flight controls can be found from Upson's words in 1942 on the topic of developing safe personal aircraft (Abzug & Larrabee, 2005),

> "Outstanding in vision, incapable of spinning, comparable with an automobile in simplicity of control, yet with unquestioned superiority of cross-country performance".

2.1.1 Safe Personal Airplanes from the 1920s to 1960s

The idea of fusing the simplicity and safety of automotive control to aircraft dates back to the mid-1920s when philanthropist Harry Guggenheim sponsored the Guggenheim Safe Aircraft Competition (SAC) from 1926 to 1929. An open invitation to aircraft manufacturers around the world resulted in twenty five entries of which only ten managed to demonstrate their designs (Abzug & Larrabee, 2005). The competition set forth the following requirements (Sellon, 2004):

- Maintain controlled, level flight at 35mph without stalling;

- Demonstrate hands-off stability for five minutes at any airspeed between 45 and 100mph in gusty air;

- Glide power-off at less than 38mph;

- Land over a 35-foot obstacle with a maximum 300-foot roll;

- Take-off over the above-mentioned 35-foot obstacle within 500 feet from a standing start.

Two entrants in particular, the Handley Page H-29 and the Curtiss Tanager (See Figure 2.1) demonstrated exceptional short-field landing capabilities by implementing full-span flaps, and leading-edge slats designed to deploy automatically, upon being adequately loaded at high angles of attack. Both aircraft also greatly improved lateral controllability with the use of floating ailerons.

Winning by a small margin, the Curtiss Tanager, achieved, "a minimum gliding speed

Figure 2.1: The Curtiss Tanager - Winner of the Guggenheim Safe Aircraft Competition

of 37 miles per hour, excellent lateral control, and a total distance from a 35-foot obstacle to a full stop of less than 300 feet" (Abzug & Larrabee, 2005).

Within a span of three years the Guggenheim SAC generated significant engineering solutions paving the way for further intellectual investment in the idea of a safe personal aircraft.

2.1.2   1929 - Study of Spiral Tendency in Blind Flying

The tendency of pilots to assume a spiral path when provided no visual reference was investigated in 1929 by the NACA at the Langley Memorial Aeronautical Laboratory in Virginia (Carroll & McAvoy, 1929). The investigation was motivated by findings in a paper published in the Journal of Morphology and Physiology (1928)

which presented experimental results indicating the tendency of blind-folded persons to follow a spiral path whether walking, driving, rowing a boat or swimming.

Unsurprisingly, the results from the NACA investigation illustrated how blind-folded pilots, when asked to maintain straight and level flight, would introduce the aircraft into a spiral dive within ninety seconds of assuming control.

The simple experiment demonstrated the significance of visual reference and the need for an artificial horizon in what we now call Instrument Flight Rules (IFR) conditions.

2.1.3 1952 - NACA's Investigation of the Effect of Control Centering Springs

The NACA technical report entitled, 'Flight Investigation of the Effect of Control Centering Springs on the Apparent Spiral Stability of a Personal-Owner Airplane' details the design, testing and results of a control system focused on improving the safety of 'hands-off' flight (Campbell et al., 1952).

The goal of this effort was to enable the pilot to, "devote adequate time to navigation problems" without worrying about large changes in heading. In addition, if caught in 'blind-flying' conditions, the pilot should be able to release the controls to ensure the aircraft remains in a safe attitude. As a result, the pilot would no longer need to rely on his or her sense of orientation; the reliability of which was illustrated by (Carroll & McAvoy, 1929).
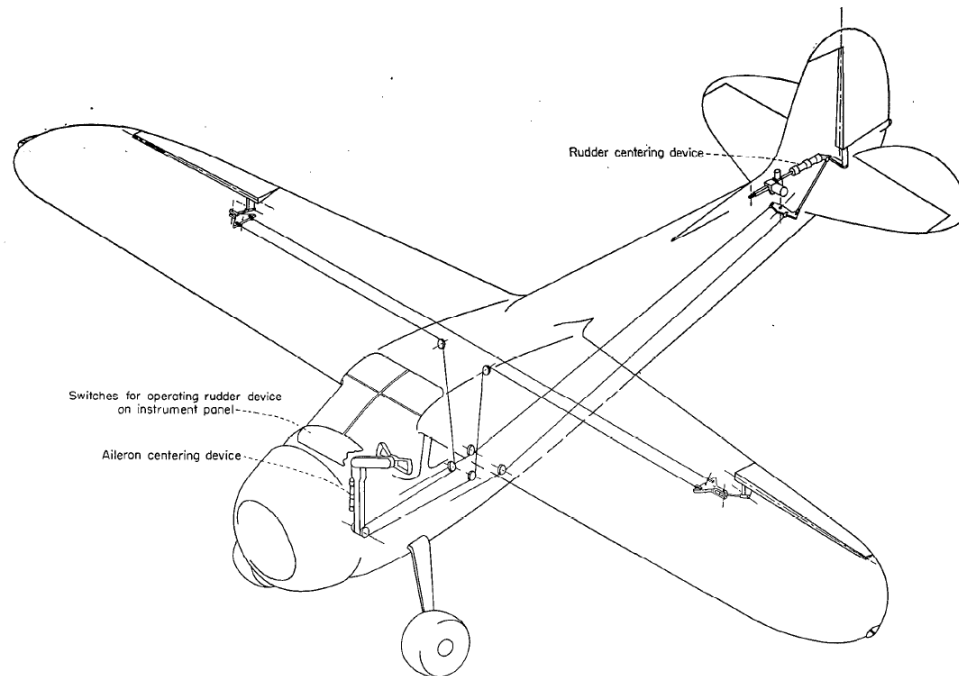
Figure 2.2: Diagram illustrating preloaded control system (Campbell et al., 1952)

The report, borrowing findings from a prior investigation, reiterated that many light airplanes with inherent spiral stability still demonstrated unstable spiral tendencies in flight due to the lack of trimming options, or as a result of the friction typically present in the control systems of light aircraft (Campbell et al., 1952).

The solution proposed and tested by (Campbell et al., 1952) comprised preloaded centering springs used in both the rudder and aileron control systems. In addition to providing a control centering mechanism, the system also facilitated trimming of the aircraft.

Flight tests were conducted with the system engaged and disengaged. According to (Campbell et al., 1952), "Records were obtained of the uncontrolled lateral motions

of the airplane starting from straight and level flight and from turns and also allowing abrupt rudder kicks" (p. 2).

The report concluded that with both centering springs engaged to hold trim, "the airplane would fly 'hands-off' for indefinite periods of time without getting into a dangerous attitude, at least, in the smooth and moderately rough air in which all the tests were made" (Campbell et al., 1952). This was not the case with both systems disengaged. Following a rudder step input the aircraft would diverge in the direction of the rudder step and fail to center due to the inherent friction in the control system.

The authors noted that even with the additional breakout force of 3.5 lbf contributed by the aileron centering system, the control forces were reasonable as reported by the test pilots. Excessive friction in the rudder system however, required a greater spring preload which resulted in a breakout force of approximately 22 lbf; a value that was objectionable to all pilots.

Additionally, it was observed that when airspeed was not held constant (elevator free) in a banked attitude, an airspeed increase tended to bank the aircraft to the right creating large divergences, once the controls were released. Finally, it was suggested by (Campbell et al., 1952) that minimization of lateral-directional trim changes due to variation in airspeed, power setting or fuel loading would be required in addition to improving the aircraft's intrinsic spiral stability to arrive at a better solution.

2.1.4   1956 - NACA's Investigation of an Auto Aileron Trim Device to Augment Spiral Stability

Building on the control augmentation solution proposed by (Campbell et al., 1952), the NACA developed and tested an automatic aileron trim device to alleviate the out-of-trim spiral divergence tendencies mentioned in Section 1.1.3.

Phillips, Kuehnel, & Whitten (1956) employed a device "designed to deflect the ailerons by shifting the trim position of preloaded control centering springs in order to maintain zero yawing velocity". Trim position was adjusted by means of an electric motor which in turn was driven in the appropriate direction based on a yaw-rate sensitive gyroscope.[1]

It was also determined that use of the device on the rudder was unnecessary as the aileron control deflection and force required to correct for an out-of-trim state were typically smaller than that of the rudder system.

Unlike an autopilot servomotor, the power requirements of the on-off electric motor were "reduced both because the total travel provided by the motor which operates the ailerons should be enough to offset only possible out-of-trim moments on the airplane, and because rate of motion can be relatively low" (W. H. Phillips et al., 1956).

To ensure effective damping of the long-period oscillation, aileron reversal was designed to occur before the yaw rate was zero, allowing the aircraft to be in a zero roll attitude when the ailerons were centered to neutral. To implement the aileron

---

[1]During a steady turn, a yaw rate gyro can serve as a roll attitude gyro, as the roll angle is proportional to yaw rate (W. H. Phillips et al., 1956).

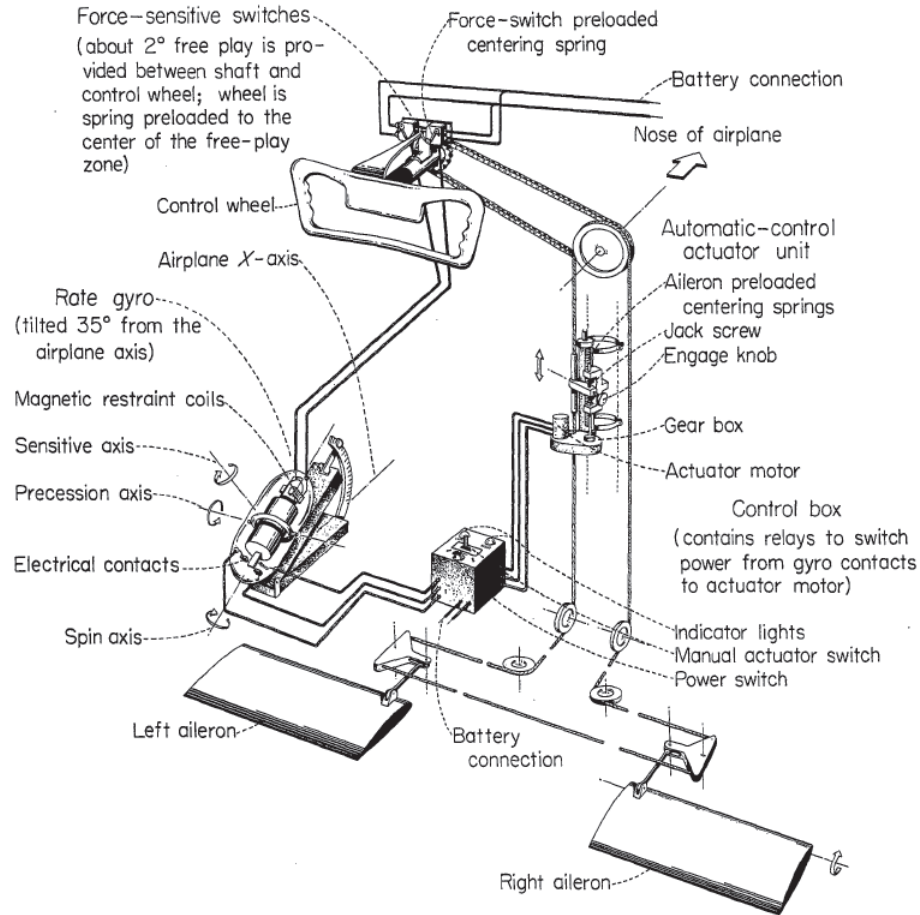Figure 2.3: Illustration of automatic aileron trim control system (W. H. Phillips et al., 1956)

reversal, the yaw rate gyro's spin axis was tilted as shown in Figure 2.3. The contacts on the gyro would reverse the motor direction, "when the resultant of the components of yawing and rolling velocities about the sensitive axis equal zero" (W. H. Phillips et al., 1956), when

$$r \cos \delta_g + p \sin \delta_g = 0 \qquad (2.1)$$

where, 'r' and 'p' are the yaw and roll rate, respectively, and δ_g was the angle subtended between the gyro spin axis and the flight path. Figure 2.3 provides a gyro tilt angle of 35 degrees to the airplane axis.

Flight testing was conducted by first trimming the aircraft and then powering the automatic trim system. No lateral trimming was performed after this point. A reasonable inclination angle was also determined for the gyroscope to achieve the desired damping. All subsequent testing was carried out at that setting.

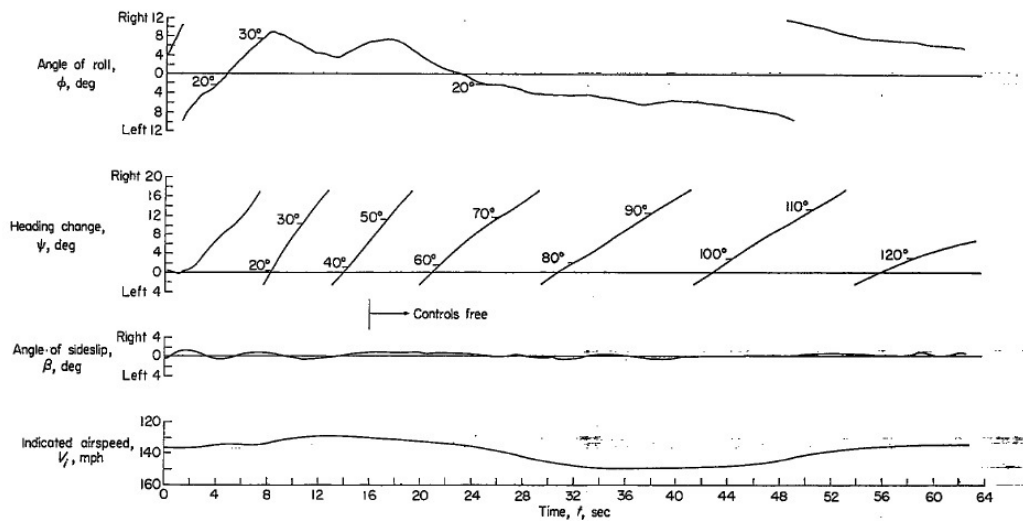Figure 2.4: Strip chart from flight test for basic aircraft (W. H. Phillips et al., 1956)

A comparison between the basic (trimming device disabled) and augmented aircraft is illustrated in Figures 2.4 and 2.5, respectively. The particular test shown began with the pilot performing a 45 degree heading change to the right after which the controls were released from a 20 degree roll angle. From Figure 2.4 the heading

angle can be seen to diverge rapidly as the aircraft continues to bank as a result of the out-of-trim state brought on by the increase in airspeed.

Conversely, Figure 2.5 demonstrates how the automatic aileron trimming device rolled the aircraft back to wings level within 10 seconds of the controls being freed, with little overshoot.
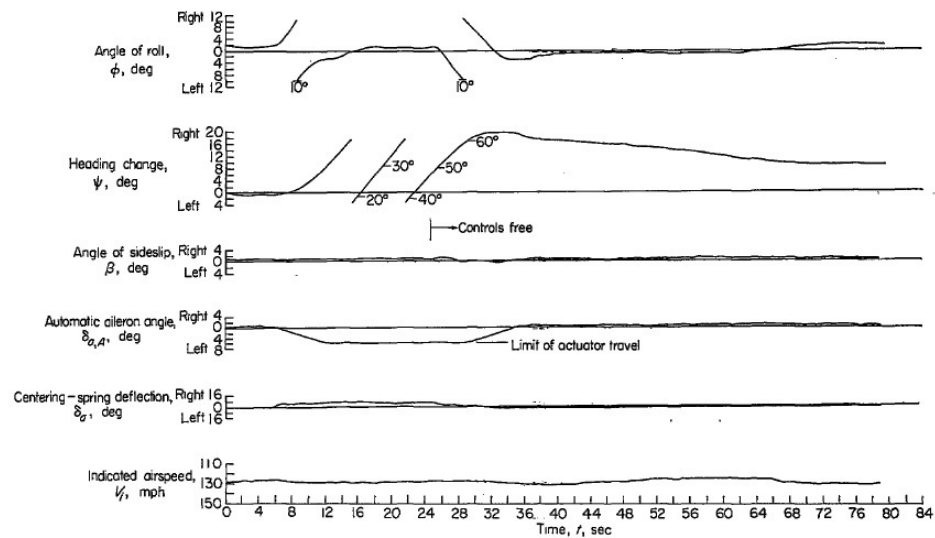

Figure 2.5: Strip chart from flight test for augmented aircraft (W. H. Phillips et al., 1956)

The investigation concluded that all four test pilots recognized the system as a useful tool in preventing divergence and enabling safe hands-free control "independent of airspeed and load changes that would cause directional trim changes" (W. H. Phillips et al., 1956).

Furthermore, the system also prevented divergence in gusty conditions and mitigated unwanted gyrations "resulting in a more comfortable ride with reduced pilot effort".

Pilots however, did object to the aileron force characteristics during takeoff and landing legs, as the preloaded spring force was objectionable when large corrective deflections were needed, especially in gusty conditions. As a result, an option to disengage the system was recommended.

Overall, the system was considered a suitable addition to improve the hands-free safety and augment the apparent spiral mode of a personal aircraft.

2.1.5   1966 - NASA's Evaluation of the Handling Qualities of Seven General Aviation Aircraft

To review the status of GA aircraft development, the NASA Flight Research Center (FRC) conducted an investigation into the handling qualities of seven late-model designs. A similar study evaluating personal-owner aircraft was carried out in 1948 (Hunter, 1948), and the almost 20 year gap since then had seen this class of aircraft undergo both physical and operational changes. Increased engine power, the replacement of the standard landing gear arrangement with a tricycle type, and the inclusion of control-system devices, contributed in justifying a fresh evaluation of the class. Furthermore, such aircraft saw increased use in adverse weather conditions as compared to those in the 1940s (Barber, Jones, Sisk, & Haise, 1966).

The quantitative evaluation of the aircraft indicated, "...satisfactory stability and control characteristics. However, these characteristics are degraded with decreasing airspeed, increasing aft center of gravity, increasing power, and extension of gear and flaps."

A summary of the investigation's flight test trials revealed that

"...the handling qualities are generally satisfactory during visual flight and during instrument flight in smooth air. Atmospheric turbulence degrades these handling qualities, with the greatest degradation noted during instrument landing system approaches. Such factors as excessive control-system friction, low levels of static stability, high adverse yaw, poor Dutch roll characteristics, and control-surface float combine to make precise instrument tracking tasks, in the presence of turbulence, difficult even for experienced instrument pilots." (Barber et al., 1966).

The report concludes with a note indicating a sharp increase in workload between the satisfactory and unsatisfactory aircraft, and specifies a need for further investigation into pilot workload in order to define superior design criteria.

2.1.6   1974 - NASA's Evaluation of Control System Modes and Displays in General Aviation Aircraft

Building on their investigation into the handling qualities of GA aircraft, NASA developed and tested a research flight control system (FCS) to mitigate the handling quality issues raised in (Barber et al., 1966).

In addition to the change in control systems, the program was divided into phases, the first of which maintained the aircraft's basic cockpit instruments, and a second phase where the cockpit was enhanced with a flight-director display (Loschke et al., 1974).

Control System Description

The FCS was comprised of hydraulic servo-actuators, rate and attitude gyros, control force sensors, and control surface position transducers. The left side controls were mechanically disconnected from the existing cable and pulley system. Fail-safe control transfer was implemented to allow for the safety pilot (right side) to take control using the aircraft's conventional control system in the event of a failure (Loschke et al., 1974).
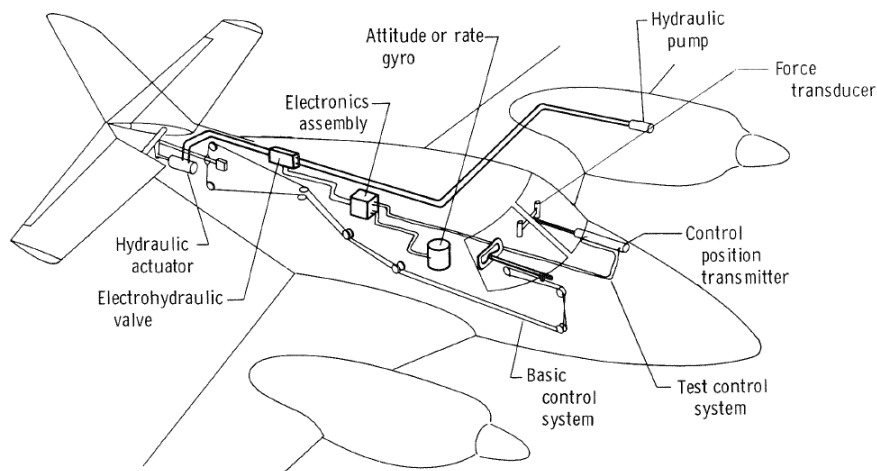

Figure 2.6: Control system mechanization in pitch axis (Loschke et al., 1974)

Control Modes

The FCS implemented three modes; (a) Basic mode, (b) Rate-command mode, and (c) Attitude-command mode.

(a) The basic mode allowed for direct control of the surface positions via the servo-actuators. This mode was intended to mimic the aircraft's existing cable-pulley system. As a result, control gains were selected to mirror the gearing ratios for wheel-to-surface and pedal-to-surface of the mechanical system (Loschke et al., 1974).

(b) The second available mode, the rate-command mode, allowed for direct pitch and roll-rate command through the control wheel. Coordinated flight was permitted by the implementation of a yaw rate damper and an aileron-to-rudder interconnect to combat adverse yaw. A washout network prevented undesired actuator responses due to a steady-state yaw rate during constant rate turns (Loschke et al., 1974).

(c) The attitude-command mode provided a direct pitch and roll attitude command signal using the wheel. Figure 2.7 illustrates the use of the shaping network to integrate the error between the actual and commanded pitch angle. Similarly, Figure 2.8 shows the roll attitude command logic.

Roll rate was used as the feedback parameter which resulted in increased loop sensitivity and smaller control gains for the axis. A heading-hold mode was used to maintain constant heading in level flight. A roll angle greater than or equal to ± 3 degrees permitted the heading-hold loop to be opened to permit turns (Loschke et al., 1974). Additionally, the loop would also open when yaw trim was activated by the pilot to correct for sideslip following a heading change.

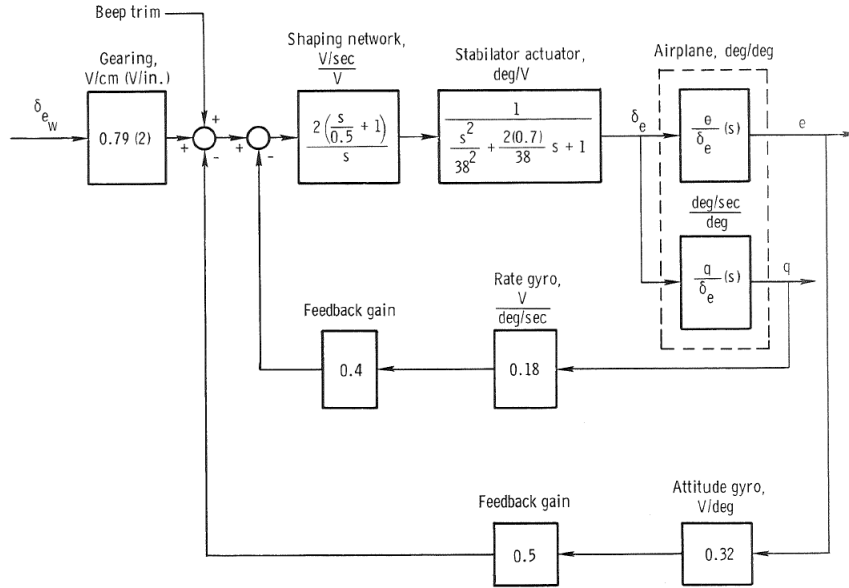*Control System Characteristics*

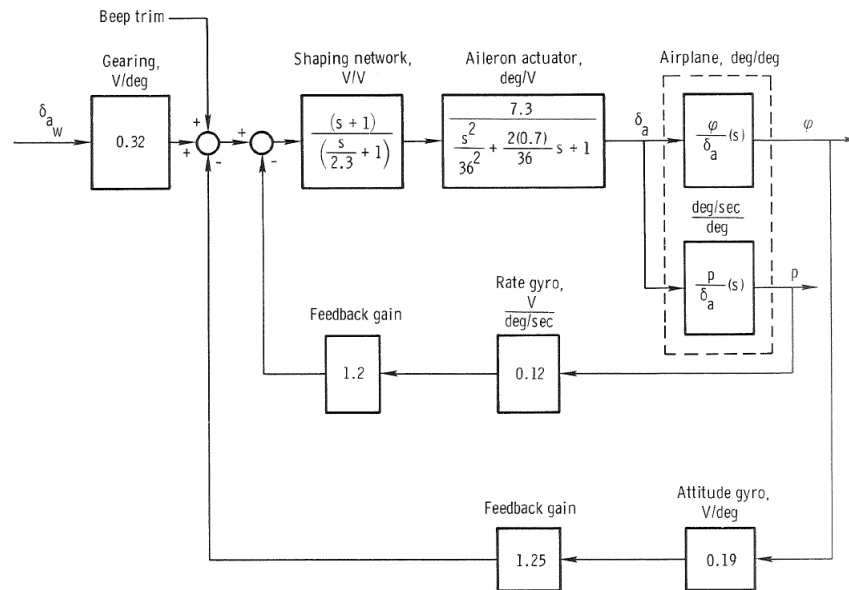Figure 2.7: Pitch-attitude control system (Loschke et al., 1974)

Figure 2.8: Roll-attitude control system (Loschke et al., 1974)

The investigation provides results from step inputs injected into the three modes to illustrate each of their longitudinal and lateral responses.

(a) Longitudinal Response

Figure 2.9 provides the longitudinal response characteristics.

The basic-mode response to a step input resulted in a near constant angle-of-attack (AoA), and varying pitch angle, pitch rate and normal acceleration. The control surface deflection followed control input as would be expected from the conventional mechanical system.

The rate-command mode response was in the form of a constant pitch-rate with a constant rate of control deflection while the command was present. Figure 2.9 also shows an increasing AoA which would result in the aircraft stalling unless the command was removed via the control wheel.

Finally, the attitude-command mode responded with a constant pitch attitude with all other longitudinal parameters varying to meet the desired signal. The pilot could enjoy almost direct flight-path control with the need to manually adjust the throttle setting, of course.

(b) Lateral Response

Figure 2.10 provides the lateral response characteristics.

The basic mode can be seen demonstrating an almost flat but increasing roll rate with the Dutch-roll and adverse yaw response clearly illustrated in the yaw rate and sideslip time traces. Roll rate divergence was indicative of the negative spiral stability of the aircraft.
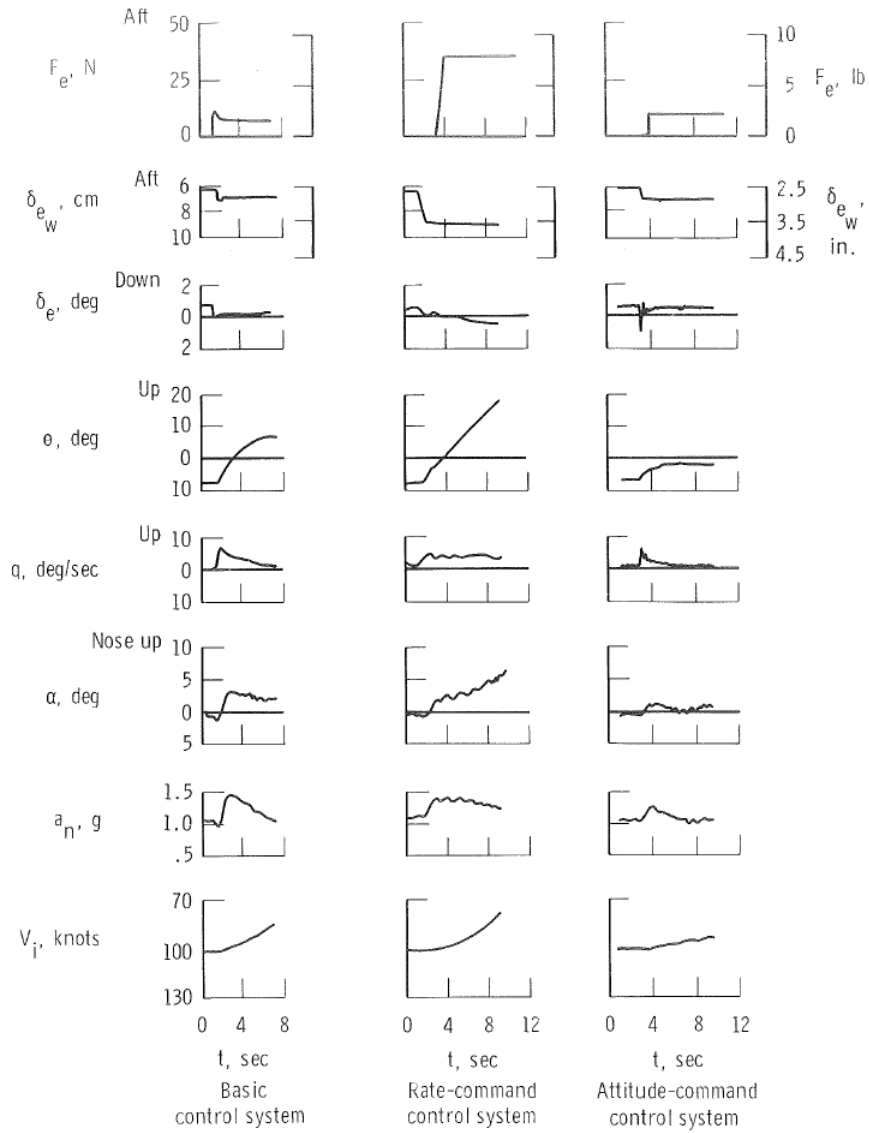
Figure 2.9: Long Response (Loschke et al., 1974)

The rate-command mode delivered a constant roll rate as expected, while the yaw

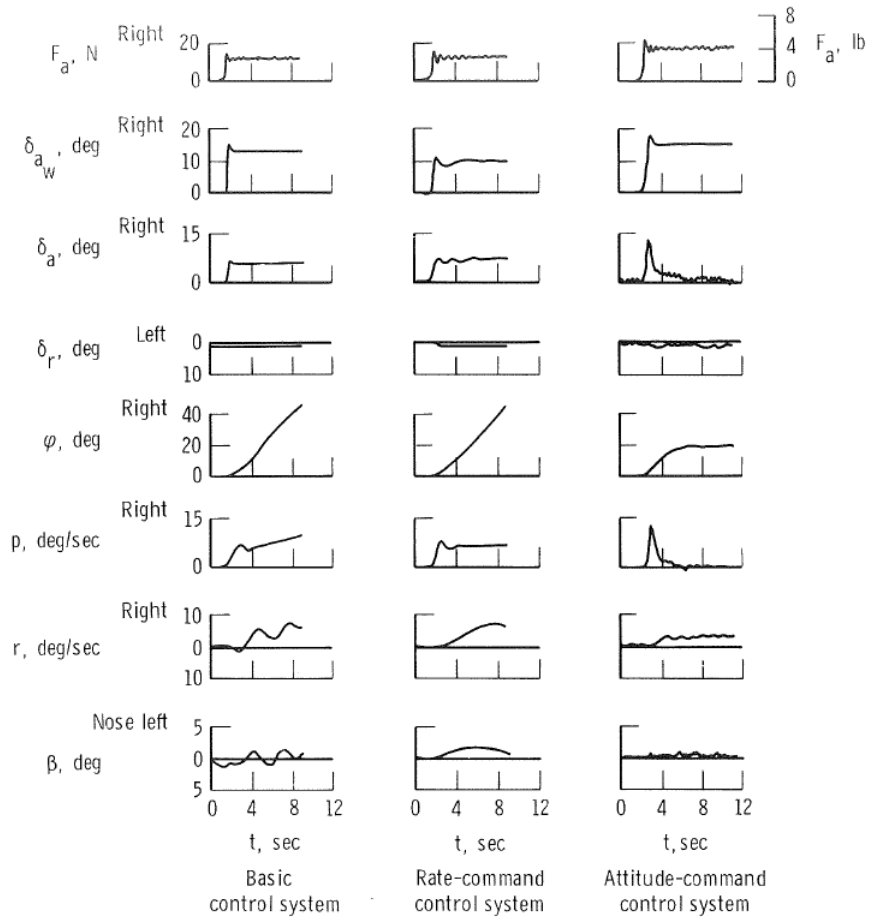damper and interconnected rudder and aileron mechanism ensured coordinated flight.

Figure 2.10: Lateral Response (Loschke et al., 1974)

Similarly, the attitude-command mode quickly met the desired roll angle commanded, and the yaw damper and heading-hold system performed well, maintaining zero sideslip more effectively than the rate-command mode.

Pilot Evaluation of Handling Qualities

To determine the real world benefits of the research FCS over the conventional control system, two experienced test pilots along with other instrument-rated pilots

with varying backgrounds were used to evaluate the aircraft. Around 20 instrument landing (ILS) approaches were flown per control system, and every pilot was made to fly "...each control system and display configuration at least once." (Loschke et al., 1974). Cooper-Harper handling qualities results for the basic mode can be seen in Figure 2.11.

With increasing turbulence during the ILS approaches, the ratings moved from, "...somewhat less than satisfactory" to '8', which is defined as unacceptable handling characteristics requiring significant pilot skill to maintain control.
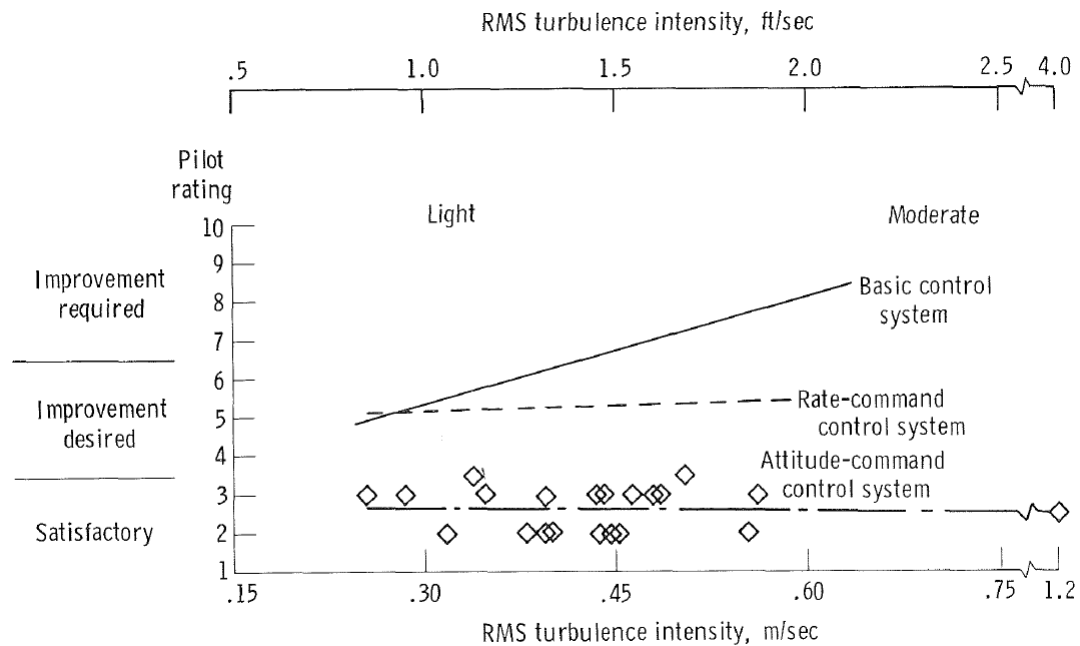

Figure 2.11: Cooper-Harper ratings for all modes (Loschke et al., 1974)

With the rate-command mode, pilots continued to rate aircraft handling as unsatisfactory, as they felt no appreciable improvement when flying in calm conditions. However, a noticeable improvement was reported in turbulence owing to the mode's ability to provide gust alleviation and limit trim changes due to throttle adjustment and flap and gear deflection. Overall trim was difficult to establish though, with pilots reporting constant pitch and roll rates drifting them off-course from the ILS beam.
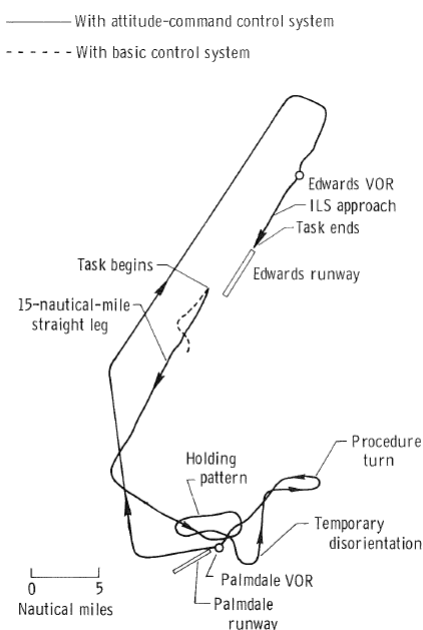

Figure 2.12: IFR mission - attitude-command vs. basic mode (Loschke et al., 1974)

Finally, the attitude-command mode received a satisfactory rating, with pilots acknowledging its performance in maintaining sufficient controllability even in high levels of turbulence. The mode managed to provide considerable stability as well, permitting the pilots to engage in navigation tasks without concern for attitude changes during the ILS approaches.

Flight testing of the attitude-command mode was extended to include 3 non-instrument rated pilots (with approximately 200 hours of flight time) to gauge the benefit of the system in the event that such pilots met with ILS conditions.

Figure 2.12 illustrates the performance of one such pilot who managed to complete the IFR mission when using the attitude-command mode, but failed to fly upright for more than 3 nautical miles whilst using the basic mode.

The findings of this investigation pointed strongly in favor of augmentation in general aviation aircraft to bolster the ease-of-use of the vehicle especially in unfavorable flying conditions.

2.2 Modern Digital FBW Controls and Displays - Investigation and Solutions, and the 'Irony of Automation'

A cross-section of research studies in FBW control system design is presented in this section. With the proliferation of such systems in military and transport category aircraft, organizations such as NASA have, and still are, exploring cost-effective techniques to simplify piloted flight in GA. Current research has focused on finding a balance between high levels of automation and manual flight control. The final products result in systems capable of limiting 'pilot error' and fatigue, whilst preserving continuous engagement with the act of flying.

2.2.1 1970s - 1980s - Boeing/NASA Development of the Velocity - Vector Control Wheel Steering System

The first series of investigations in this chronology of FBW solutions was targeted at addressing pilot workload, and flight safety of commercial transports operating in congested terminal areas, under the sponsorship of the Terminal Configured Vehicle Program (TCVP). One of these studies, described below, focused on flight operations requiring manual pilot control in complex environments. The objective of the study was the development of a system capable of providing (Lambregts & Cannon, 1979):

- automatic tracking of the established flight path to eliminate the need for pilot attention to control the effects of trim changes due to speed, configuration changes, turbulence and windshear;

- direct control over the inertial flight path using column/wheel and suitable displays, thereby reducing the need for attitude inner loop control;

- anticipatory flight path information display, to allow early assessment of the required pilot control input to achieve longer term airplane position objectives.

The solution comprised of: (a) development of a Velocity Control Wheel Steering system, and (b) the development of displays which provide anticipatory flight path information.

Central to manually flying the Velocity CWS system was the expectation that, "The pilots maneuvering task will further be simplified if the control augmentation/display system allows the pilot to make each path change with a single well-planned control input." (Lambregts & Cannon, 1979)

The initial implementation of the Velocity CWS was comprised of a longitudinal and lateral control law.

The longitudinal control law was designed to track the established vertical flight path. Pilot column input would introduce a γ_{cmd} input, initiating a synchronization to the actual flight path angle. This action would effectively open the automatic control loop. Upon returning the column to detent, γ_{cmd} would become the new reference for the automatic control loop. Pilot input was guided by the presence of a gamma indication on a display instrument (Lambregts & Cannon, 1979).

The control law was also scheduled with airspeed to maintain satisfactory stick force per 'g' sensitivity and aircraft damping response.

The lateral control law consisted "of a ground track hold mode, a roll maneuvering and a bank angle hold submode." (Lambregts & Cannon, 1979). Ground track hold engagement was a function of bank angle control wheel position. Setting a bank angle below 5 degrees and centering the control wheel would engage the mode. Commanding the wheel out of its detent would engage the roll maneuver mode, permitting the pilot to roll the aircraft freely. If the wheel were to be released at a bank angle greater than 5 degrees, the roll attitude hold mode would take over.

Several deficiencies related to handling qualities and mode confusion identified during simulation trials and flight test resulted in redesigns for the both control laws and their corresponding display symbology.

The replacement of the gamma feedback signal with a computed $\dot{\gamma}_{cmd}$ signal helped increase system damping while decreasing gamma response overshoot in response to a column input.

The lateral control law's mode confusion issues "were experienced when transitioning between the bank hold and track hold and when making small track angle adjustments." (Lambregts & Cannon, 1979). The threshold of 5 degrees was difficult to perceive given the inherent sluggishness of the system, and test pilots found themselves applying a trial and error method to engage the desired track hold mode.

Thus, it was determined that submodes should not be activated "by a logical function based on an imperceptible combination of control states." (Lambregts & Cannon, 1979). Instead, activation was only made possible by discrete pilot control action. Pilot displays were also updated to replace instantaneous bank angle with the commanded bank angle for the predicted track display. This alleviated the unsteady behavior of the track display in turbulence.

Another improvement added the ability for the pilot to maintain a constant radius ground track in crosswind conditions, eliminating the need for bank angle adjustments during a turn to line up with the desired track.

Lastly, a decrab enhancement was added to simplify touchdowns. The feature permitted the pilot to only make a rudder pedal input to decrab without having to correct for the aircraft's roll attitude.

The study indicated that the Velocity CWS concept could substantially reduce workload during manual control; however no formal simulation studies or flight test data were available at the time of publication.[2]

2.2.2 1980s - 1994 - NASA's Development and Evaluation of the E-Z Fly Control System in Simulation

Since the mid-80s, the LaRC was engaged in developing technologies to improve the efficiency and safety of general aviation. A study comparable to the one associated with this thesis was conducted by the LaRC in the early 1990s. The motivation was also to enable simplified flight for the non-or-novice pilot, reducing training time, and limiting 'recurring proficiency requirements' by implementing a digital FBW control system in a piloted simulator (Stewart, 1994).

The complete system was comprised of two parts; (a) a decoupled fly-by-wire control system named the 'E-Z Fly' (Easy-to-Fly) control system, and, (b) a pictorial display called the Highway-in-the-Sky (HITS) display (See Figure 2.13). As it happens this name has since been used for a variety of display systems attempting to guide the pilot through some kind of virtual path in the sky.

---

[2]A subsequent study tested the longitudinal improvements in isolation and the results were published in NASA TP-1664.
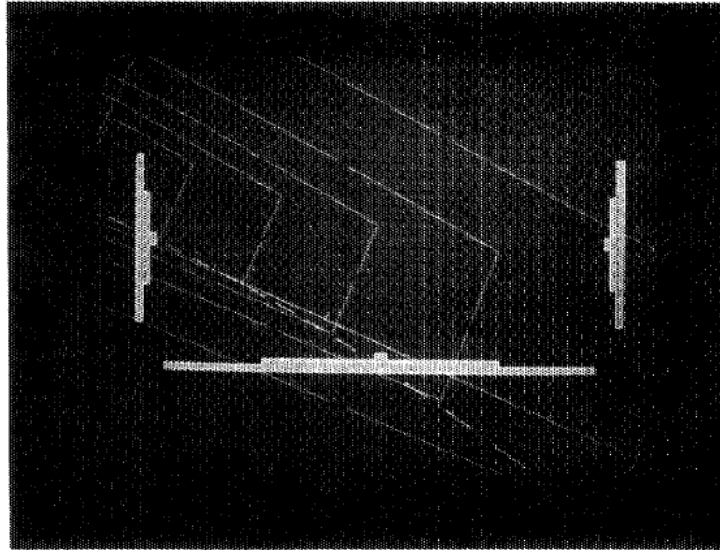
Figure 2.13: Highway-in-the-Sky display system used in the Langley GA Simulator (Stewart, 1994)

The collective system, E-Z Fly and HITS, was assembled in a simulation cockpit mounted on a limited full-motion base with a hydraulic control loading system (Stewart, 1994).

The E-Z Fly system provided three cockpit controls: the longitudinal wheel, the lateral wheel, and the throttle. Rudder pedals were only required during crosswind landings to control the sideslip angle. The three main cockpit controls were intended to "individually and uniquely determine the three primary response parameters (vertical speed, airspeed, and heading rate)." (Stewart, 1994).

Control laws for the E-Z Fly system provided direct control over the vertical speed, airspeed, roll angle, and the sideslip angle (See Figure 2.14). The longitudinal wheel provided vertical speed control using "proportional plus integral (PI) forward

paths" with, "Gain scheduling as [a] function of airspeed and dynamic pressure..." to deliver pitch damping (Stewart, 1994). The throttle was a direct airspeed (PI) controller, and implemented a feed-forward path to limit engine transients brought on by large commanded changes in airspeed. Roll angle control was afforded by the lateral wheel through a "...gain with roll rate used to provide damping." (Stewart, 1994). As mentioned above, the rudder pedals simply controlled the sideslip angle, and the yaw rate was fed back to deliver damping about the vertical axis. Trimming of control forces was provided by two separate automatic trimming functions for both longitudinal and lateral motion. The system was designed to alleviate increased wheel forces when it was held in a deflected position for a few seconds. Finally, the control law authority was limited by flight envelope protection (FEP) to prevent stalls and other situations brought on by unreasonable commanded inputs (Stewart, 1994).

The test program recruited three test pilots with some flight training, and thirteen subjects with no experience of piloting an aircraft. A racetrack pattern, including "...a takeoff, straight climbs, a climbing run, a level downwind section, a descending turn, and a two-segment straight-in approach to a flare and landing" was flown with a 200 ft ceiling. All participants were required to fly three different configurations; (a) with both the E-Z Fly system and HITS engaged, (b) with the E-Z Fly disengaged (conventional control system) but the HITS engaged; and (c) with the E-Z Fly engaged but the HITS disabled. Other runs with specific features turned off, were also flown to separate evaluation variables (Stewart, 1994).

Pilot Control Motion   **Airplane Motion Response**

Throttle lever ———————▶ Airspeed

Longitudinal wheel ———————▶ Vertical speed

Lateral wheel ———————▶ Heading rate

Pilot Control Motion   **Airplane Motion Response**

Throttle lever ———————▶ Airspeed

Longitudinal wheel ———————▶ Vertical speed

Lateral wheel ———————▶ Heading rate
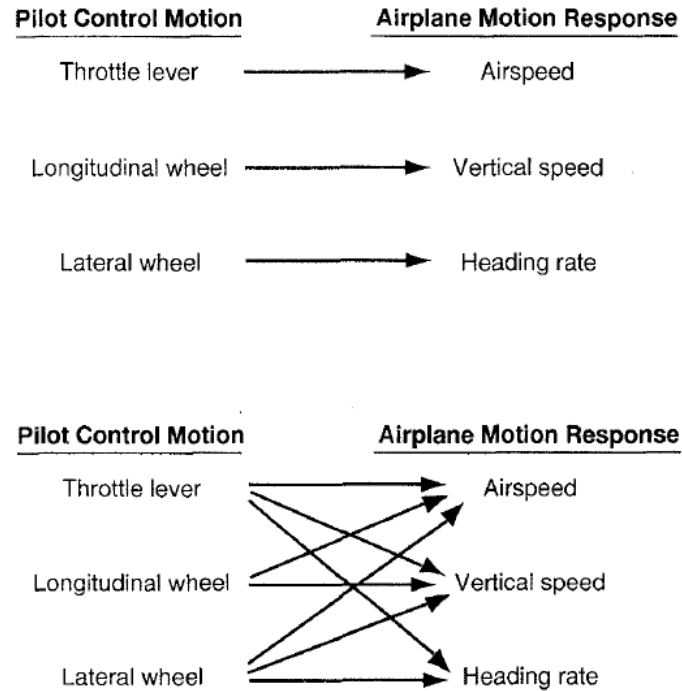
Figure 2.14: Mapping of pilot inputs to aircraft response for the decoupled control vs. the conventional system (Stewart, 1994)

Results from the trials with the E-Z Fly and HITS systems being engaged showed that all non-pilots successfully completed the assigned piloting tasks without prior training. Other pertinent observations made were as follows:

- Poor-performing pilots performed poorly in all the runs

- Non-pilots took their first turns with some difficultly, flying 'out of the highway'. Pilots did not have this problem.

- Non-pilots managed to track the glideslope well (to within ±0.35 deg) even when presented with virtual cloud cover, thereby having to rely solely on the HITS display.

- Non-pilots showed significant improvement from their first attempt with the E-Z Fly system, correcting for overshoots in turns and generating less control activity with experience.

- With the E-Z Fly system off, only 2 out of 7 runs were successfully flown by the non-pilots.

- As expected, trained pilots completed all the different configuration runs successfully.

Figure 2.15 presents the performance of one non-pilot using the E-Z Fly system, and Figure 2.16 provides results for the same pilot attempting to fly with the conventional control system.

The findings of this investigation indicate dramatic benefits in the implementation of FBW in GA aircraft.

2.2.3   2002 - FAA Civil Aerospace Medical Institute: Applying Performance-Controlled Systems, Fuzzy Logic, and Fly-By-Wire Controls to GA

The goals set out by the AGATE consortium in the 90s motivated the development of a fuzzy-logic control system (FLC) by a doctoral candidate at Wichita State University. The idea was to develop a system capable of being fitted in "different
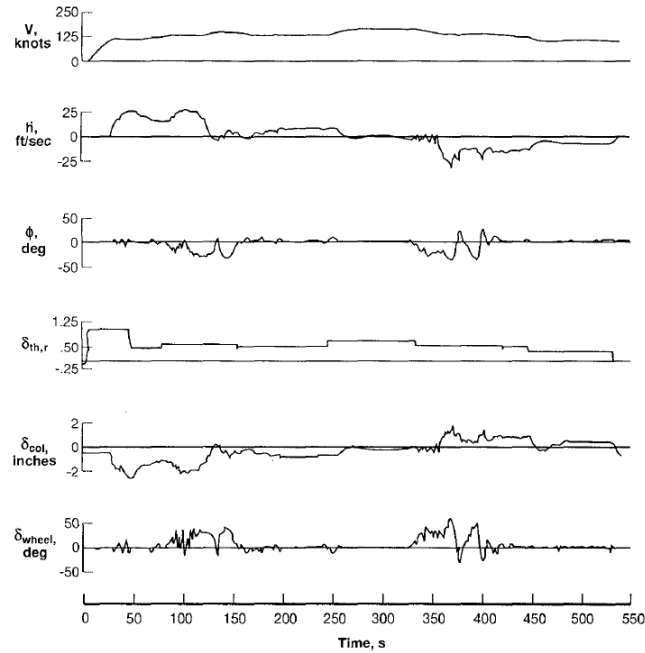
Figure 2.15: Performance of a non-pilot particpant using the E-Z control system (Stewart, 1994)

airframes without the usual individual 'tuning' associated with autopilot systems..." The FLC would also provide some form of FEP to prevent stalls or excessive airspeeds (Beringer, 2002).

Code developed in this dissertation by Duerksen was implemented by the FAA's Civil Aerospace Medical Institute in the Advanced General Aviation Research Simulator (AGARS) for purposes of piloted evaluations (Beringer, 2002).

The simulator, as in the previous study mentioned above, was equipped with both conventional controls and the experimental FLC hardware which was comprised of a "spring-centered and damped 4-axis side-arm controller, with those axes representing
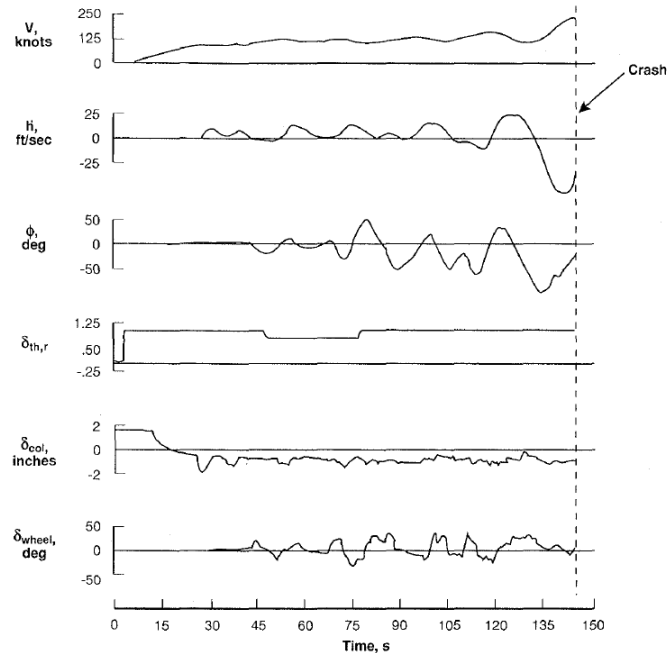
Figure 2.16: Performance of a non-pilot particpant using the conventional control system (Stewart, 1994)

turn rate (wrist rotation), climb or descent rate (vertical wrist flexion), and airspeed (fore-aft slide axis)." (Beringer, 2002). See Figure 2.17.

Driving the simulation was a math model of the Piper Malibu (a single piston engine, 6 person GA aircraft). The display was configured to be a HITS system with a "3-D courseline", and guidance vector (Beringer, 2002).

Evaluations were conducted by 24 participants, broken into 4 groups: high-time pilots, low-time pilots, student pilots, and non-pilots. A short pre-flight briefing without hands-on training was provided. Participants were tasked with taking-off, climbing, and executing a base-leg turn before descending on approach to land at the
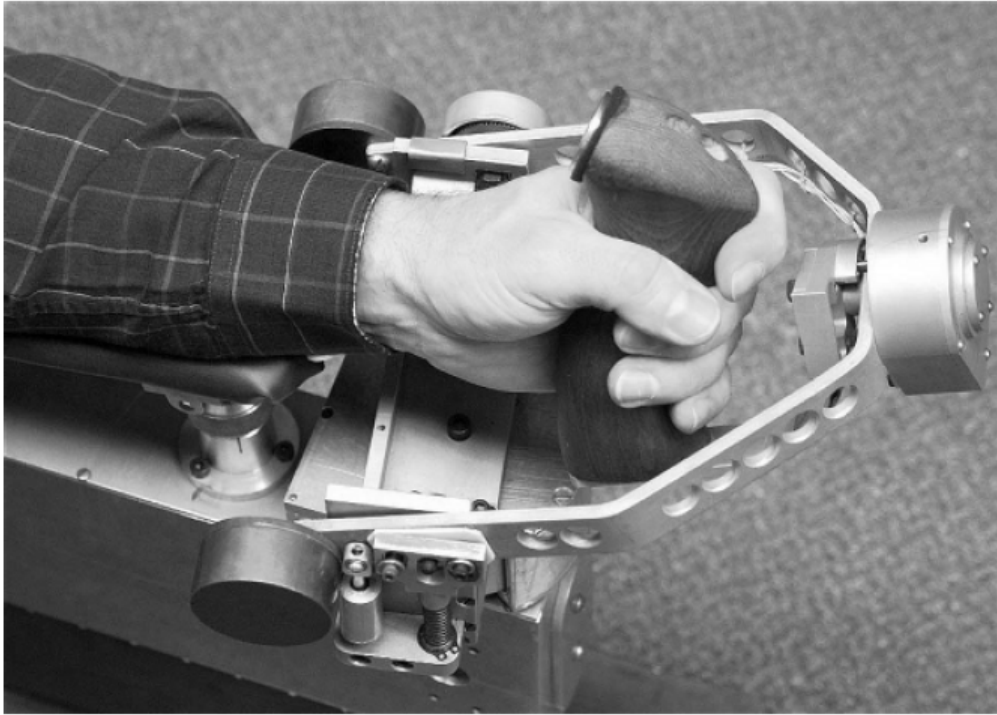
Figure 2.17: 4-axis side arm controller used in the FLC-system (Beringer, 2002)

starting airport. Throughout the extended pattern, the visual system provided a virtual pathway to follow. The 15-17 minute flights ended with a post-test questionnaire. Quantitative data was recorded as well.

As previous studies have shown, augmented control systems have received favorable responses from evaluating participants. This study was no different, with both pilots and non-pilots expressing their preference for the FLC system. Non-pilots also indicated that the FLC system was easier to learn. Quantitative data, as is presented for one non-pilot in Figures 2.18 and 2.19, shows the marked improvement over the conventional yoke in both vertical and lateral tracking when using the FLC system.
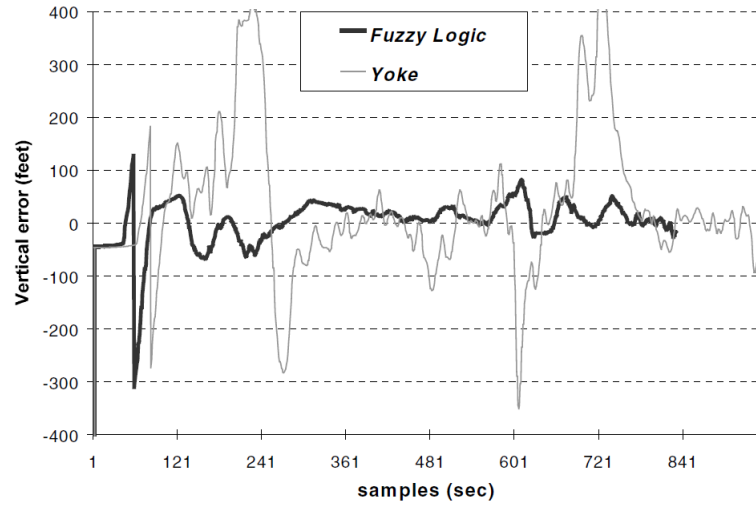
Figure 2.18: Vertical error of a non-pilot particpant (Beringer, 2002)
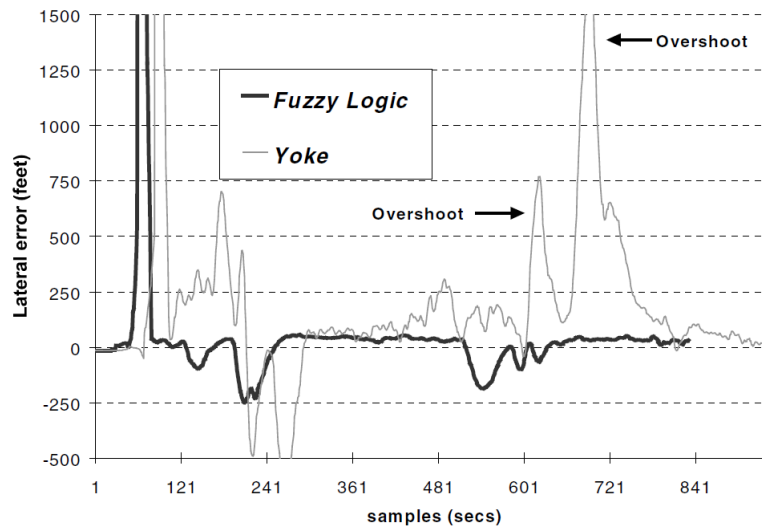
Figure 2.19: Lateral error of a non-pilot particpant (Beringer, 2002)

An expected yet noteworthy outcome of the evaluations was that of reduced control input frequency with the FLC system engaged. A reduction ratio of almost 3:1 was achieved across the sample, signifying considerable workload alleviation for the

participant. A complaint against the FLC system was that of having to hold the side-stick in position to maintain a desired climb or descent rate. This was straining for the wrist, and was subsequently rectified with 'lock-in and release' functionality which could be disabled once the desired end-state was achieved.

2.2.4   2003 - Raytheon's GA Research Aircraft

Under the direction of the SATS program, Duerksen's research in advanced flight controls for GA continued at the Raytheon Aircraft Company. A 1978 Beech F33C Aerobatic Bonanza was retrofitted with a programmable FBW control system and two 10 inch Avidyne LCDs (Duerksen, 2003).

Echoing similar motivation, the goal was to enable "people with little or no piloting experience" to successfully fly instrument approaches to minimums after about 15 minutes of instruction.

The F33C's flight control system was designed as a 'velocity vector command system'. The pilot is provided a joystick to command the vertical flight path angle, γ and desired turn rate. The second inceptor is a speed command lever to set the desired airspeed. Sideslip related functions are automatic to ensure yaw damping, coordinated flight and compensation for engine torque and p-factor (Duerksen, 2003). To accomplish the command tasks, the FBW system controlled throttle, elevator, aileron and rudder positions.

FEP was built into the system as well, protecting against stalls, over-g, over-bank and over-speed.

With regard to lateral flight path control, Duerksen claims the design philosophy behind turn-rate command rather than the more direct heading command was driven by the

> "vast wealth of experience in the target population that correlates control effector position with turn rate (e.g. steering wheel in a car). Using this convention would allow for positive transfer of learning from other vehicle types" (Duerksen, 2003).

As a result, a steep turn in instrument conditions was demonstrated to be an easy task for an inexperienced pilot. The maximum turn rate would be achievable by fully deflecting the stick to either side and holding it there. With appropriate airspeed, the aircraft could attain a maximum 55 degree bank angle and with the stick centered longitudinally, the airplane would maintain altitude and commanded airspeed. With the stick spring loaded to the center, the airplane would hold current altitude, heading and speed until manipulated by the pilot. Of course, adjusting the speed lever would affect a change from the steady-state condition as well.

This idea of lateral flight path control in this, and the preceding section, is echoed in the methodology adopted for this thesis. See Section 3.2.1 for details on the Ω-inceptor as a direct horizontal flight path inceptor.

Evaluation flights flown by low- and no-time pilots demonstrated a high level of confidence in flying the aircraft after "a few minutes". Furthermore, it was noted that if autopilot-type tracking was allowed, the pilots felt completely disengaged from the

task of flying. Instead, a primary display providing a moving map with "weather, traffic, terrain and other hazards along the flight path" granted situation awareness under low workload conditions. However, pilots did complain that the constant stick displacement required in a long climb or descent was "annoying" (Duerksen, 2003).

A rigorous flight test program was planned but no results have been found in the literature.

At this stage in the presentation of literature, a summary of control laws covered through Sections 2.2.1-3 would be useful before proceeding to detail the motivation and design behind the path-oriented control and display augmentation system developed at Delft University. The table below lists the primary control parameters for the decoupled FBW systems from each section.

Table 2.1: FBW sytems summary

	Long.	Lat-Dir	Speed control
E-Z Fly	$\dot{h}$	$\dot{\psi}$ CMD & Pilot δ_r	Pilot δ_t
FLC	$\dot{h}$	$\dot{\psi}$ CMD & β control	Airspeed CMD
Raytheon	γ	$\dot{\psi}$ CMD &β control	Airspeed CMD
Delft FBW+	γ	curvature-rate CMD	Fixed Speed 150kts

2.2.5 2006 Delft University of Technology's Path-Orientated Augmentation Concept

In 2006, Borst et al. published a comparative study of flight-path predictor display and flight-path vector control augmentation concepts (Borst et al., 2006). The study sought to demonstrate the relative efficacy of a curvature-command based, display and control augmentation system designed by the authors.

The investigators based their design on Boeing's Velocity CWS system described in Section 2.2.1.

The goal of the design was to enable the pilot to fly "circular curved ground-referenced trajectories, irrespective of crosswinds...", much like Boeing's system (see Section 2.2.1) and "relieve the pilot from holding the side stick deflected during turns." The latter requirement was met by allowing the pilot to command a "curvature-rate of the future aircraft trajectory" (Borst et al., 2006). Pilot inputs were interpreted by a fast-time simulation (FTS) to determine the curvature-rate and climb-angle rate commands which in turn were output as real-time reference signals for the control augmentation system to track.
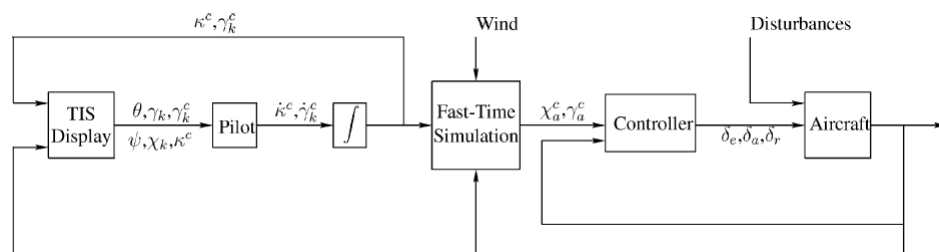
Figure 2.20: Block diagram from a 'velocity error' in a curve (Borst et al., 2006)

The pilot interface included an augmented command tunnel display "representing a 3D analog of the future trajectory that will be flown" (Borst et al., 2006). The command and reference tunnels were designed to be of equal dimensions to permit easy detection of path deviation.

The resulting pilot control task was a, "pursuit-tracking task with preview" (Borst et al., 2006). To remain on-course, the pilot would have to align the command tunnel (future trajectory) to the reference tunnel. Longitudinal stick deflection would result in a climb-angle-rate/climb-angle hold command, while lateral deflection would initiate a curvature-rate/curvature hold command. As expected, a zero-stick deflection would hold the current climb angle and or curvature.
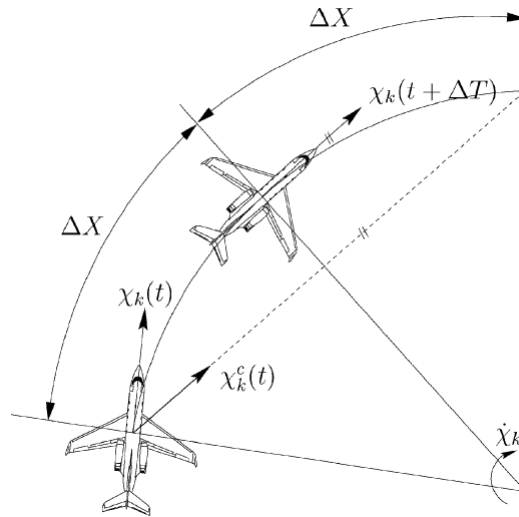
Figure 2.21: Lag effects from a 'velocity error' in a curve (Borst et al., 2006)

The longitudinal control law tracks the aerodynamic flight-path angle and in doing so effectively controls the climb or descent rate of the aircraft. The inner loop employs a pitch-attitude hold controller and turn compensation assists with steady-state turns.

The lateral control law is a heading-hold (HH) controller with yaw-damping and turn coordination. The inner loop of the HH control law tracks yaw-rate.

For the sake of simplicity, the experiment was conducted using an auto-throttle which regulated the airspeed to a constant 150 ± 5 kts. An experiment was conducted with six professional pilots. The experiment used a factorial within-subjects design to expose each subject to four different augmentation concepts, including the one detailed in this paper, and two weather conditions. Each pilot flew four blocks of sixteen runs, where each block had "sixteen randomly ordered runs". The subjects also completed a questionnaire on the usability of each augmentation concept in assisting with tracking a trajectory (Borst et al., 2006).

Results indicated that the path-oriented augmentation concept yielded the best performance in path-following and ride comfort. However, what was not hypothesized was that the new concept would increase pilot control activity and workload. It was inferred that the increase in activity owed much to the availability of precise tracking information with the display system. This could have resulted in pilots attempting to correct errors imperceptible in other augmentation and display concepts. Subjective responses from the pilots confirmed this idea, with none of them preferring the newer concept, as it demanded far too much attention to minimizing errors between the command and reference tunnels. Additionally, the prediction time of the

command tunnel resulted in pilots focusing on capturing longer-term tracking goals whilst 'corner-cutting' in the interim (Borst et al., 2006).

The research team concluded that their concept had not significantly improved upon other solutions.

2.2.6 2003-2012 NASA's H-Mode (Horse Metaphor) and Haptic Flight Control System

An extensive study in vehicle automation, control augmentation and interaction was initiated by NASA at the Langley Research Center. The literature, almost spanning a decade (2003-2012), established a new design metaphor for tackling the realm of highly automated vehicles and their interactions with human users.

With aviation, the concern was that highly automated aircraft had not only "led to a reduction of physical workload, but also to severe problems like mode confusion, human-out-of-the-loop, and many more." (Flemisch et al., 2003). This was echoed in the words of Bainbridge who coined the term 'irony of automation' to describe a situation where "by taking away the easy parts of his tasks, automation can make the difficult parts...more difficult" (Bainbridge, 1983).

Furthermore, criticism was also directed at the additive nature of cockpit design, where the highly automated cockpit of a typical passenger jet had become a collection of incremental advances in systems with little regard for the overall cockpit concept.

The proposed design metaphor, named the Horse-metaphor (H-metaphor), highlighted the fact that a distracted (or out-of-loop) horse rider could rely on the animal

to maintain a safe path, without colliding into obstacles. Conversely, direct control could be asserted by tightening the reigns (Flemisch et al., 2003).

The application of the metaphor to flying was summarized as the ability to focus on other tasks while knowing the aircraft would sense and avoid any perceived obstacle. Equally important to the development of the concept was the elimination of activity spikes seen when transitioning from purely automated flight to manual flight. Instead it was desired that the pilot would regularly interact with the vehicle via the inceptor to make periodic tracking commands. The underlying system would provide control augmentation and inner-loop closure on the relevant states to simplify the task of manual control, and automation would not be an exclusive state of control; rather the physical loop would include both the pilot and the automation simultaneously (Goodrich, Schutte, & Williams, 2011).

Subsequent publications introduced the design of a Haptic-Multimodal Flight Control System (HFCS). Central to the design of the HFCS was the idea that it combined three command 'languages' (Schutte, Goodrich, & Williams, 2012). The command languages were introduced as the mainstay of highly automated aircraft of the day.

The first language was the manipulation of the control surfaces and propulsion via three inceptors (stick/yolk, rudder pedals, and throttle).

The second language addressed speed and direction whereby the pilot would interact with an autopilot guidance panel of some sort to set desired heading, airspeed and altitude commands.

The third and final language brought "earth-referenced locations and clock time" into the scenario. This of course required interacting with an FMS display and abiding by its unique set of rules to configure it for navigation to specific locations (Schutte et al., 2012).

The HFCS aimed to combine these languages and their unique inceptors into a simpler paradigm where tasks related to manual flight as well as navigation to a specific location could all be accomplished using the stick, throttle and a pair of displays (Schutte et al., 2012).

Also of note was the intent to create a system that could "serve as a bridge between today's state of the art aircraft that are highly automated but have little autonomy and can only be operated by highly trained experts (i.e., pilots) to a future in which non-experts (e.g., drivers) can safely and reliably use autonomous aircraft to perform a variety of missions." (Goodrich et al., 2011). With a focus on the Personal Air Vehicle (PAV), the design requirements stated that the intended training time would ideally decrease to a level comparable with driver education, especially if FBW were leveraged to limit the need for conventional flight skills. A follow-up demand was to simplify piloting the vehicle to the point where maintaining proficiency could be accomplished by flying once a month.

Evaluations of the HFCS alongside a manual control system, and a fully automated system resulted in a response in favor of the HFCS reducing pilot workload, and improved situational awareness (Schutte et al., 2012).

This chapter has introduced the reader to a brief history of control augmentation for the purpose of simplifying flight. More importantly, research presented from the last 25 years has demonstrated, via simulator evaluations that FBW control systems can substantially increase the EoU of a typical GA aircraft making it more accessible to an audience unable to acquire extensive flight training and fulfill regular recurrency requirements.

The following chapter will present a unique implementation of automotive-like inceptors in a FBW-type control system which attempts to integrate the familiarity of driving a car with simplified piloted flight.

3. Methodology

This chapter is divided into three sections. The first presents a basic definition of the Ω-inceptor or steering wheel, the second details the functional design of each control mode, employing the stick shifter and pedals to change and manipulate each mode, respectively, and the third section describes the experiment design for the piloted trials.

3.1 Mathematical Basis for the Ω - Inceptor and Envelope Protection

From basic flight mechanics, a relationship exists between the rate-of-turn, Ω, bank angle, ϕ, and the aircraft's true airspeed, V_{TAS}. This relationship determines Ω to be a required output from the inceptor (steering) in order to manipulate the horizontal flight path of the aircraft.

The relationship is given in Mechanics of Flight (W. F. Phillips, 2009) as

$$\phi = \arctan \frac{\Omega V}{g} \qquad (3.1)$$

where Ω is the output received from deflection of the Ω - inceptor.

In Section 3.2.1, details on how the resulting bank angle, ϕ, will be used to command a roll rate to achieve the desired rate-of-turn requested by the pilot will be provided.

3.1.1 Load/Stall Limited Rate-of-Turn

To determine an upper limit for the commanded turn rate allowed by the Ω - inceptor, the maximum attainable rate-of-turn based on stall and load limitation can be expressed as,

$$\Omega_{max} = \sqrt{\frac{C_{L_{max}}}{2}\left(\frac{n_{pll}W_{max}}{W} - \frac{W}{n_{pll}W_{max}}\right)g}\sqrt{\frac{\rho}{W/S_w}} \tag{3.2}$$

where n_{pll} is the positive load limit (W. F. Phillips, 2009). The maximum rate-of-turn for the Navion model and IO-360 combination at $V_{TAS} = 110kts$ and $W = 2150lbs$ is estimated to be,

$$\Omega_{max} \approx 41deg/s \tag{3.3}$$

well above the design maximum Ω of 15 deg/s for the Ω - inceptor (5 times faster than a standard rate turn).

3.2 Flight Modes & Control Law Design

As introduced in Chapter 1, the pilot can manipulate the mode selector between six modes to cover the typical flight profile - from takeoff (mode 1) through climb (mode 2) and into low-speed cruise (mode 3) and high-speed cruise (mode 4), followed by descent (mode 5), and finally approach (mode 6), at a 3 degree glide scope.

3.2.1 Takeoff Mode (Mode 1)

Engaged at the start of the simulation, Mode 1 enables the pilot to increase throttle from idle. Takeoff roll is initiated by pressing down on the right pedal inceptor. Upon reaching a predefined ground speed, the aircraft rotates to climb out. Once off the ground, horizontal flight path can be changed using the $\Omega-inceptor$ or steering wheel. The pilot is free to switch to Mode 2, or if desired can remain in Mode 1 without causing the aircraft to become unsafe.

The control logic defining this mode is expanded below. For brevity, deflections of the right and left pedal inceptors will be abbreviated as δ_{+R} and δ_{-R}, respectively.

Right Pedal Inceptor as Direct Throttle Control

Exclusive to the takeoff mode, this simple logic serves to link the deflection of the right pedal inceptor to direct throttle control. A simple first-order relationship between deflection of the right pedal inceptor and commanded throttle, $\delta_{th_{cmd}}$, as manifold air pressure (MAP) can be represented by,

$$\delta_{th_{cmd}} = 8\delta_{+R} \quad \text{(inHg of MAP)} \tag{3.4}$$

where δ_{+R} ranges from 0 to 1 (full deflection).

Through the use of what would conventionally be the accelerator pedal in an automobile, the pilot can increase the engine power setting, above the default setpoint, demanding the throttle setting, $\delta_{th_{dem}}$, from the engine,

$$\delta_{th_{dem}} = \delta_{th_{cmd}} + P_{base} \quad \text{(inHg of MAP)} \tag{3.5}$$

where P_{base} is the base power setting of 20 inHg of MAP and $\delta_{th_{dem}}$ is 28 inHg of MAP with full deflection of δ_{+R}. This outputs a maximum of 177.5 bhp at 2,700 RPM for takeoff.

Ω - Inceptor for Direct Ground Steering

Again, control logic only found in mode 1 permits the use of the Ω - inceptor as a conventional steering wheel linked directly to the rudder while the aircraft is on the ground. The following illustrates the relationship between the controller and the control surface,
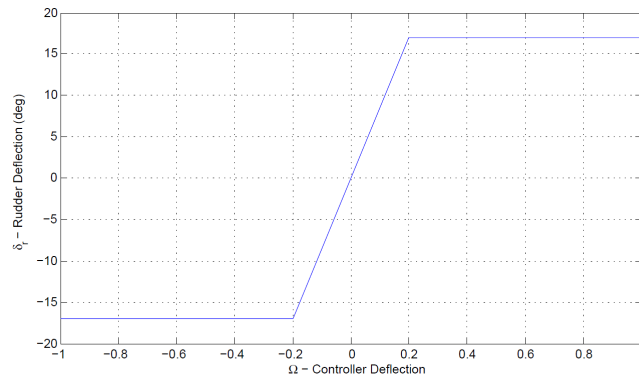
Figure 3.1: Rudder surface deflection vs. Ω - inceptor deflection

Once a $\delta_{th_{cmd}}$ results in a true airspeed (TAS) value greater than the 62 KIAS, a second control law is triggered to initiate takeoff rotation. The following section provides a detailed description. Additionally, the direct Ω - inceptor to rudder link

is replaced with the control law described under Ω - *inceptor for Direct Horizontal Flight Path Control.*

$\dot{h}$-q *Control Law and the Right and Left Pedal Inceptors*

The activation of the takeoff mode enables the aircraft to maintain a predefined climb angle of 2 degrees without pilot input. The active control law demands a rate-of-climb based on ground speed, V_{gnd}, appropriate to maintain the climb angle, γ, as shown below,

$$\dot{h}_{cmd} = V_{gnd} \tan \gamma \; (ft/s) \tag{3.6}$$

Note: Small α approximation in use.

The activation of this logic depends on a minimum airspeed, V_{rot}, requirement being met to prevent a stall during the takeoff rotation.

$$\dot{h}_{cmd}(ft/s) = \begin{cases} V_{gnd} \tan \gamma & for V_{gnd} > V_{rot} \\ 0 & for V_{gnd} < V_{rot} \end{cases}$$

The right pedal inceptor manipulates the throttle setting as shown in 3.4, while maintaining the predefined climb angle. This control logic will be referred to as the **$\dot{h}$-q** control law. Figure 3.2 illustrates the top-level logic of the $\dot{h}$-q control law as implemented for the takeoff mode.
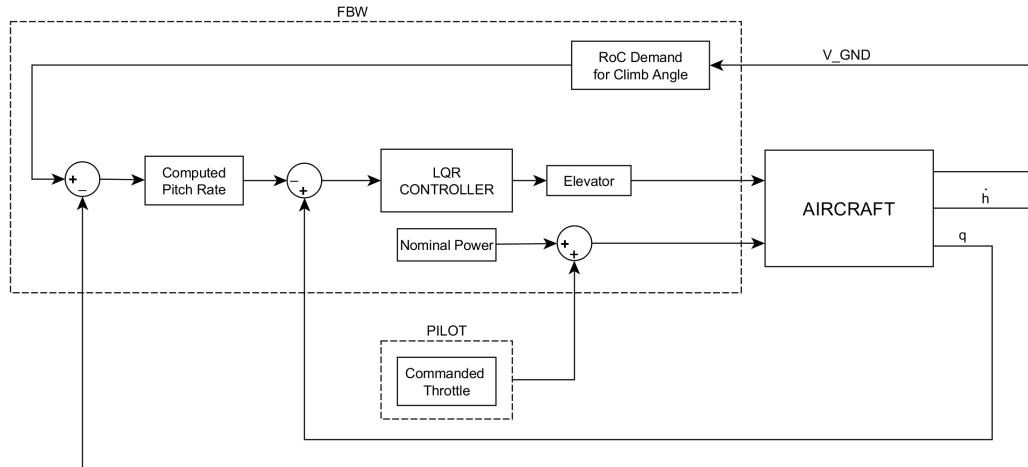
Figure 3.2: Block diagram illustrating $\dot{h}$-q control logic for the takeoff mode

With this relationship in hand, the piecewise function shown below relates the desired rate-of-climb to a commanded pitch rate, q_{cmd},

$$
q_{cmd}(deg/s) = \begin{cases} K_q(\dot{h}_{cmd} - \dot{h}) & for\ 0 < |\dot{h}_{cmd} - \dot{h}| \leq 1.25ft/s \\ 10°/s & for|\dot{h}_{cmd} - \dot{h}| > 1.25ft/s \end{cases}
$$

The $\dot{h}$-q control law relates a commanded $\dot{h}$ to a proportional pitch rate, q_{cmd}. Driving the *error* between the current aircraft pitch rate, q, and q_{cmd} to zero poses itself as a tracker problem, warranting the implementation of a linear quadratic regulator (LQR) with output feedback manipulating the elevator.

The tracker/regulator problem for an aircraft is described by the following linear time-invariant (LTI) system of the form

$$
\dot{x} = Ax + B\delta \tag{3.7}
$$

$$
y = Cx \tag{3.8}
$$

is addressed through use of the standard quadratic performance index shown below,

$$J = \frac{1}{2} \int_0^\infty (x^T Q x + \delta^T R \delta) dt \tag{3.9}$$

where

$$x(t) = \left\{ \begin{array}{c} \dot{h} \\ u \\ w \\ \theta \\ q_e \end{array} \right\} \quad \& \quad u(t) = \left\{ \delta_e \right\}$$

and Q and R are the state and control penalizing weighting matrices, respectively. The performance index of Equation 3.9 is minimized by the control gain, K, computed by solving the algebraic Riccati equation for P,

$$-A^T P - PA + PBR^{-1}B^T P - Q = 0 \tag{3.10}$$

using the chosen Q and R matrices. The final Q matrix was selected after several trial-and-error tuning attempts to capture the commanded rate-of-climb at a reasonable rate while limiting sharp changes in load factor during mode transition and pedal input. The design for the state penalizing, Q, and control penalizing, R, matrices are shown below,

$$\mathbf{Q} = \begin{bmatrix} 3.73\text{x}10^{-7} & 0 & 0 & 0 & 0 \\ 0 & 0.0037 & 0 & 0 & 0 \\ 0 & 0 & 2.611\text{x}10^{-4} & 0 & 0 \\ 0 & 0 & 0 & 3.73\text{x}10^{-7} & 0 \\ 0 & 0 & 0 & 0 & 66021 \end{bmatrix} \tag{3.11}$$

where, the state order is u, w, θ, q_e, and $\dot{h}$. The control order for R matrix below is δ_e,

$$\mathbf{R} = \begin{bmatrix} 7.479\text{x}10^9 \end{bmatrix} \tag{3.12}$$

A positive definite solution of the Ricatti equation yields the control command,

$$\delta = -Kx \tag{3.13}$$

or,

$$\delta = \left\{ \delta_e \right\} = -K \left\{ \begin{array}{c} \dot{h} \\ u \\ w \\ \theta \\ q_e \end{array} \right\} \tag{3.14}$$

where $\dot{h}$, u and w (V_{GND}), and q_e are the feedback terms shown in Figure 3.2. The control gain matrix, K, for the elevator is

$$K = R^{-1}B^T P = \begin{bmatrix} -0.1982 & -0.0099 & 0.0648 & -31.2569 & -3.7572 \end{bmatrix} \tag{3.15}$$

<u>Ω - *Inceptor for Direct Horizontal Flight Path Control*</u>

Once airborne, the Ω-inceptor enables the pilot to command a rate-of-turn without requiring additional control input to remain in coordinated flight. The result is *carefree* manipulation of the aircraft's horizontal flight path.

The simulator receives pilot input from the Ω-inceptor as a normalized value of deflection to translate it to a desired rate-of-turn via the piecewise function for a 1-D lookup table shown below:

$$\Omega_{cmd}(deg/s) = f(\delta_s) = \begin{cases} \mp 15 & for \pm 1.0 \le \delta_s \le \pm 0.6 (\text{normalized}) \\ -30\delta_s - 3 & for \pm 0.6 < \delta_s \le \pm 0.2 (\text{normalized}) \\ -15\delta_s & for -0.2 < \delta_s \le +0.2 (\text{normalized}) \end{cases}$$
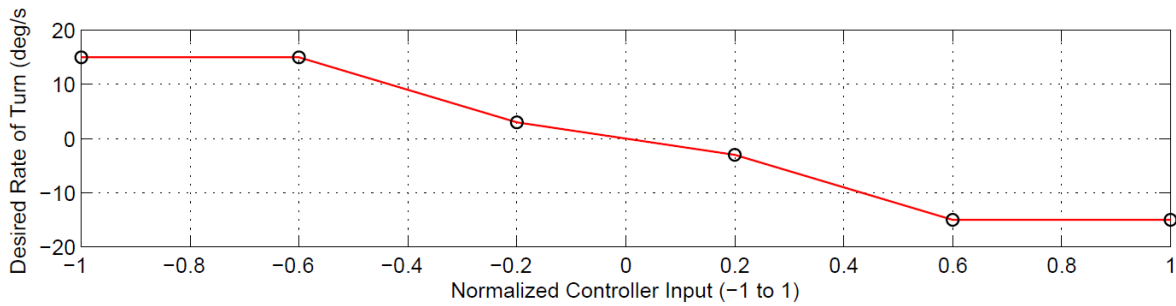
Figure 3.3: Ω - inceptor normalized input vs. desired rate of turn

The relationship between the inceptor input and Ω_{cmd}, shown in Figure 3.3, enables smaller heading adjustments limiting the tendency for a pilot to over-correct.
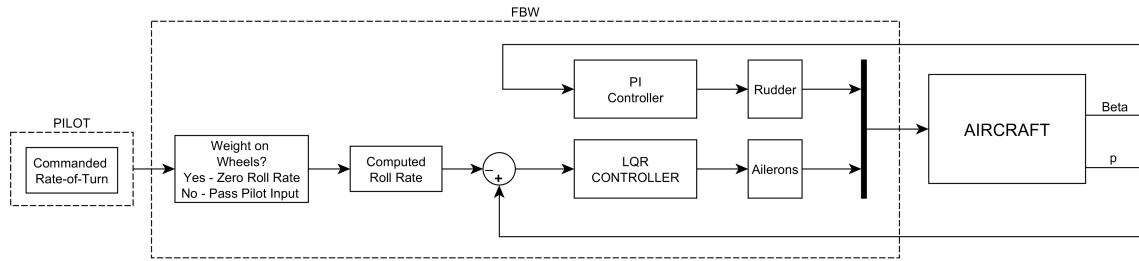
Figure 3.4: Top-level diagram illustrating carefree control of horizontal flight path for the takeoff mode

Larger deflections of the inceptor result in increasing rate-of-turn (RoT) commands up to the 15 deg/s limit.

The commanded rate-of-turn, Ω_{cmd}, is then used to determine the necessary roll angle, ϕ_{cmd}, based on the aircraft's true airspeed using the equation below,

$$\phi_{cmd} = \cos^{-1}\left(\frac{1}{\sqrt{\Omega_{cmd}^2 V_{TAS}^2/g^2 + \cos^2\gamma}}\right) = \tan^{-1}\left(\frac{\Omega_{cmd}V_{TAS}}{g}\right) \qquad (3.16)$$

The difference between ϕ_{cmd} and the current roll angle, ϕ, determines the commanded roll rate, p_{cmd}, as shown below:

$$p_{cmd}(deg/s) = \begin{cases} K_{roll}(\phi_{cmd} - \phi) & for\ 0 < |\phi_{cmd} - \phi| \le 5° \\ 7°/s & for \qquad |\phi_{cmd} - \phi| > 5° \\ 0 & for\ \ \text{Wheels on Ground} \end{cases}$$

A p_{cmd} of zero is demanded while the aircraft wheels are in contact with the ground.

The problem of tracking the commanded roll rate here is identical in nature to the regulator problem posed for $\dot{h}$-q control. Therefore, to drive the error between the current roll rate, p, and the commanded value, p_{cmd}, the following state and control vectors are formed,

$$
x(t) = \begin{Bmatrix} u \\ v \\ w \\ \phi \\ \theta \\ p_e \\ q \\ r \end{Bmatrix} \quad \& \quad \delta(t) = \begin{Bmatrix} \delta_a \end{Bmatrix}
\tag{3.17}
$$

where p_e is the error between p_{cmd} and p.

The design input diagonal Q matrix to penalize the states is shown below. Heavier penalties on θ and ϕ ensured coordinated flight and a benign system response to sharp or aggressive Ω - inceptor inputs.

$$\mathbf{Q} = \begin{bmatrix} 1.7 & 0 & 0 & 0 & 0 & 0 & 0 & 0 & 0 \\ 0 & 1.7 & 0 & 0 & 0 & 0 & 0 & 0 & 0 \\ 0 & 0 & 1.7 & 0 & 0 & 0 & 0 & 0 & 0 \\ 0 & 0 & 0 & 13.26 & 0 & 0 & 0 & 0 & 0 \\ 0 & 0 & 0 & 0 & 13.09 & 0 & 0 & 0 & 0 \\ 0 & 0 & 0 & 0 & 0 & 1.7 & 0 & 0 & 0 \\ 0 & 0 & 0 & 0 & 0 & 0 & 1.7 & 0 & 0 \\ 0 & 0 & 0 & 0 & 0 & 0 & 0 & 1.7 & 0 \\ 0 & 0 & 0 & 0 & 0 & 0 & 0 & 0 & 28.475 \end{bmatrix} \tag{3.18}$$

The control weighting matrix, R, is only a function of aileron control,

$$\mathbf{R} = \begin{bmatrix} 52620 \end{bmatrix} \tag{3.19}$$

The final control gain matrix, K, is

$$K = \begin{bmatrix} 6.7982 \text{x} 10^{-4} & -0.0015 & -0.0019 & -0.0799 & 0.6378 & -2.7828 & 0.0818 & -0.0198 \end{bmatrix}$$

The rudder was separated from the LQR implementation and instead, was driven by a Proportional-Integral controller (PI) to maintain a zero sideslip angle, β. The controller can be represented in the Laplacian domain as

$$P + I\frac{1}{s} = \frac{P}{s}(s + \frac{I}{P}) \tag{3.20}$$

where the Simulink PID tuning utility was used to limit overshoot such that the final gains were determined to be $P = -5.7$ and $I = -0.532$.

3.2.2 Climb/Descend Modes (Modes 2 & 5)

Logic almost identical to Mode 1 drives the climb and descend modes affording the pilot to maintain a fixed rate-of-climb (or descent), $\dot{h}_{base}$, once engaged. If required the pilot can increase or decrease that fixed rate through manipulation of the right pedal inceptor and left pedal inceptor, respectively. Turning flight, to change horizontal flight path, can also be performed in these modes without adding to pilot workload beyond the steering of the $\Omega - inceptor$.

Figure 3.5 provides a top-level description of the longitudinal climb/descend control portion of modes 2 and 5.
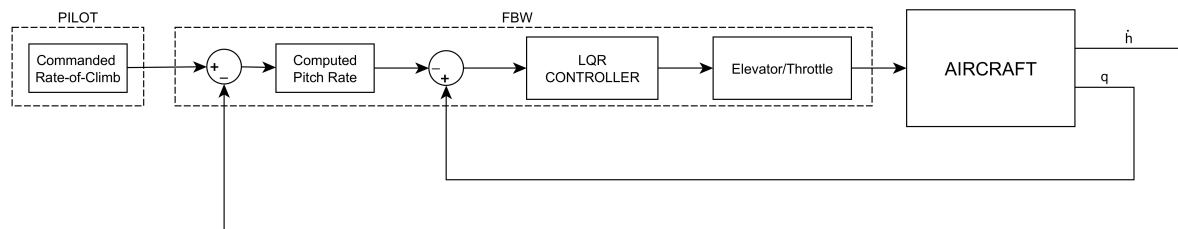
Figure 3.5: Block diagram illustrating rate-of-climb/descent logic for the climb and descend modes

$\dot{h}$-q Control Law and the Positive/Negative Rate Inceptors (for Modes 2 & 5)

Unlike the takeoff mode described previously, which implemented direct throttle control through the right pedal inceptor, deflection of the δ_{+R} or δ_{-R} inceptor by the pilot manipulates the rate-of-climb/descent via the following relationship,

$$\dot{h}_{cmd} = \dot{h}_{base} + k_1\delta_{+R} - (k_2\delta_{-R} + k_2)ft/s \qquad (3.21)$$

where k_1 and k_2 are scaling terms to translate the normalized pedal input values to $\dot{h}$ terms. The expression within parentheses represents the left pedal inceptor's lookup table. The constant bias term allows for the lookup table to output zero when δ_{-R} is zero.

With this relationship in hand, the piecewise function shown below relates the desired rate-of-climb to a commanded pitch rate, q_{cmd},

$$q_{cmd}(deg/s) = \begin{cases} K_q|\dot{h}_{cmd} - \dot{h}| & for \ 0 < |\dot{h}_{cmd} - \dot{h}| \leq 1.25 ft/s \\ 10°/s & for |\dot{h}_{cmd} - \dot{h}| > 1.25 ft/s \end{cases}$$

As is described in the previous section, the $\dot{h}$-q control law relates a commanded $\dot{h}$ to a proportional pitch rate, q_{cmd}. The LQR controller implemented contains δ_{th} as an additional control term. As a result, the control vector is now,

$$\delta(t) = \begin{Bmatrix} \delta_e \\ \delta_{th} \end{Bmatrix}$$

with the chosen Q and R matrices (see below),

$$\mathbf{Q} = \begin{bmatrix} 3.73\text{x}10^{-7} & 0 & 0 & 0 & 0 \\ 0 & 0.0037 & 0 & 0 & 0 \\ 0 & 0 & 2.611\text{x}10^{-4} & 0 & 0 \\ 0 & 0 & 0 & 3.73\text{x}10^{-7} & 0 \\ 0 & 0 & 0 & 0 & 66021 \end{bmatrix} \tag{3.22}$$

where the state order is $\mathbf{x} = \begin{bmatrix} u & w & \theta & q_e & \dot{h} \end{bmatrix}^T$. The control order for the R matrix below is $\delta = \begin{bmatrix} \delta_e & \delta_{th} \end{bmatrix}$,

$$\mathbf{R} = \begin{bmatrix} 7.479\text{x}10^9 & 0 \\ 0 & 193.9 \end{bmatrix} \tag{3.23}$$

and the positive definite solution of the Ricatti equation yields the same control command as shown in the previous section,

$$\delta = -Kx \tag{3.24}$$

or,

$$\delta = \begin{Bmatrix} \delta_e \\ \delta_t \end{Bmatrix} = -K \begin{Bmatrix} \dot{h} \\ u \\ w \\ \theta \\ q_e \end{Bmatrix} \tag{3.25}$$

where, K, the control gain matrix for the elevator and throttle is,

$$K = \begin{bmatrix} -0.1982 & -0.0099 & 0.0648 & -31.2569 & -3.7572 \\ \\ 0.0191 & 0.1317 & -0.0089 & 1.9085 & 0.0336 \end{bmatrix} \quad (3.26)$$

Ω - *Inceptor for Direct Horizontal Flight Path Control*

With the climb or descend modes being enabled in-flight, the control logic no longer requires the presence of the 'weight on wheels' condition and can be removed. As a result, the $\Omega - inceptor$ simply continues to provide the pilot the ability to change the aircraft's horizontal flight path. Carefree flight is again made possible in these modes. Figure 3.6 reiterates the top-level structure of this control law.
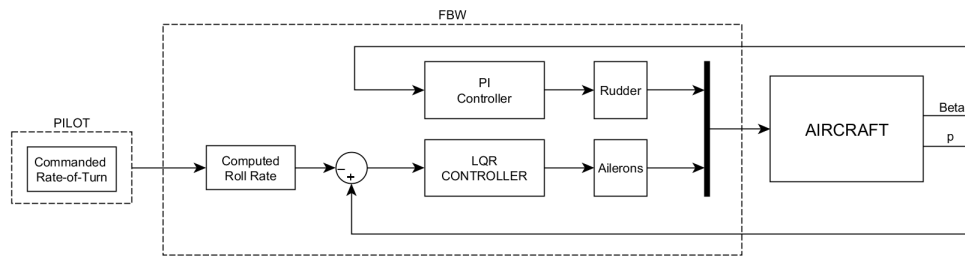
Figure 3.6: Top-level diagram illustrating carefree control of horizontal flight path for all modes.

In contrast to the takeoff mode, the commanded bank angle is limited to 20° after a predefined $\dot{h}$ of 300 ft/min is exceeded. Below this climb rate, bank angles of up to 30° are permitted allowing for smaller radius turns.

$$\phi_{cmd} = \begin{cases} 20° & for \ \dot{h} > 300 ft/min \ \text{(Climb Mode only)} \\ 30° & for \ \dot{h} < 300 ft/min \ \text{(Climb Mode only)} \\ 45° & for \ \forall \dot{h} \ \ \text{(Descend Mode only)} \end{cases}$$

As before, the difference between ϕ_{cmd} and the current roll angle, ϕ, determines the commanded roll rate, p_{cmd}, as shown below,

$$p_{cmd} = \begin{cases} K_{roll}(\phi_{cmd} - \phi)\pi & for \ 0 < |\phi_{cmd} - \phi| \le 5° \\ 7°/s & for \ \ \ |\phi_{cmd} - \phi| > 5° \end{cases}$$

The problem of tracking the commanded roll rate here is identical to the regulator problem described in Section 3.2.1 and the same LQR and PI controllers have been implemented. Therefore, the P and I gains remain the same and no further discussion is required regarding these modes.

3.2.3 Low/High-Speed Cruise Modes (Modes 3 & 4)

Once engaged, the two cruise modes are designed to maintain altitude by ensuring a zero rate of climb while automatically commanding a baseline MAP of 22.4 inHg or 65% power (75% power in the case of Mode 4) and an engine speed of 2400 RPM without the need for pilot input. The pilot is free to change the aircraft's horizontal flight path via the Ω-inceptor without compensating for variation in altitude. Further control augmentation is achieved via a simple sideslip-to-rudder feedback which prevents undesirable flight characteristics such as adverse yaw and Dutch roll by ensuring coordinated flight.

Altitude Hold

The control logic of the altitude hold function serves two scenarios, valid only when the Cruise modes are engaged.

1. The aircraft transitions to either of the two cruise modes from the takeoff or climb modes. If the absolute difference between the actual altitude, h, and the commanded altitude, h_{cmd},

$$\Delta h = |h - h_{cmd}| \tag{3.27}$$

is *smaller than* an upper threshold, Δh_{max}, and *greater than* zero, then the following rate of descent is commanded:

$$\dot{h}_{cmd} = -K_{\dot{h}}\Delta h \tag{3.28}$$

For the scenario where the value of Δh is *greater than* Δh_{max}, the following rate of descent is commanded:

$$\dot{h}_{cmd} = -300 \; ft/min \tag{3.29}$$

In short, the bounds for the altitude hold control logic are summarized as the piece-wise function shown below,

$$\dot{h}_{cmd} = \begin{cases} -K_{\dot{h}}\Delta h & for \; 0 < \Delta h \leq \Delta h_{max} \\ -300 ft/\min & for \; \Delta h > \Delta h_{max} \end{cases}$$
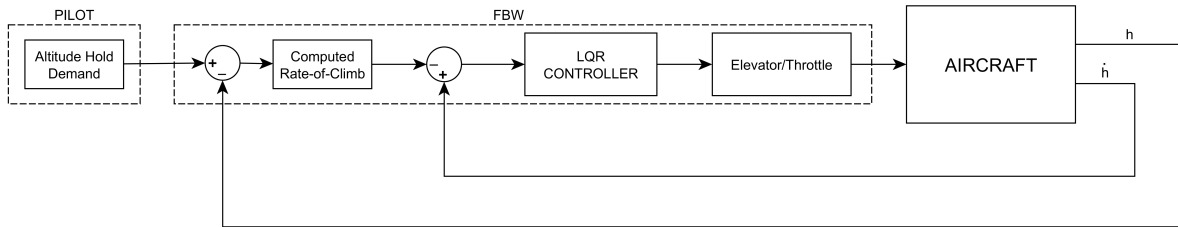
Figure 3.7: Block diagram illustrating the altitude hold function for the cruise modes.

2. The aircraft transitions to a cruise mode from either the descend or approach modes. This scenario of course, is the inverse of the control problem described in item 1. and can be summarized as follows,

$$
\dot{h}_{cmd} =
\begin{cases}
-K_{\dot{h}}(-\Delta h) & for\ 0 < \Delta h \le \Delta h_{max} \\
\\
300\,ft/\min & for\ \Delta h > \Delta h_{max}
\end{cases}
$$

Throttle Control

Working in conjunction with the altitude hold control law described in the previous section, the throttle control law enables the pilot to use the right or left pedal inceptors $(\delta_{+R}, \delta_{-R})$ to increase or decrease the aircraft's manifold air pressure from a nominal predefined power setting, P_{base}. As a result, the pilot has the ability to increase or decrease airspeed without compensating for a change in altitude.

$$
\delta_{th_{cmd}} = P_{base} + 1.6\delta_{+R} - (2\delta_{-R} + 2)\ \ \text{inHg of MAP} \tag{3.30}
$$
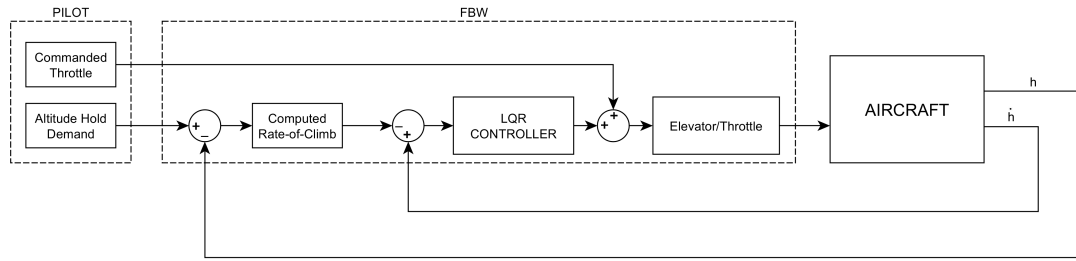
Figure 3.8: Block diagram illustrating the throttle control functionality coupled with the altitude hold law (cruise modes only).
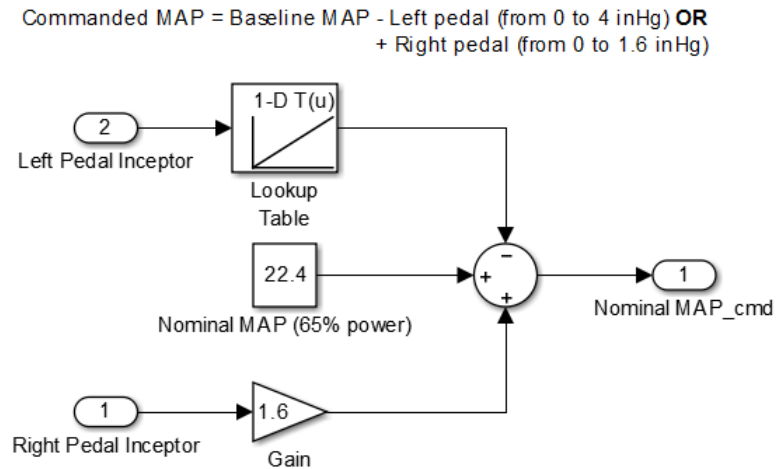
Figure 3.9: Simulink block diagram of the throttle/MAP control logic.

The equation above provides a total commanded throttle (MAP value) with a baseline power setting, P_{base}, of 65% (MAP of 22.4 inHg) for Mode 3. Figure 3.9 illustrates the implemented throttle control in Simulink. Both the positive and negative rate controllers allow the pilot to regulate the power above and below the 65% nominal setting. See Table 3.1 below.

Table 3.1: Throttle control in cruise mode.

Controller	Output
No control input	P_{base}, Baseline 22.4 inHg
Right pedal inceptor, δ_{+R}	Increase MAP from 22.4 to 24 inHg
Left pedal inceptor, δ_{-R}	Decrease MAP from 22.4 to 18.4 inHg

3.2.4 Landing Approach Mode (Mode 6)

When the pilot has lined up for final approach and is flying through the center of the highway-in-the-sky visual projection, enabling Mode 6 guarantees a 3 degree glide slope down to the runway. If the pilot visualizes being short of this mark, i.e. has fallen below the HITS projection; then pressing the left pedal inceptor will 'lift' the aircraft trajectory to assist the pilot in maneuvering back into the virtual highway. Upon re-entry into the glide slope tunnel, the pilot can release the inceptor. The opposite effect can be achieved by the right pedal inceptor if the pilot will overshoot the target.

$\dot{h}$-**q** Control Law for Glide Slope Control

A simple modification of the same $\dot{h}$-q control law implemented in modes 1, 2 and 5 allows the aircraft to demand a rate-of-climb and in turn an appropriate pitch rate, q, to track a glide slope. The right and left pedal inceptors can directly adjust the

aircraft flight path angle to be centered within the glide slope. Equation (3.31) below relates the commanded rate-of-climb to the glide slope.

$$\dot{h}_{cmd} = V_{gnd} \ tan\gamma \ (ft/s) \tag{3.31}$$

where

$$\gamma = \gamma_{ref} + (k_3\delta_{-R} + k_3) - k_4\delta_{+R} \ \text{(degrees)} \tag{3.32}$$

and, $\gamma_{ref} = -3$ (predefined flight path angle).k_3 and k_4 are scaling terms to translate the normalized pedal input values to γ terms.

As can be seen above, both inceptors play the role of manipulating the glide slope to realize a new rate of climb and as a result, a new commanded pitch rate. The same LQR controller and gains implemented for modes 1,2, and 5 can be used.

3.3   Experiment

The goal of the experiment was to determine if the control concept assisted non-pilots in achieving performance comparable to trained pilots. Eighteen subjects participated in the experiment - 9 pilots (XP) and 9 non-pilots (NP). See Tables 3.2 and 3.3 for subject specifics.

Table 3.2: Pilot participants

Subject	Age	Hours
Pilot#1	27	100
Pilot#2	34	232
Pilot#3	18	22
Pilot#4	21	260
Pilot#5	20	20
Pilot#6	22	420
Pilot#7	23	500
Pilot#8	25	270
Pilot#9	36	165

Table 3.3: Non-pilot participants

Subject	Age
Non-Pilot#1	24
Non-Pilot#2	50
Non-Pilot#3	22
Non-Pilot#4	51
Non-Pilot#5	15
Non-Pilot#6	40
Non-Pilot#7	69
Non-Pilot#8	51
Non-Pilot#9	47

3.3.1 Procedure

After a 10-minute presentation, each subject flew the same set of three unique scenarios with the goal of using the available controls to remain centered in the HITS boxes.

The scenarios were designed as follows:

1. A 10 min 'pattern' flight which originated and ended at KSFO. The flight required the subject to climb to a reference altitude, complete the pattern which comprised of four 90 degree legs, and descend for the final approach to land.

2. A 15 min flight from KSFO to KSQL. The subject was guided to two target altitudes; an initial climb to 1,000 ft followed by a climb to 1,500 ft. Major heading changes were only required during the cruise phase-of-flight. The scenario concluded with a final approach into KSQL.

3. A 20 min flight from KSFO to KOAK. This last scenario guided the subject to climb and maintain 1,500 and 2,000 ft. On descent, the subject was guided to four target altitudes, 1,700, 1,500, 1,100, and 600 ft, respectively, before having to initiate the final approach into KOAK. This scenario required 10 major heading changes during the climb, cruise and descent phases-of-flight. The flight concluded with a final approach into KOAK.
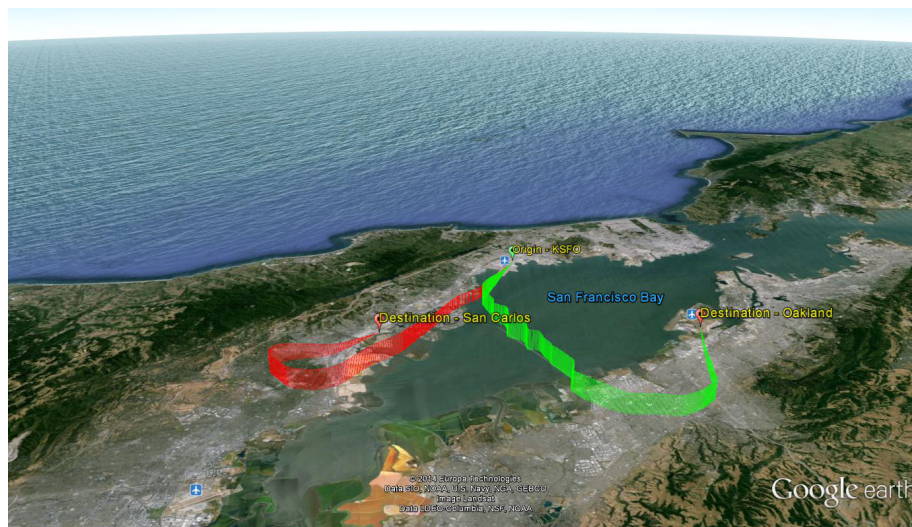
Figure 3.10: 3D view of Google Earth rendering of the KSFO - KSQL and KSFO - KOAK scenarios

Figure 3.11: Top view of Google Earth rendering of the KSFO - KSQL and KSFO - KOAK scenarios

3.3.2 Dependent Measures

The dependent measures were:

1. Path-tracking performance - subject path-tracking compared against the reference trajectory, and expressed as a normalized value.

2. Lateral control activity - the RMS of the subject's control input via the Ω-inceptor.

3. Lateral control activity - RMS and frequency input for maneuver slices taken from each scenario.

3.3.3 Data Reduction

Path-Tracking Performance: the k-nearest neighbors (k-NN) algorithm has been used to compute a normalized value for both lateral and 3D path-tracking performance of each participant.

The thresholds used for the Euclidean distance to determine whether the aircraft is in or out of a HITS box are,

- Threshold for lateral exit from HITS box = 25 m (82 ft) left or right of center.

- Threshold for vertical exit from HITS box = 12.5 m (41 ft) above or below center.

where each HITS box is 50 x 50 m (164 x 164 ft) in size.

RMS of Lateral Control Activity: The RMS, Eq.3.33 below, of lateral control activity, i.e. the Ω-inceptor input, provides a simple statistical measure of the average input magnitude during each scenario.

$$\delta_{RMS} = (\frac{1}{N}\sum_{n=1}^{N}|\delta_n|^2)^{\frac{1}{2}} \tag{3.33}$$

where δ_n is the n-th sample value.

Additionally, the standard deviation is computed to provide a measure of data consistency across each group.

Magnitude Spectrum of Lateral Control Activity: Applying the Fast Fourier Transform (FFT) to the control activity quantifies participant control input magnitude as a function of frequency. The results from this are compared to a typical handling qualities metric. See Table 3.4.

Table 3.4: Typical control input frequency ranges (Field & Giese, 2005)

Frequency Range	Description
0.25 - 0.8 rad/s	Typical open-loop control associated with trimming and flight path modulation.
0.80 - 2.0 rad/s	Typical closed-loop control associated with transport aircraft maneuvering.
2.0 - 4.0 rad/s	Higher-gain closed-loop control associated with increased task urgency or handling issues with the aircraft, such as a PIO.
4.0 - 10.0 rad/s	Very high-gain closed-loop control, almost certainly associated with control difficulties.

This chapter has detailed the control law logic and its functional modes. Furthermore, the design of the experiment has been described along with the methods used to analyze data retrieved from participant flights.

The following chapter presents the results and analysis from experimental data.

4. Results and Analysis

This chapter presents results from the experiment and provides a qualitative assessment of participant performance.

4.1 Averaged Results from Scenarios

The following plots show tracking performance and the RMS of control input for the average pilot and non-pilot across all three scenarios.

Plots in Figures 4.1 and 4.2 both indicate a trend of improving path-tracking performance for the non-pilot group.

Unexpectedly, the pilot group's performance decreases with the non-pilots outperforming them (on average) in scenarios 2 and 3. However, with the standard deviation being considerably high in both groups, an explanation isn't readily available. A possible cause for degraded pilot performance could be attributed to boredom with the assigned tasks.

Control activity presented in Figure 4.3 shows small control input activity across the pilot group with relatively high consistency.

Non-pilot control activity values suggest the participants are gaining familiarity with the Ω-inceptor as their average input drops 10-20% across the scenarios. Here

too, a significant standard deviation limits the scope of drawing any meaningful conclusions.

Furthermore, the comparison of control activity across scenarios can not be precise simply because each scenario is different. Although the difficulty of the tracking task is intended to increase as the participant progresses from one scenario to the next, the increasing flight duration can add significant periods of limited activity which would drive down the mean RMS value.
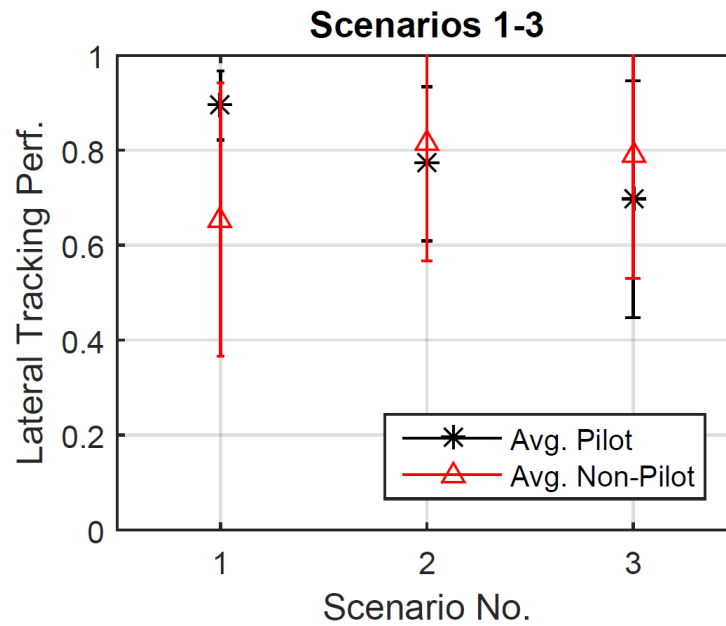
Figure 4.1: Tracking performance across scenarios
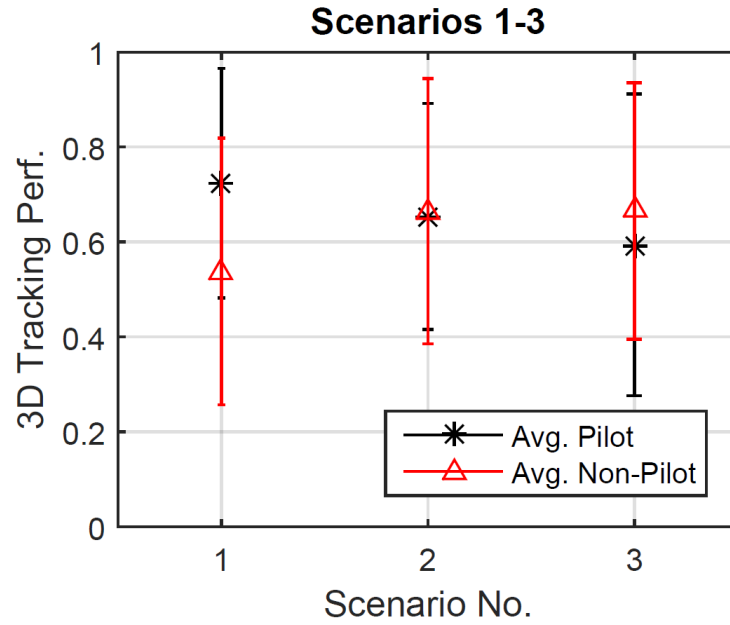
Figure 4.2: Lateral tracking performance across scenarios
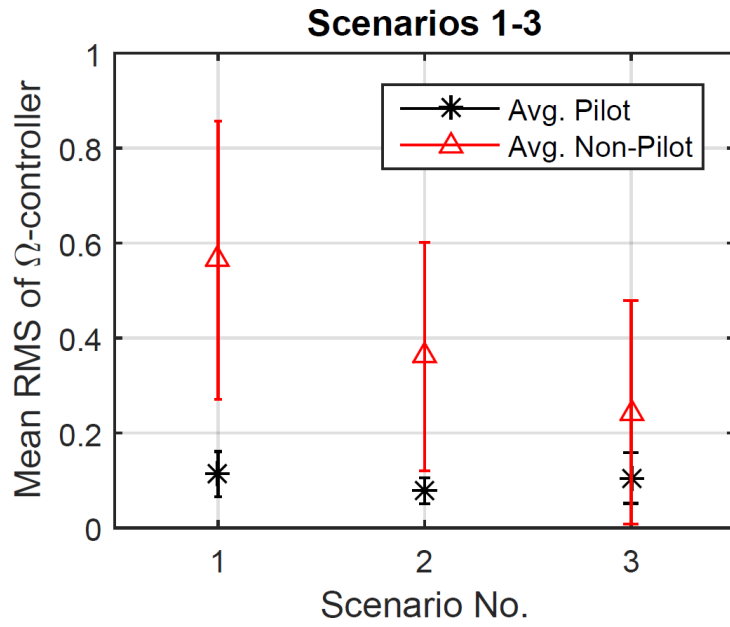
Figure 4.3: Control activity across scenarios

Observing a sample individual pilot across each scenario raises a question about pilot attention and or boredom. The following pilot was chosen based on an average performance in the first scenario within the pilot group. The pilot's performance in the subsequent scenarios is shown in Figures 4.5 and 4.6. The pilot's tracking performance increasingly dips below the group average from Scenario 2 to 3. This pilot starts out as an average performer but ends the experiment performing 25-27% below the pilot group average.
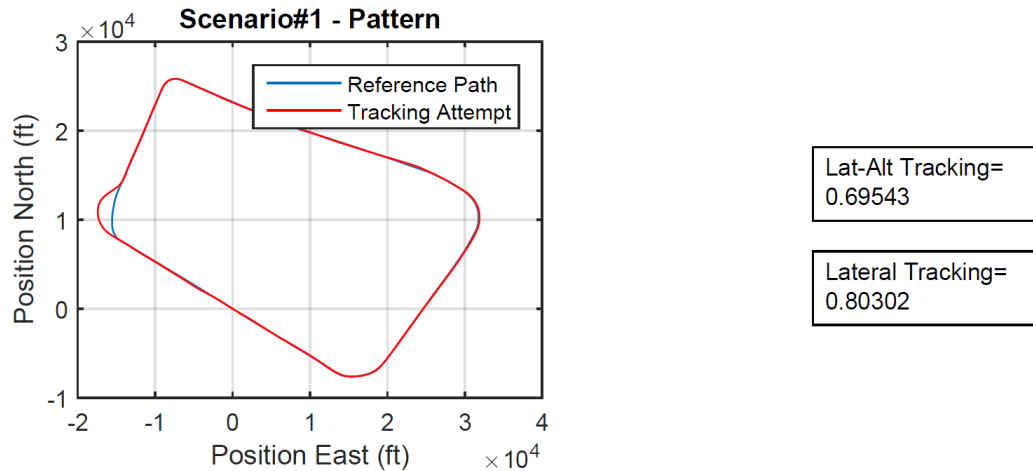
Figure 4.4: Pilot XP-7 - Tracking performance in Scenario 1
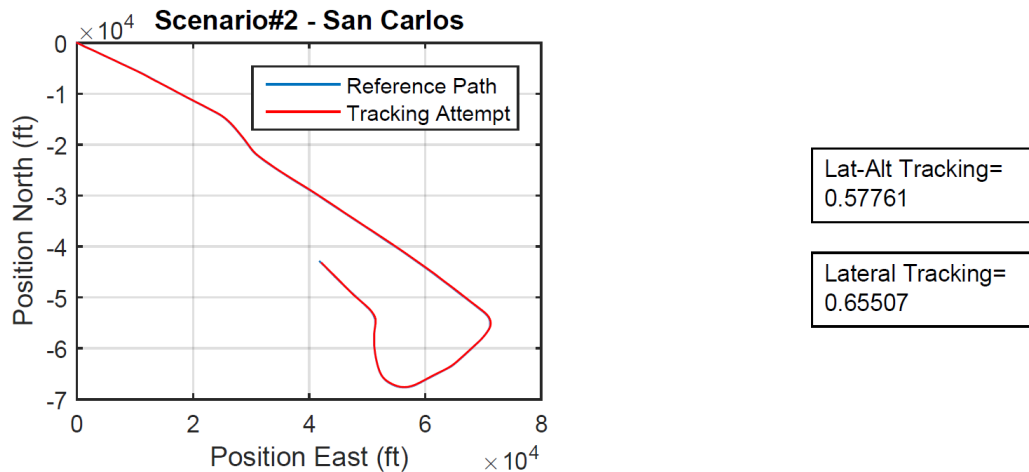
Figure 4.5: Pilot XP-7 - Tracking performance in Scenario 2
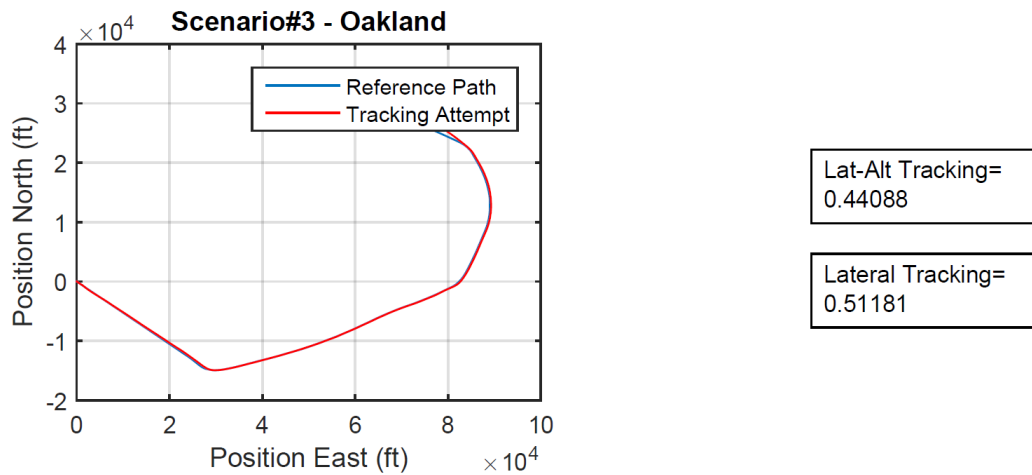
Figure 4.6: Pilot XP-7 - Tracking performance in Scenario 3

Applying the same selection criteria used to sample a pilot, a sample non-pilot has been selected. The performance across scenarios is presented in Figures 4.7, 4.8 and 4.9 below.
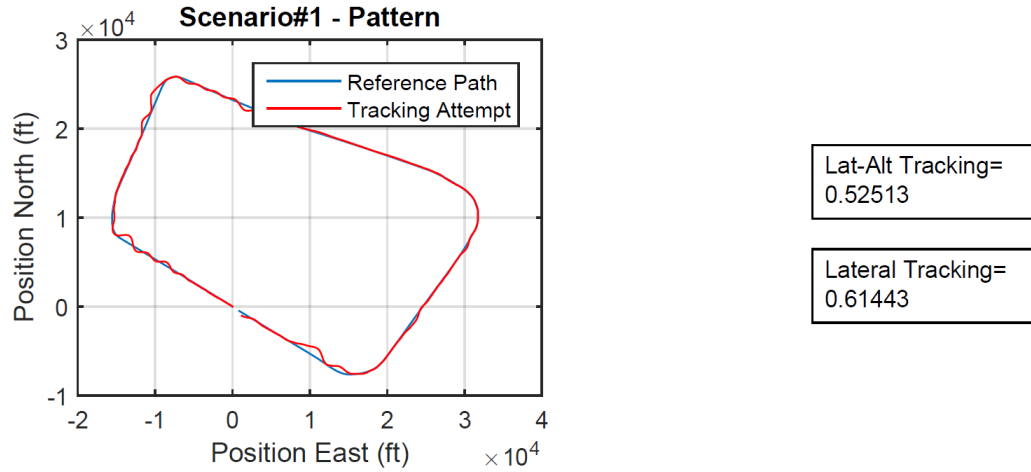
Figure 4.7: Pilot NP-9 - Tracking performance in Scenario 1
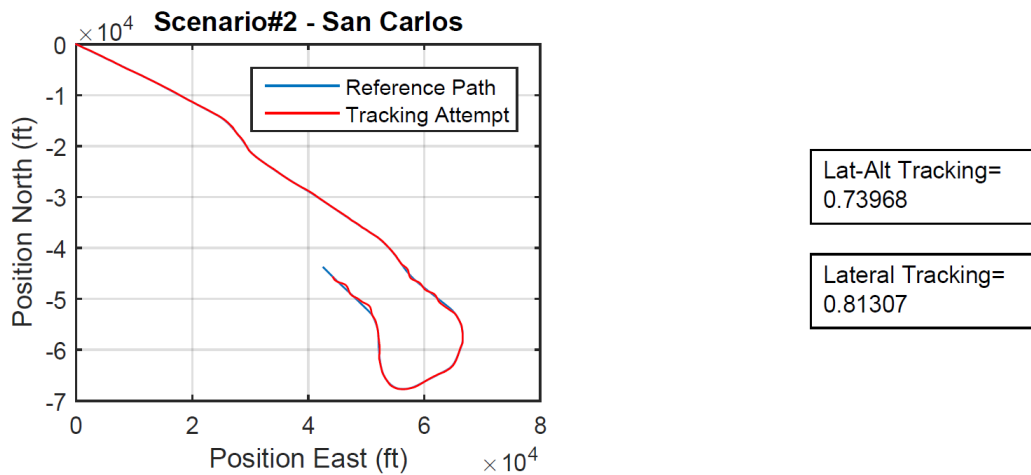
Figure 4.8: Pilot NP-9 - Tracking performance in Scenario 2
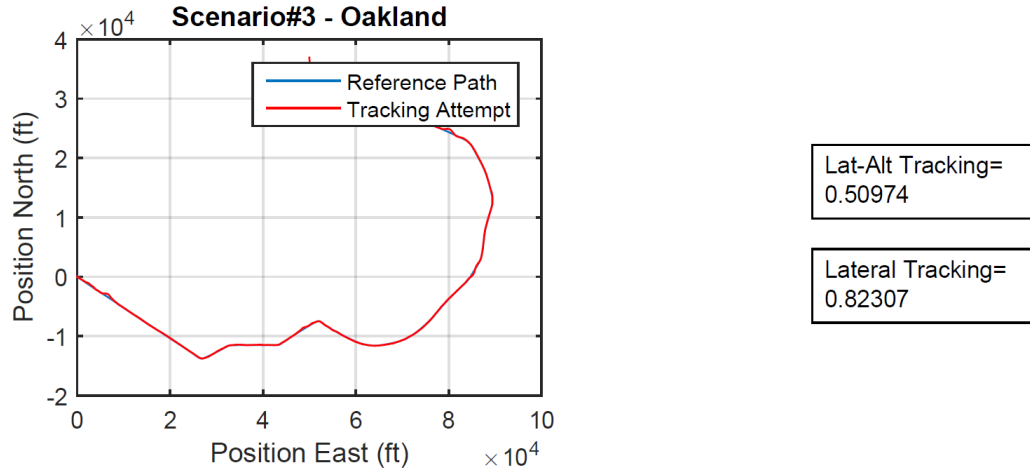
Figure 4.9: Pilot NP-9 - Tracking performance in Scenario 3

The non-pilot's performance remains average to above average in Scenario 2 for both lateral and 3D tracking. Scenario 3 sees the subject maintaining above average lateral tracking performance however, performance suffers in 3D tracking.

4.2   Averaged Results from Maneuver Cuts

Analyzing entire scenario flights can hide details associated with the entry into maneuvers required by a flight path change in the course.

To address this limitation, a turning maneuver, between 30-60 seconds, was selected from each scenario in an attempt to better understand control activity between both groups.

Figures 4.10 and 4.11 below provide the Ω-inceptor mean RMS, and the dominant frequency for each maneuver, respectively.
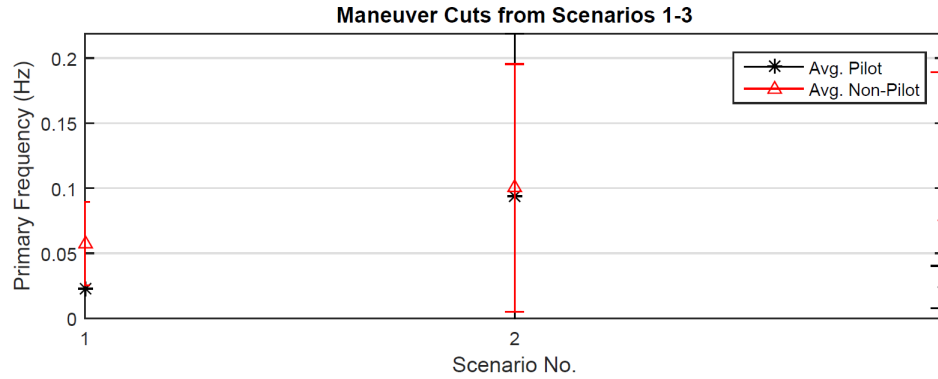
Figure 4.10: Average input frequency from maneuver cuts
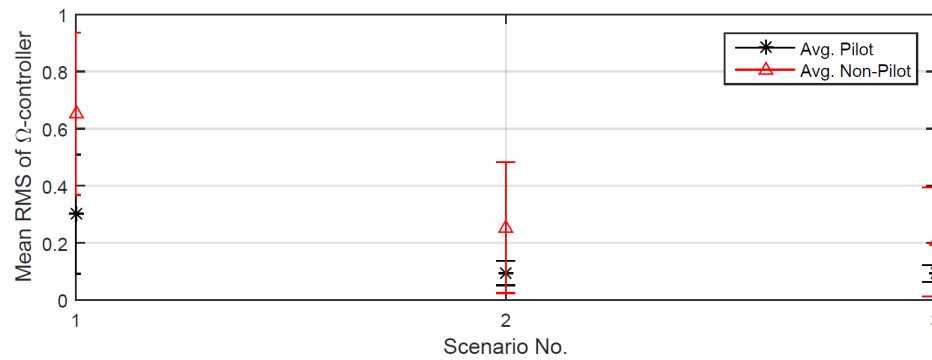
Figure 4.11: Mean RMS of Ω - inceptor from maneuver cuts

The first maneuver, from Scenario 1, happens to be the first major heading change of the experiment. The pilot group inputs smaller control deflections than the non-pilot group; however, a significant standard deviation value could imply differing control strategies employed by each pilot as they execute the turn. The dominant input frequency, however, doesn't vary among the pilots, possibly indicating their familiarity with typical aircraft response to control inputs.

The non-pilots make larger control inputs at a higher average frequency. However, the input frequencies are well within typical open-loop maneuvering per Table 3.4.

The second maneuver (Scenario 2) has the pilot group making consistent inceptor deflections yet differing greatly as far input frequency is concerned. This too could be indicative of control strategy differences as some pilots may opt to correct continuously while others make delayed corrections at higher rates.

The non-pilots show significant reduction in inceptor deflection. This could be attributable to their increased familiarity with the system.

The third and final maneuver sees the pilots maintaining consistent inceptor deflections and input frequencies. This maneuver presents the participant with a sharper turn that straightens out relatively quickly. The pilot group acts consistently, almost identically, in anticipating and executing the turn.

Although more challenging than the previous two maneuvers, the non-pilots manage a smaller inceptor deflection on average but show considerable variation when modulating the Ω-inceptor.

Table 4.1 provides a summary of pilot and non-pilot input frequencies during maneuvers across all three scenarios.

Table 4.1: Pilot and non-pilot control input frequency summary

		Frequency (Hz)	Frequency (rad/s)
Scenario 1	Pilots	0.0225	0.1420
	Non-Pilots	0.0574	0.3608
Scenario 2	Pilots	0.0943	0.5925
	Non-Pilots	0.1002	0.6299
Scenario 3	Pilots	0.0240	0.1510
	Non-Pilots	0.0779	0.4893

The decreasing trend in inceptor deflection by the non-pilots indicates their increased familiarity with the aircraft's response to their inputs. It can be observed that they limit turning the Ω-inceptor beyond 8-9 deg/s commanded RoT.

Sample pilot data from the previous section is presented in Figures 4.12, 4.13 and 4.14 below. The subject's control activity is half of the average for the group in Scenario 1. See Figure 4.11. The low control activity continues to be below the average value for the pilot group in both Scenarios 2 and 3. The low control activity combined with decreasing path tracking performance probably points to pilot boredom or an acceptable level of deviation decided upon by the subject.
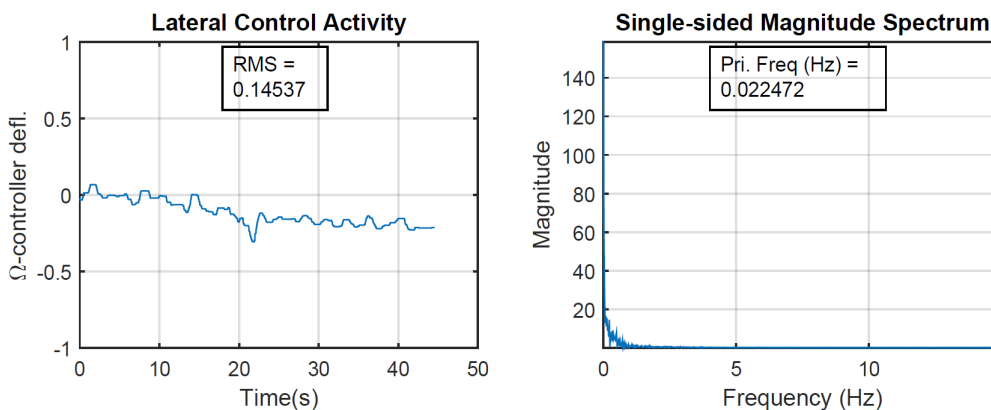
Figure 4.12: Pilot XP-7 - Lateral control activity for Scenario 1 maneuver
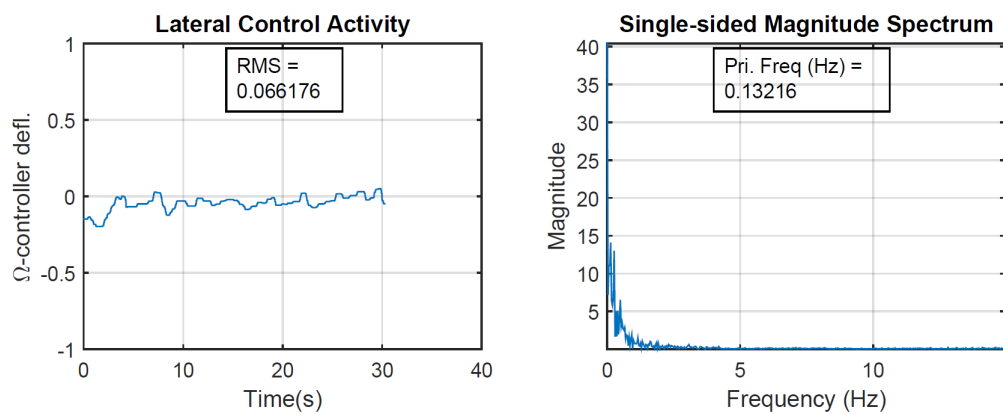
Figure 4.13: Pilot XP-7 - Lateral control activity for Scenario 2 maneuver
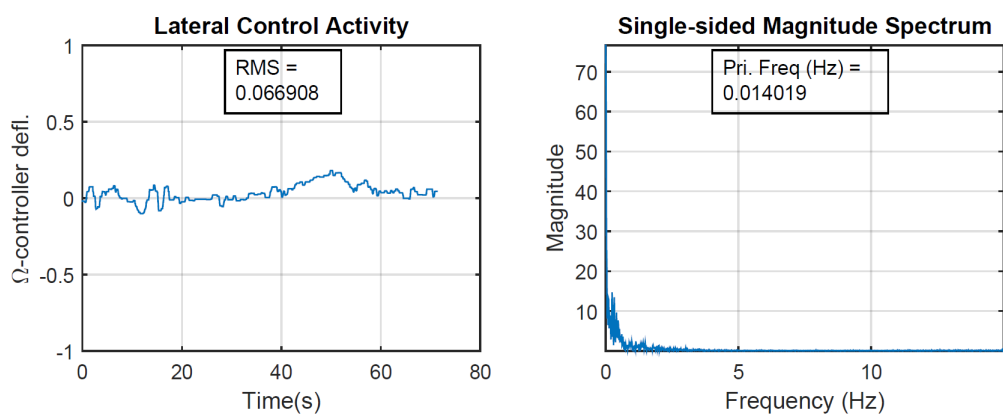
Figure 4.14: Pilot XP-7 - Lateral control activity for Scenario 3 maneuver

Sample non-pilot data from the previous section is presented in Figures 4.15, 4.16 and 4.17 below. Although demonstrating average path tracking performance in Scenario 1, the subject makes above average inputs to the Ω-inceptor with several maximum deflection inputs when negotiating the first 90 degree leg. Control activity across the remaining scenarios continues to decrease. By Scenario 3, the subject's control activity is average for the non-pilot group whereas the control input frequency value, although commensurate with the flying task, is above average when compared to the non-pilot group.
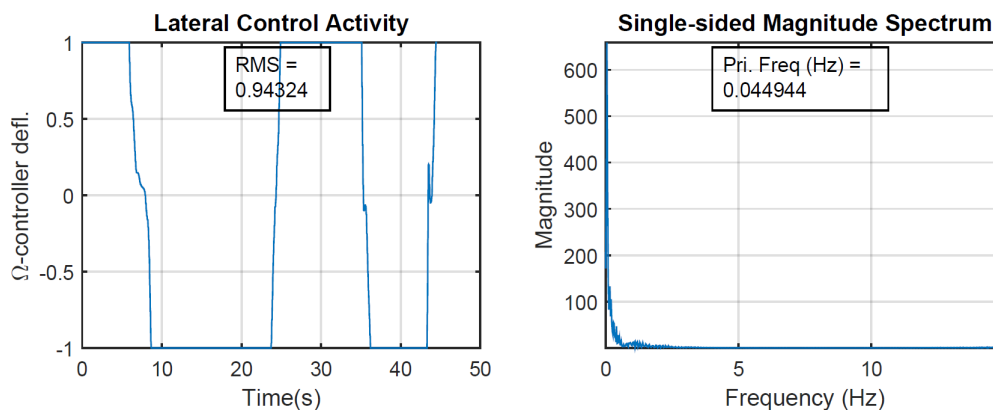
Figure 4.15: Non-pilot NP-9 - Lateral control activity for Scenario 1 maneuver
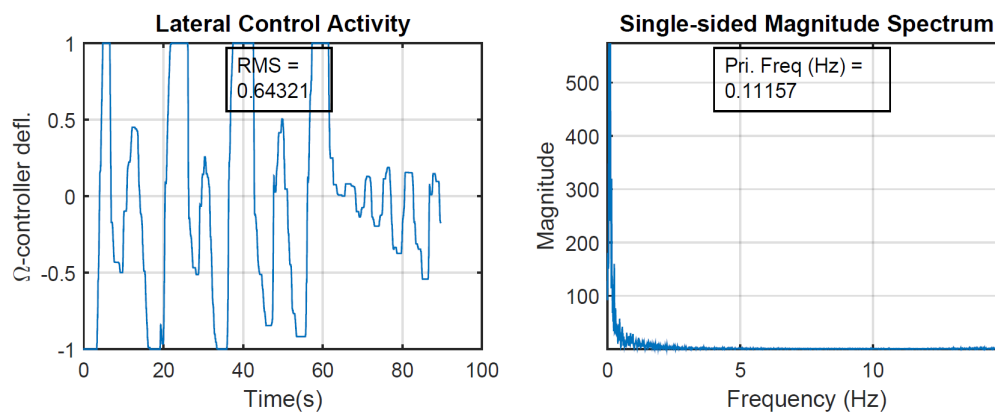
Figure 4.16: Non-pilot NP-9 - Lateral control activity for Scenario 2 maneuver
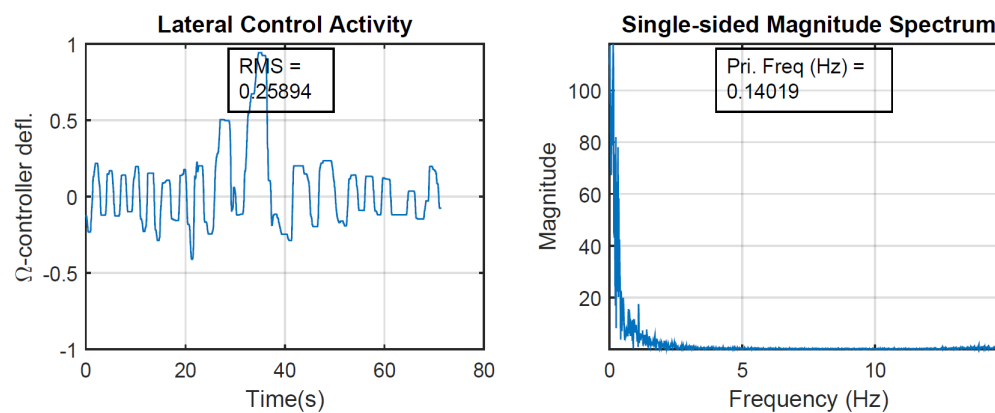
Figure 4.17: Non-pilot NP-9 - Lateral control activity for Scenario 3 maneuver

This chapter presented the results and observations from the experiment. The next chapter highlights the limits of this project and proposes improvements for future efforts.

5. Conclusion

This project set out to develop a simulator-based experiment to determine the potential in having automotive-inspired inceptors as a means to closing the gap between the non-pilot and the pilot. It was hypothesized that the non-pilot's familiarity with automotive controls could be leveraged to develop an interface which could enable the user to perform at a level comparable to a conventionally trained pilot. It should be noted that the level of performance desired for the non-pilot was limited to basic maneuvering tasks.

Both quantitative and qualitative data from the experiment suggest that non-pilots found the system challenging at first, mainly due to the Ω-inceptor's sensitivity. With continued exposure to the simulation, their performance tended to improve whilst their mean control activity decreased.

However, the evidence in support of the hypothesis is not without its limitations.

- The high values of the standard deviations for path-tracking performance and control activity suggest that the sample did not have adequate statistical power.

- That said, the computation of tracking performance depended on a fixed threshold for lateral and vertical deviation. Loosening up the threshold might have a significant impact on the spread of the standard deviation.

- Non-pilots flew the concept without flying the same aircraft model with conventional controls. Therefore, any potential improvement facilitated by the control concept goes untested against conventional controls and aircraft response - for the given simulator setup.

- Participants flew three different scenarios which complicates the task of determining performance changes for a given participant. Though care was taken to increase the number of tasks and their complexity with each scenario, large portions of the second and third path did involve straight and level flight.

- Any input lag to the OTW system was not characterized before the experiment was conducted. This could result in over-correcting the vertical or horizontal flight path.

6. Recommendations

6.1 Future Work

The experiment provided insight into how the control concept affected basic non-pilot performance. Several improvements, to the inceptors, control law logic, and experiment could be of value to the future development of this, or any other concept attempting to simplify flight.

- A larger sample of participants would be useful in providing greater statistical power.

- A more scientific approach to scenario creation for the experiment.

- The concept can be refined by using a formal control design methodology to develop the control law implementation.

- The display of a HITS is only one way of representing the flight path in simulation. Other, more subtle visual cues may reduce pilot workload.

- A more obvious difference between modes 3 and 4.

- Wavelet based technique to generate power vs. frequency vs. time plots. Such plots are a valuable bridge between the time and frequency domains.

- The presence of a control group using conventional aircraft controls. This would provide a baseline for comparative analysis.

- The completion of the auto-flare and touchdown control law functionality to provide an end-to-end simulator experience.

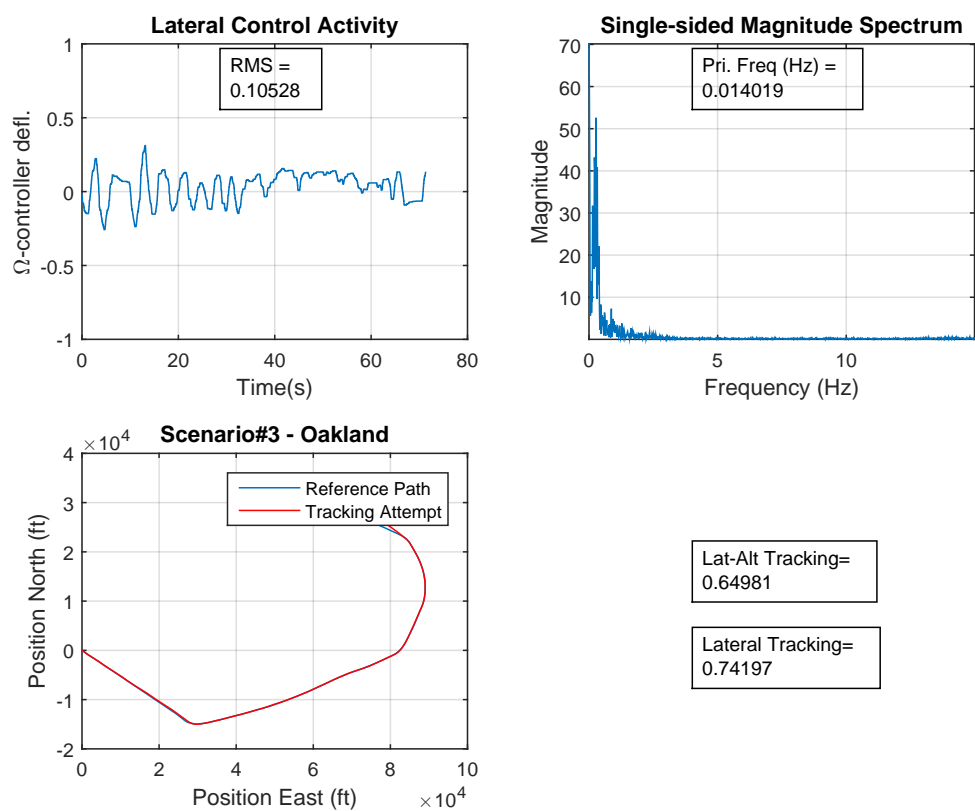# A. Experimental Results

A.1   Scenario 1 - Pattern (Pilots)
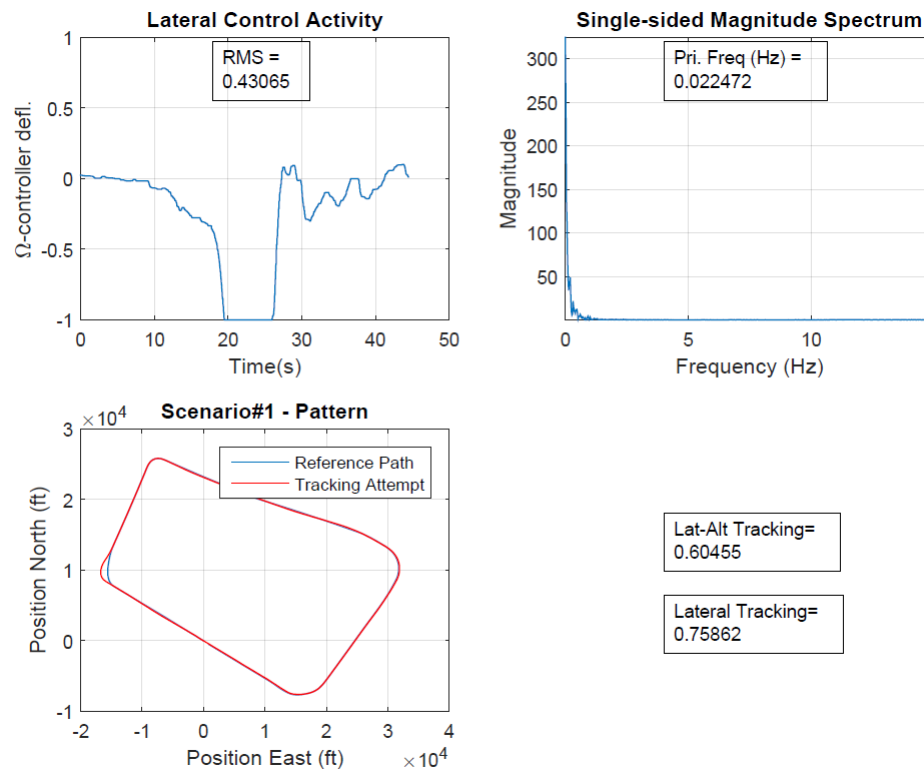
Figure A.1: Participant XP-1 Performance - Scenario 1
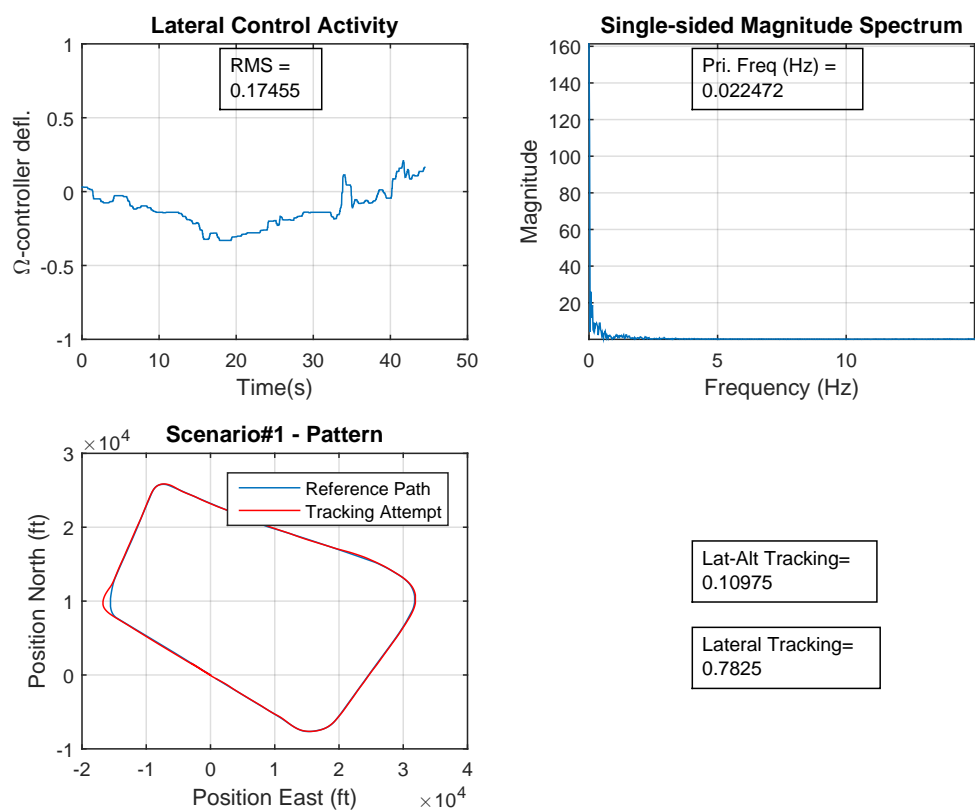
Figure A.2: Participant XP-2 Performance - Scenario 1
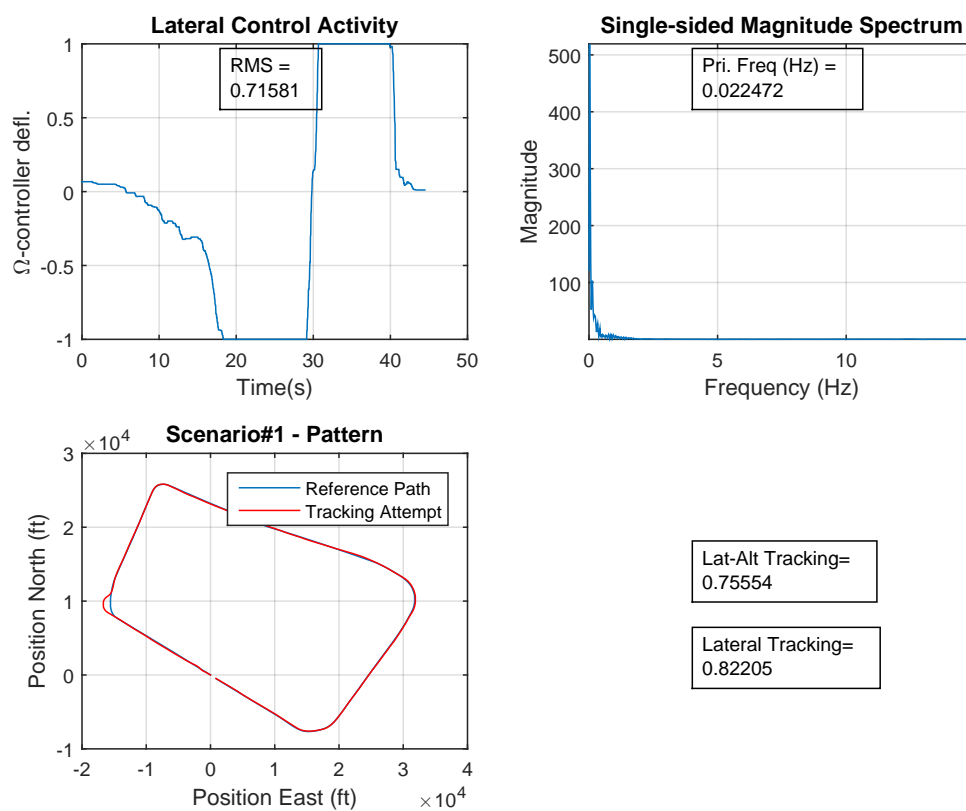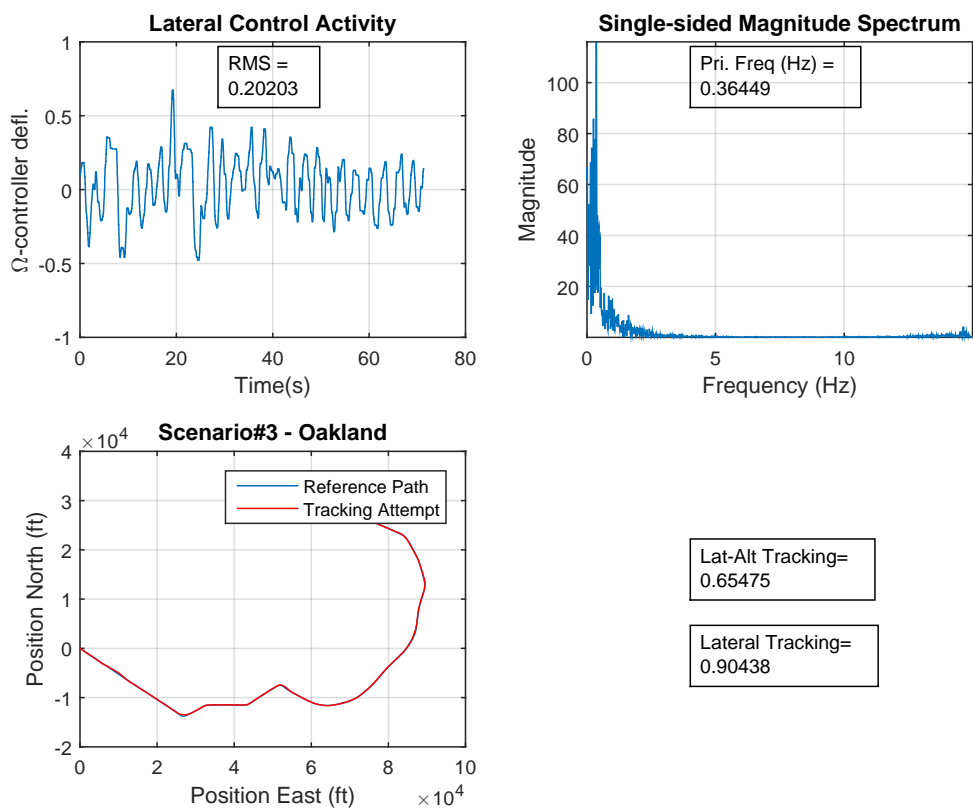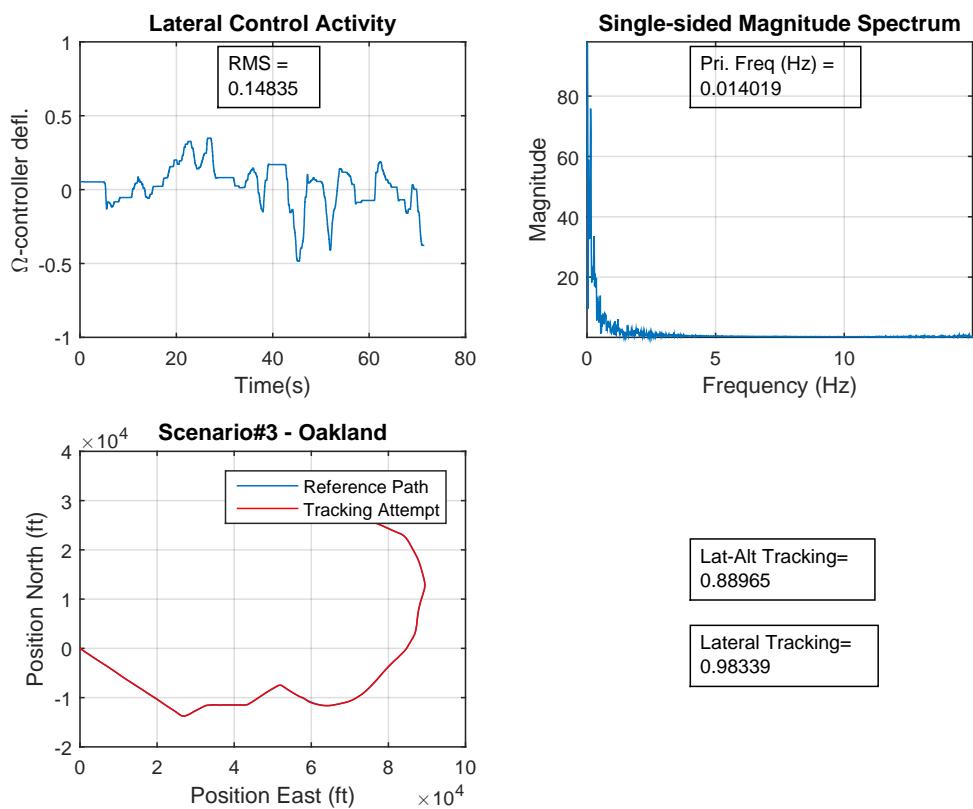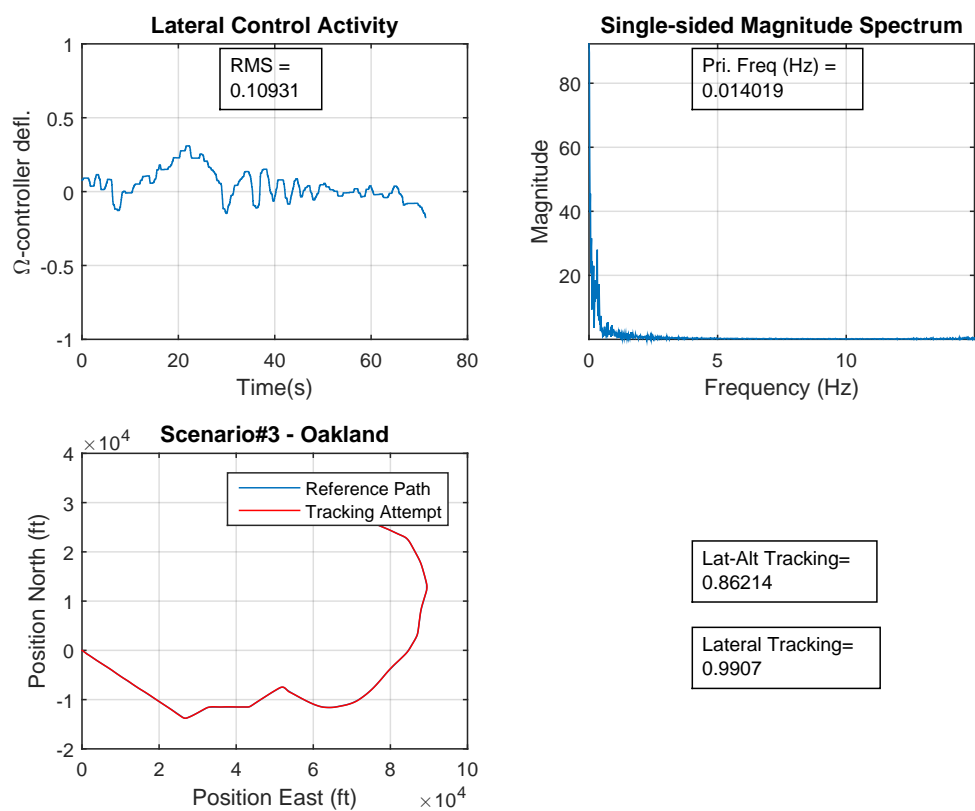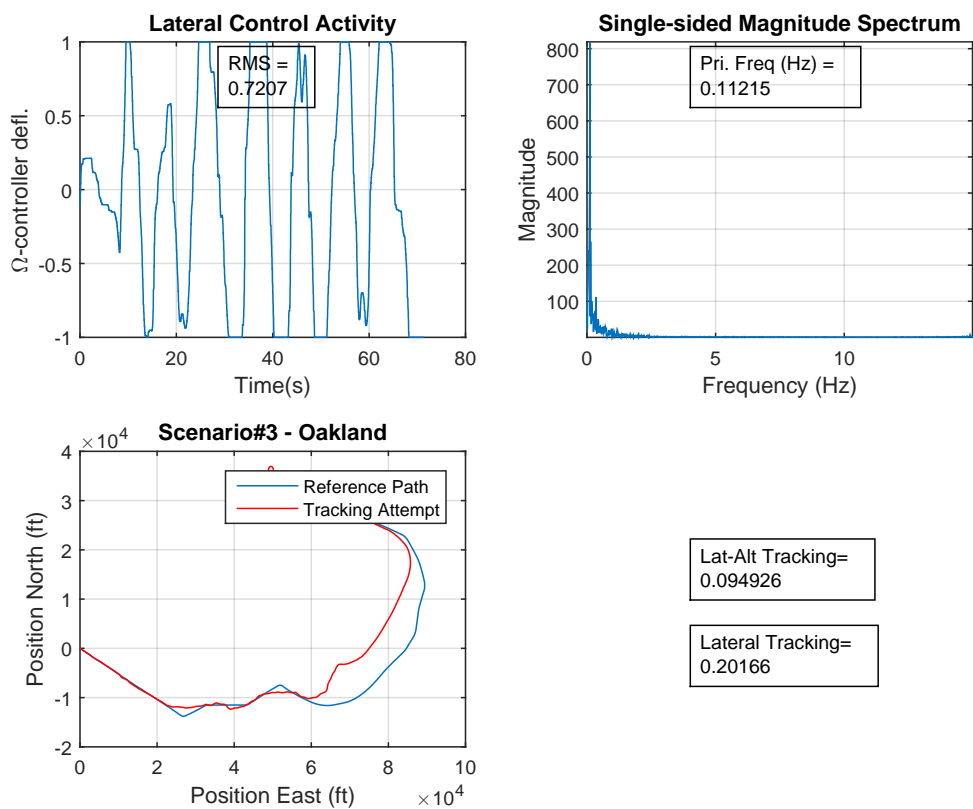
Figure A.3: Participant XP-3 Performance - Scenario 1
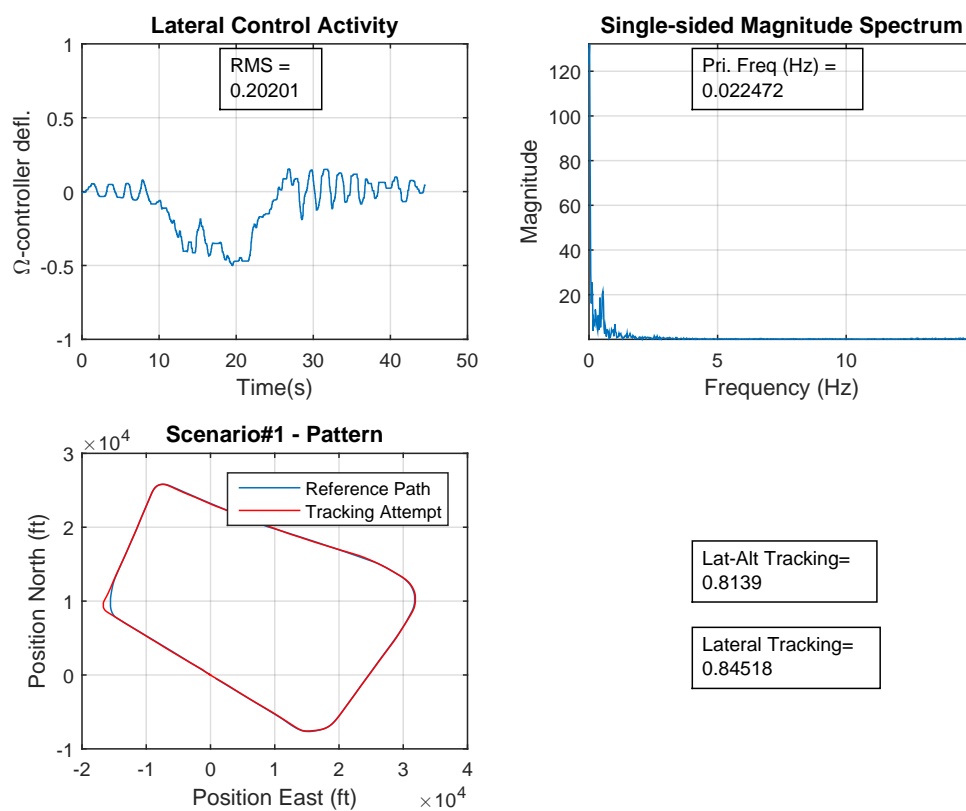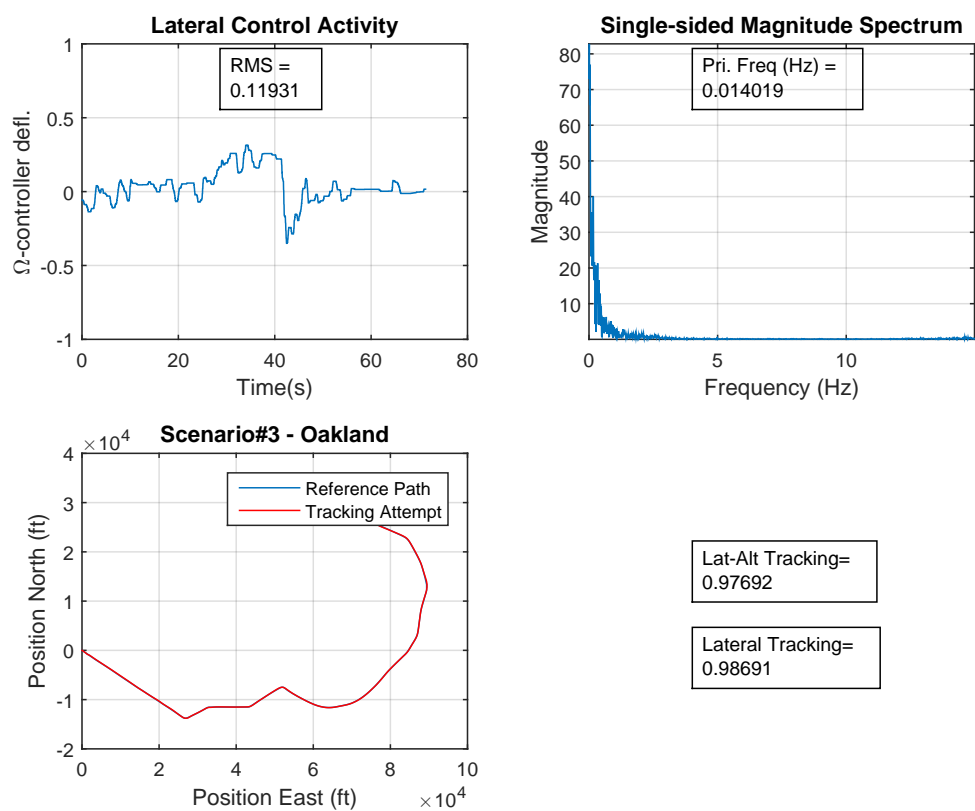
Figure A.4: Participant XP-4 Performance - Scenario 1
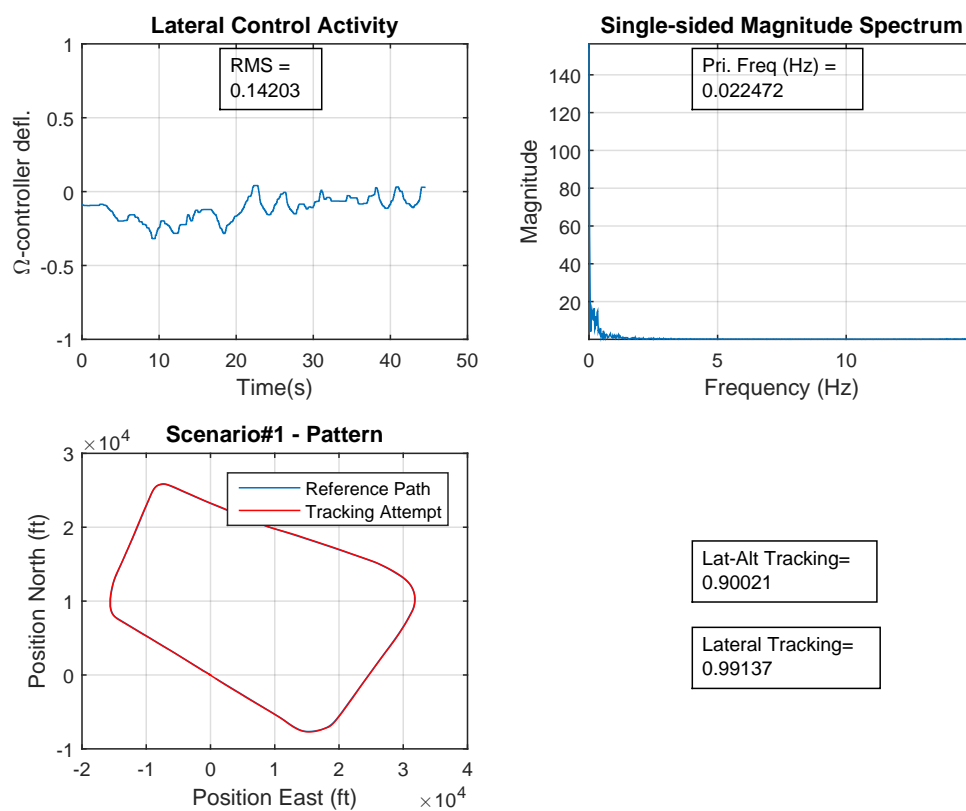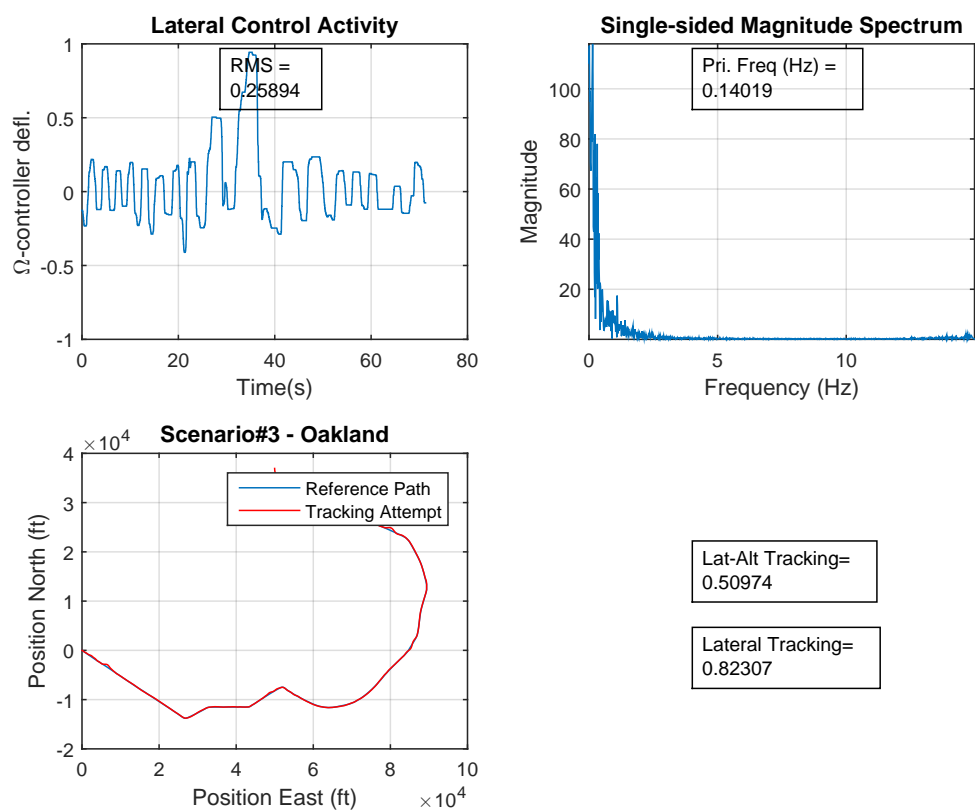
Figure A.5: Participant XP-5 Performance - Scenario 1

Lateral Control Activity

RMS =
0.59127

Ω-controller defl.

Time(s)

Single-sided Magnitude Spectrum

Pri. Freq (Hz) =
0.022472

Magnitude

Frequency (Hz)

Scenario#1 - Pattern

Position North (ft)

Reference Path
Tracking Attempt

Position East (ft)

Lat-Alt Tracking=
0.79026

Lateral Tracking=
0.82003
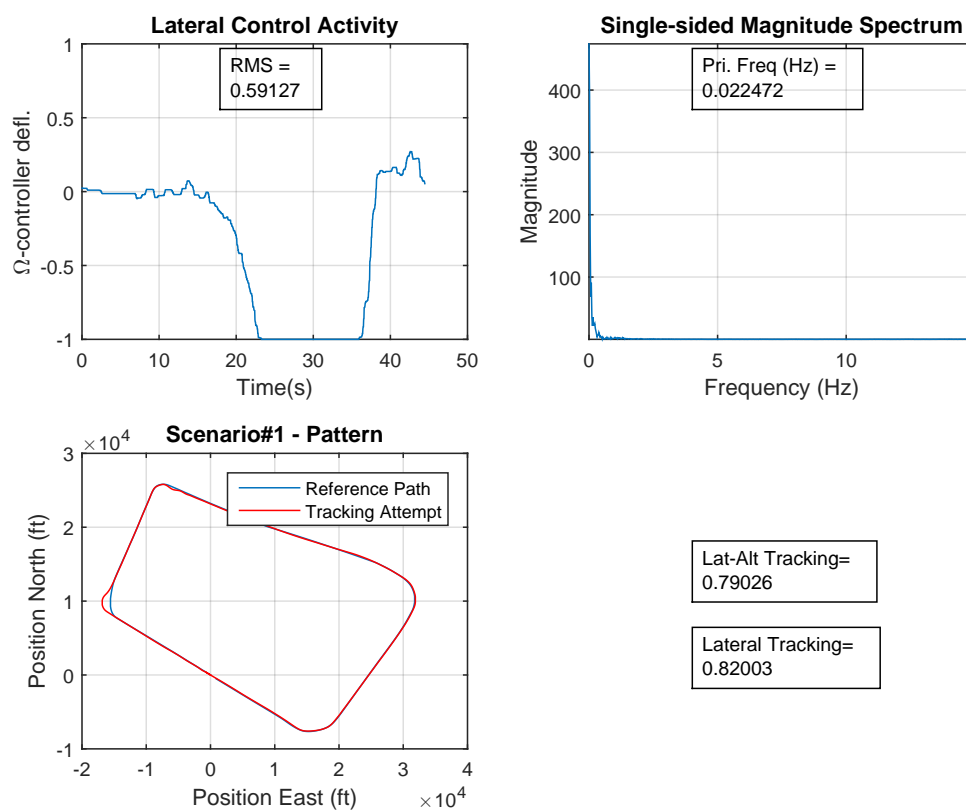
Figure A.6: Participant XP-6 Performance - Scenario 1
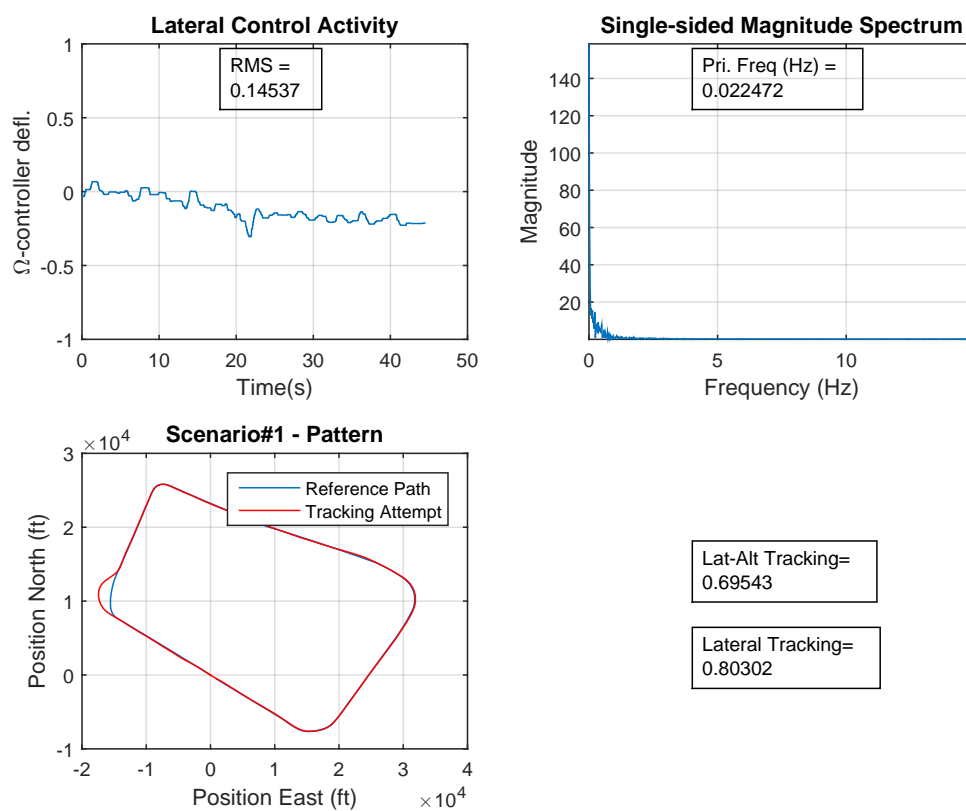
Figure A.7: Participant XP-7 Performance - Scenario 1
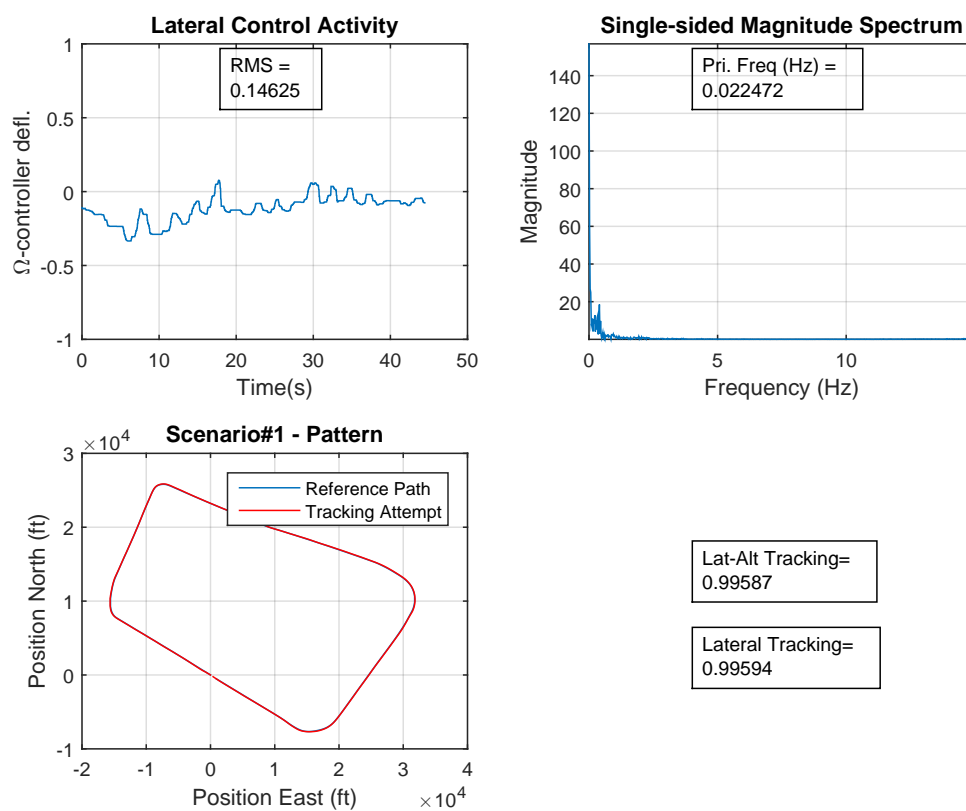
Figure A.8: Participant XP-8 Performance - Scenario 1

Lateral Control Activity

RMS = 0.15563

Single-sided Magnitude Spectrum

Pri. Freq (Hz) = 0.022472

Scenario#1 - Pattern

Reference Path
Tracking Attempt

Lat-Alt Tracking= 0.85095

Lateral Tracking= 0.9802
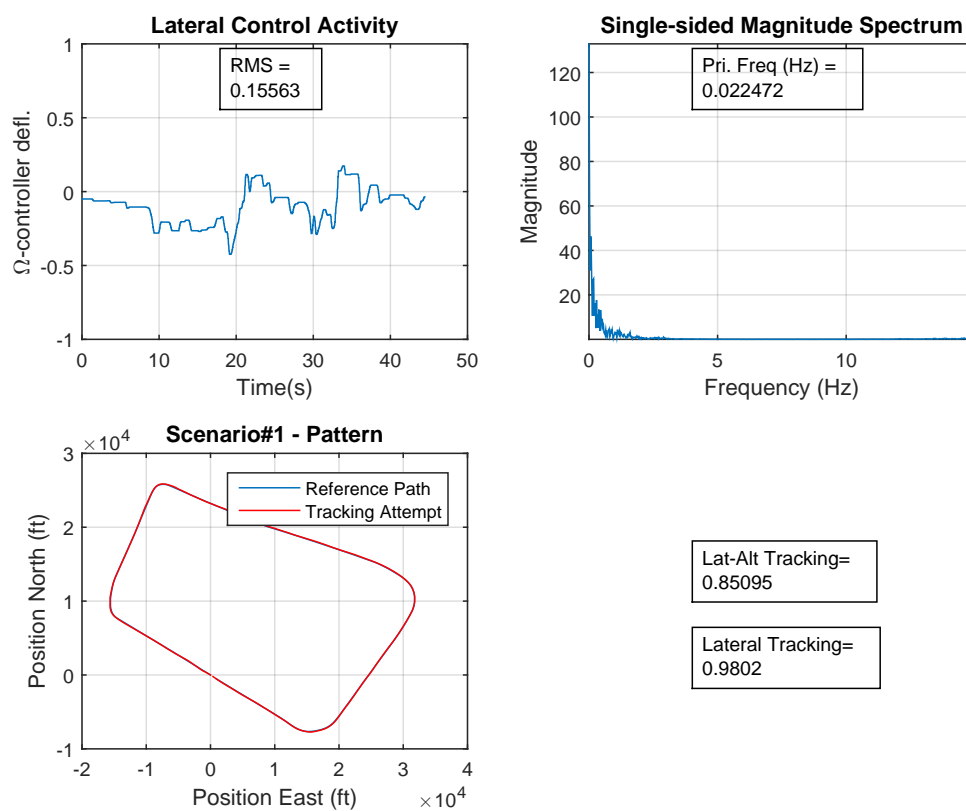
Figure A.9: Participant XP-9 Performance - Scenario 1

A.2 Scenario 1 - Pattern (Non-Pilots)
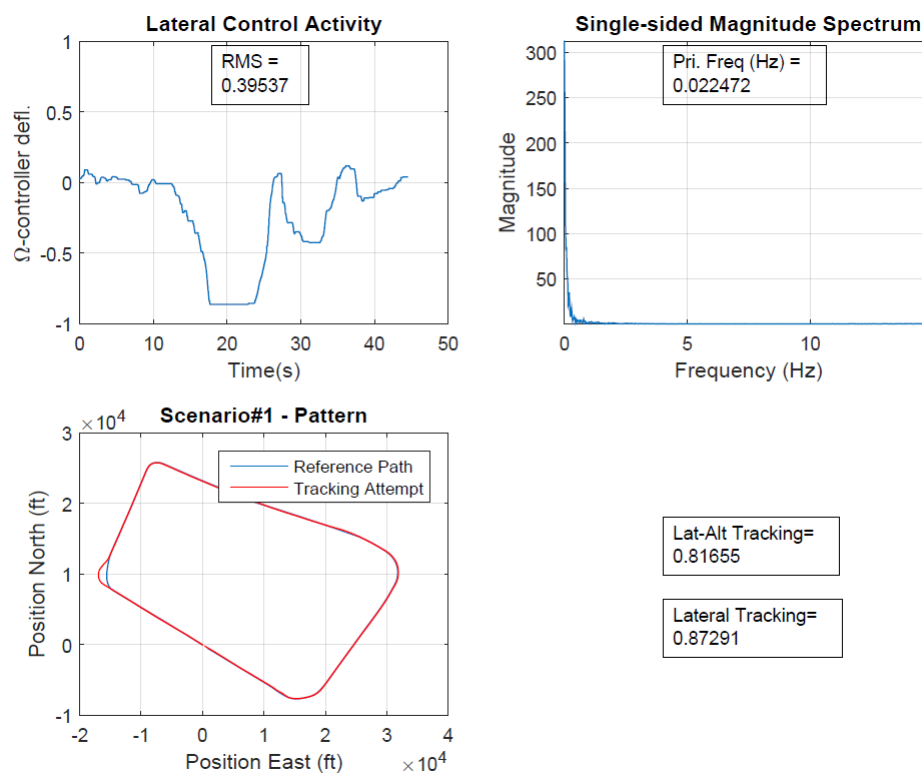
Figure A.10: Participant NP-1 Performance - Scenario 1
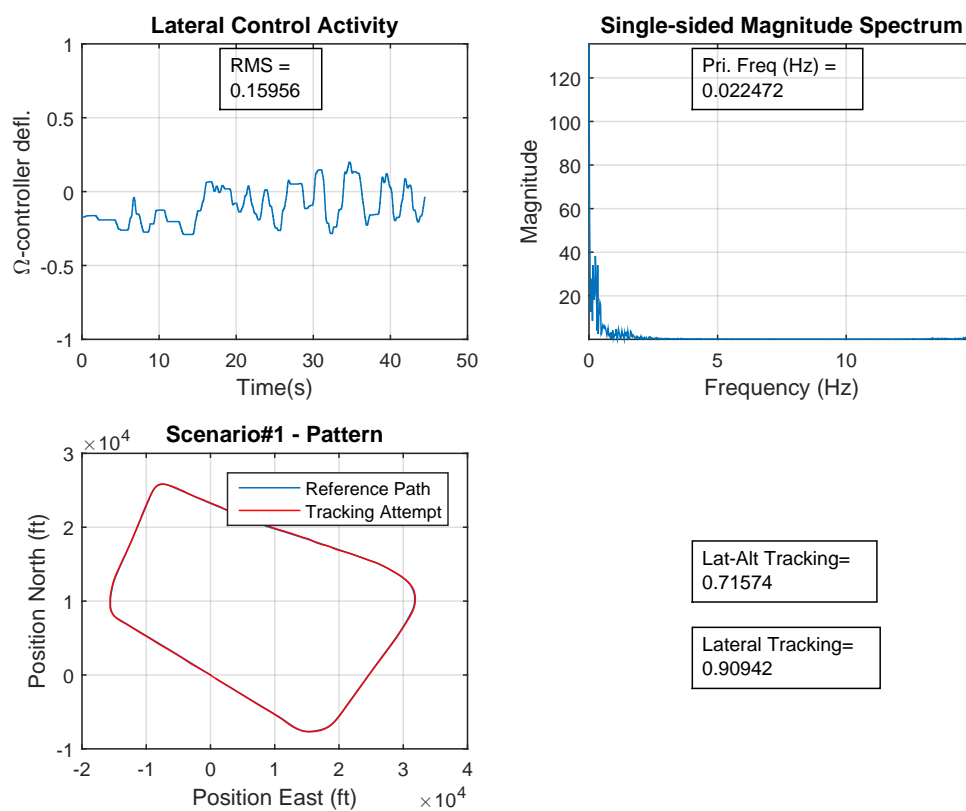
Figure A.11: Participant NP-2 Performance - Scenario 1
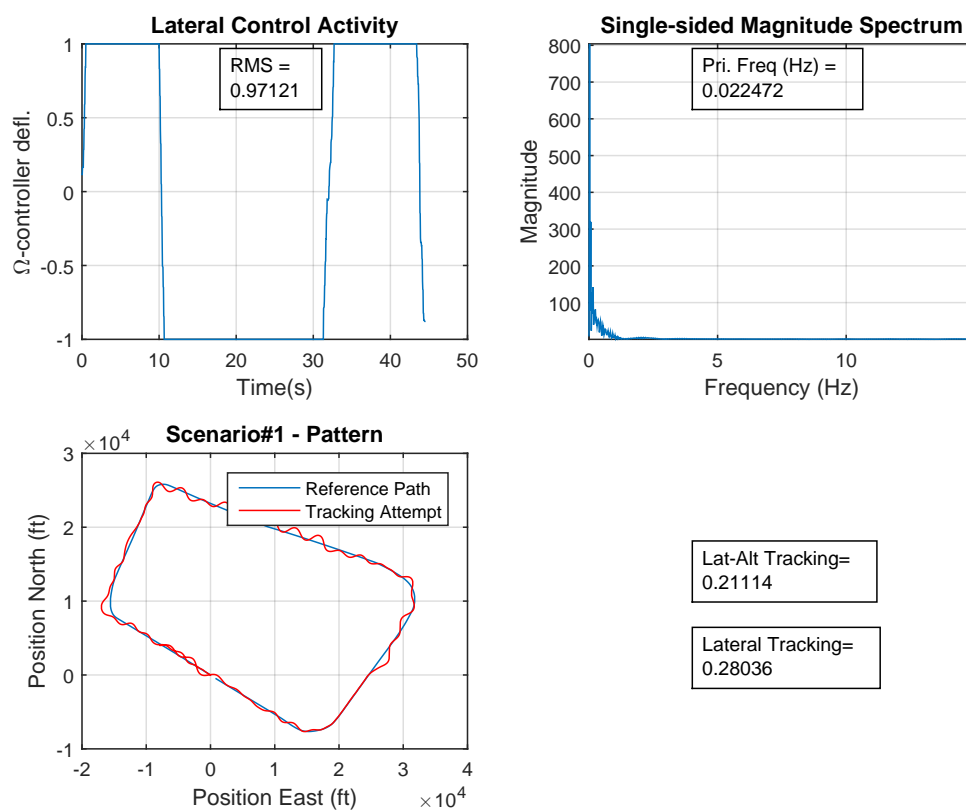
Figure A.12: Participant NP-3 Performance - Scenario 1
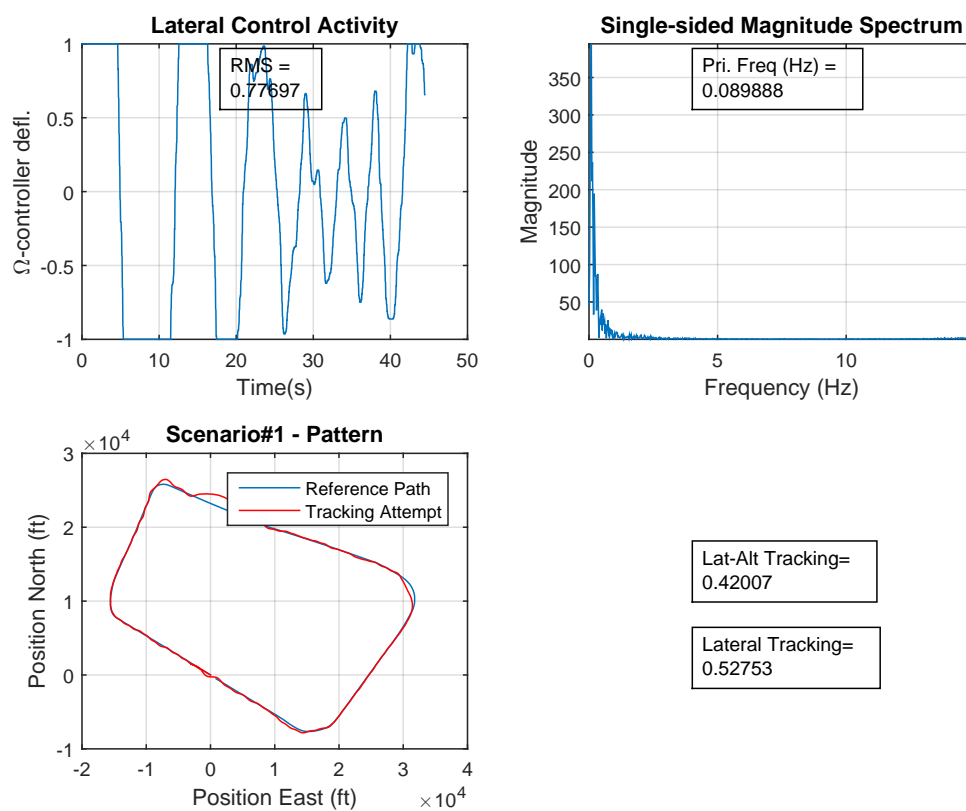
Figure A.13: Participant NP-4 Performance - Scenario 1
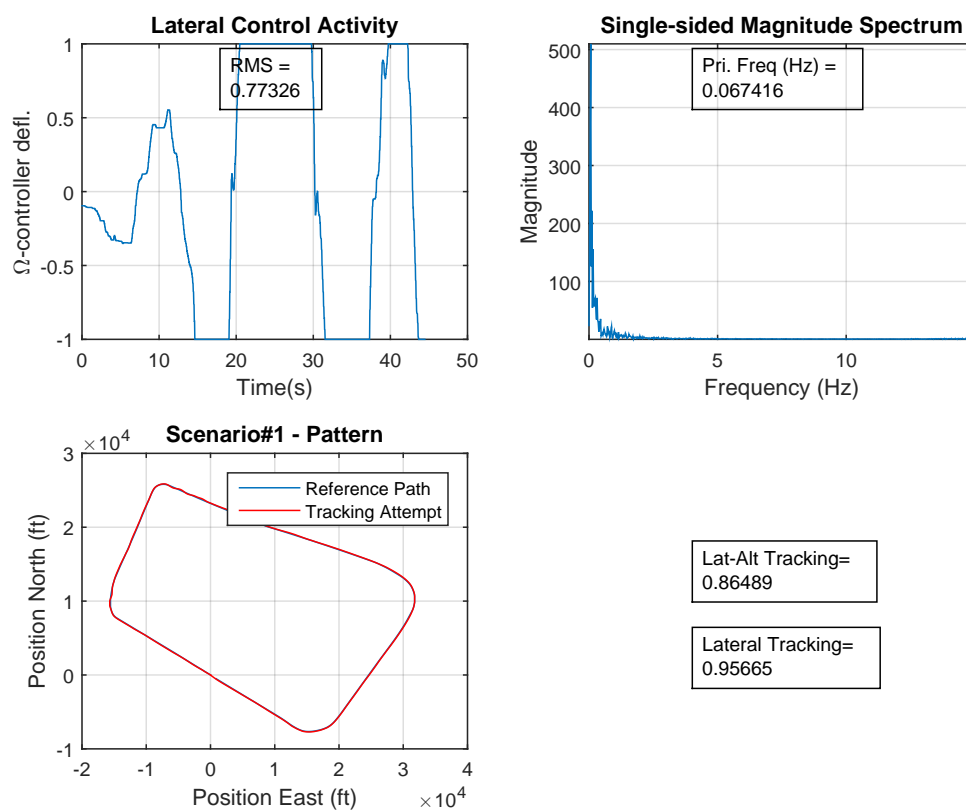
Figure A.14: Participant NP-5 Performance - Scenario 1
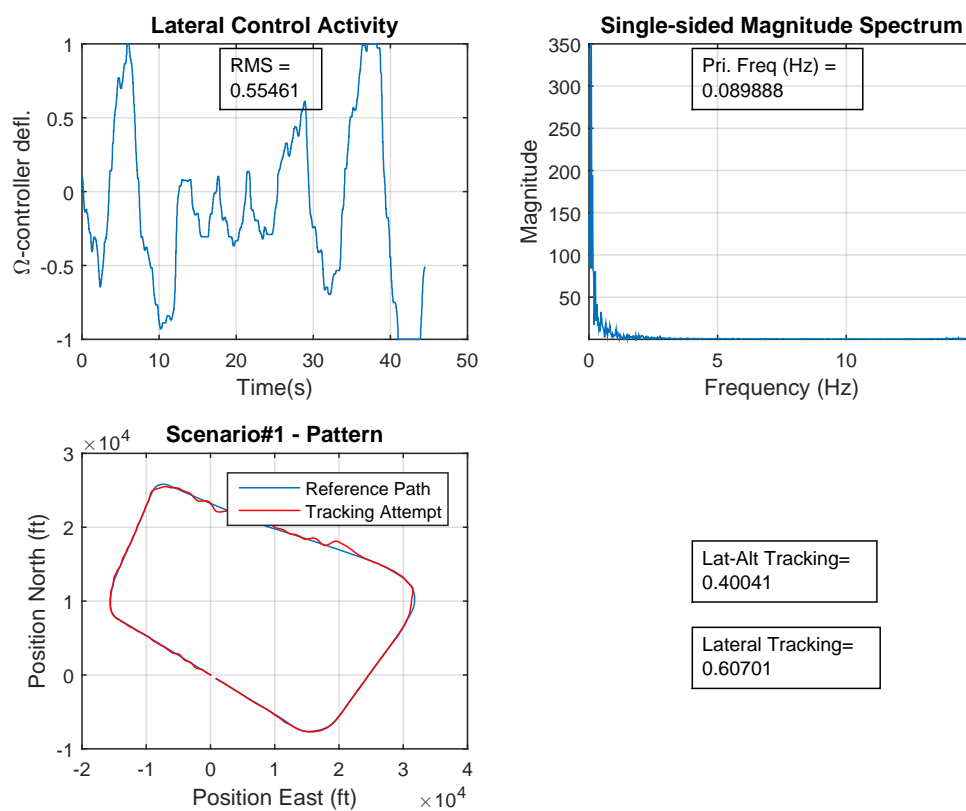
Figure A.15: Participant NP-6 Performance - Scenario 1
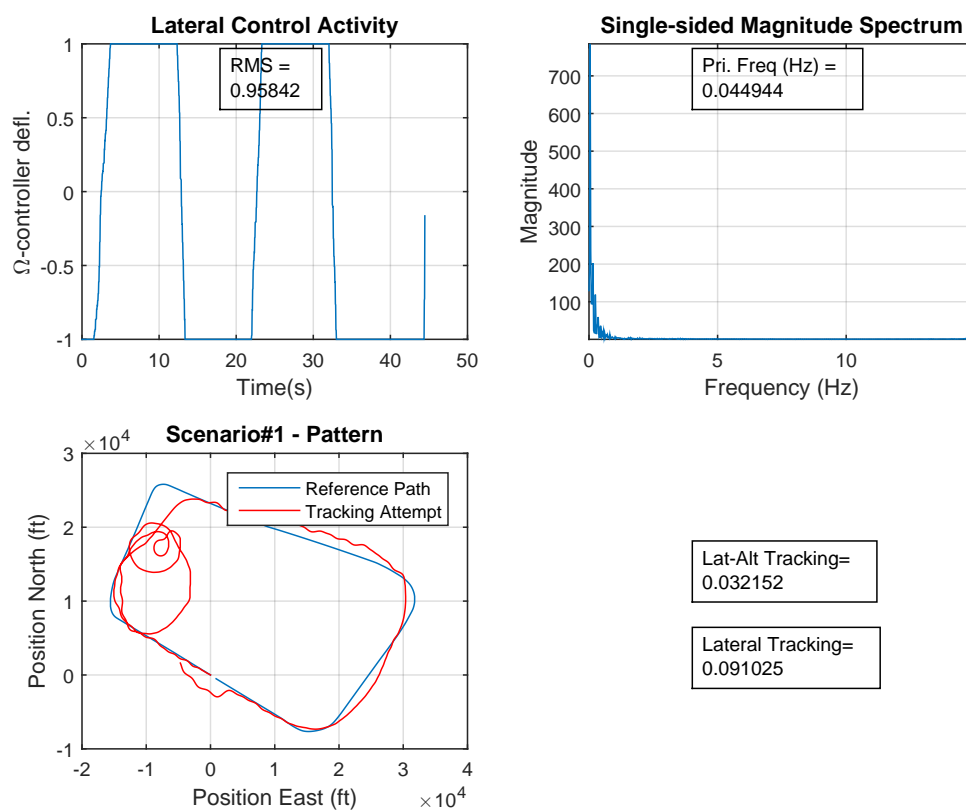
Figure A.16: Participant NP-7 Performance - Scenario 1
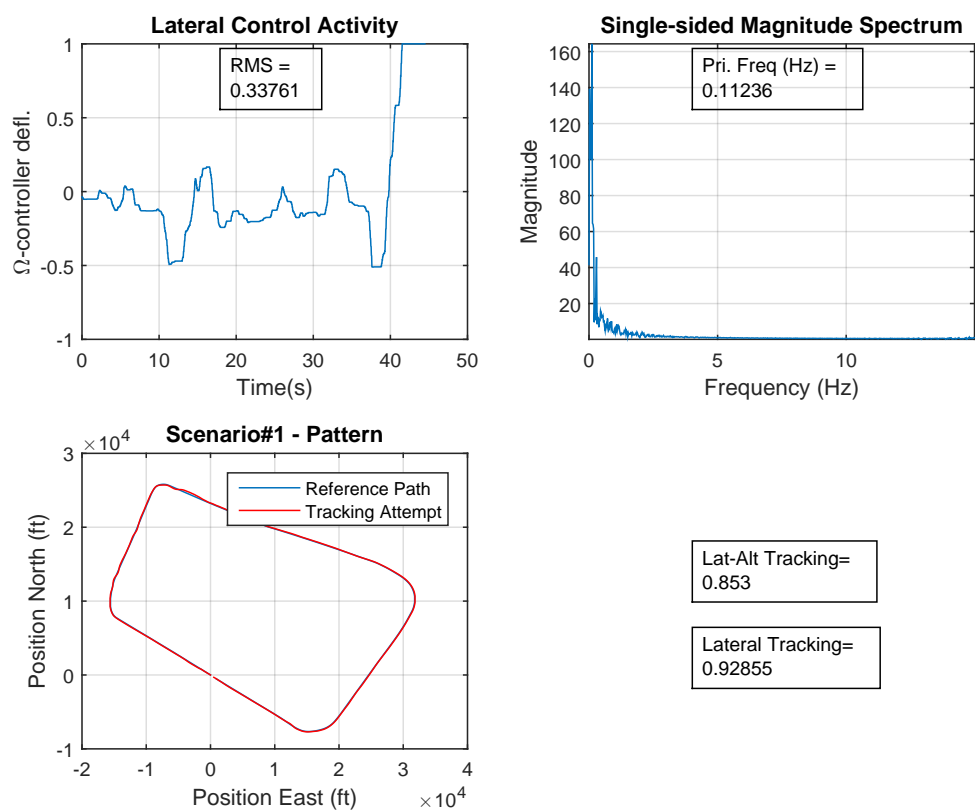
Figure A.17: Participant NP-8 Performance - Scenario 1
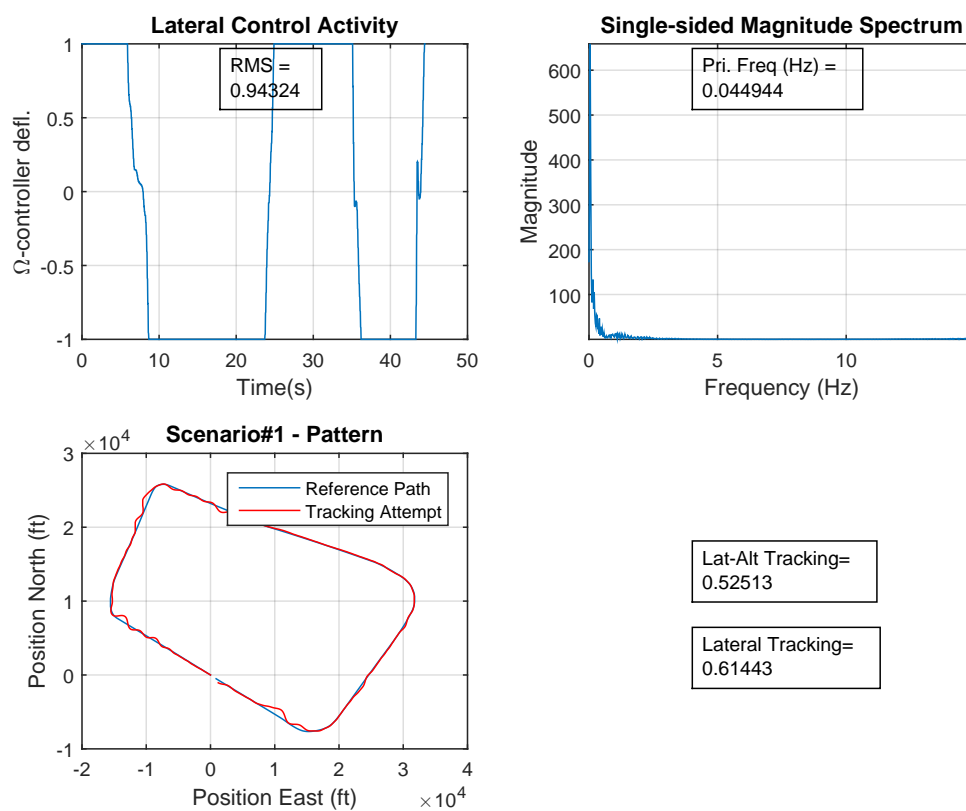
Figure A.18: Participant NP-9 Performance - Scenario 1

A.3 Scenario 2 - San Carlos (Pilots)
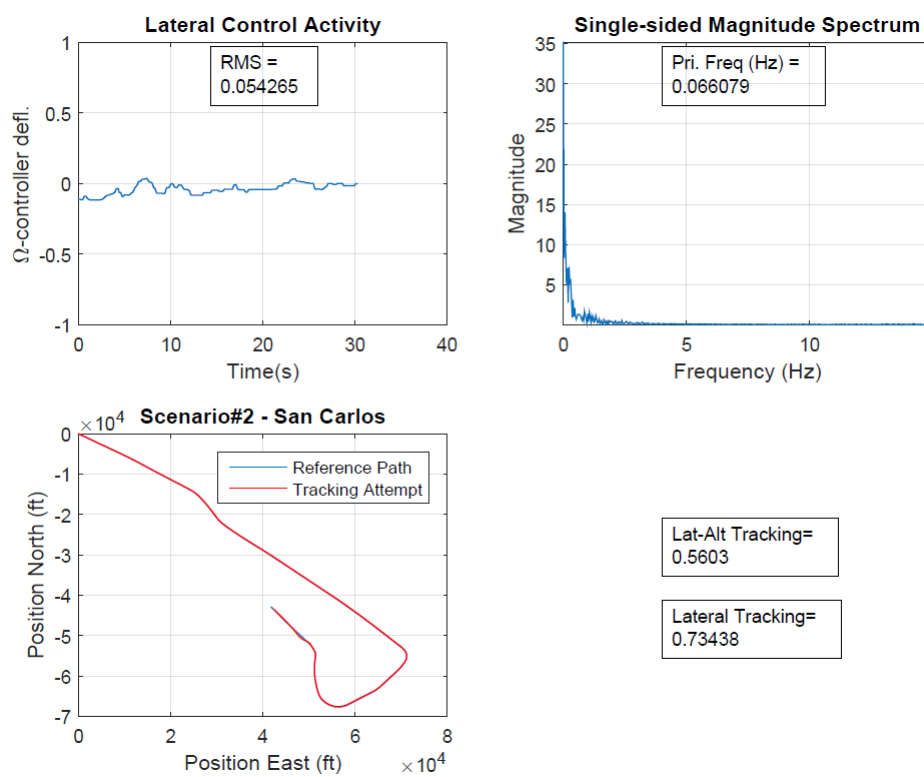
Figure A.19: Participant XP-1 Performance - Scenario 2
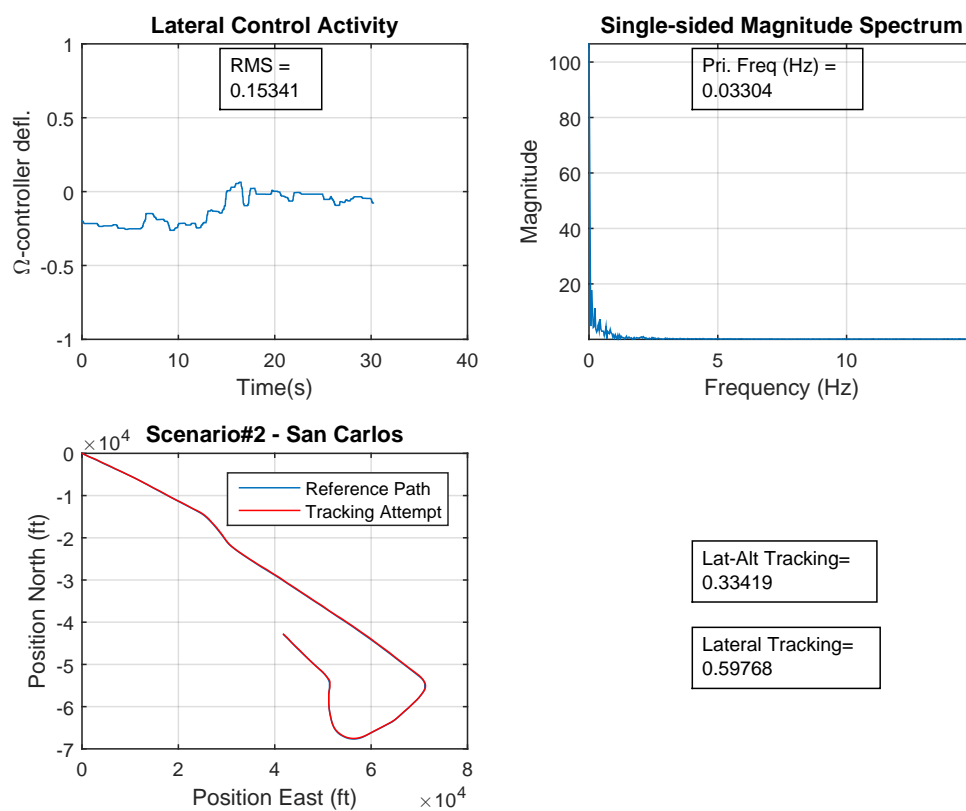
Figure A.20: Participant XP-2 Performance - Scenario 2
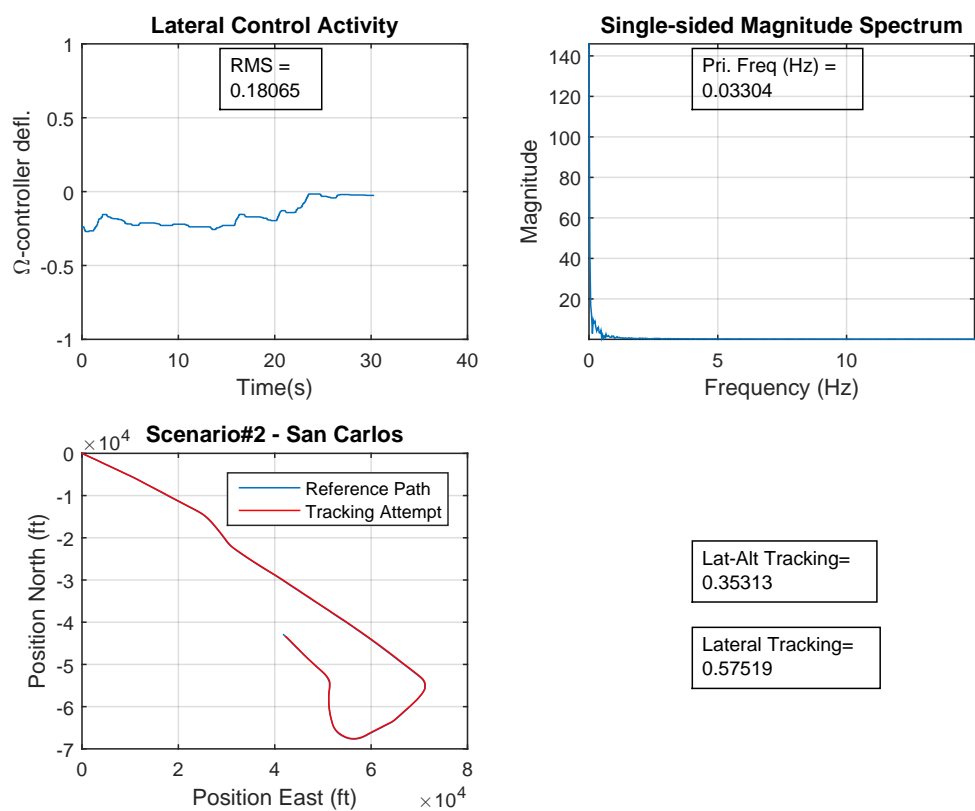
Figure A.21: Participant XP-3 Performance - Scenario 2
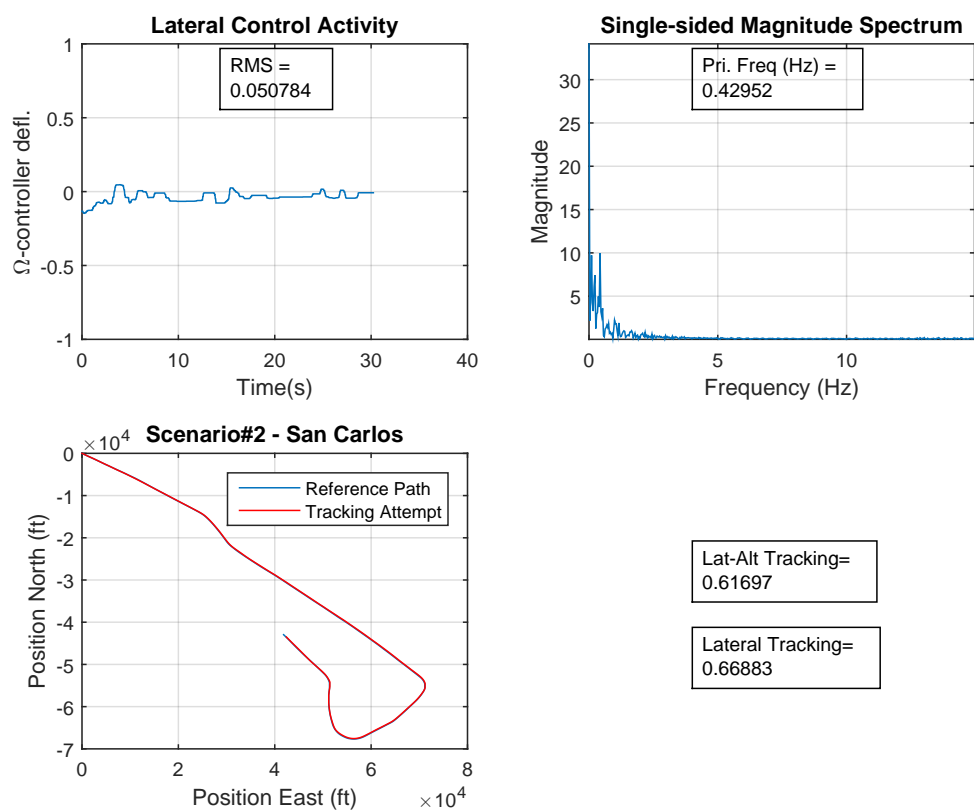
Figure A.22: Participant XP-4 Performance - Scenario 2
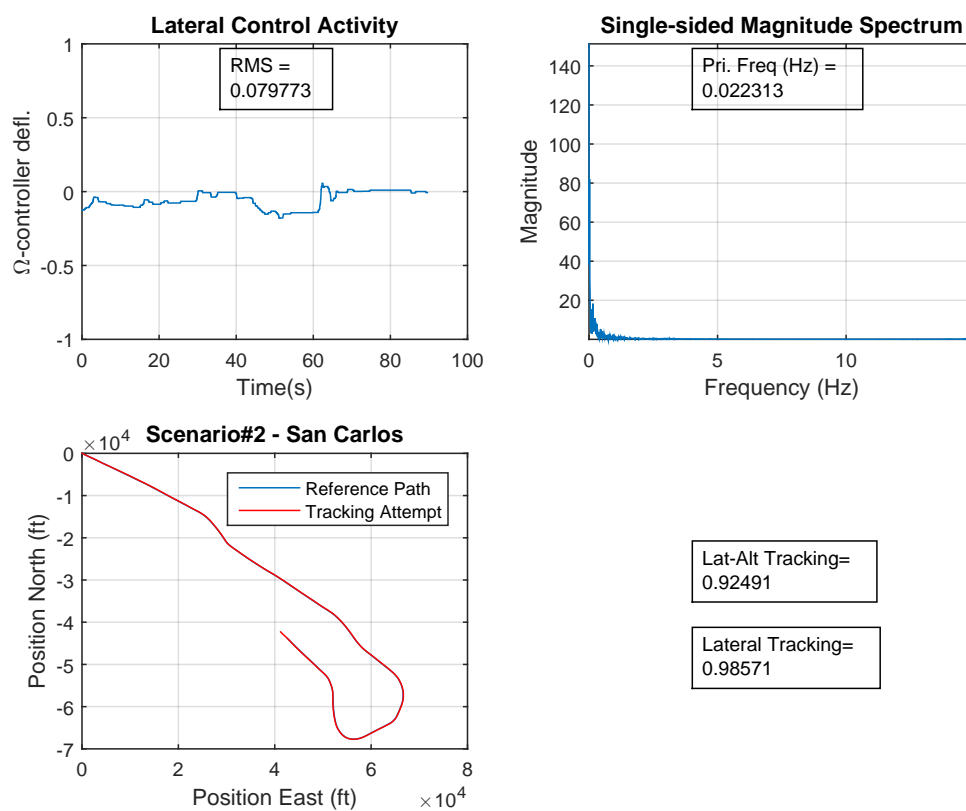
Figure A.23: Participant XP-5 Performance - Scenario 2
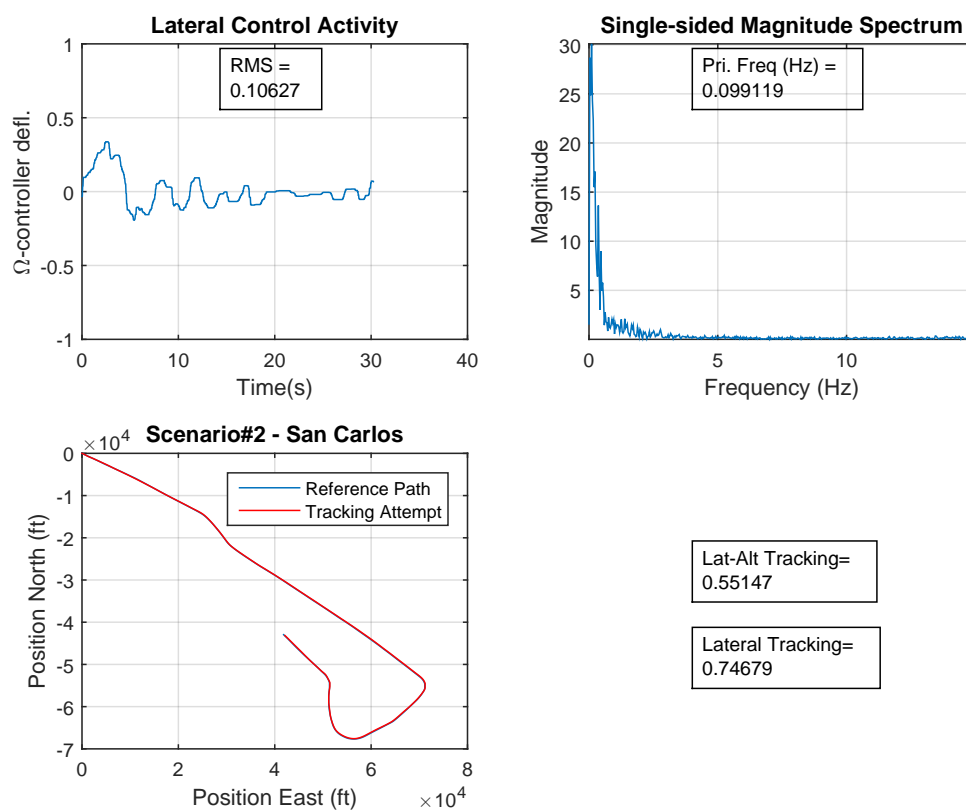
Figure A.24: Participant XP-6 Performance - Scenario 2

Lateral Control Activity

RMS =
0.066176

Ω-controller defl.

Time(s)

Single-sided Magnitude Spectrum

Pri. Freq (Hz) =
0.13216

Magnitude

Frequency (Hz)

Scenario#2 - San Carlos

Position North (ft)

Reference Path
Tracking Attempt

Lat-Alt Tracking=
0.57761

Lateral Tracking=
0.65507

Position East (ft)
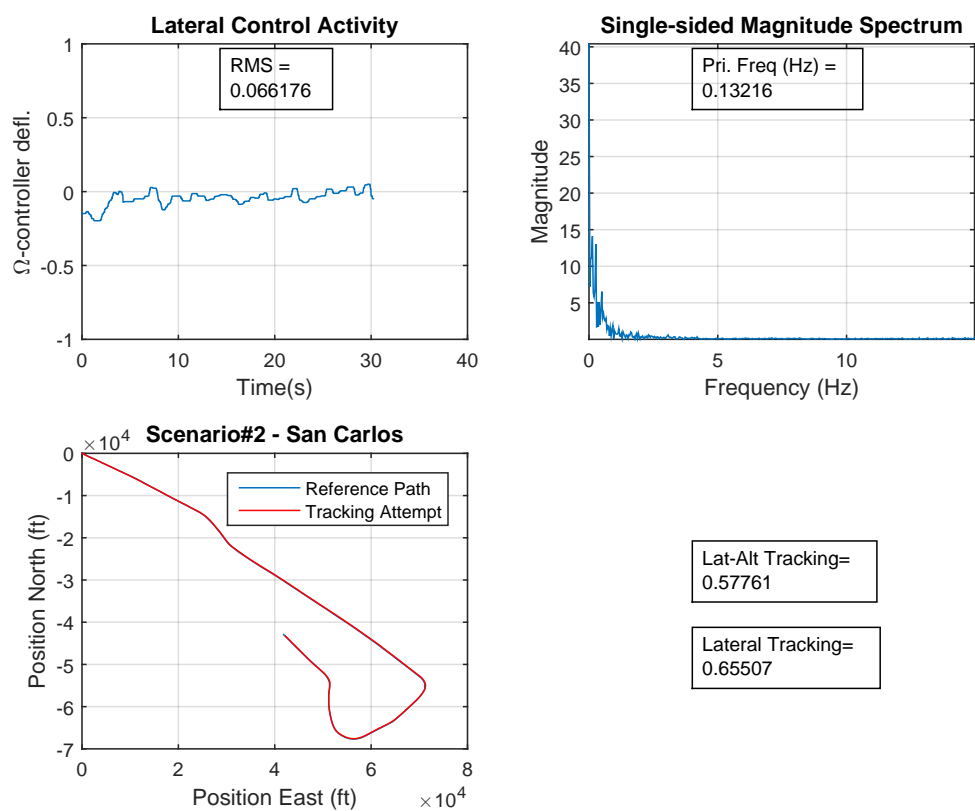
Figure A.25: Participant XP-7 Performance - Scenario 2
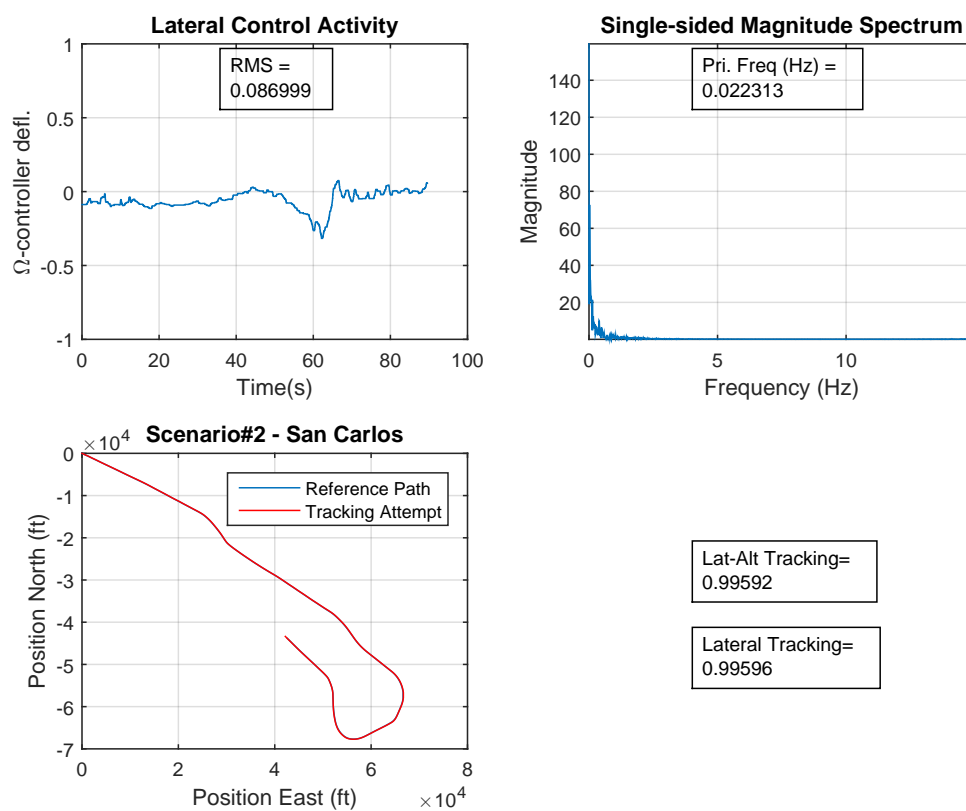
Figure A.26: Participant XP-8 Performance - Scenario 2
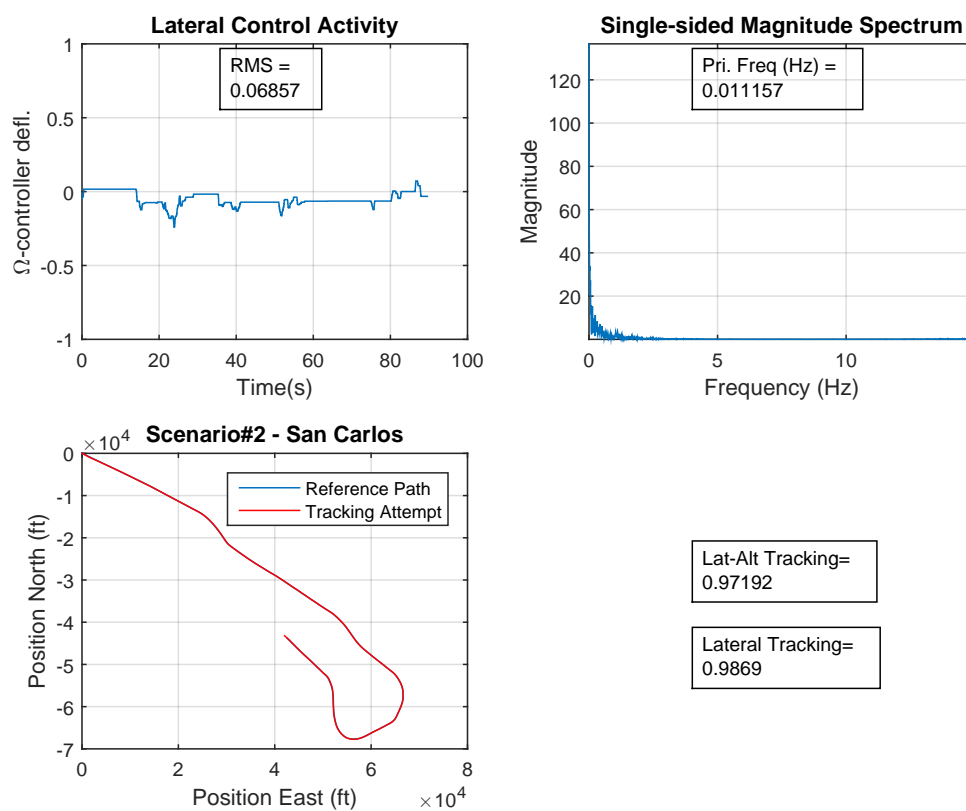
Figure A.27: Participant XP-9 Performance - Scenario 2

A.4 Scenario 2 - San Carlos (Non-Pilots)
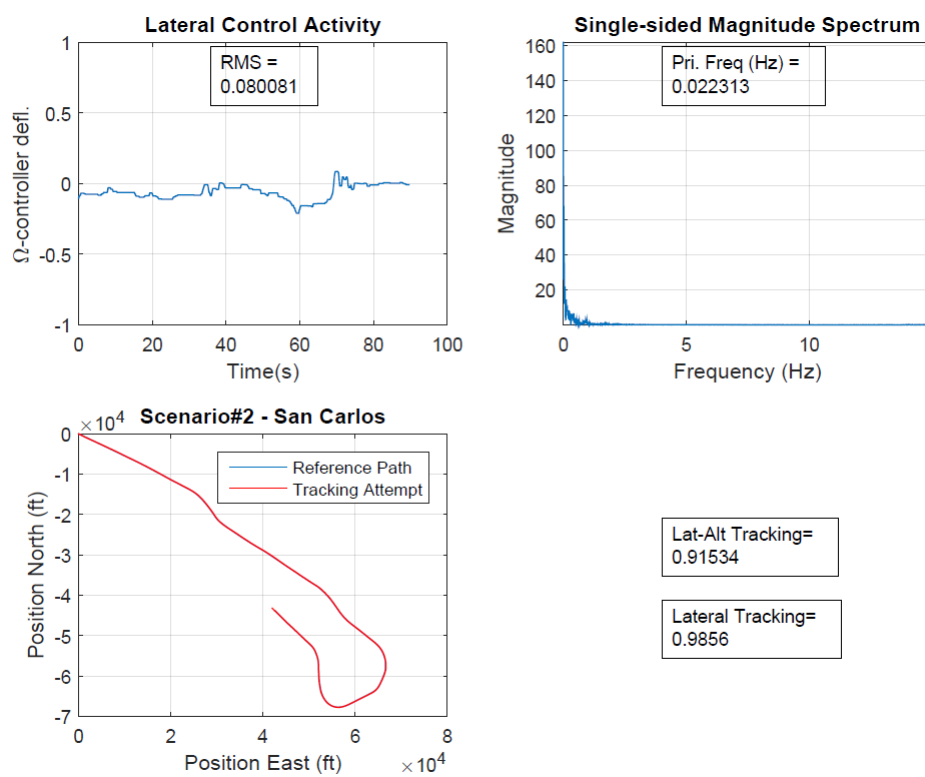
Figure A.28: Participant NP-2 Performance - Scenario 2
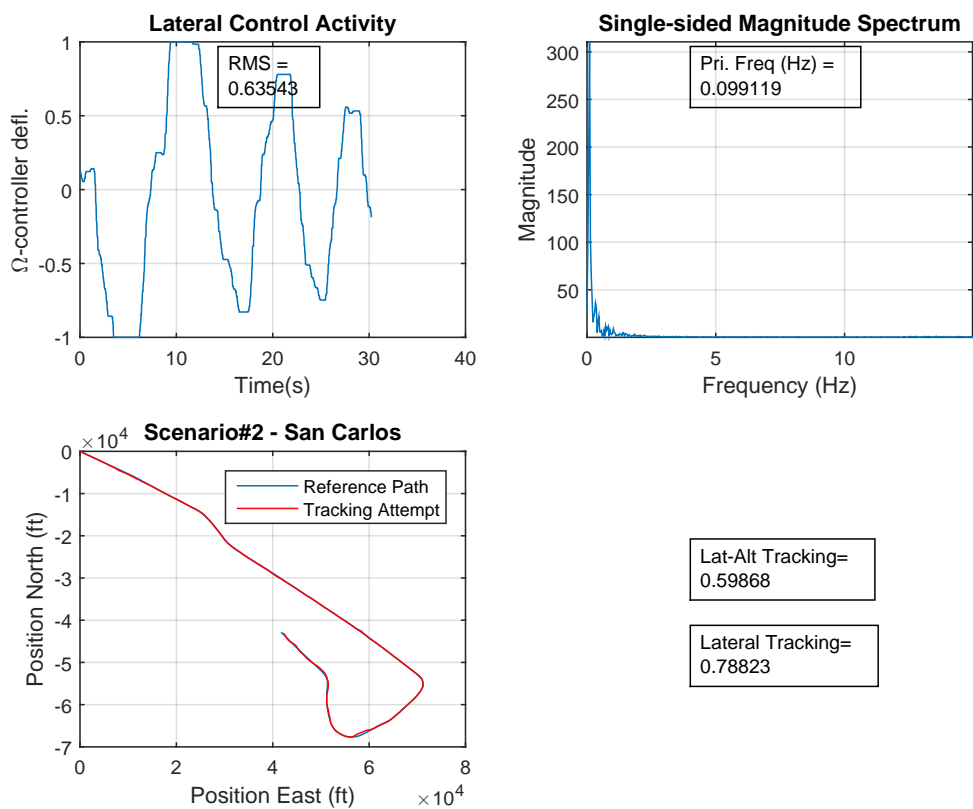
Figure A.29: Participant NP-3 Performance - Scenario 2
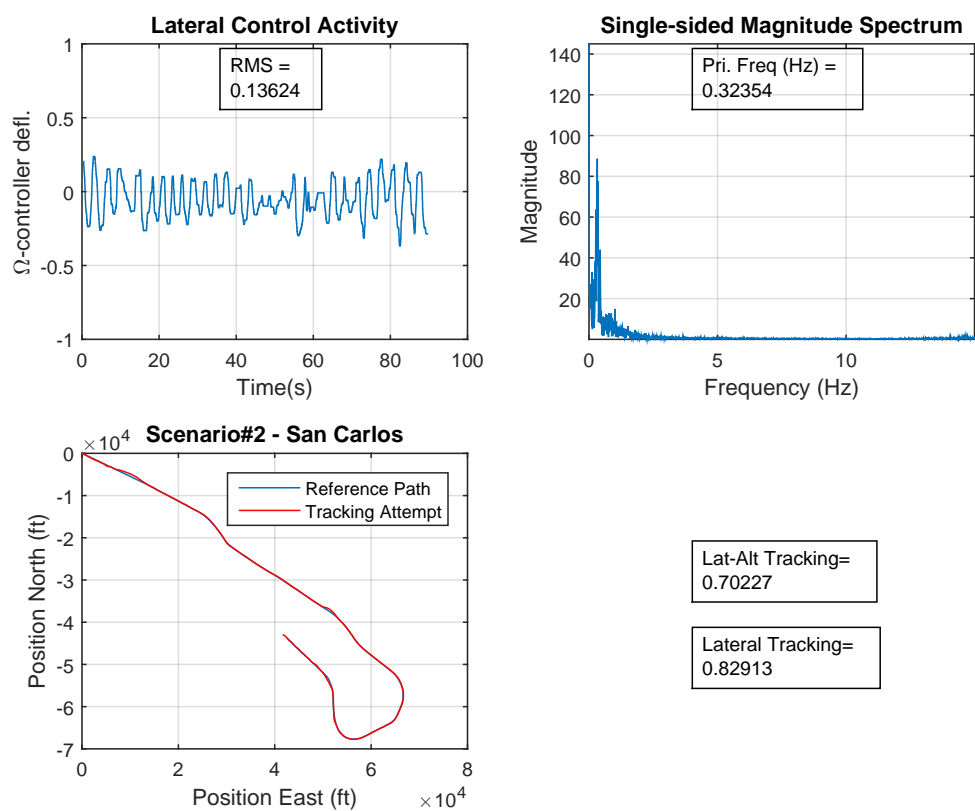
Figure A.30: Participant NP-4 Performance - Scenario 2
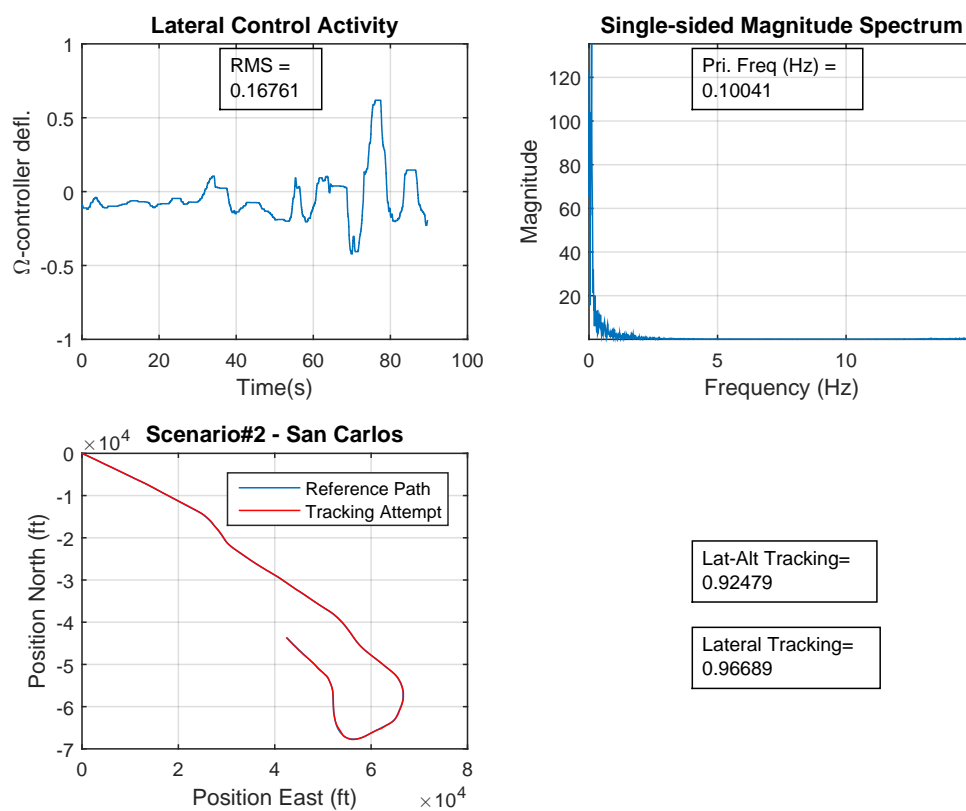
Figure A.31: Participant NP-5 Performance - Scenario 2
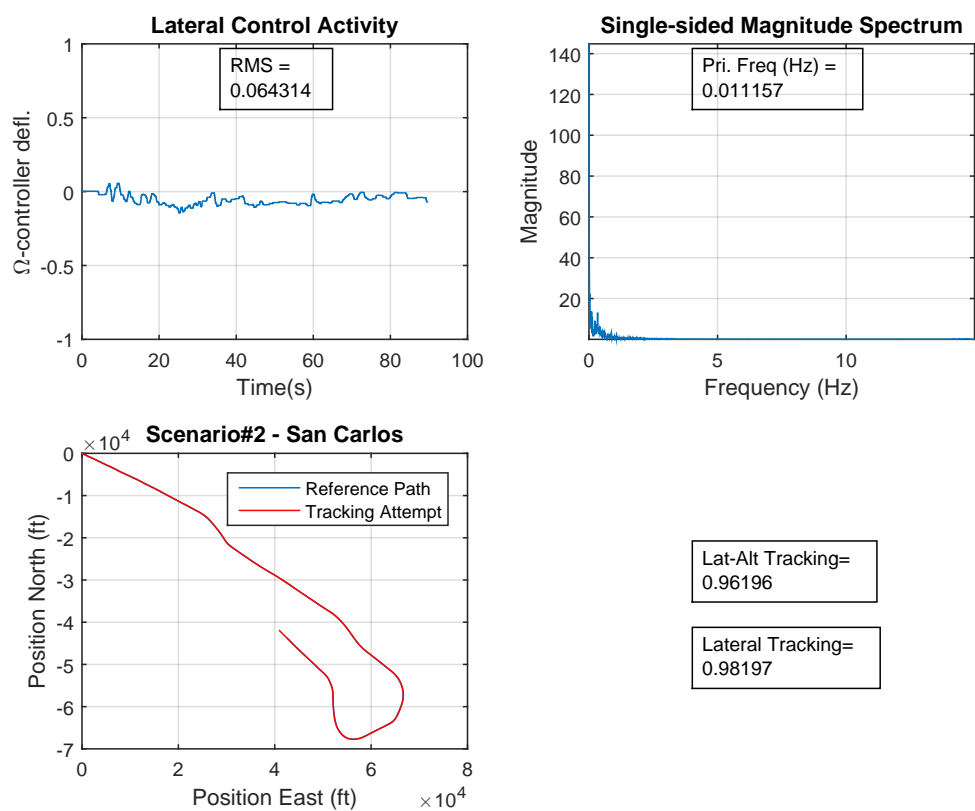
Figure A.32: Participant NP-6 Performance - Scenario 2
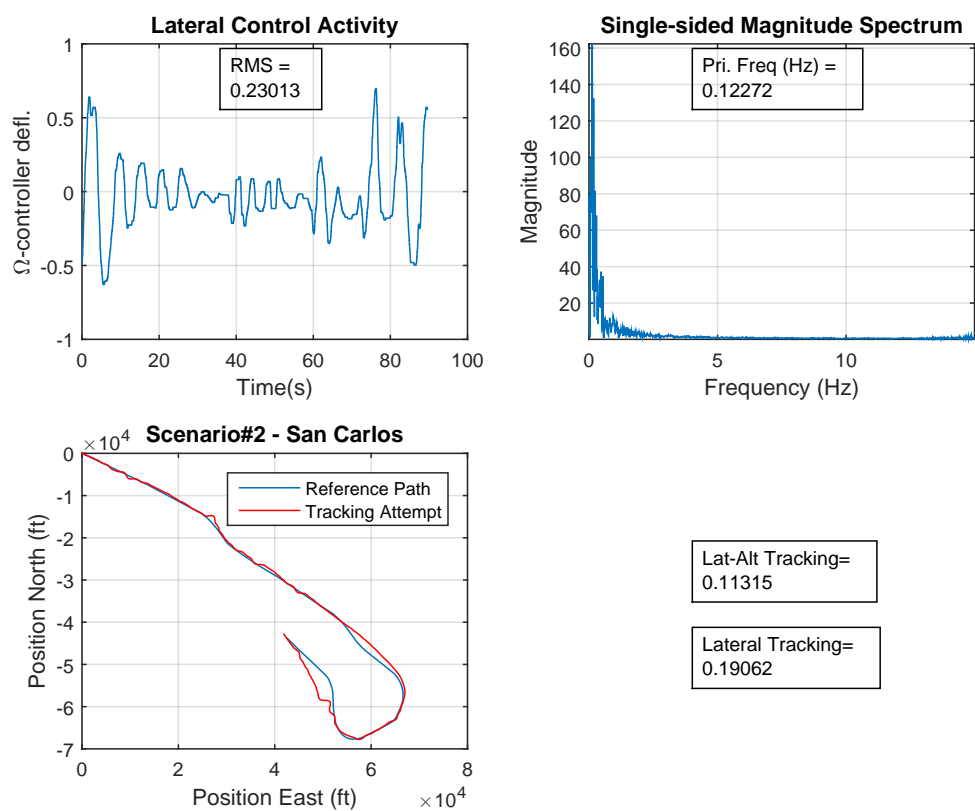
Figure A.33: Participant NP-7 Performance - Scenario 2
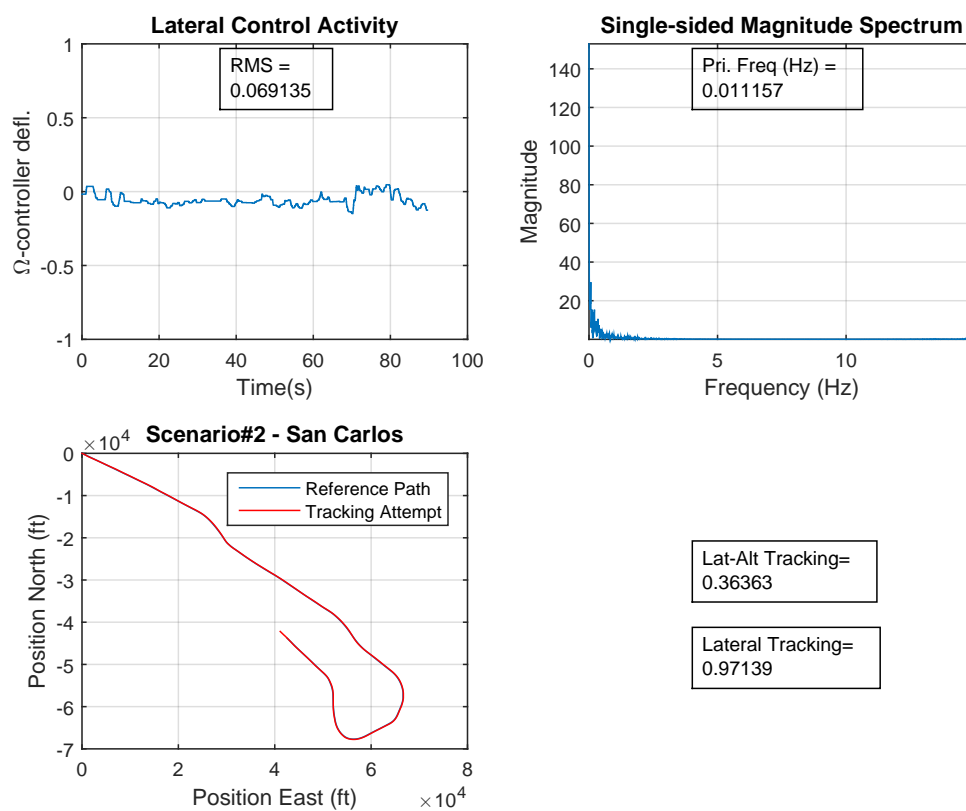
Figure A.34: Participant NP-8 Performance - Scenario 2
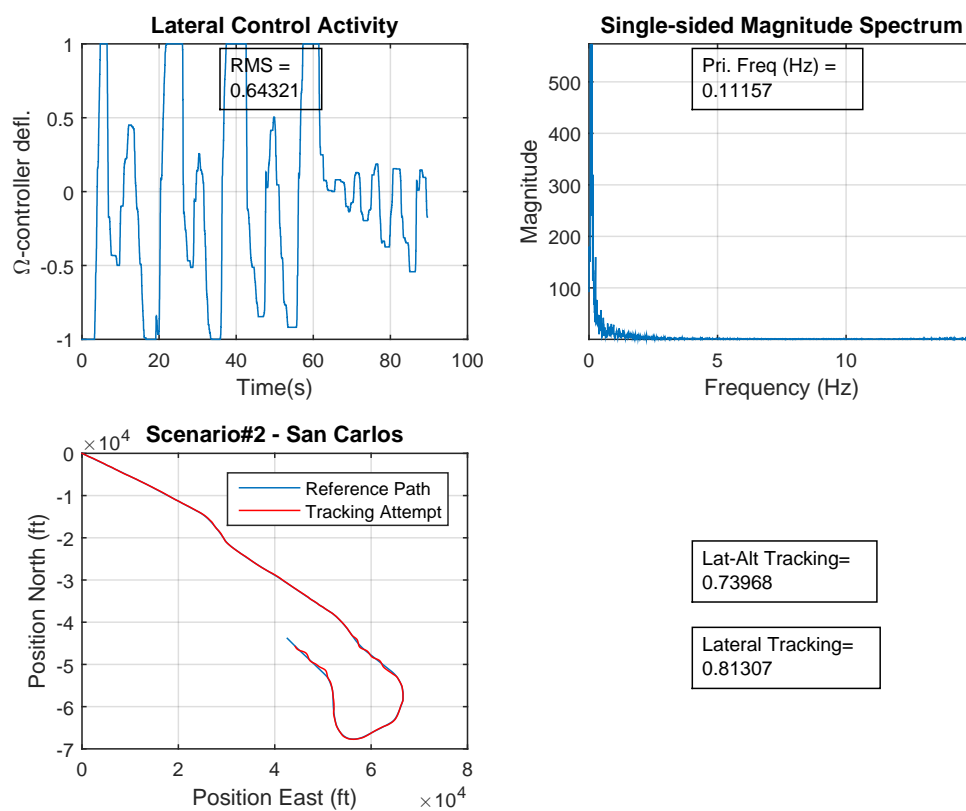
Figure A.35: Participant NP-9 Performance - Scenario 2

A.5   Scenario 3 - Oakland (Pilots)
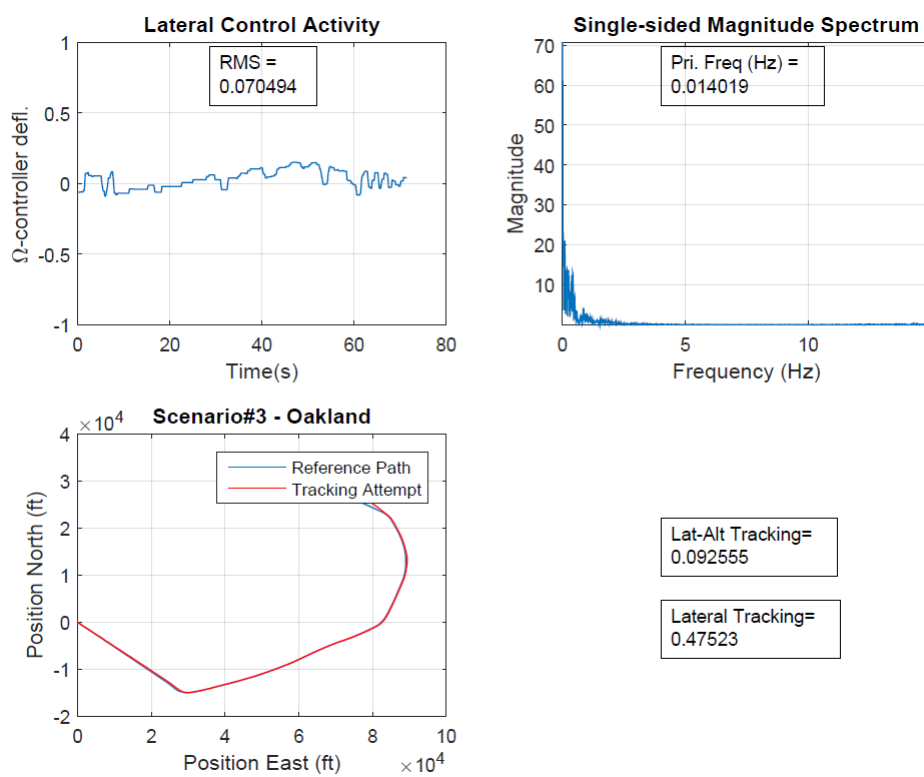
Figure A.36: Participant XP-2 Performance - Scenario 3

Lateral Control Activity

RMS =
0.064003

Single-sided Magnitude Spectrum

Pri. Freq (Hz) =
0.014019

Scenario#3 - Oakland

Reference Path
Tracking Attempt

Lat-Alt Tracking=
0.41785

Lateral Tracking=
0.47026
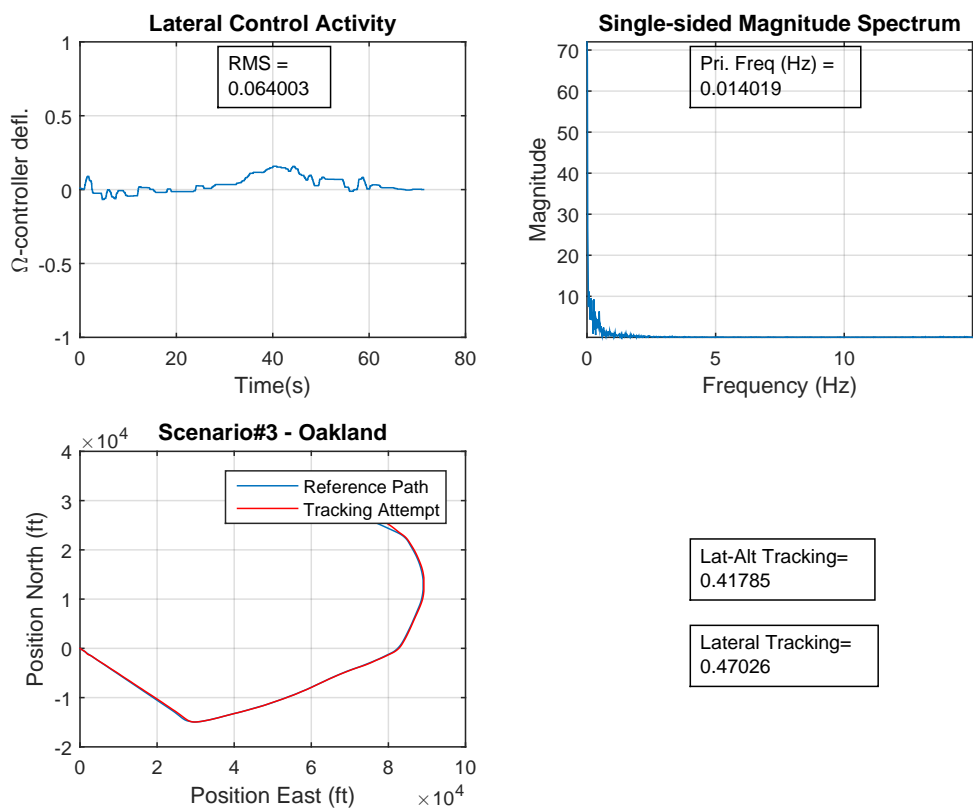
Figure A.37: Participant XP-3 Performance - Scenario 3
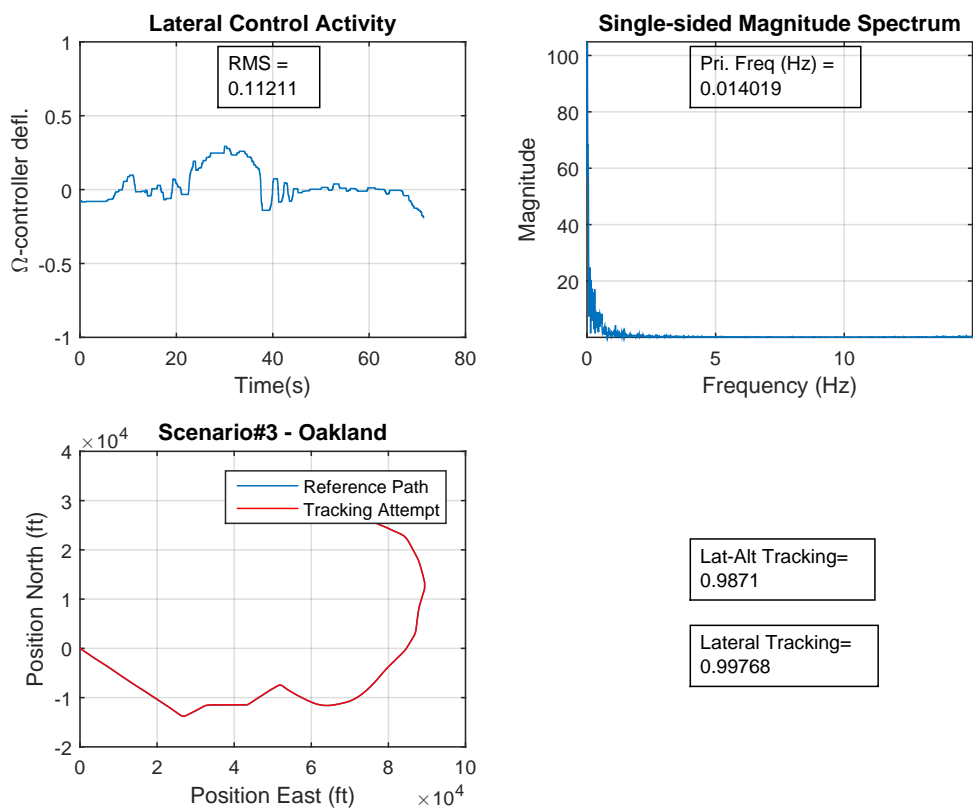
Figure A.38: Participant XP-5 Performance - Scenario 3
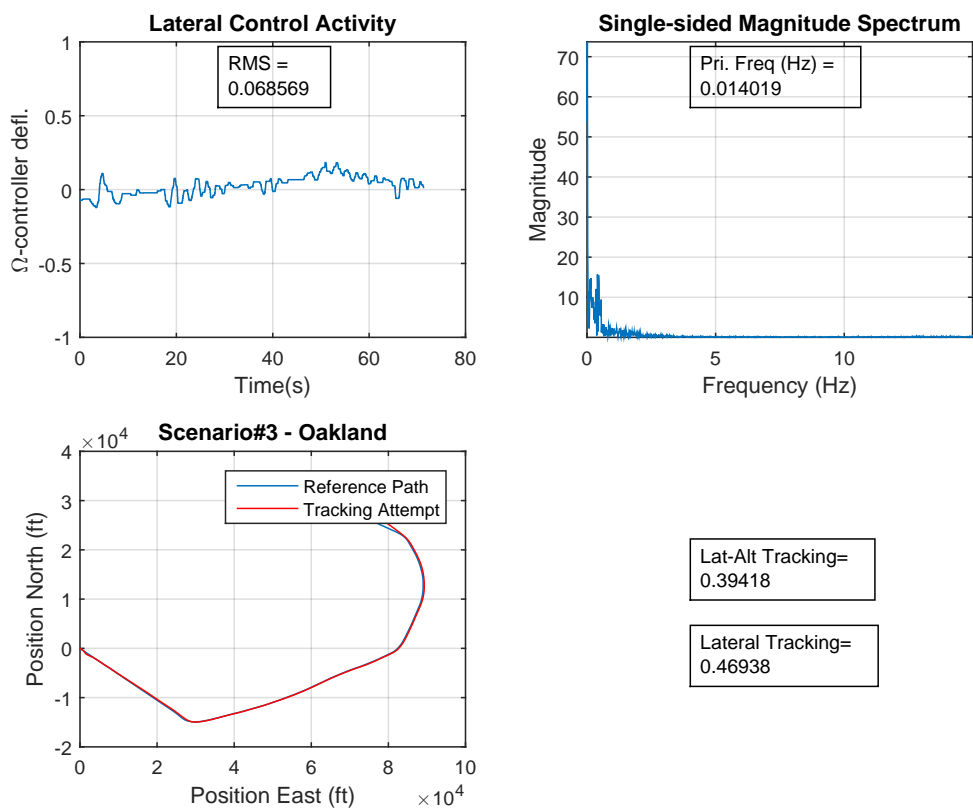
Figure A.39: Participant XP-6 Performance - Scenario 3
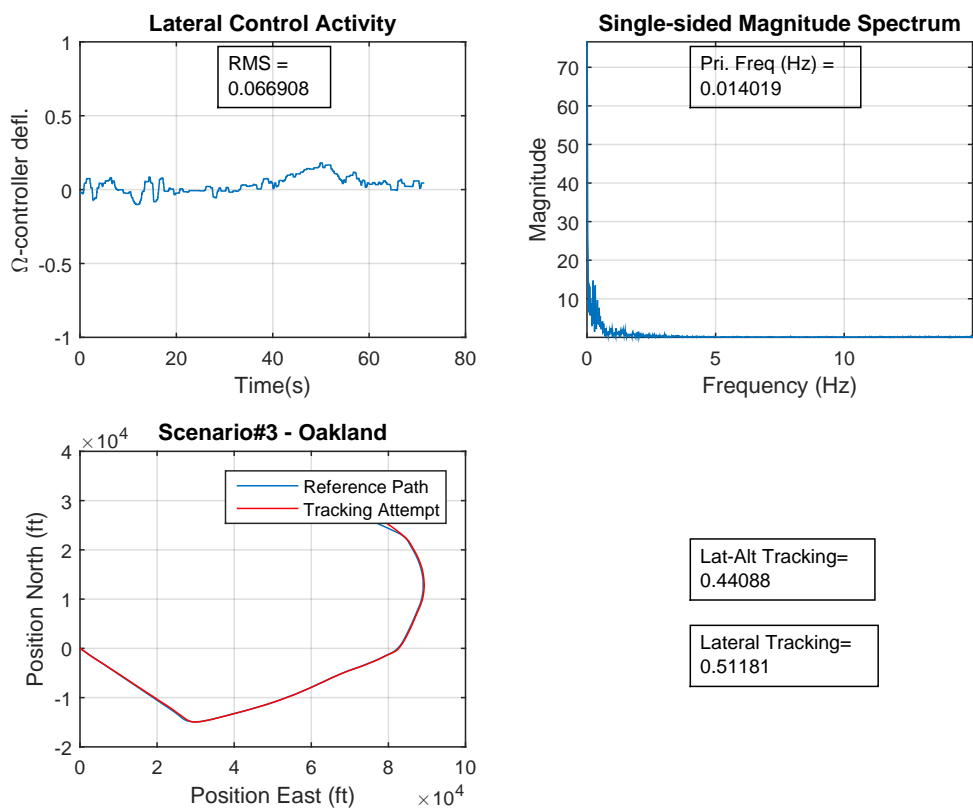
Figure A.40: Participant XP-7 Performance - Scenario 3
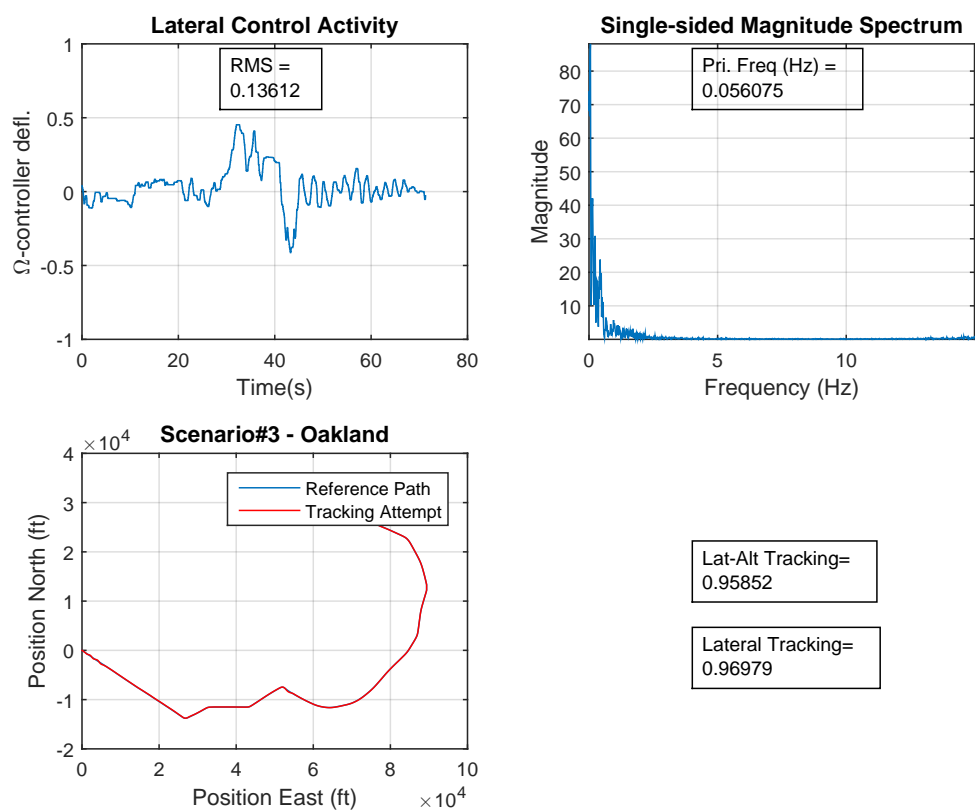
Figure A.41: Participant XP-8 Performance - Scenario 3
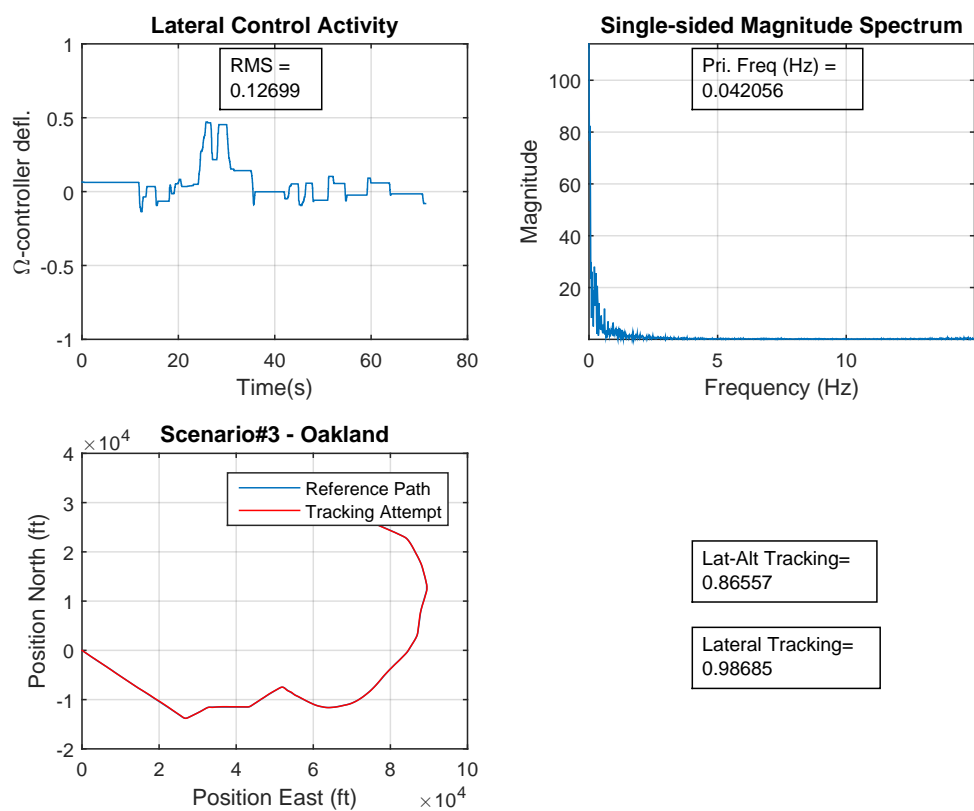
Figure A.42: Participant XP-9 Performance - Scenario 3

Scenario 3 - Oakland (Non-Pilots)
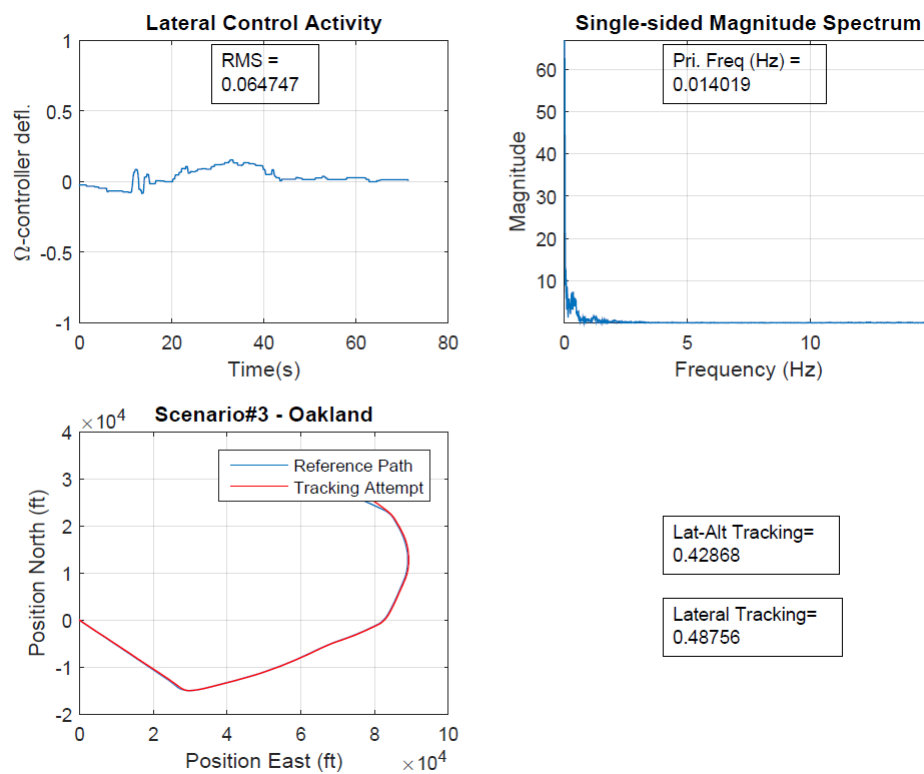
Figure A.43: Participant NP-1 Performance - Scenario 3

Lateral Control Activity

RMS = 0.10327

Single-sided Magnitude Spectrum

Pri. Freq (Hz) = 0.014019

Scenario#3 - Oakland

Reference Path
Tracking Attempt

Lat-Alt Tracking= 0.91985

Lateral Tracking= 1
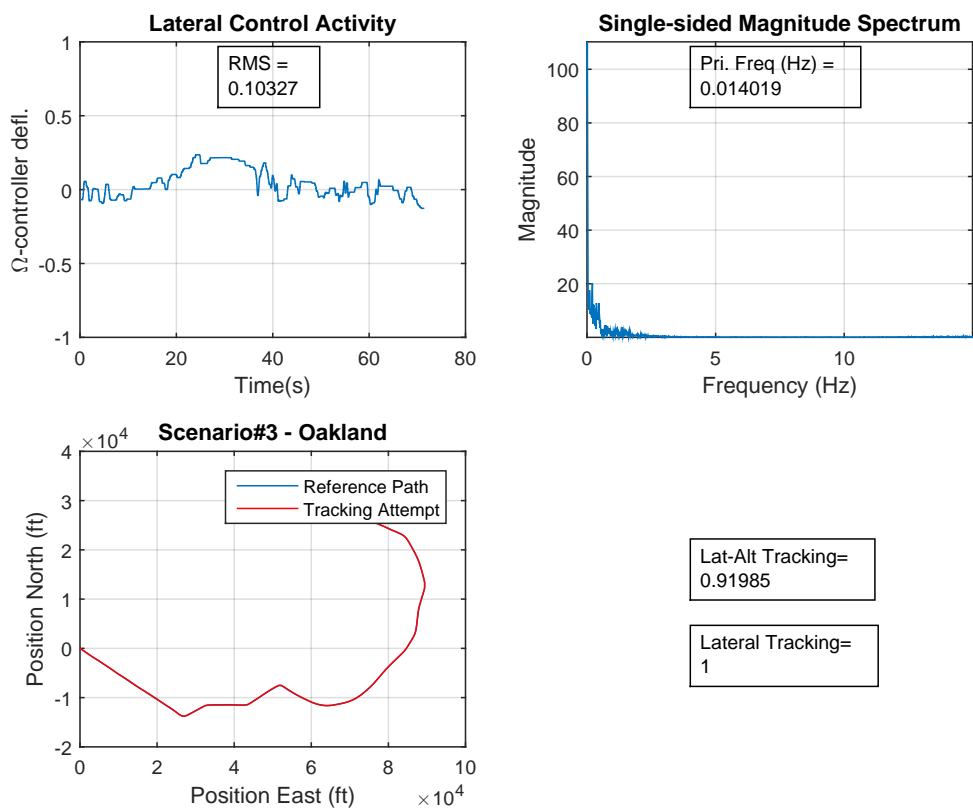
Figure A.44: Participant NP-2 Performance - Scenario 3

Figure A.45: Participant NP-3 Performance - Scenario 3

Figure A.46: Participant NP-4 Performance - Scenario 3

Figure A.47: Participant NP-5 Performance - Scenario 3

Figure A.48: Participant NP-6 Performance - Scenario 3

Figure A.49: Participant NP-7 Performance - Scenario 3

Figure A.50: Participant NP-8 Performance - Scenario 3

Figure A.51: Participant NP-9 Performance - Scenario 3

B. Time Histories of Control Law Modes

A series of simulation flights were captured to highlight each control mode. The following sections present observations for the relevant parameters recorded during each flight mode's operation.

B.1 Takeoff Mode Simulation Data

This section provides data from a takeoff run. The aircraft begins its ground roll and takes off remaining in Takeoff Mode throughout the flight. The data has been divided into four segments.

B.1.1 Takeoff Mode Flight - 1st Segment

A full power takeoff at 28 inHg of MAP is performed with the aircraft auto-rotating at t=26s. The aircraft tracks a 2 degree climb angle at t≈32s with no appreciable Ω - controller input. This results in a fairly benign rate of climb of approximately 300 ft/s. Inaccuracies from the ground reaction model introduce high frequency noise in the angular rates, accelerations, and, as a result, in the control surface deflections. This noise disappears once ground contact is 'false'.
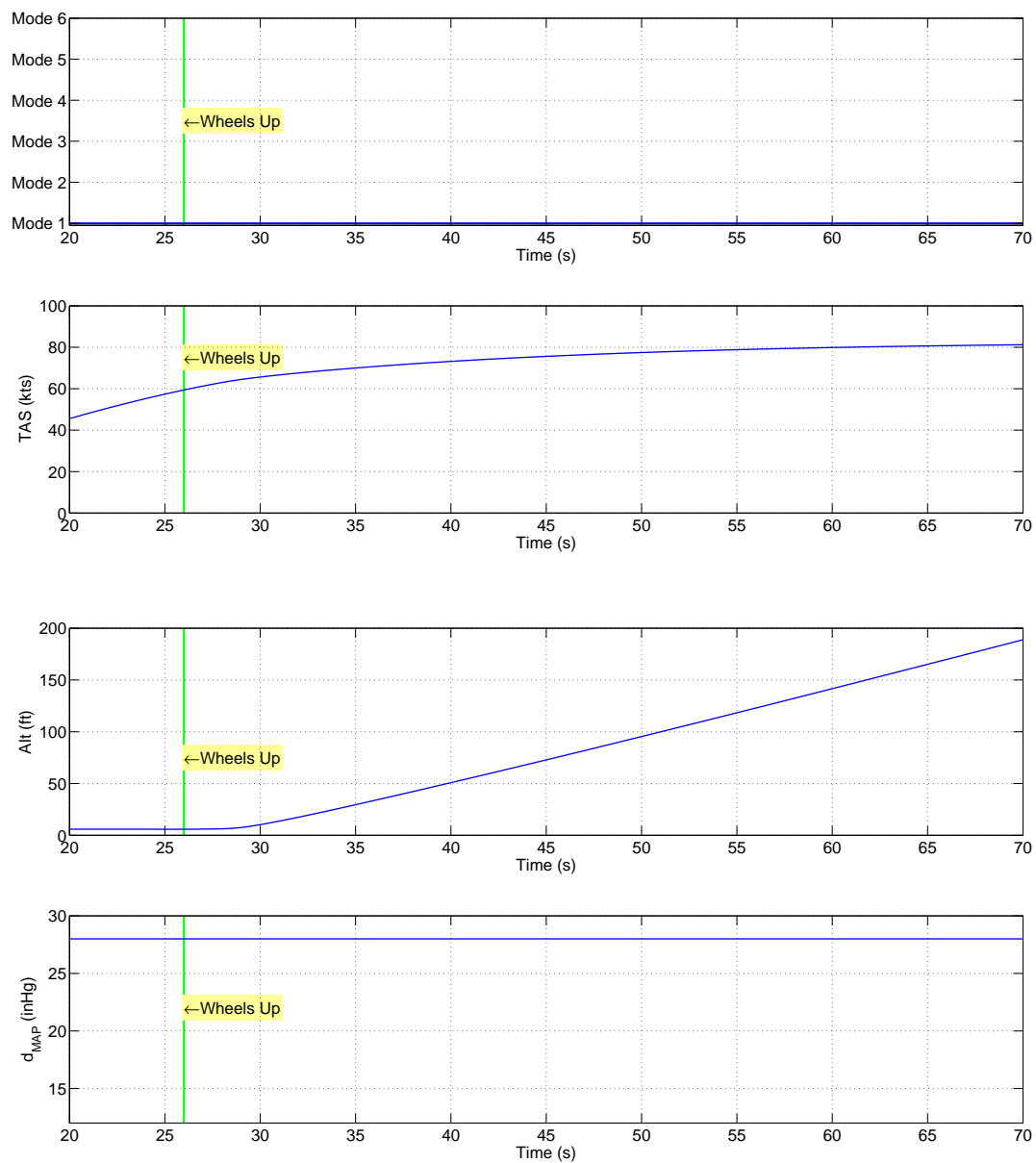
Figure B.1: Ground roll to T-O in mode 1
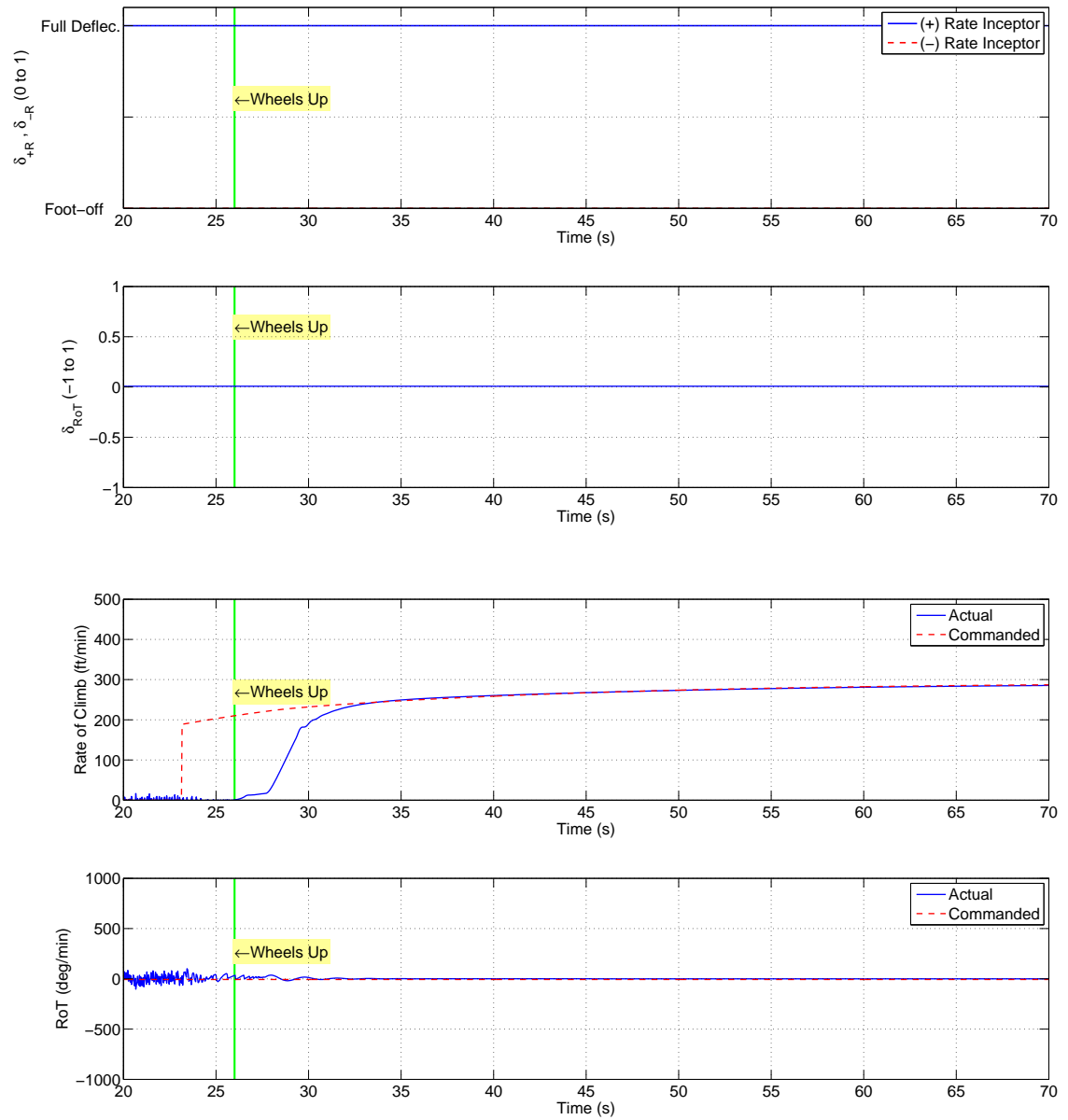
Figure B.2: Ground roll to T-O in mode 1
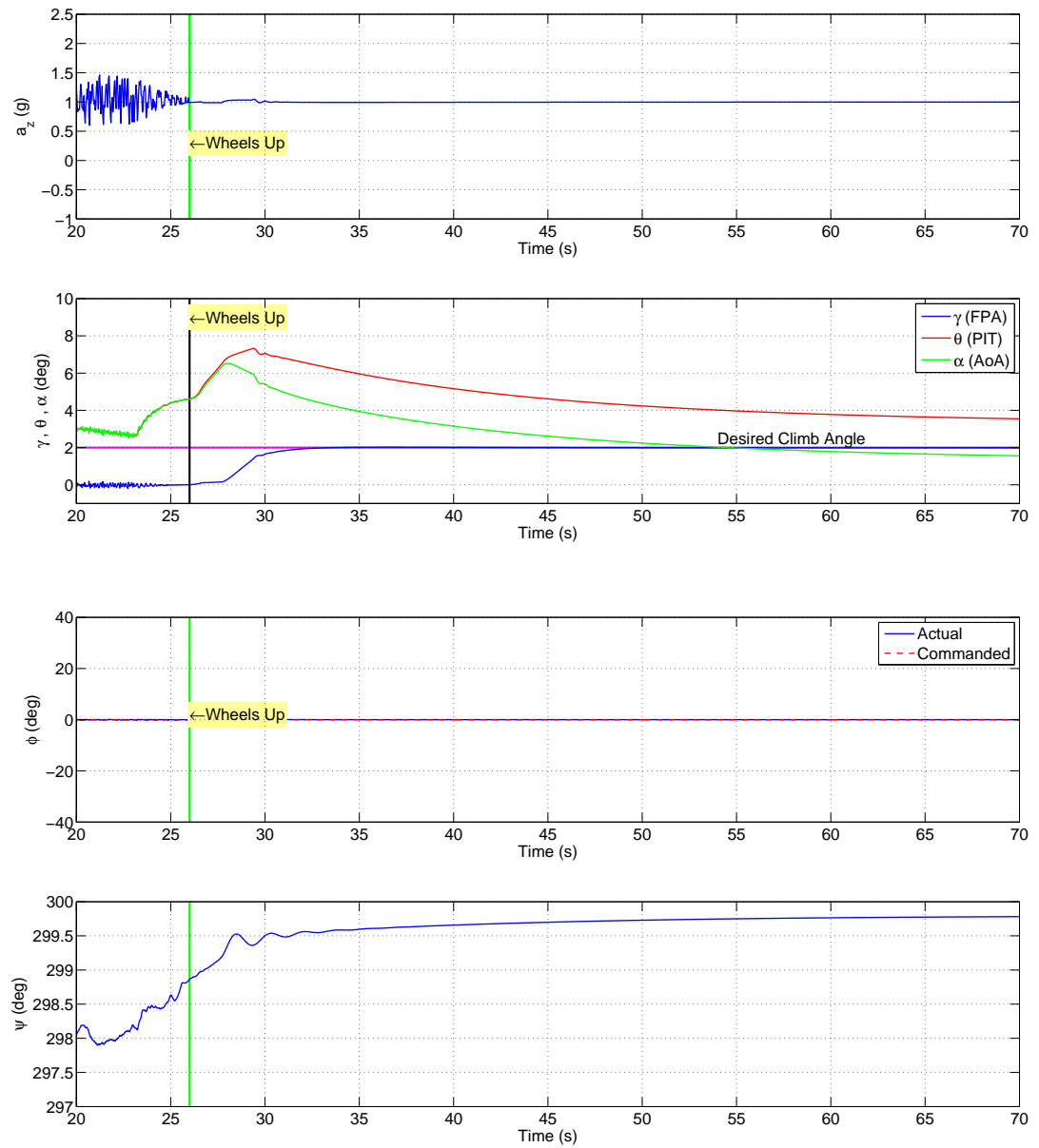
Figure B.3: Ground roll to T-O in mode 1
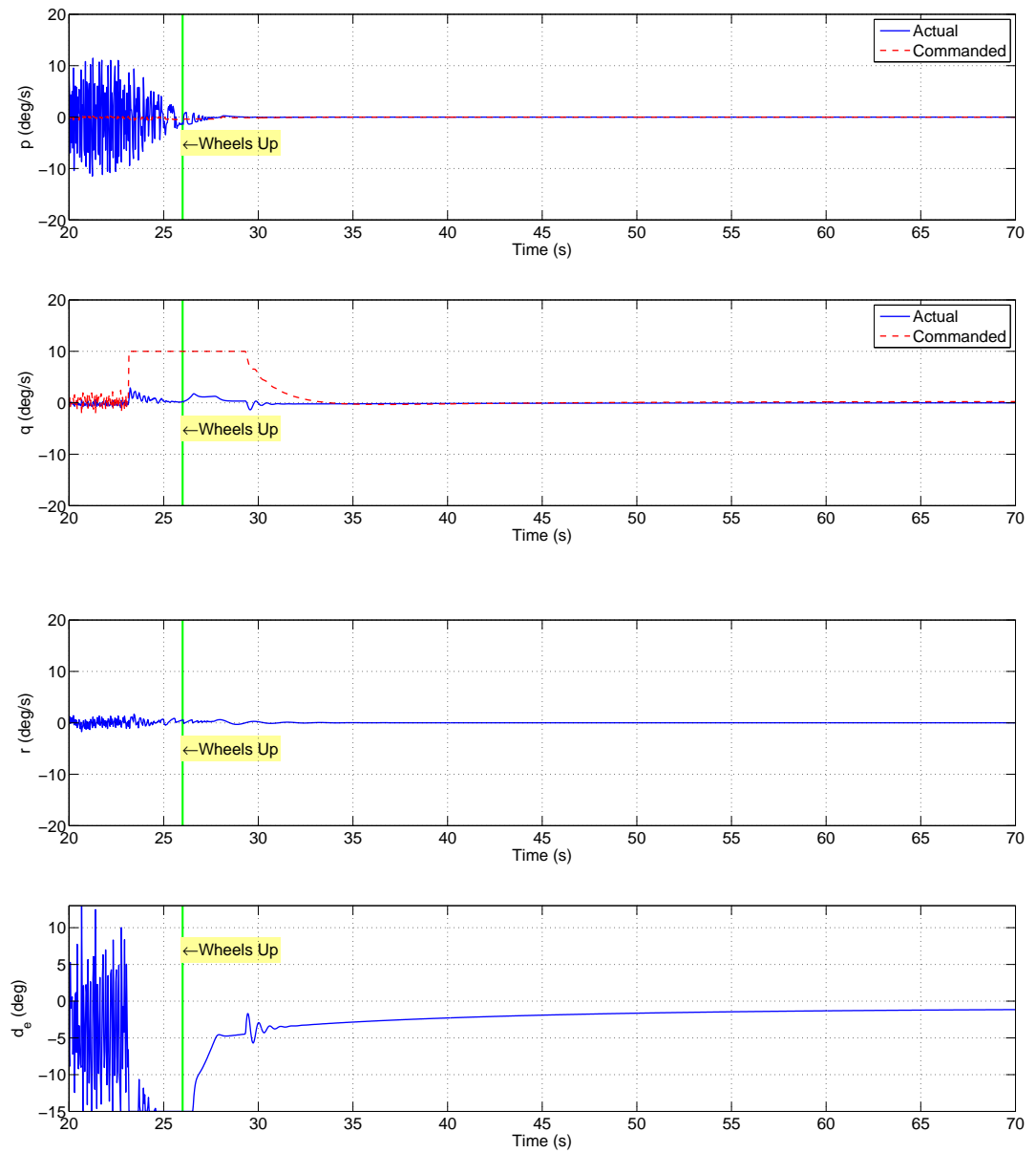
Figure B.4: Ground roll to T-O in mode 1
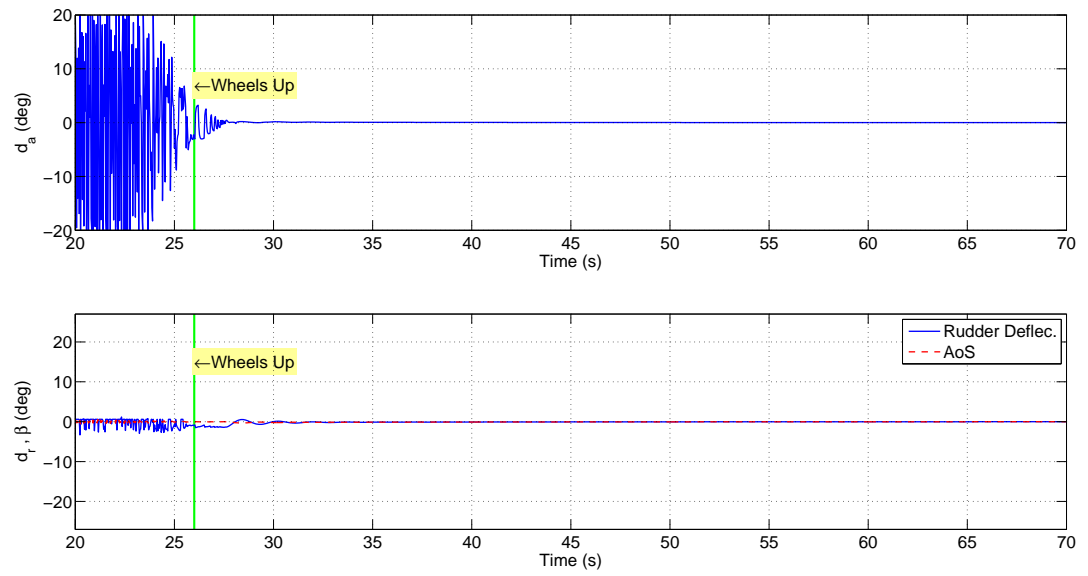
Figure B.5: Ground roll to T-O in mode 1

B.1.2   Takeoff Mode Flight - 2nd Segment

Following climb-out a minimum RoT (44% of a standard rate turn) to the right

is commanded while in Takeoff Mode while maintaining the 2 degree climb angle.
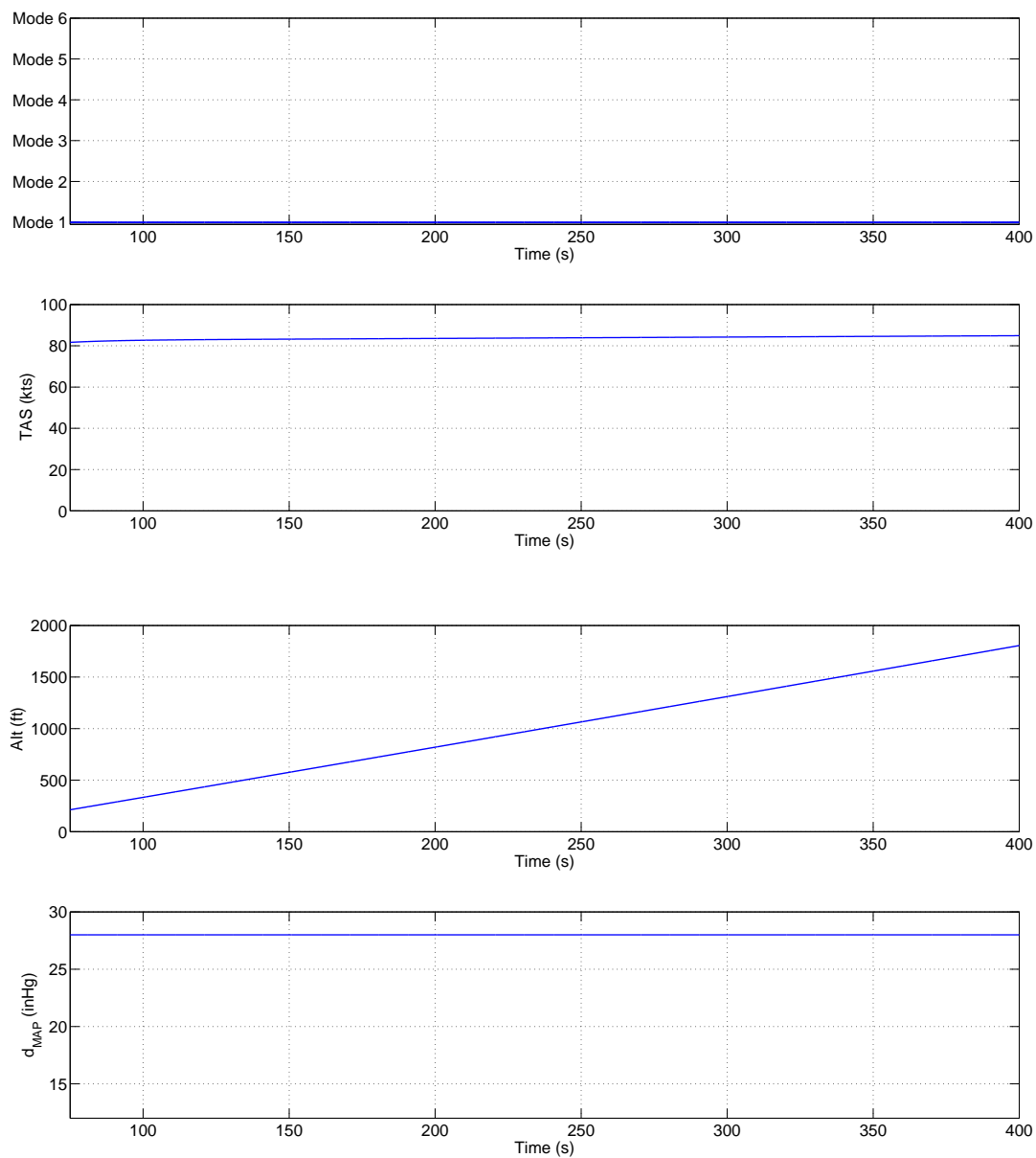
Figure B.6: Minimum RoT maneuver in mode 1
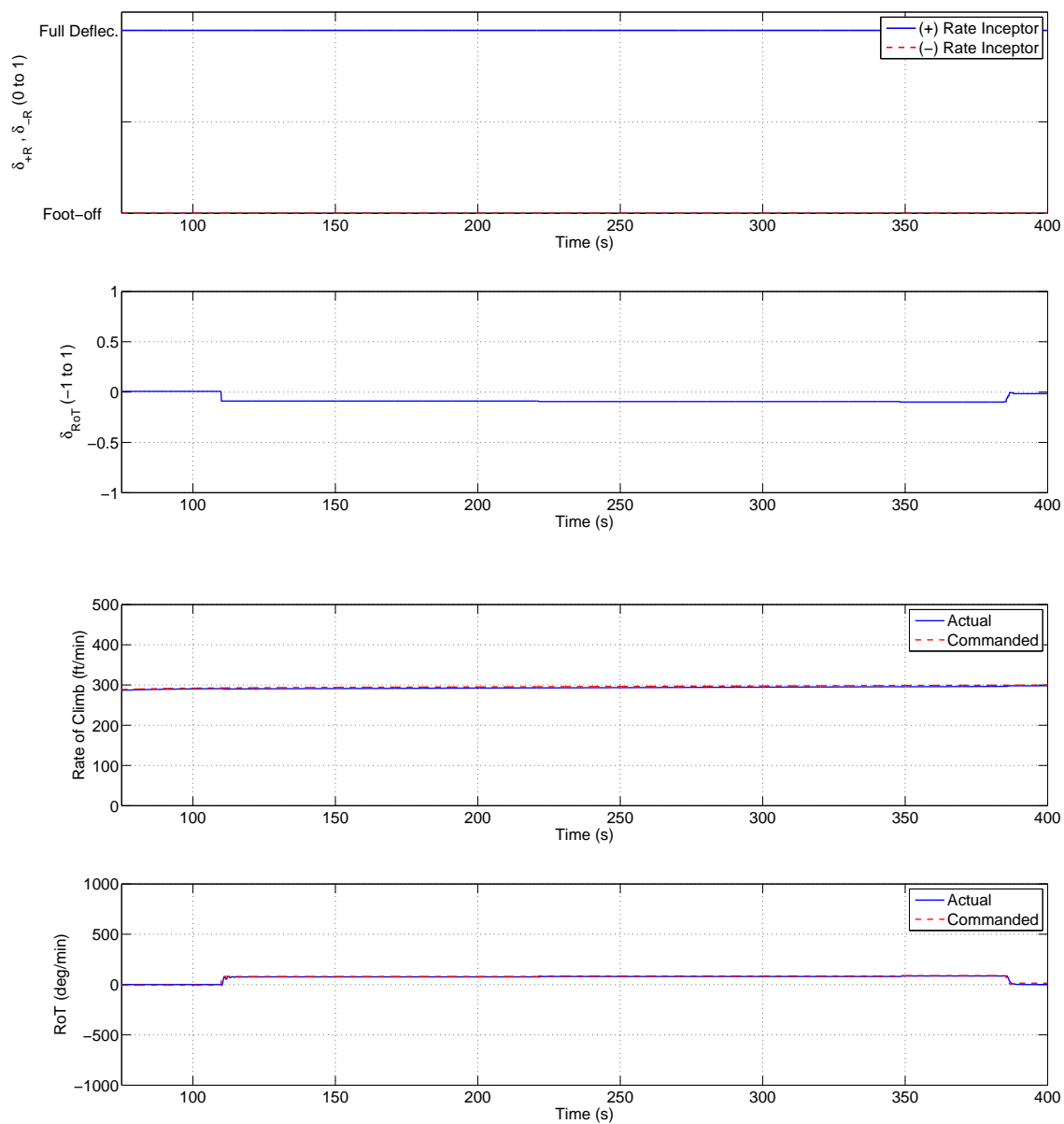
Figure B.7: Minimum RoT maneuver in mode 1
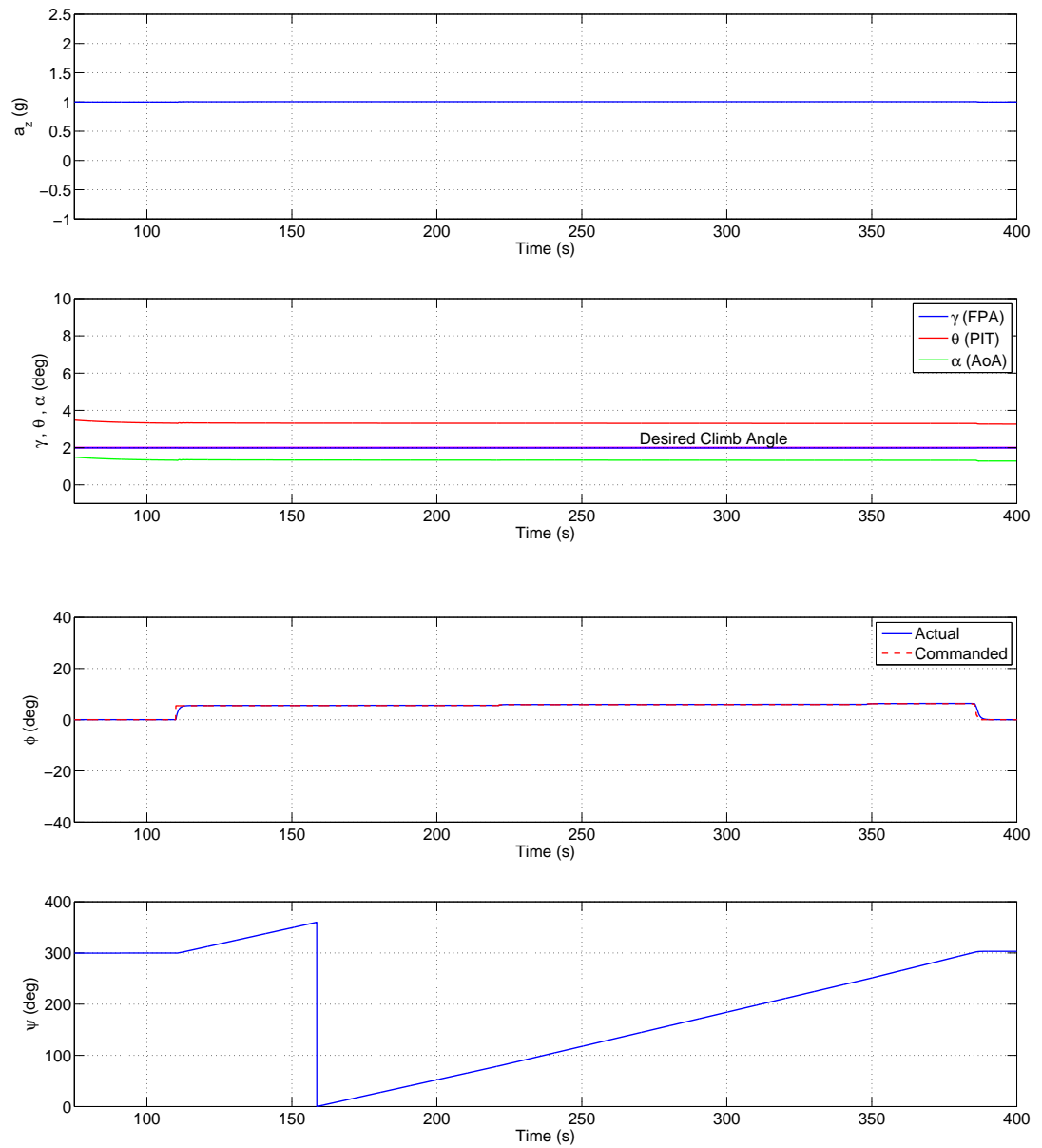
Figure B.8: Minimum RoT maneuver in mode 1
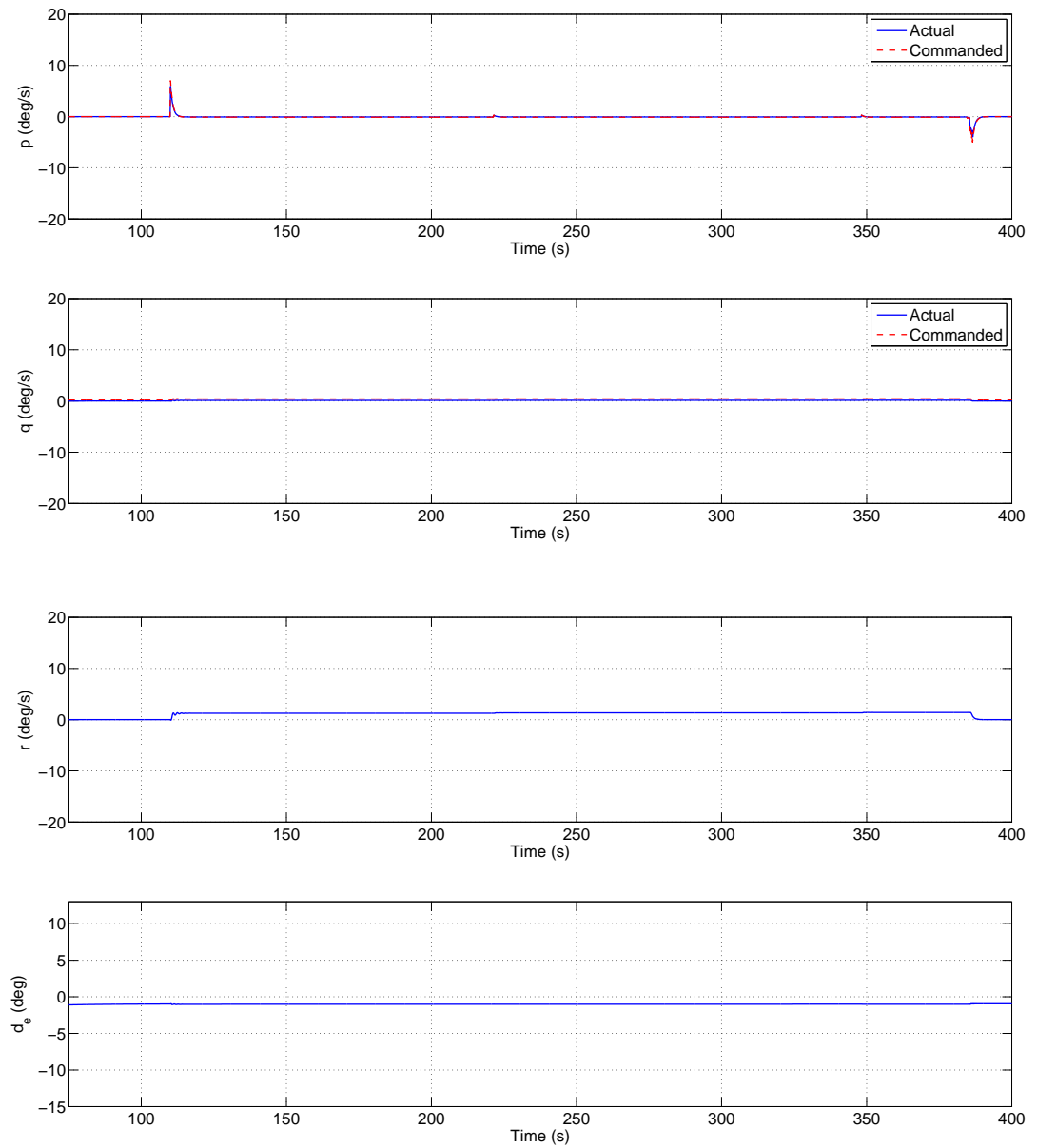
Figure B.9: Minimum RoT maneuver in mode 1
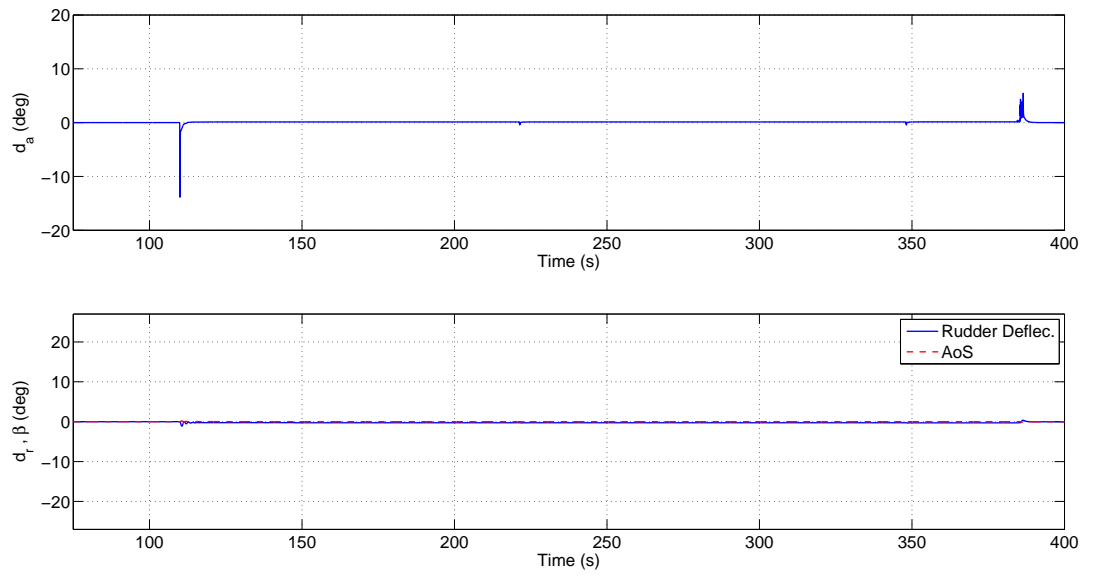
Figure B.10: Minimum RoT maneuver in mode 1

B.1.3 Takeoff Mode Flight - 3rd Segment

A second right turn is performed with the Ω-controller commanding a 600 deg/min RoT. However, due to a 25 degree bank angle limit imposed in Takeoff Mode the effective RoT is reduced to 360 deg/min as shown in the RoT or ψ trace. The climb angle remains at 2 degrees.
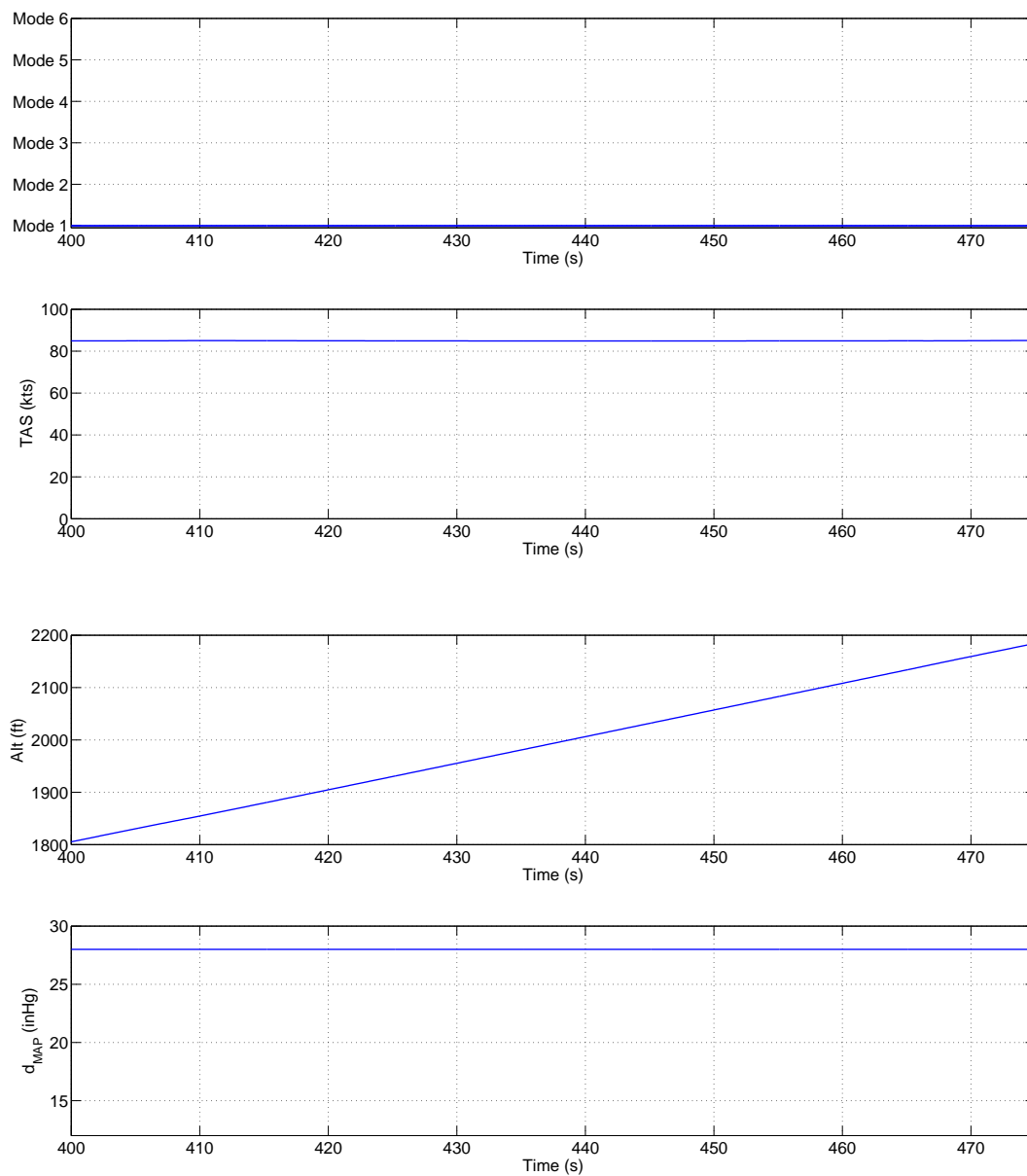
Figure B.11: Climbing to T-O in mode 1
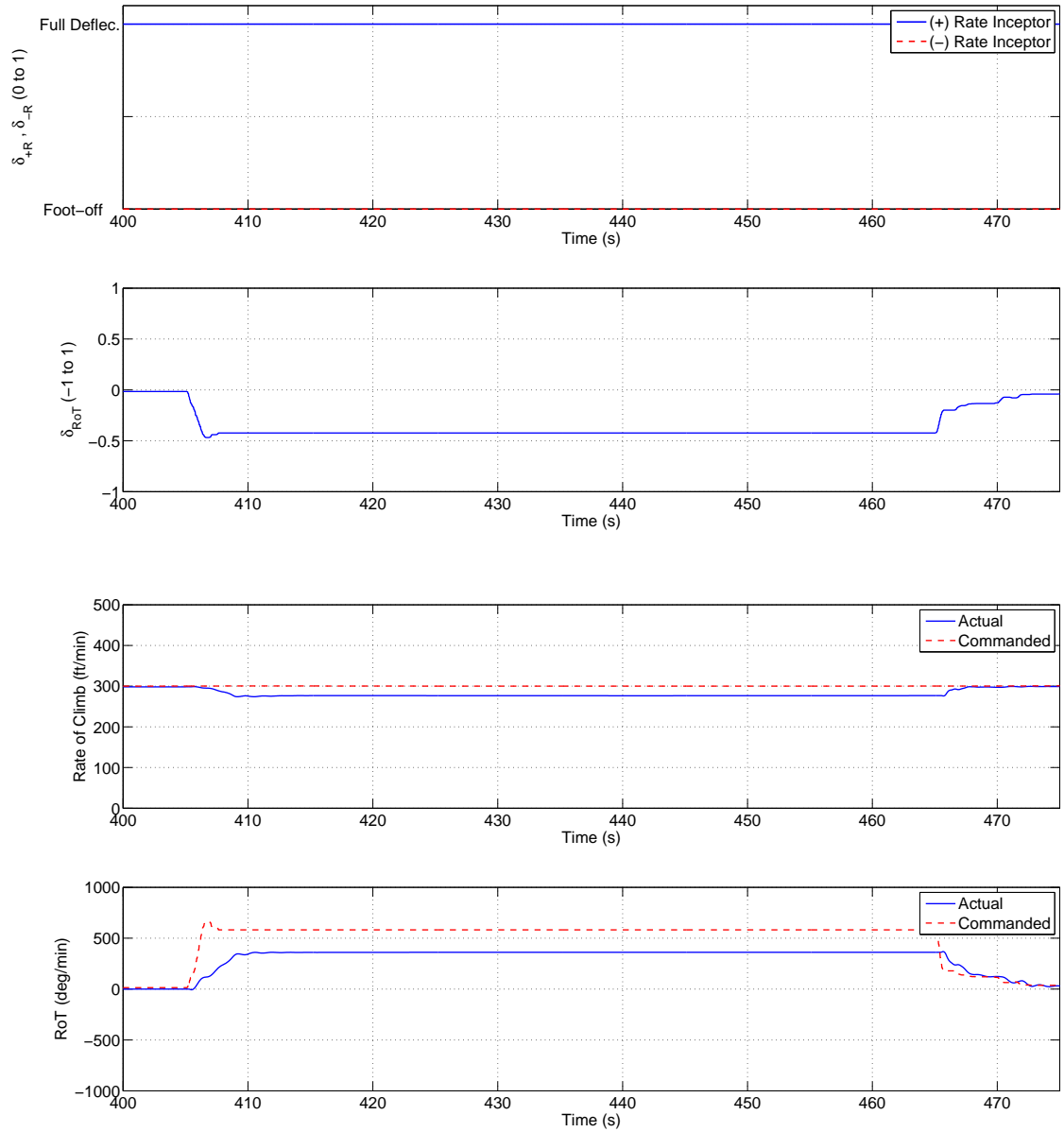
Figure B.12: Climbing to T-O in mode 1
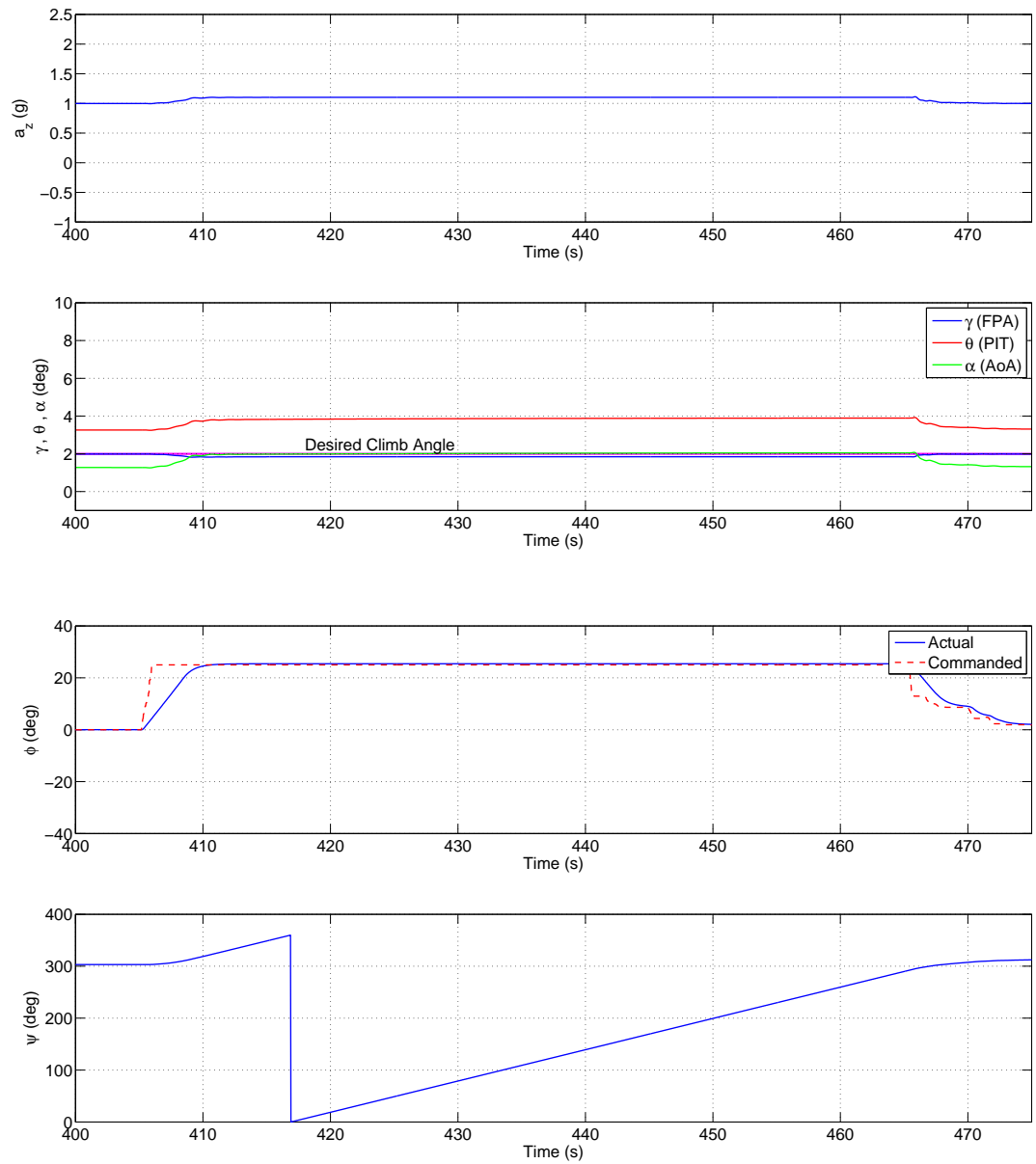
Figure B.13: Climbing to T-O in mode 1
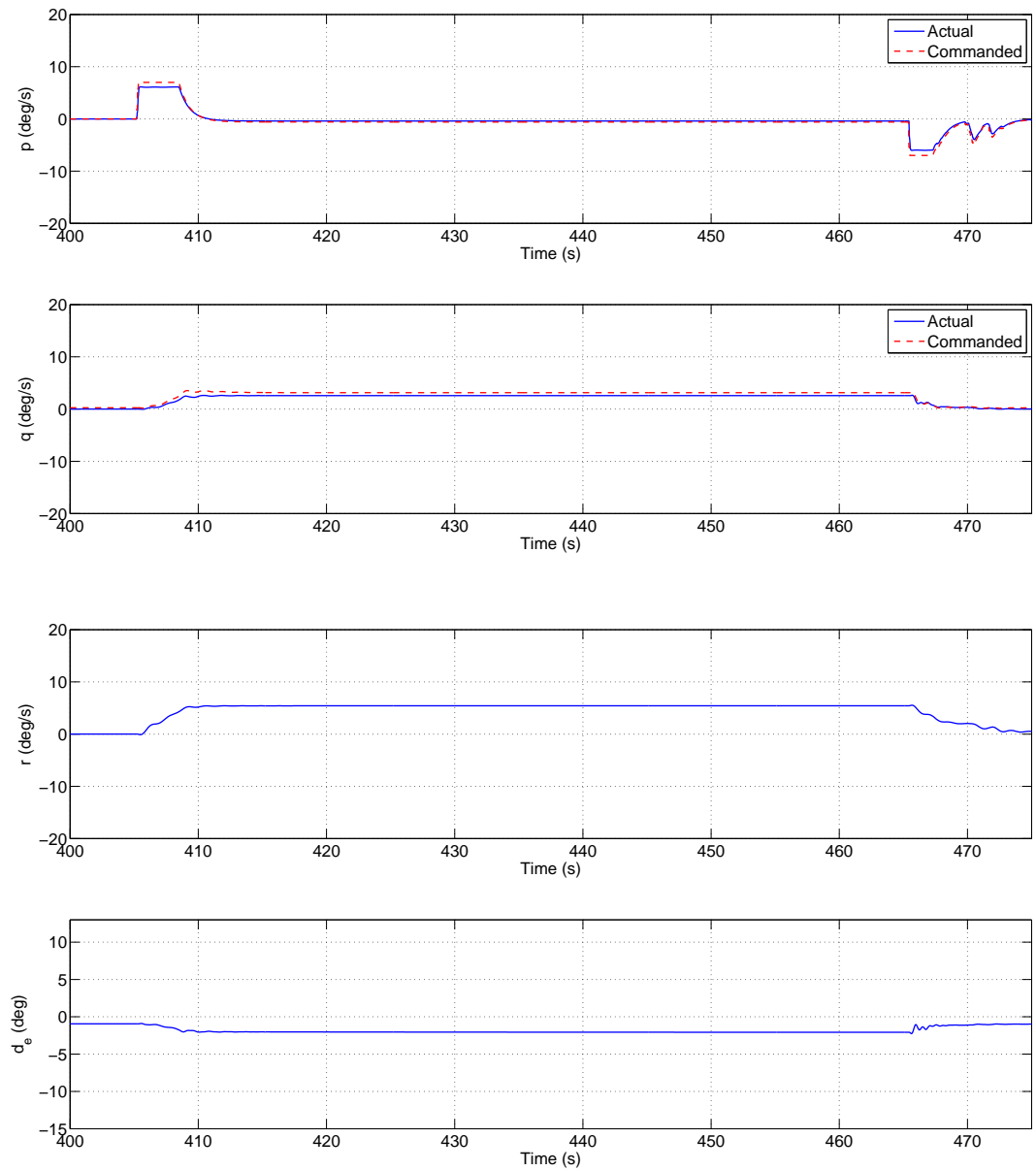
Figure B.14: Climbing to T-O in mode 1
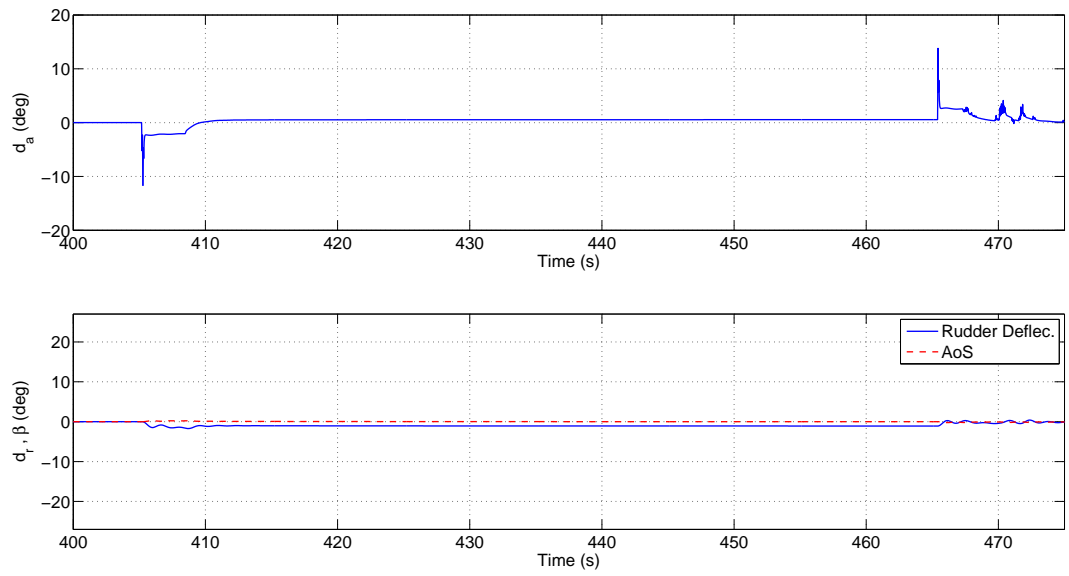
Figure B.15: Climbing to T-O in mode 1

B.1.4 Takeoff Mode Flight - 4th Segment

The final maneuver was a left turn performed at standard rate. Again, the aircraft maintained the commanded 2 degree climb angle. Figure 4.20 provides a ground track for all three turning maneuvers performed in the Takeoff Mode.
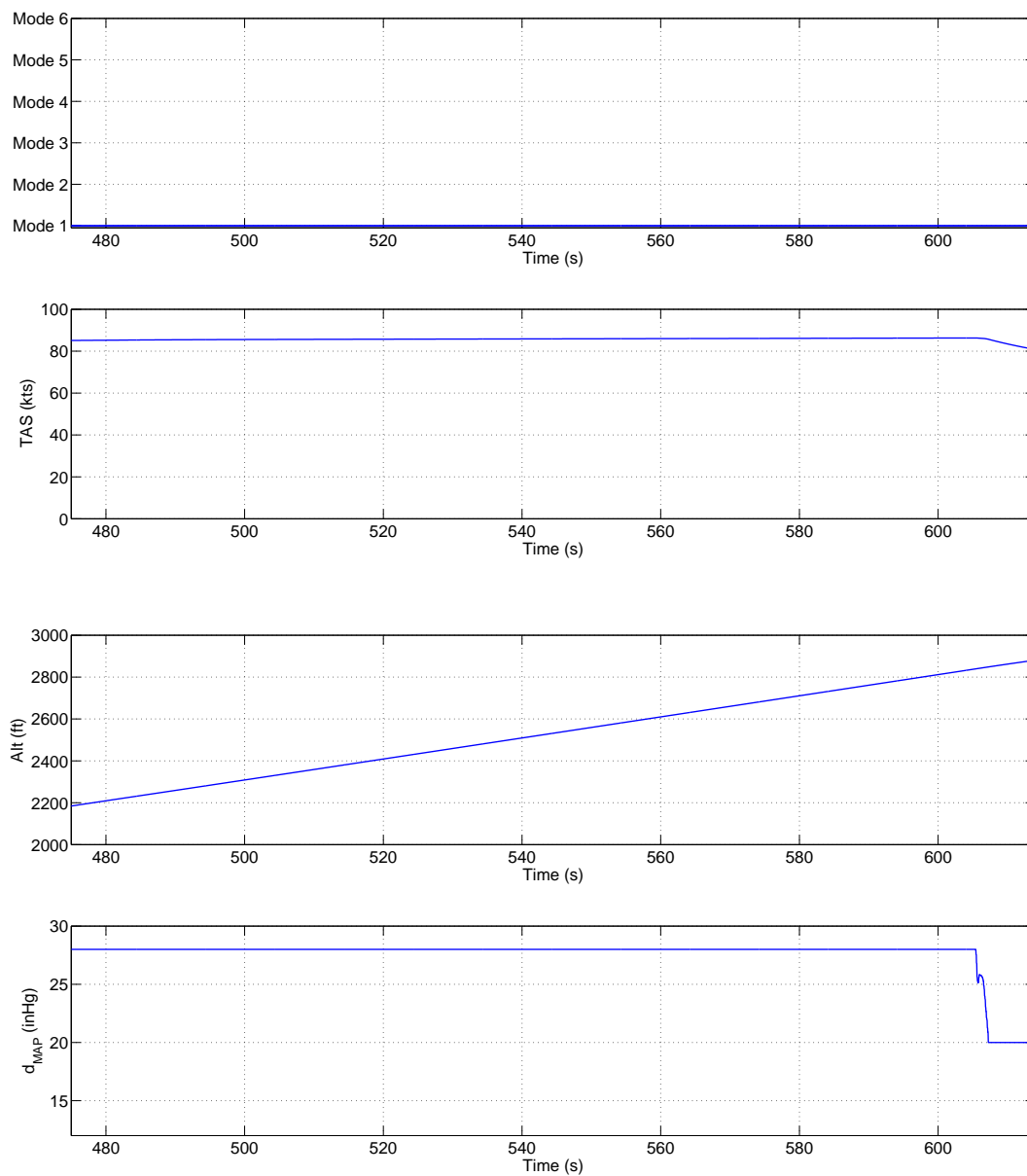
Figure B.16: Climbing to T-O in mode 1
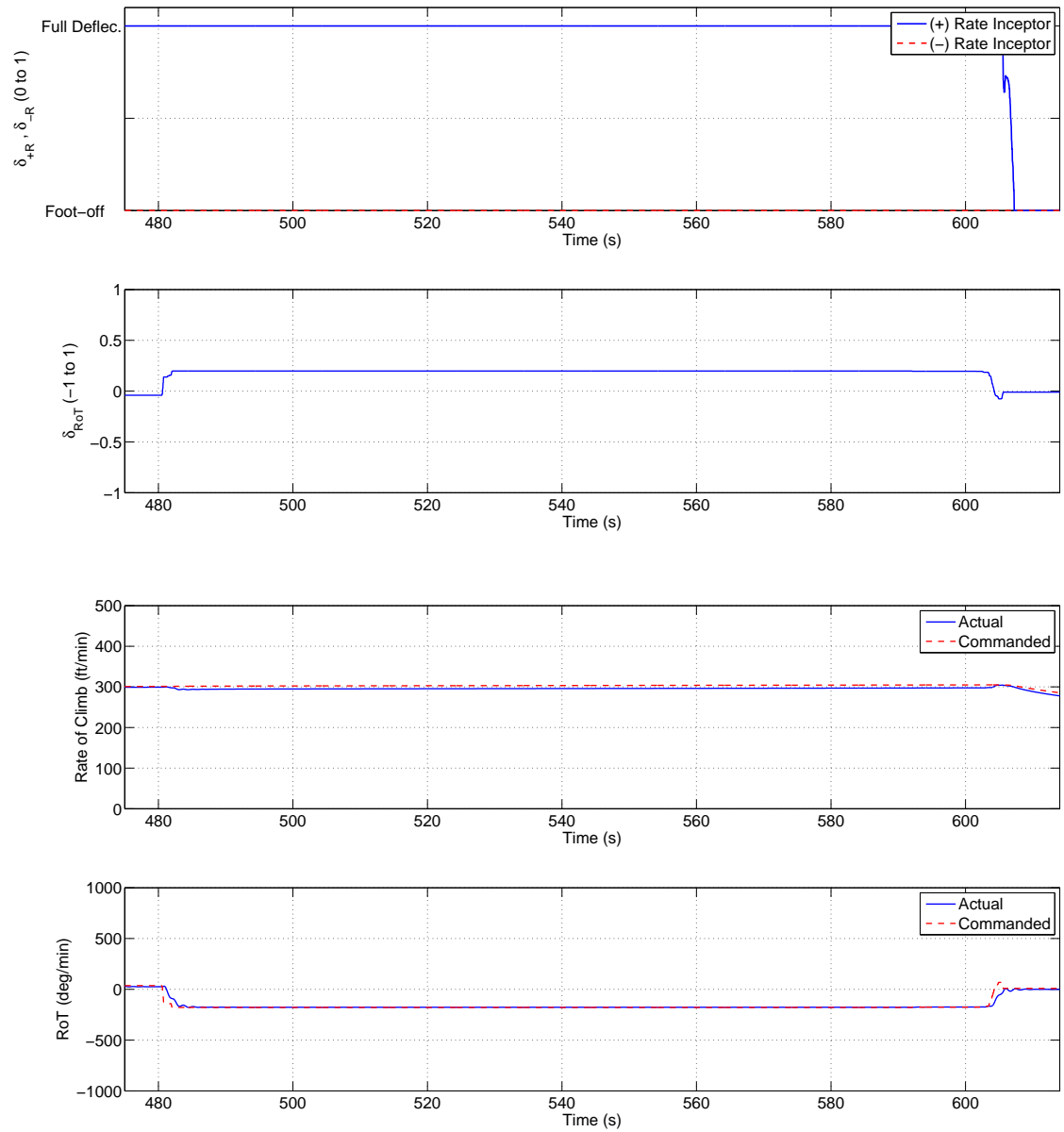
Figure B.17: Climbing to T-O in mode 1
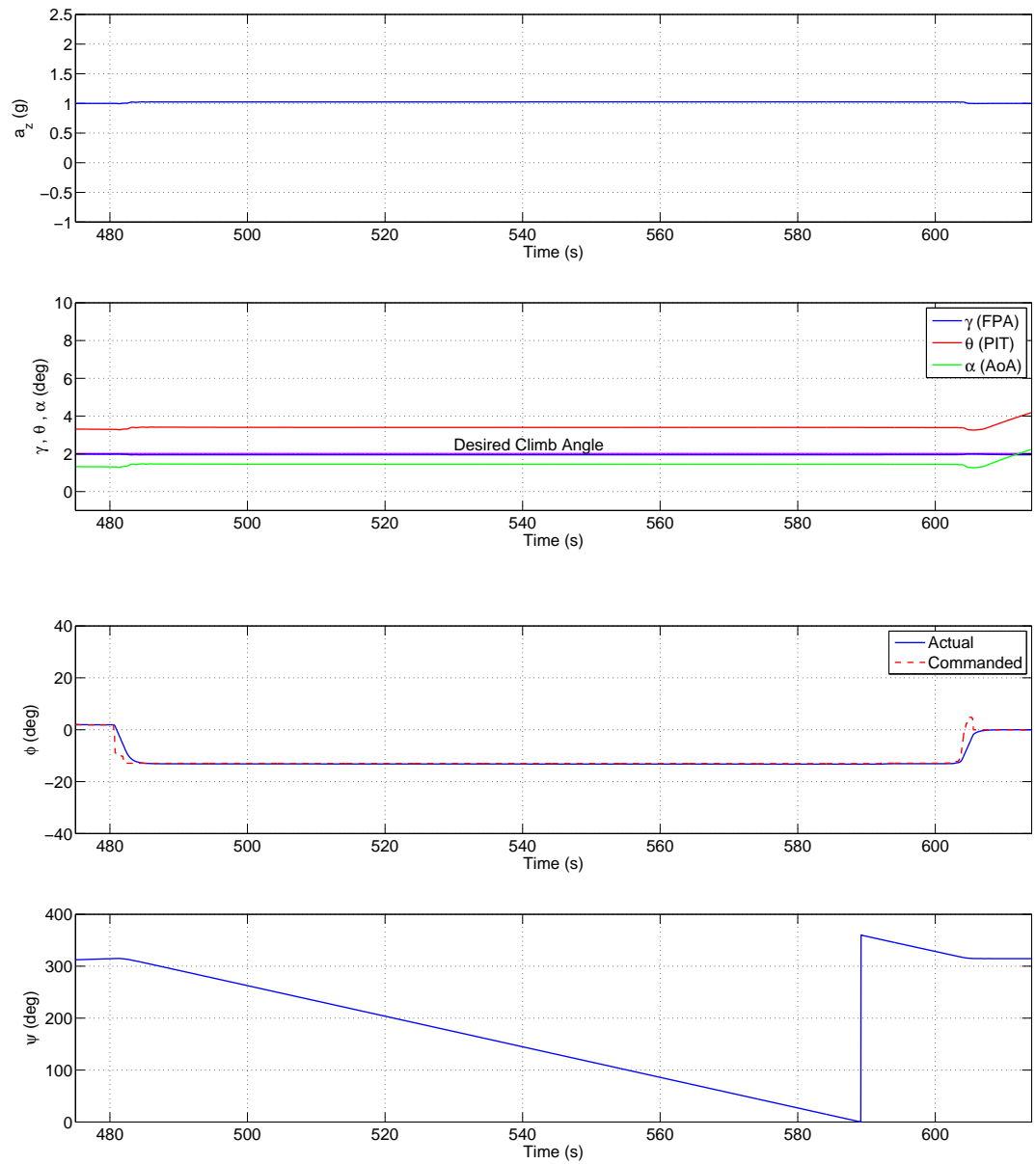
Figure B.18: Climbing to T-O in mode 1
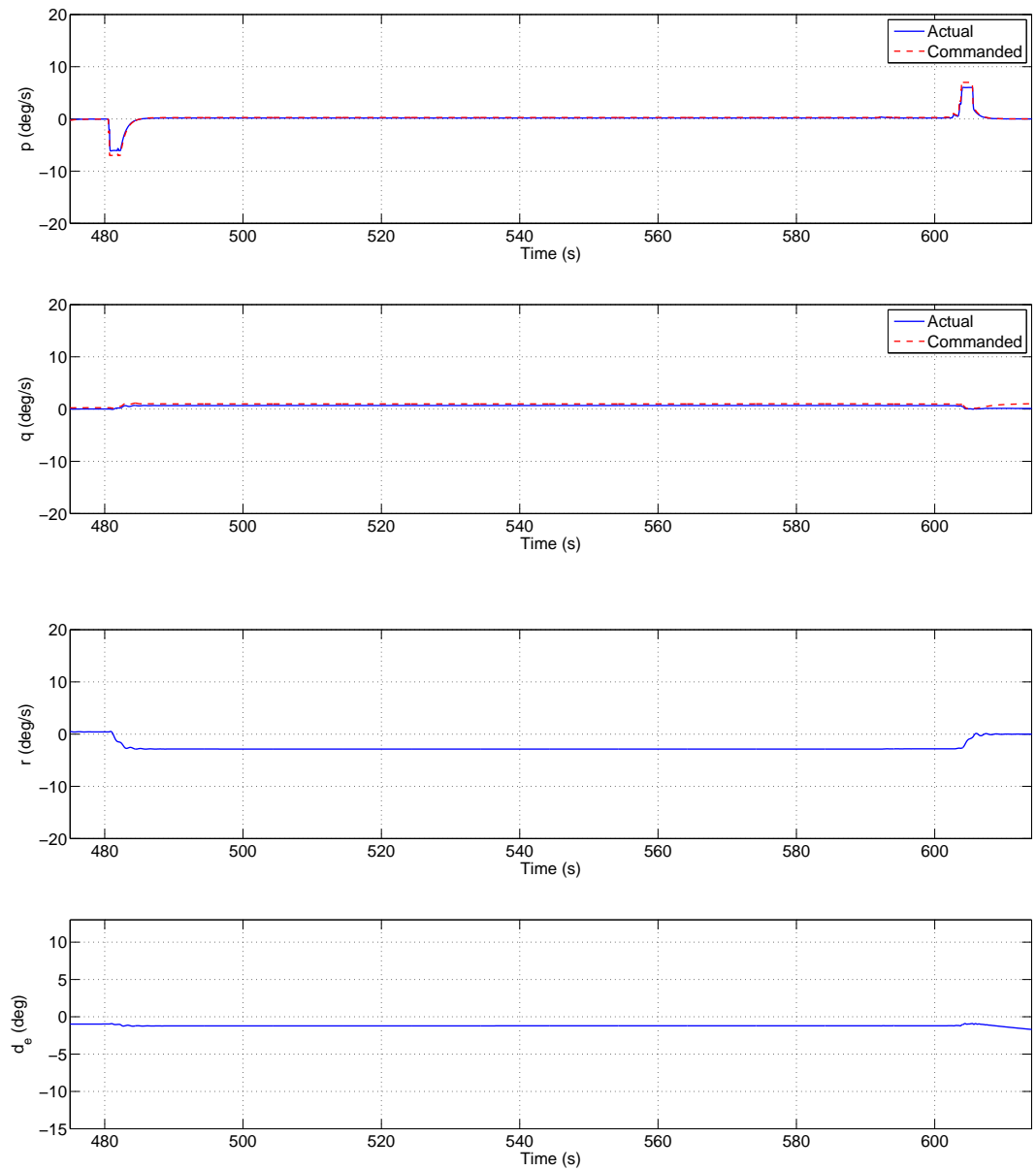
Figure B.19: Climbing to T-O in mode 1
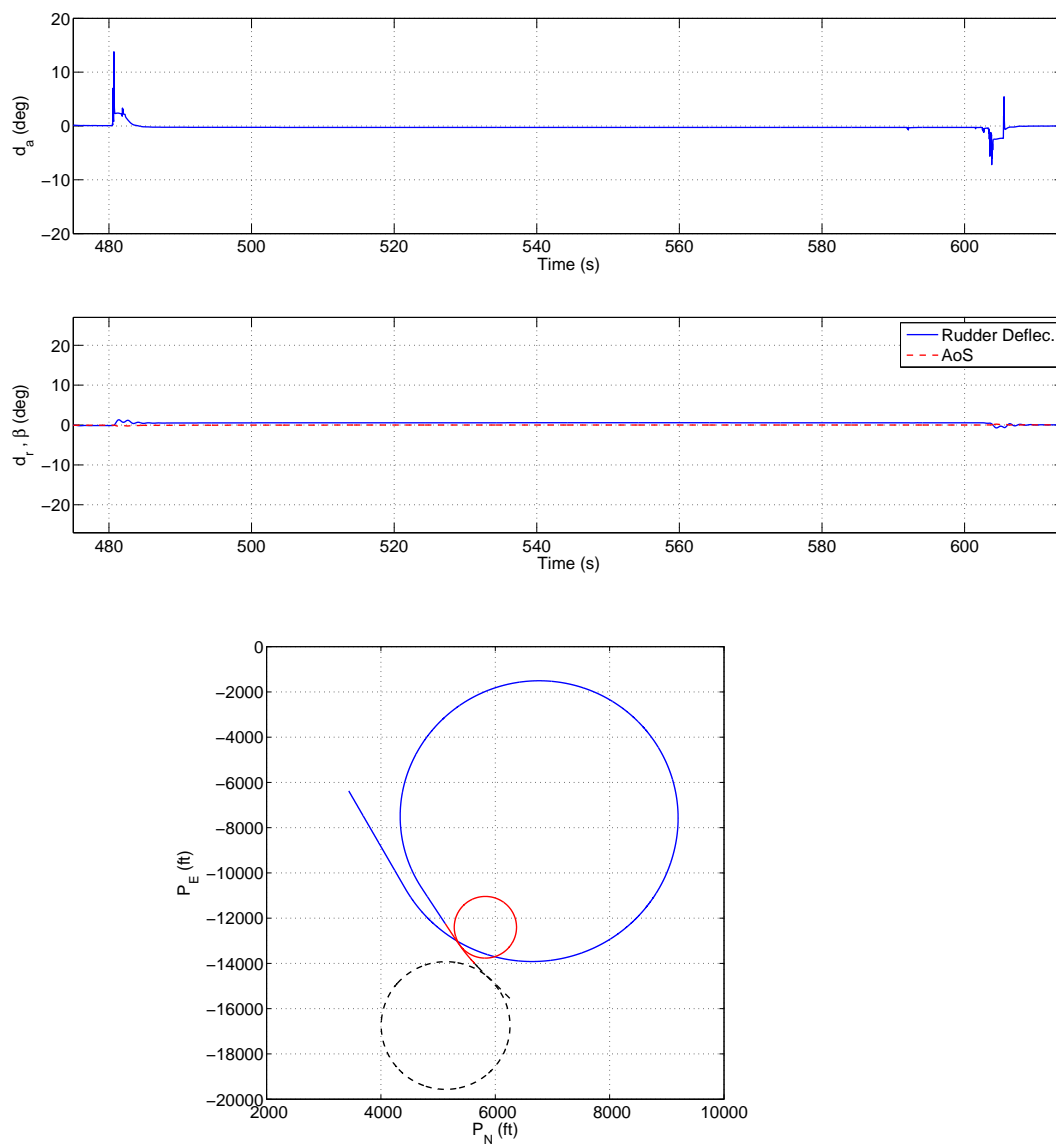
Figure B.20: Climbing to T-O in mode 1

B.2 Climb Mode Simulation Data

Similar to the Takeoff Mode data, the Climb Mode results have been divided into segments as well. Sections 4.2.1-4.2.3 illustrate a steady heading climb, variable RoT climbs with no δ_{+R} or δ_{-R} inceptor deflections, and variable RoT climbs with full δ_{+R} input.

B.2.1 Climb Mode Flight - 1st Segment

The data begins with the aircraft in Mode 2 (Climb Mode) maintaining a baseline RoC of 300 ft/min. Around the 20 second mark, a full deflection of the δ_{+R} inceptor commands a 480 ft/min RoC. This is followed by an increase in MAP which subsides with the increase in pitch angle, θ, and reduced airspeed. Figures B.22 and B.24 indicate a failure to capture the commanded RoC and pitch rate, q. The result is a 470 ft/s maximum climb rate.

Past the 160 second mark, the δ_{-R} inceptor is fully deflected to command level flight (RoC = 0 ft/s). Within 9 seconds the aircraft decreases its RoC from the 300 ft/min baseline value, to $\approx$ 3 ft/min. See Figure B.22.

Since the Simulink code did not include actuator models representative of a typical mechanical system for any given control surface, the elevator response can be seen in Figure B.24 as a high frequency signal driven purely by the LQR control gains.
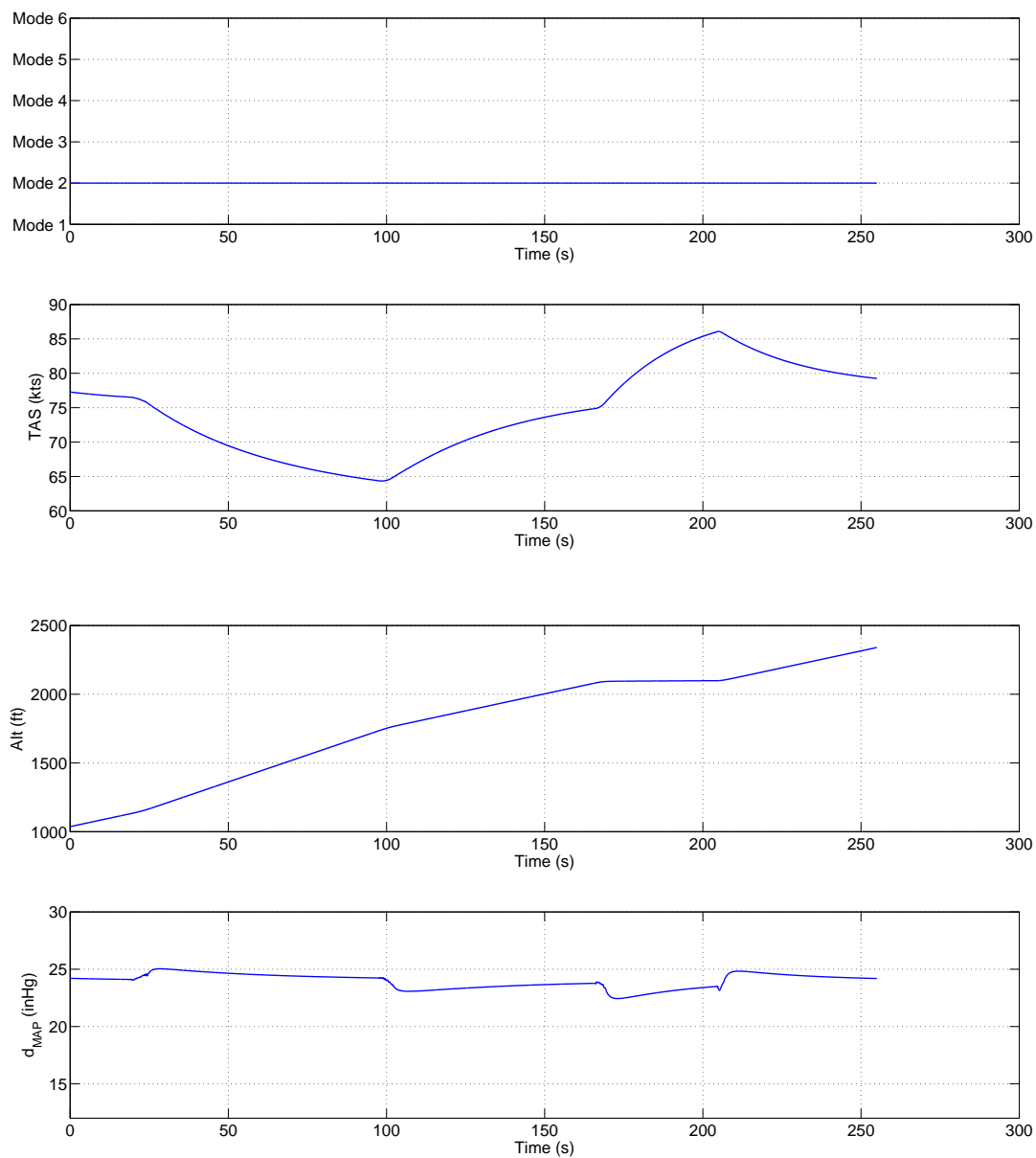
Figure B.21: Climbing in mode 2
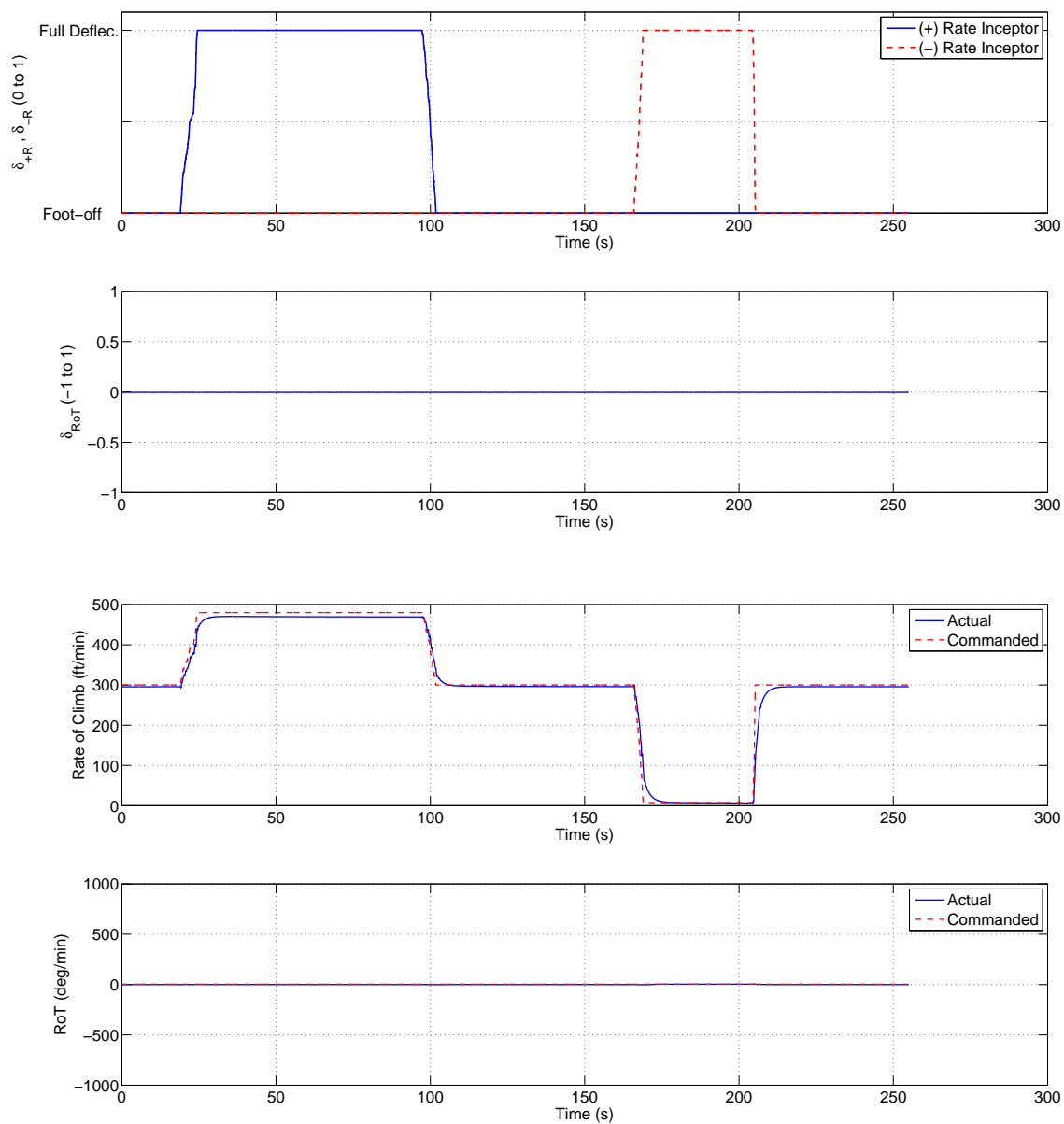
Figure B.22: Climbing in mode 2
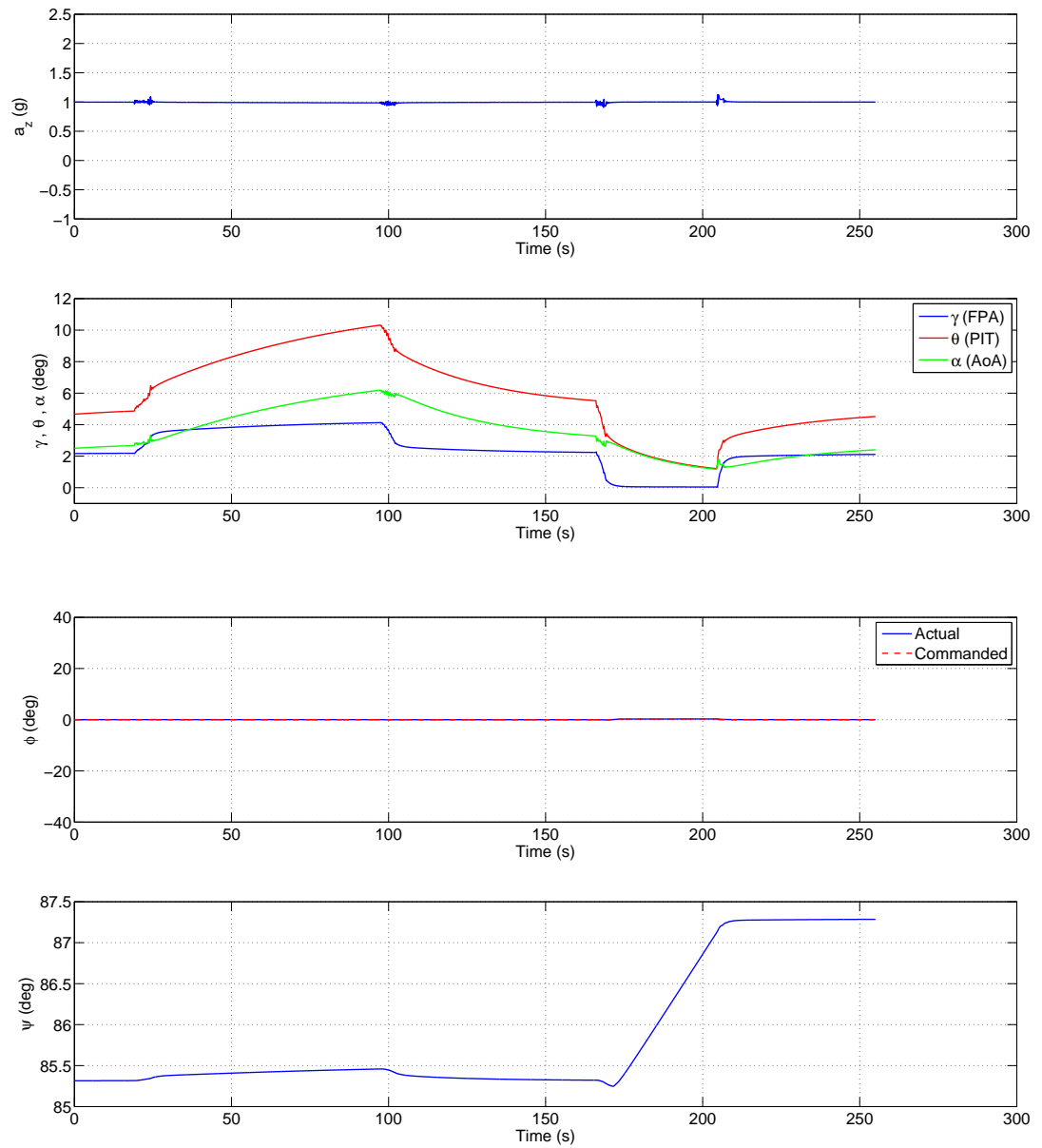
Figure B.23: Climbing in mode 2
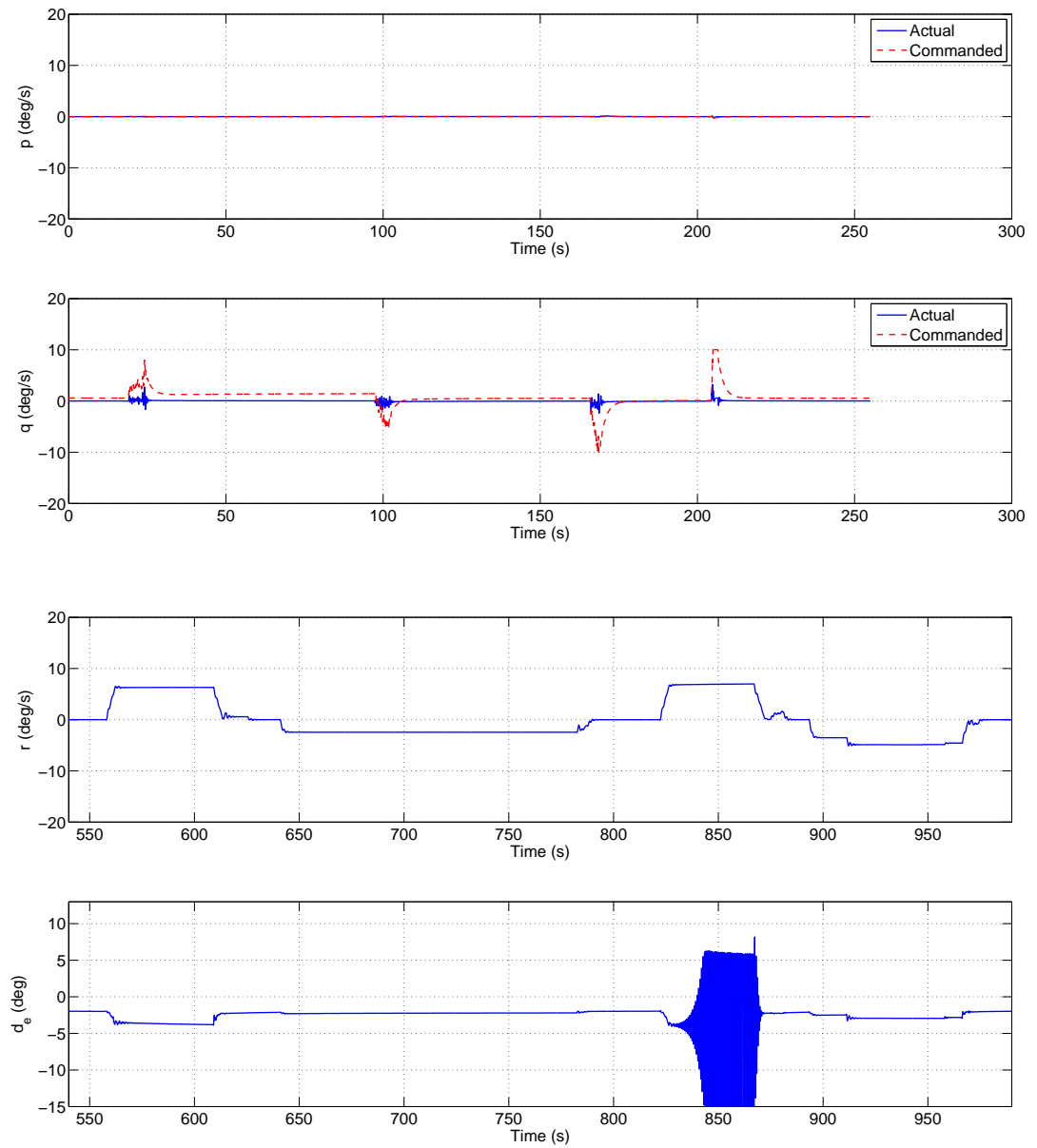
Figure B.24: Climbing in mode 2
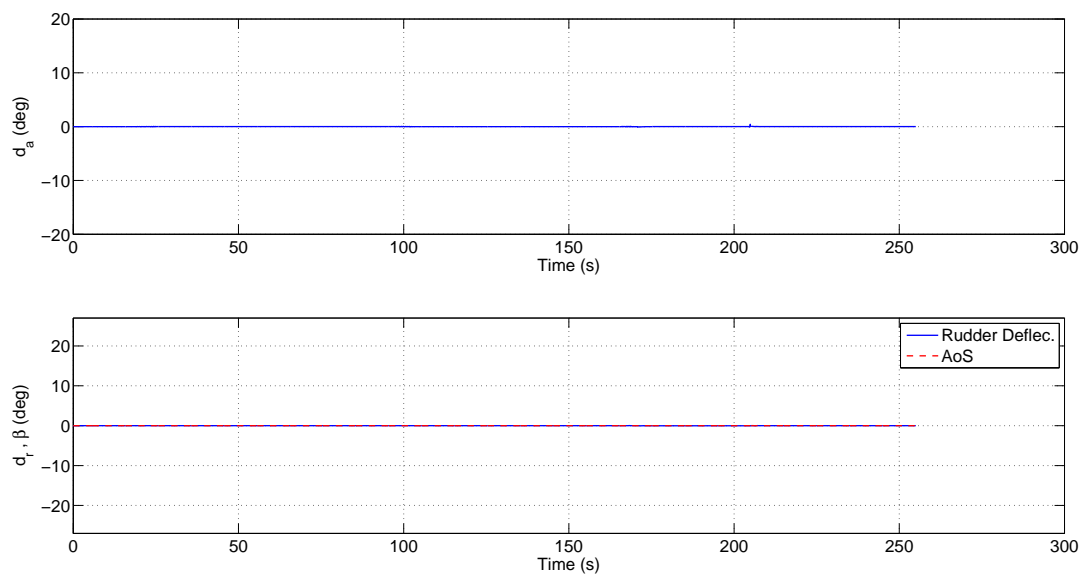
Figure B.25: Climbing in mode 2

B.2.2 Climb Mode Flight 2nd Segment

A second segment is presented below illustrating turning performance while climbing. Four complete 360 degree turns are attempted with varying δ_{RoT} inputs. The aircraft attempts to maintain the baseline 300 ft/min RoC without any δ_{+R} and δ_{+R} pilot input.

The first input ($\approx 33\%$ deflection) at t $= 557$s to the Ω-controller commands a 420 deg/min right turn which results in a 27 degree bank allowing the aircraft to complete a full circle in ≈ 53 seconds. The turning maneuver reduces the effective RoC to 268 ft/min. With the Ω-controller centered, the aircraft reestablishes its baseline RoC and new bank angle in ≈ 3 seconds and 4.5 seconds, respectively. See Figures B.27 and B.28.

At t $= 640$s, a second, left-hand turn is performed. The Ω-controller is deflected $\approx 17\%$ of its maximum range resulting in a 152 deg/min RoT with a 10 degree bank angle. This shallower turn results in the aircraft maintaining a ≈ 292 ft/min climb rate. The full turn takes ≈ 147 seconds.

With a maximum deflection of the Ω-controller, a 900 deg/min RoT is commanded (5x standard rate turn). As the RoT approaches 500 deg/min the aircraft enters an aggressive longitudinal oscillation. The oscillation grows into a constant frequency response seen in the RoC, RoT, q, and δ_e data traces in Figures B.27 and B.29. This particular oscillation was not observed during human factors testing as pilots avoided

sustained maximum deflections of the Ω-controller. Releasing the controller mitigated the issue with the aircraft returning to wings-level climbing flight.

The last turn is a $\approx 25\%$ deflection of the Ω-controller resulting in a 315 deg/min RoT with a 21 degree bank angle. As expected, the RoC drops to 280 ft/min; a value between that observed for RoC in the first and second turns. The complete turn takes 74 seconds.
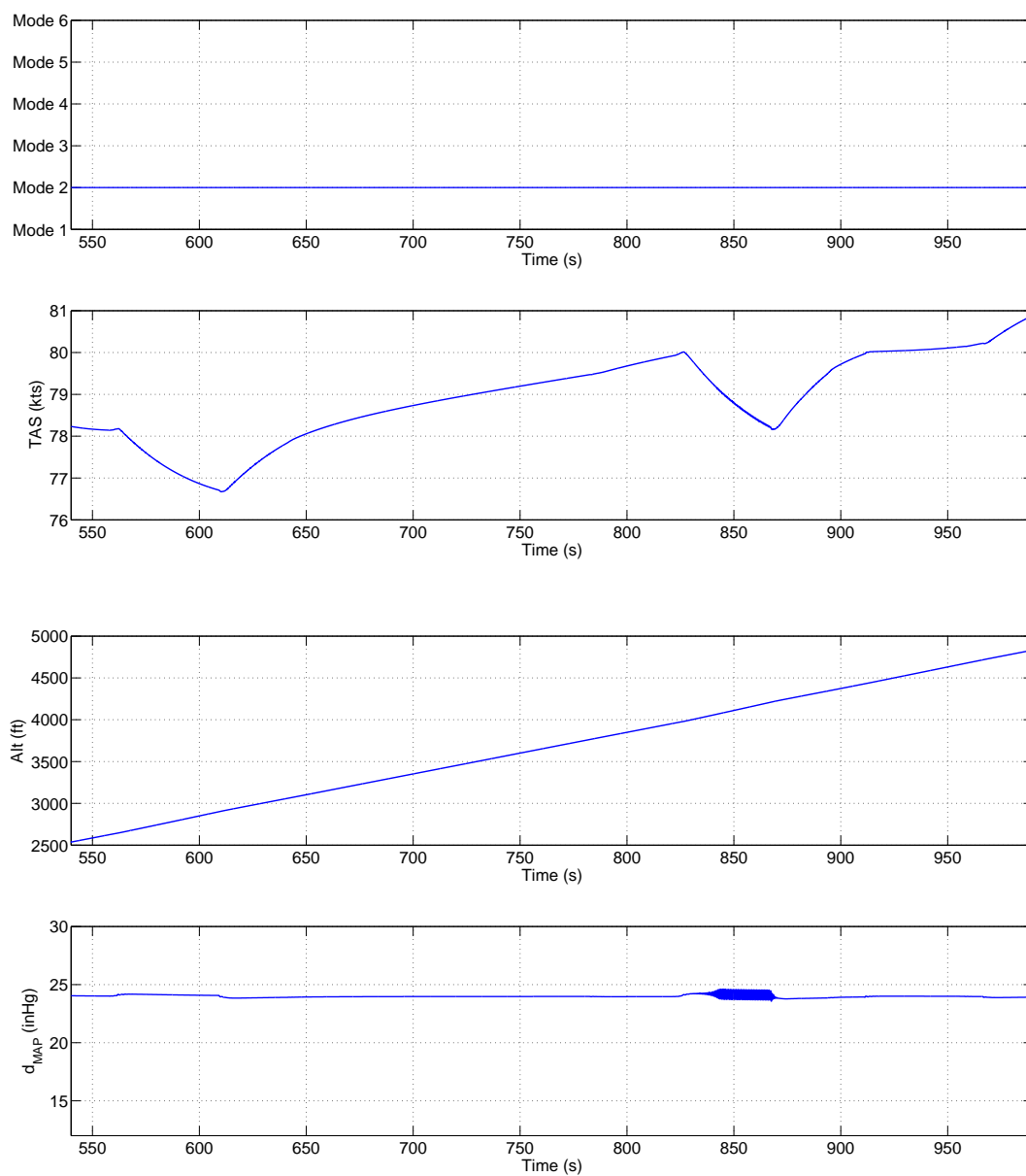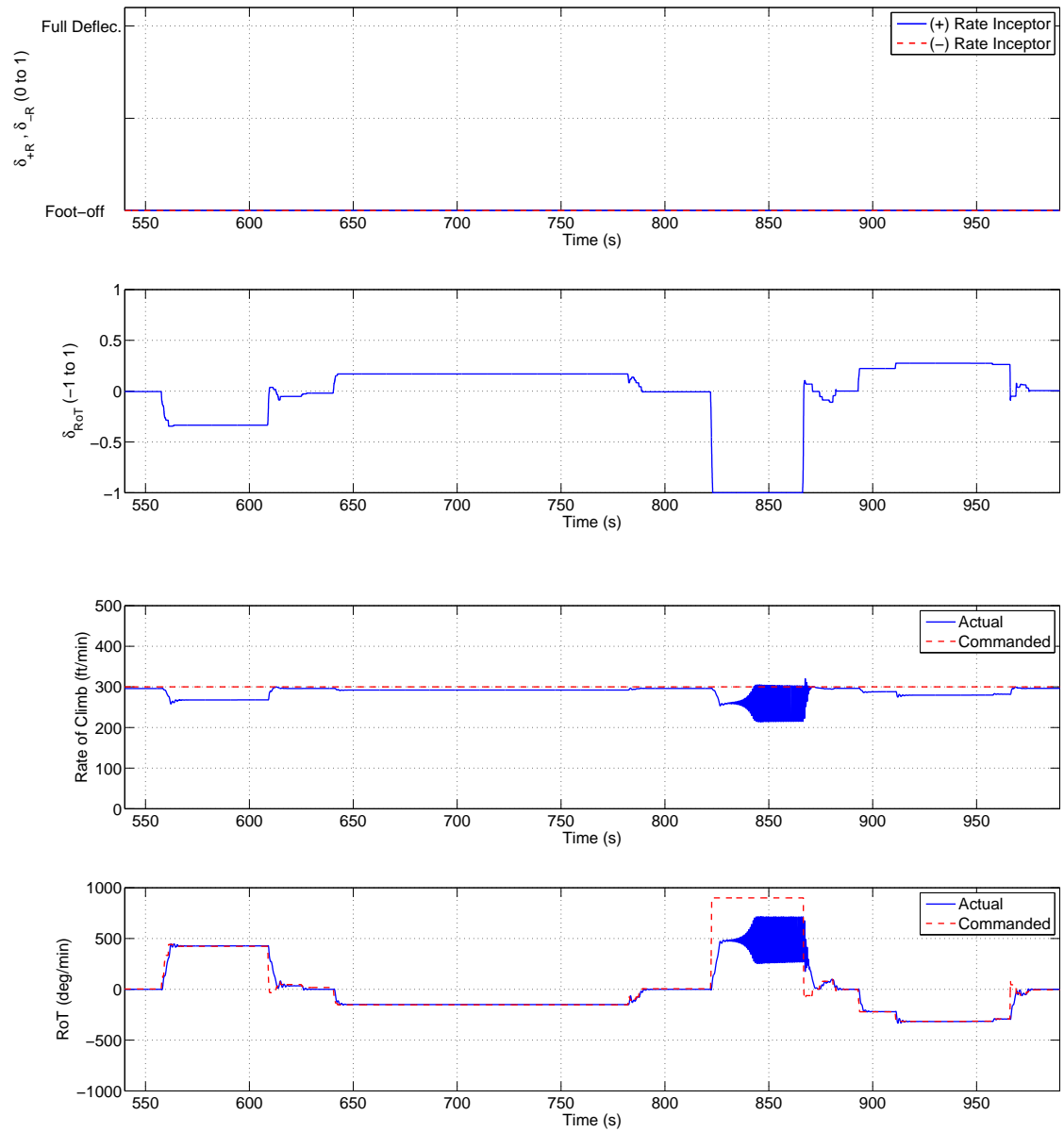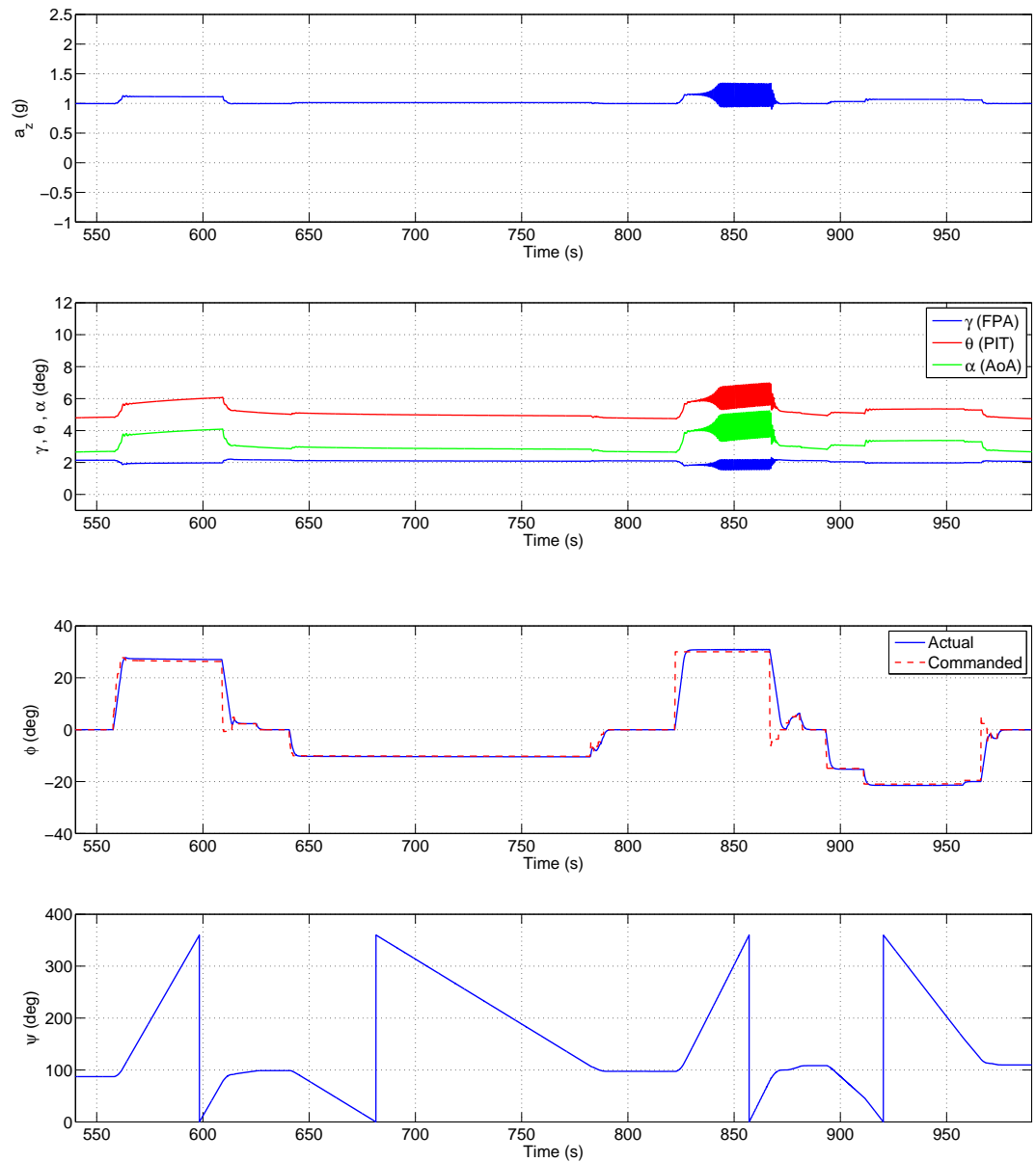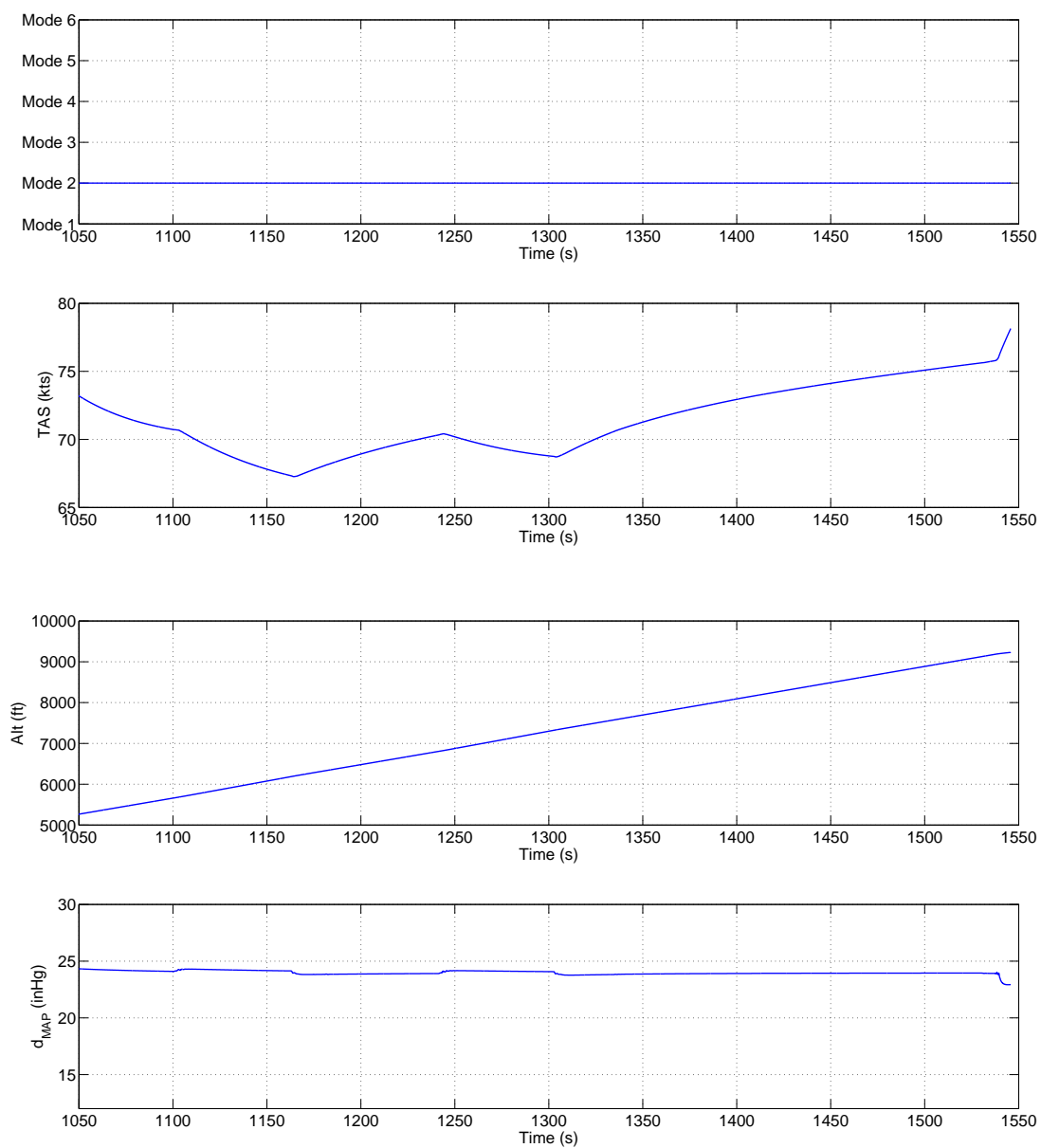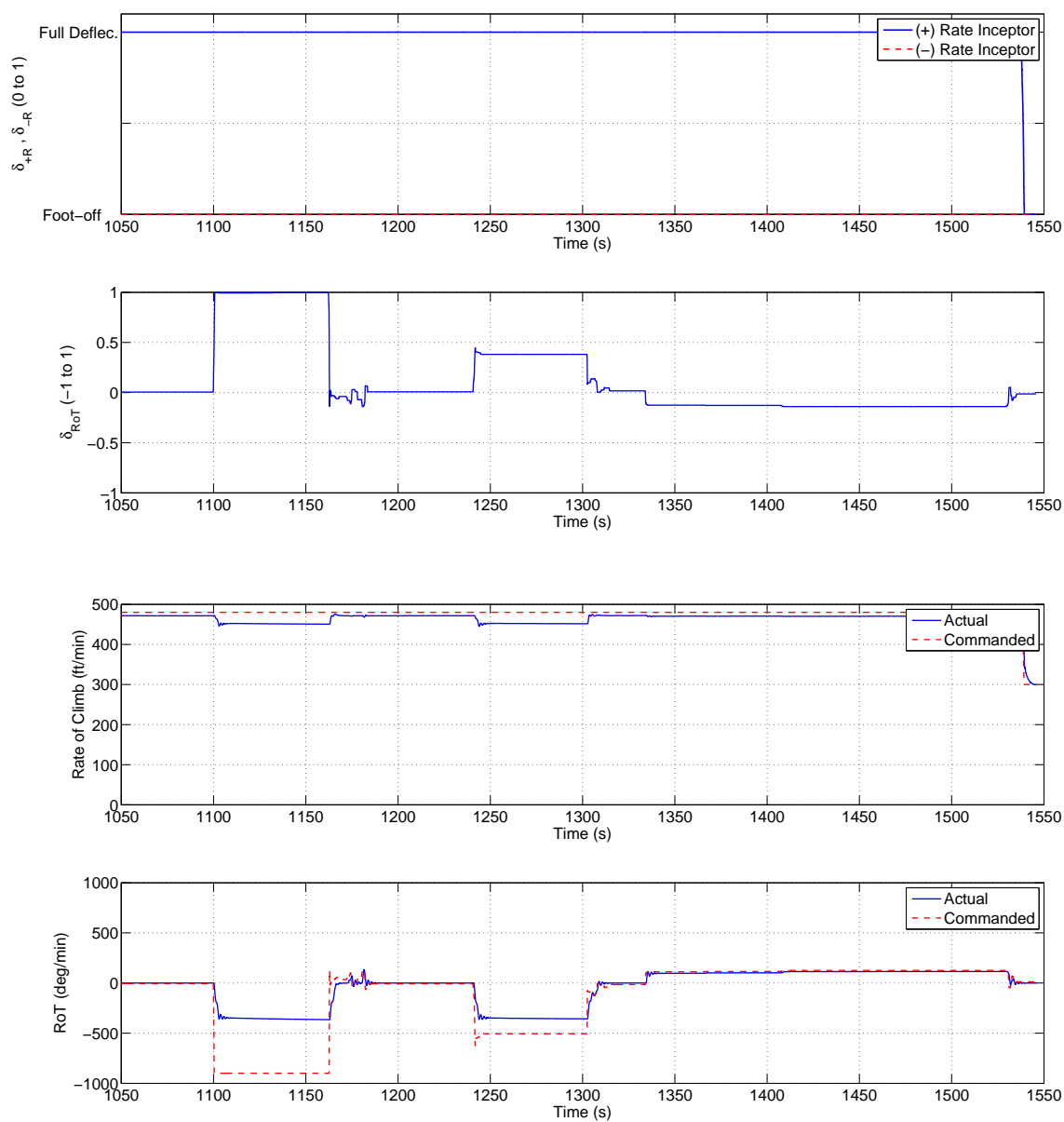
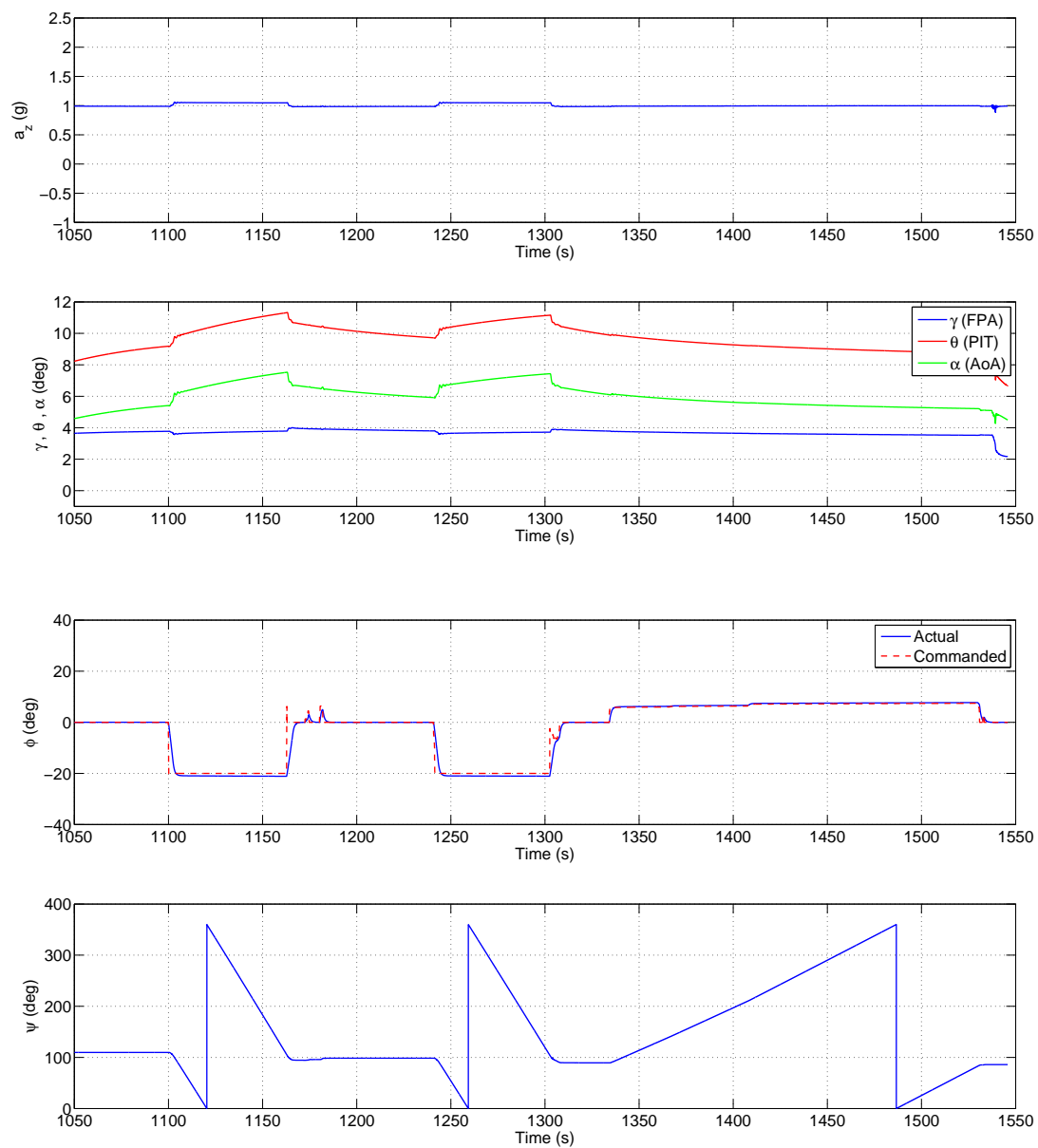Figure B.26: Climbing in mode 2

Figure B.27: Climbing in mode 2

Figure B.28: Climbing in mode 2
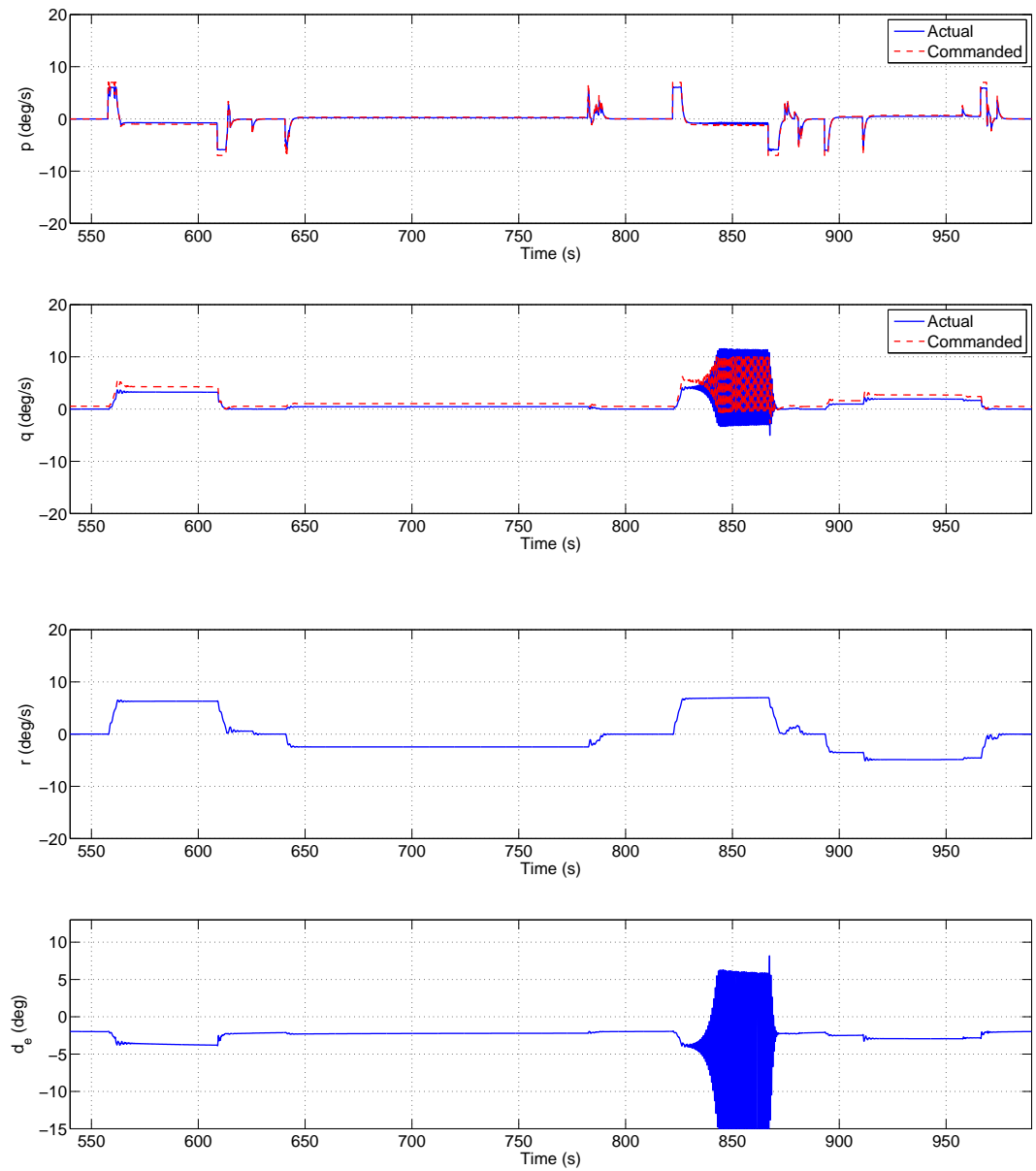
Figure B.29: Climbing in mode 2
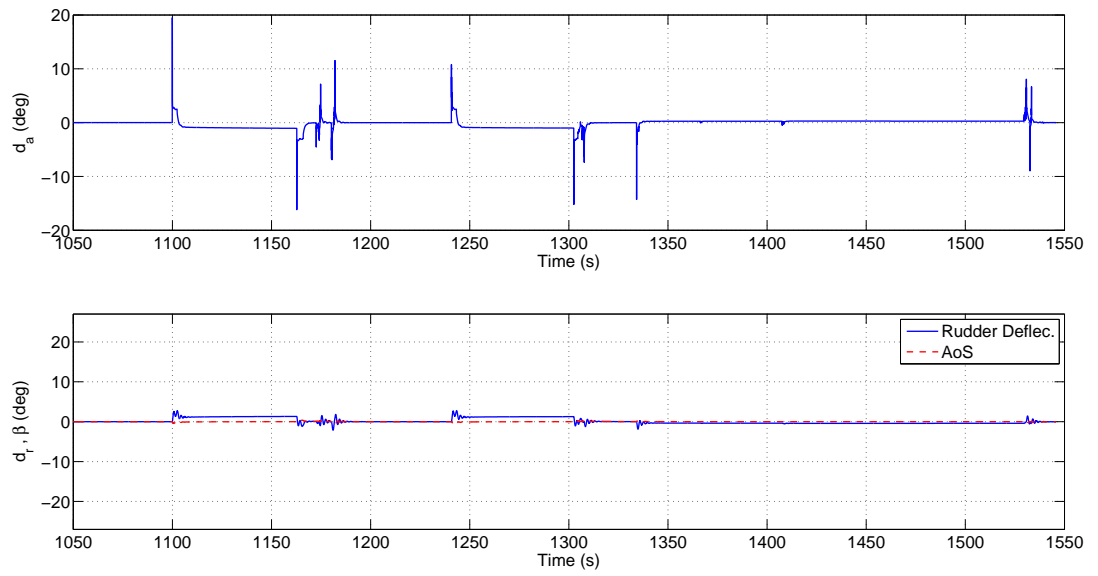
Figure B.30: Climbing in mode 2

B.2.3 Climb Mode Flight 3rd Segment

The last segment of flight data for the Climb Mode illustrates turning performance while demanding a maximum RoC (480 ft/min); a maximum δ_{+R} deflection.

The first turn is initiated at t=1100 s

A second segment is presented below illustrating turning performance while climbing. Four complete 360 degree turns are attempted with varying δ_{RoT} inputs. The aircraft attempts to maintain the baseline 300 ft/min RoC without any δ_{+R} and δ_{+R} pilot input.

The first input ($\approx 33\%$ deflection) at t $= 557$s to the Ω-controller commands a 420 deg/min right turn which results in a 27 degree bank allowing the aircraft to complete a full circle in ≈ 53 seconds. The turning maneuver reduces the effective RoC to 268 ft/min. With the Ω-controller centered, the aircraft reestablishes its baseline RoC and new bank angle in ≈ 3 seconds and 4.5 seconds, respectively. See Figures B.27 and B.28.

At t $= 640$s, a second, left-hand turn is performed. The Ω-controller is deflected $\approx 17\%$ of its maximum range resulting in a 152 deg/min RoT with a 10 degree bank angle. This shallower turn results in the aircraft maintaining a ≈ 292 ft/min climb rate. The full turn takes ≈ 147 seconds.

With a maximum deflection of the Ω-controller, a 900 deg/min RoT is commanded (5x standard rate turn). As the RoT approaches 500 deg/min the aircraft enters an aggressive longitudinal oscillation. The oscillation grows into a constant frequency

response seen in the RoC, RoT, q, and δ_e data traces in Figures B.27 and B.29. This particular oscillation was not observed during human factors testing as pilots avoided sustained maximum deflections of the Ω-controller. Releasing the controller mitigated the issue with the aircraft returning to wings-level climbing flight.

The last turn is a $\approx 25\%$ deflection of the Ω-controller resulting in a 315 deg/min RoT with a 21 degree bank angle. As expected, the RoC drops to 280 ft/min; a value between that observed for RoC in the first and second turns. The complete turn takes 74 seconds.

Figure B.31: Climbing in mode 2

Figure B.32: Climbing in mode 2

Figure B.33: Climbing in mode 2
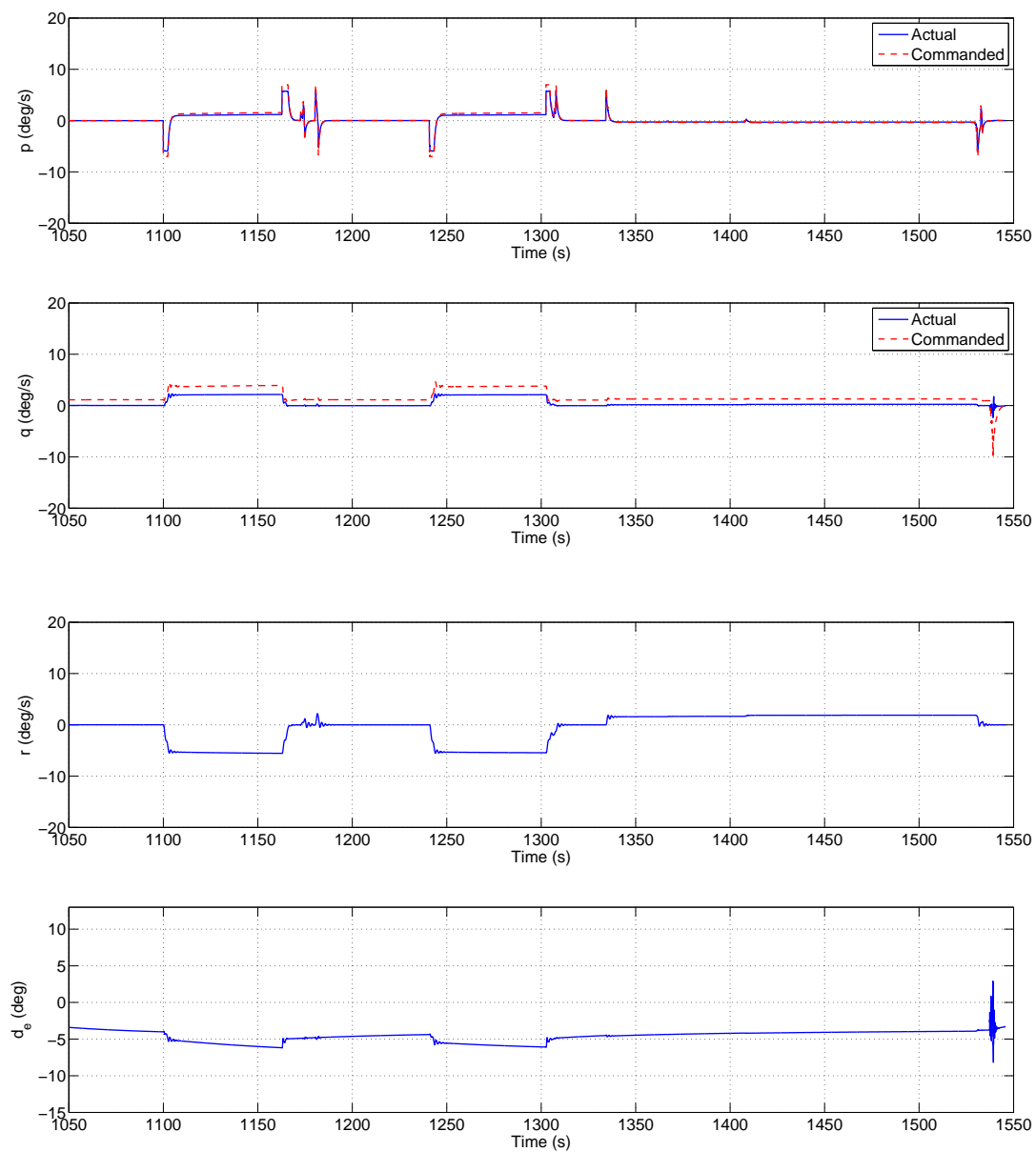
Figure B.34: Climbing in mode 2
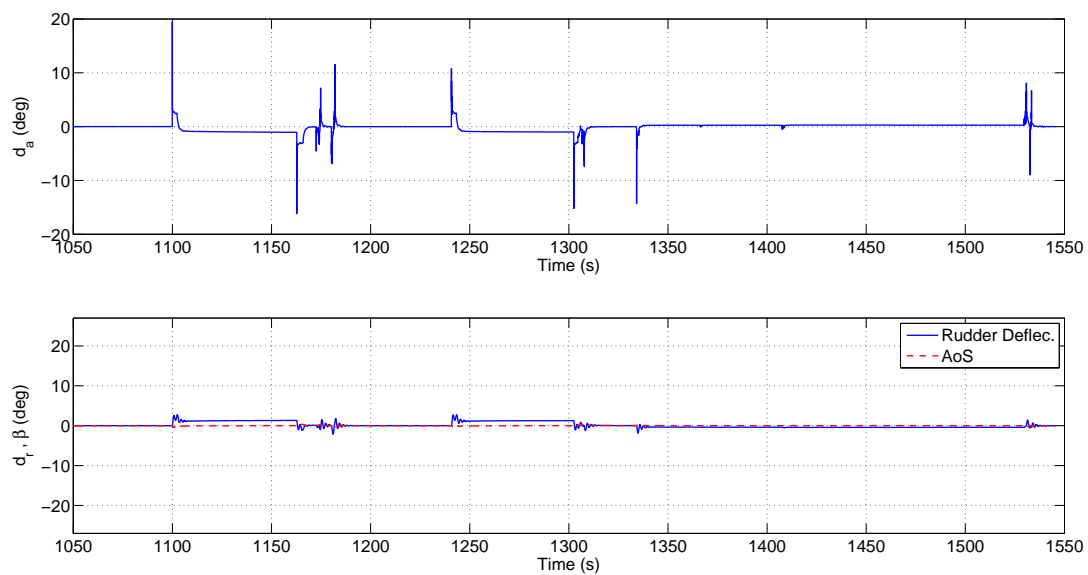
Figure B.35: Climbing in mode 2

B.3   Low-Speed Cruise Mode Simulation Data

This section provides data from the low-speed cruise portion of the run. The following plots show the aircraft transitioning from Climb to Low-Speed Cruise, pilot Ω - inceptor inputs to execute level turns and pedal inceptor inputs to modulate airspeed.

When Mode 3 is engaged the Altitude Hold function sets the current altitude as the capture target. The altitude strip chart shows a small overshoot as the control law begins to track the command.

The remainder of the data shows aircraft response to increasing Ω-inceptor inputs and pedal modulation. Deviations in altitude during higher RoT maneuvers are within 10-15 ft but the control law returns the aircraft to the original set point soon after rolling back to wings level.
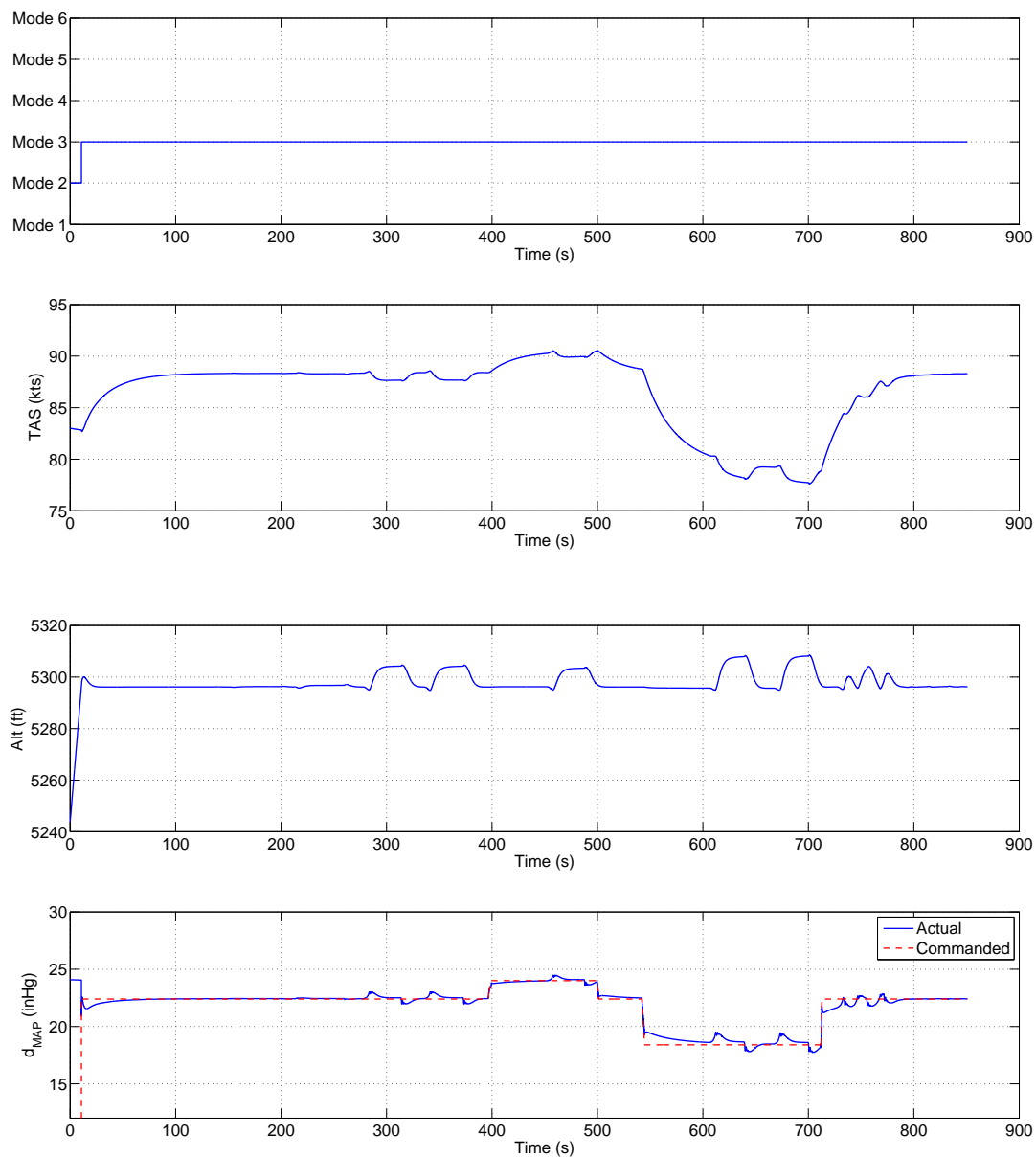
Figure B.36: Maneuvering in mode 3
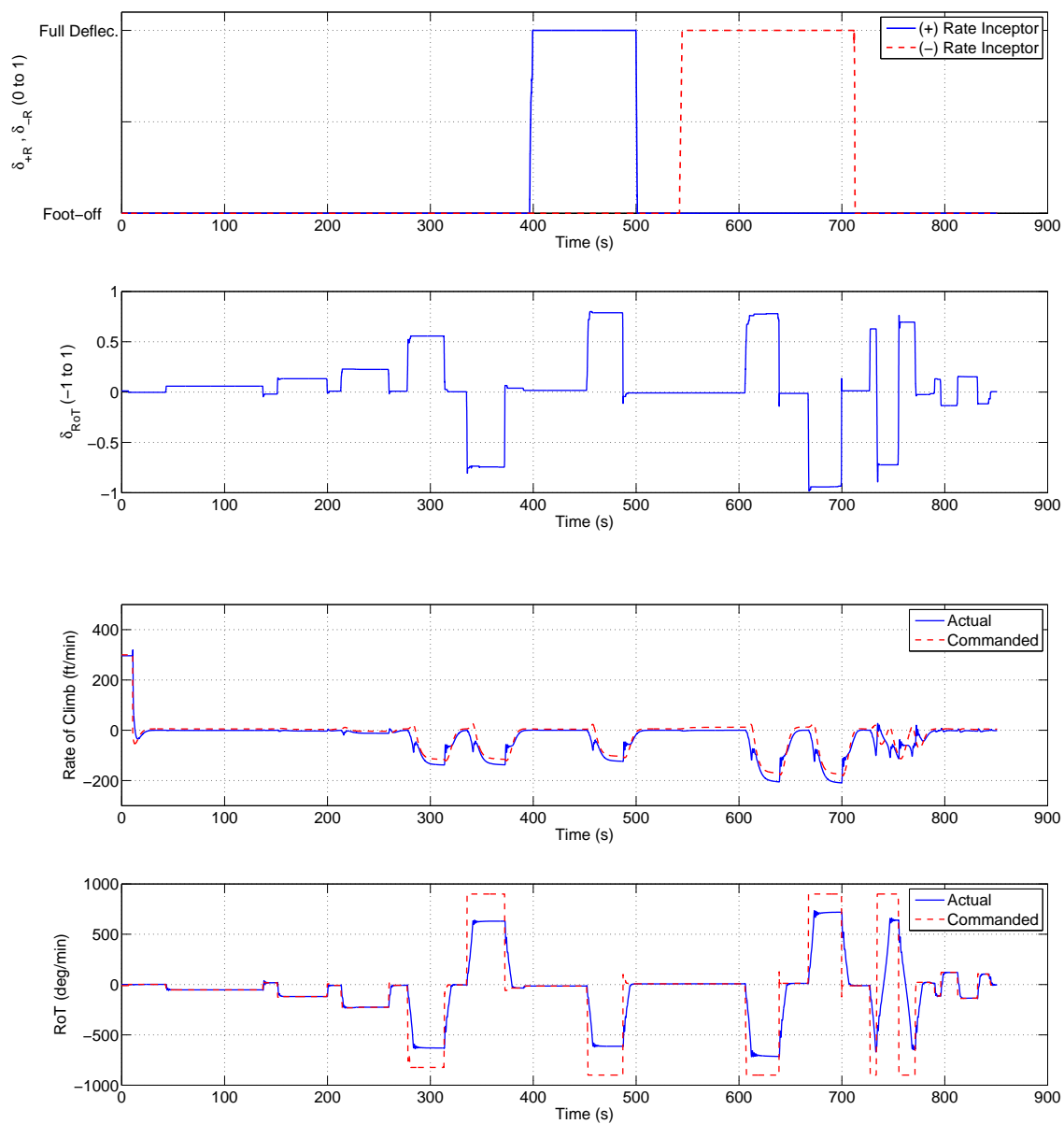
Figure B.37: Maneuvering in mode 3
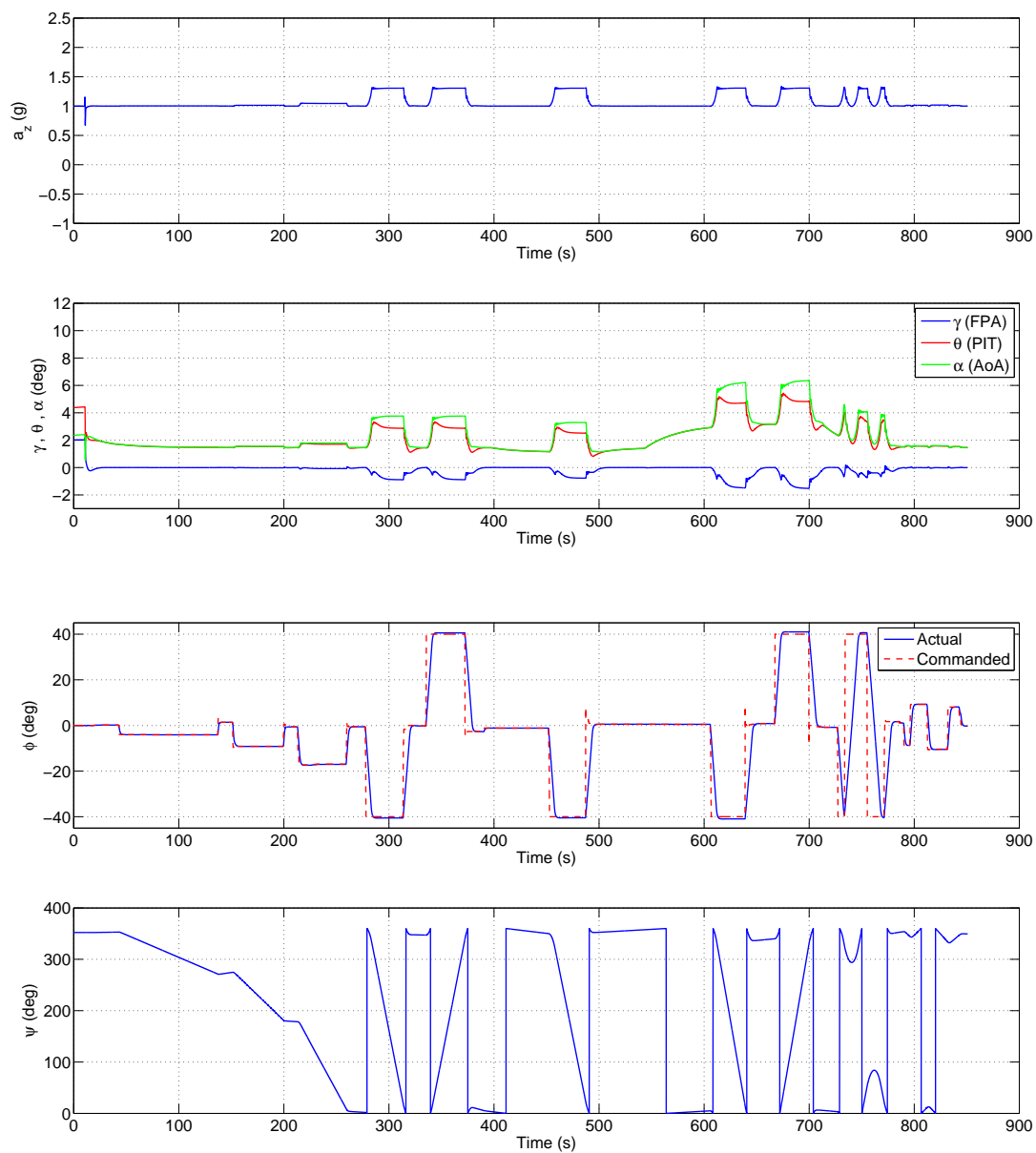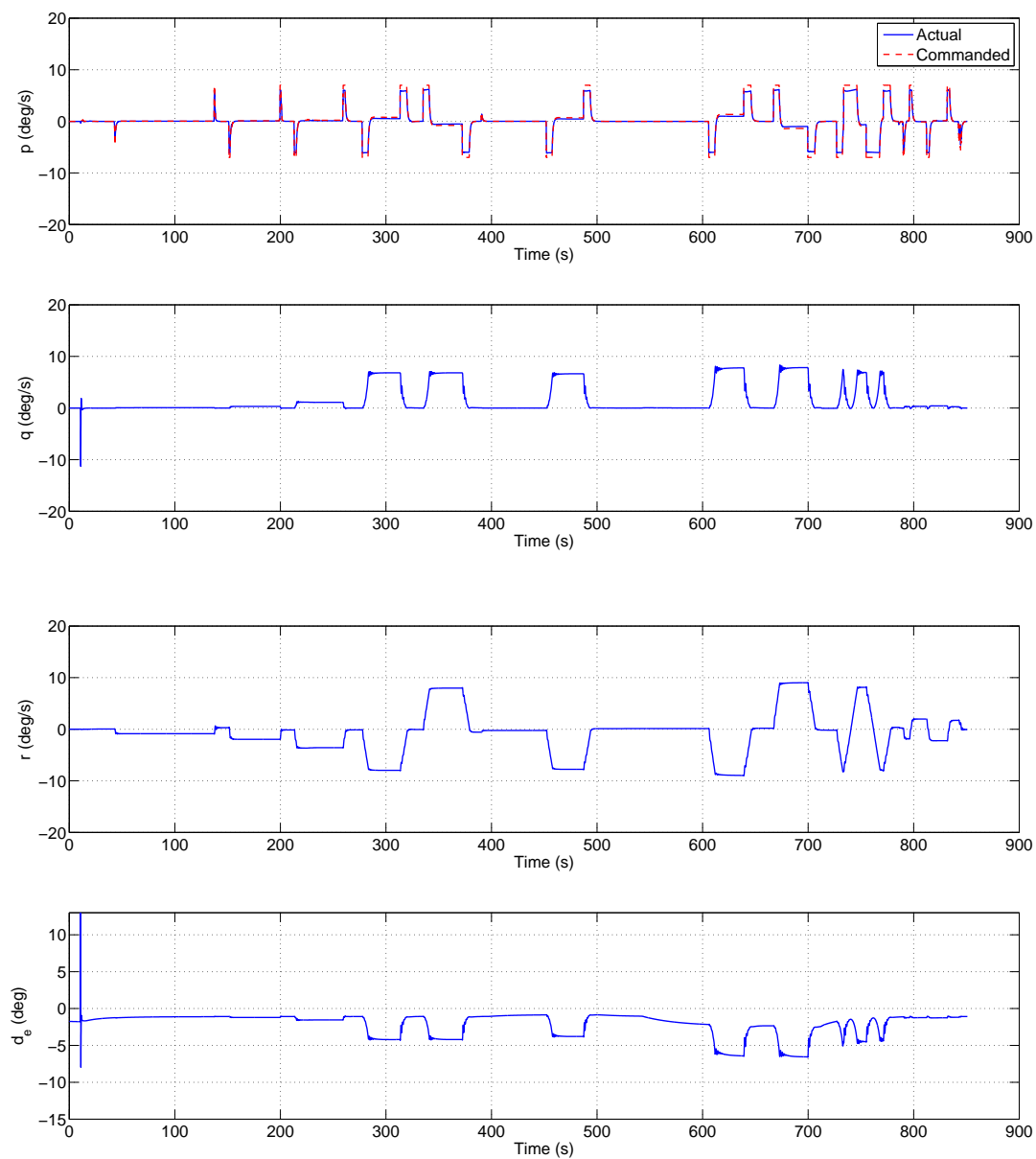
Figure B.38: Maneuvering in mode 3
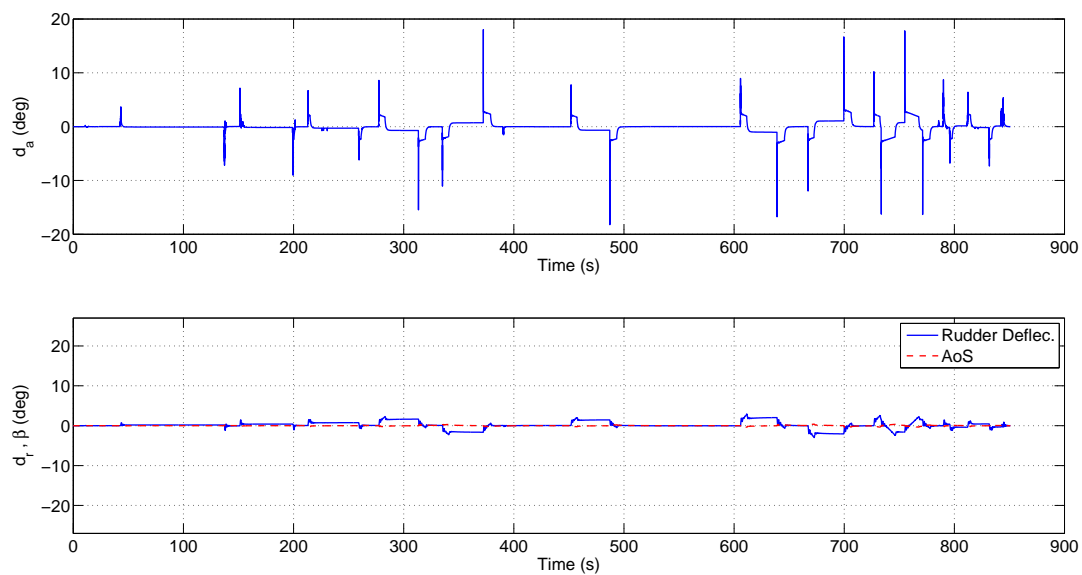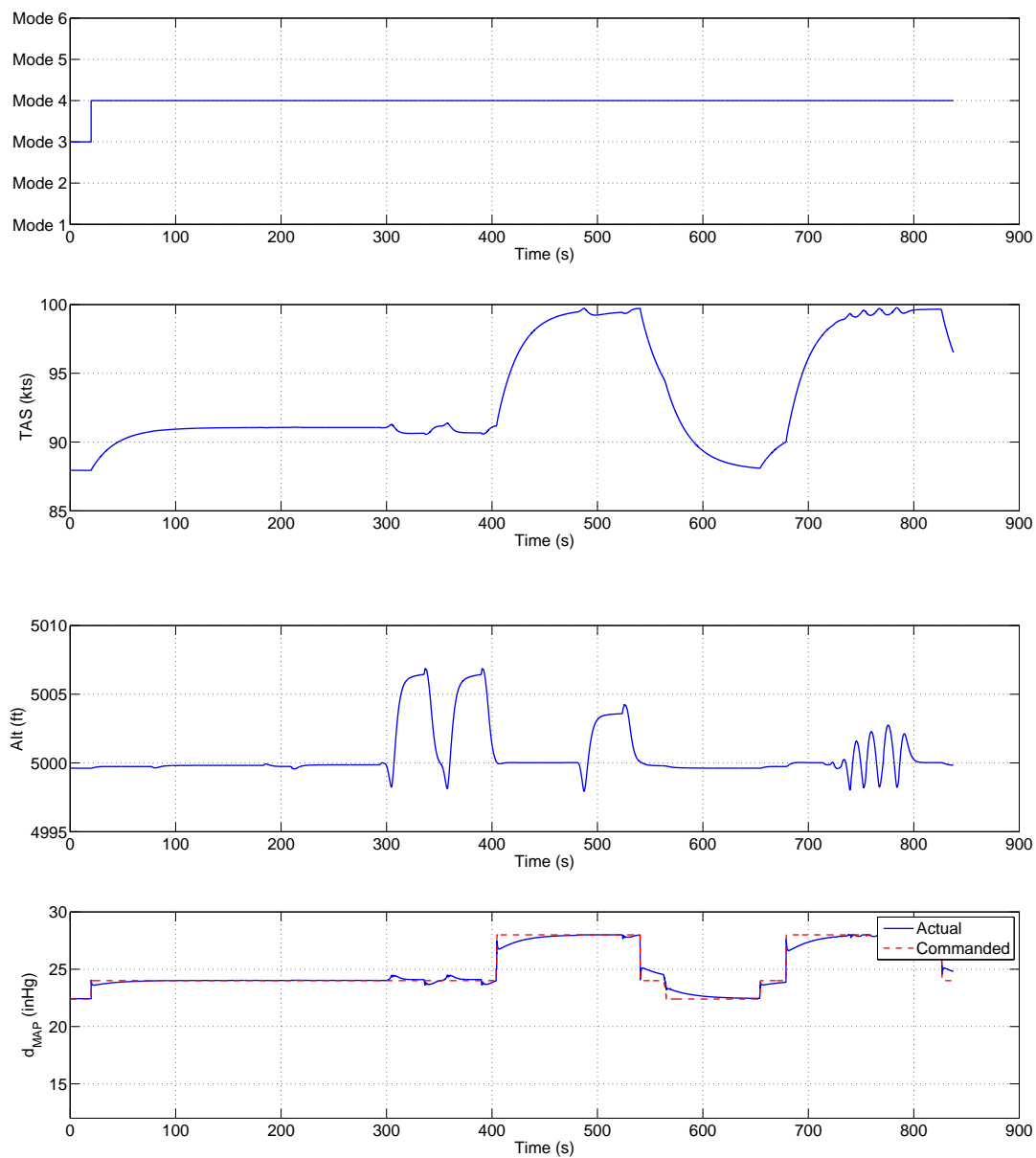
Figure B.39: Maneuvering in mode 3

Figure B.40: Maneuvering in mode 3

B.4   High-Speed Cruise Mode Simulation Data

This section provides data from the high-speed cruise portion of the run. The following plots show the aircraft transitioning from Low-Speed Cruise to High-Speed Cruise. Since this mode is functionally equivalent to Mode 3, barring a small airspeed difference, further details are not necessary.

Figure B.41: Maneuvering in mode 4
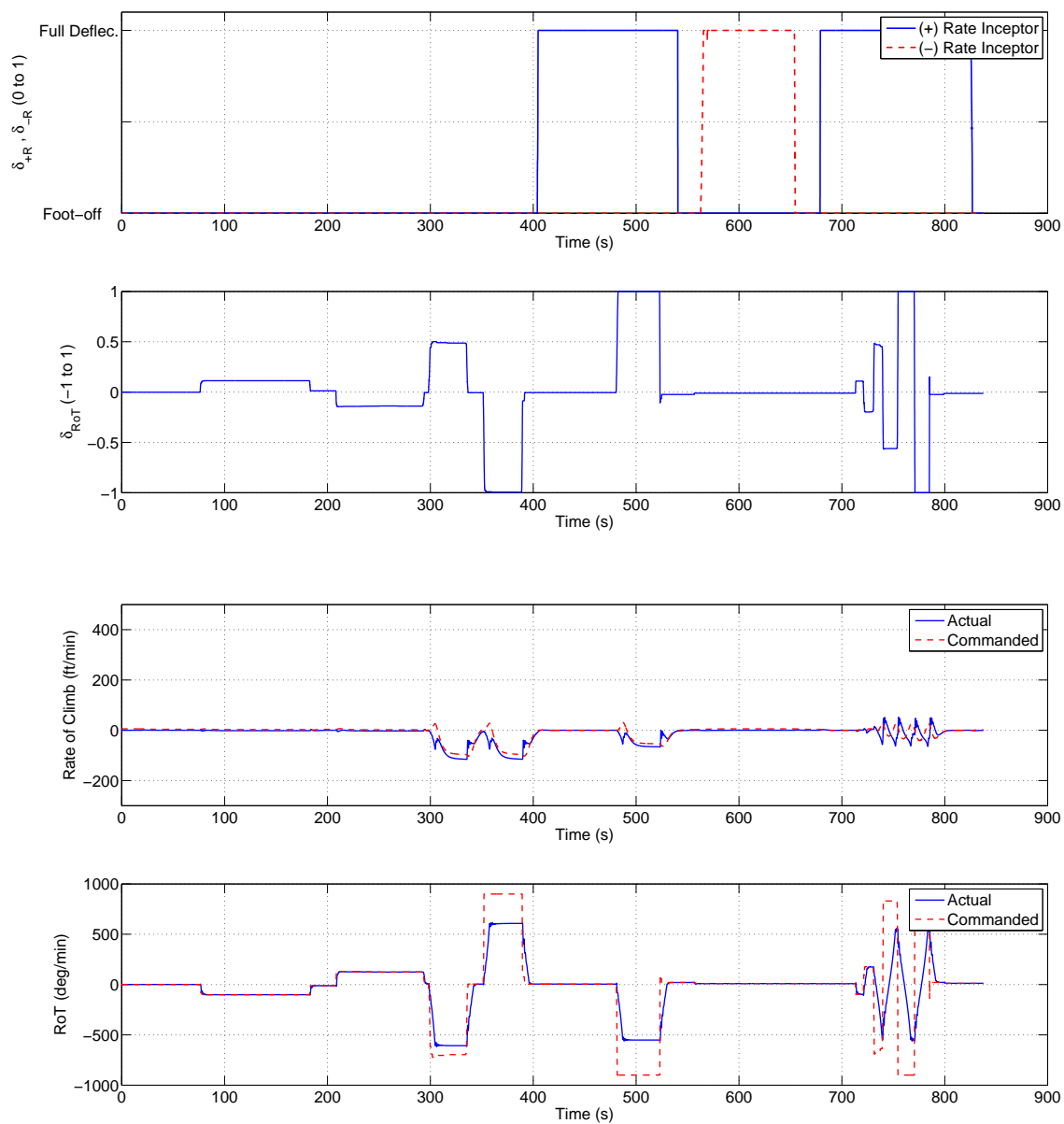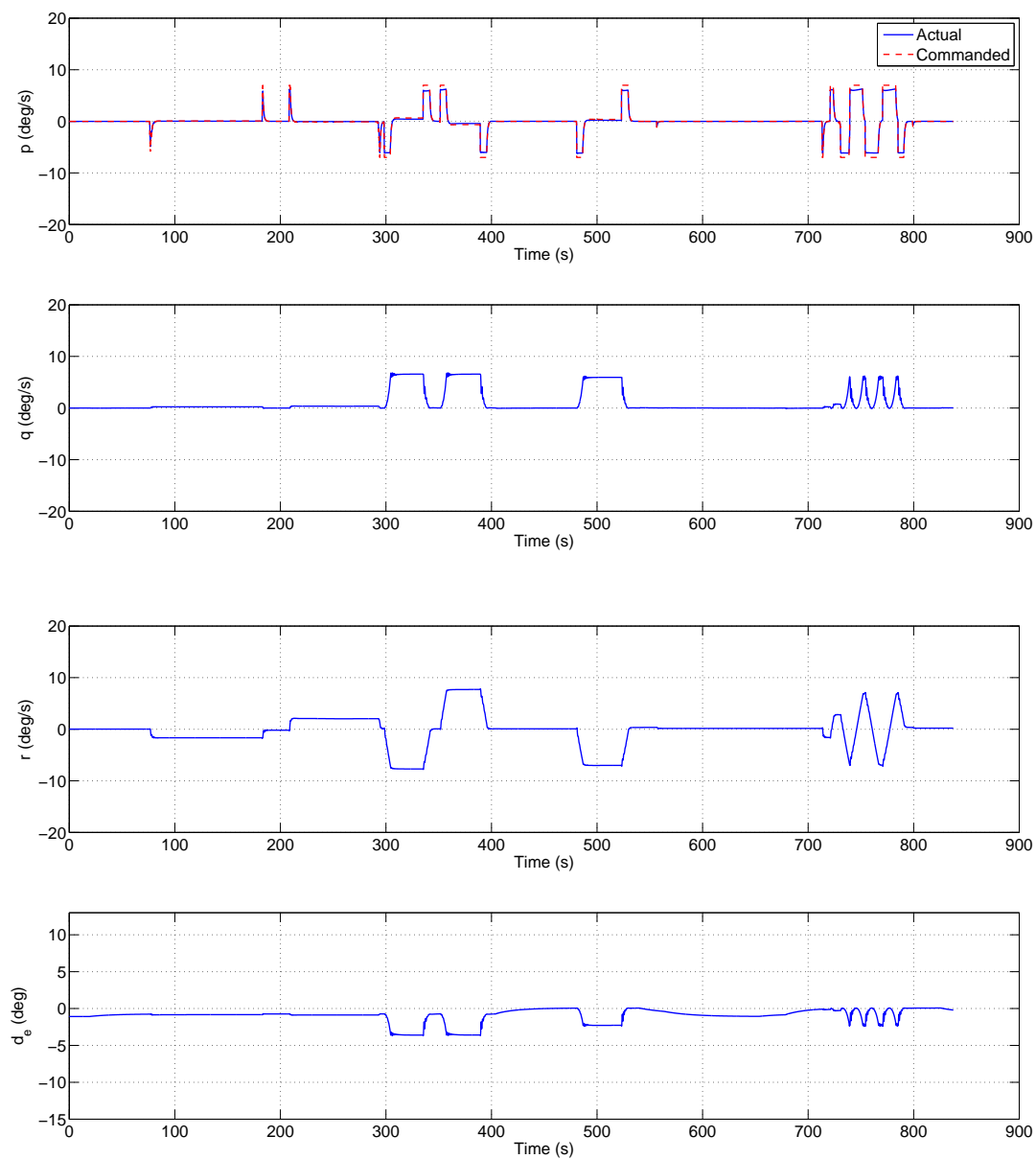
Figure B.42: Maneuvering in mode 4

Figure B.43: Maneuvering in mode 4
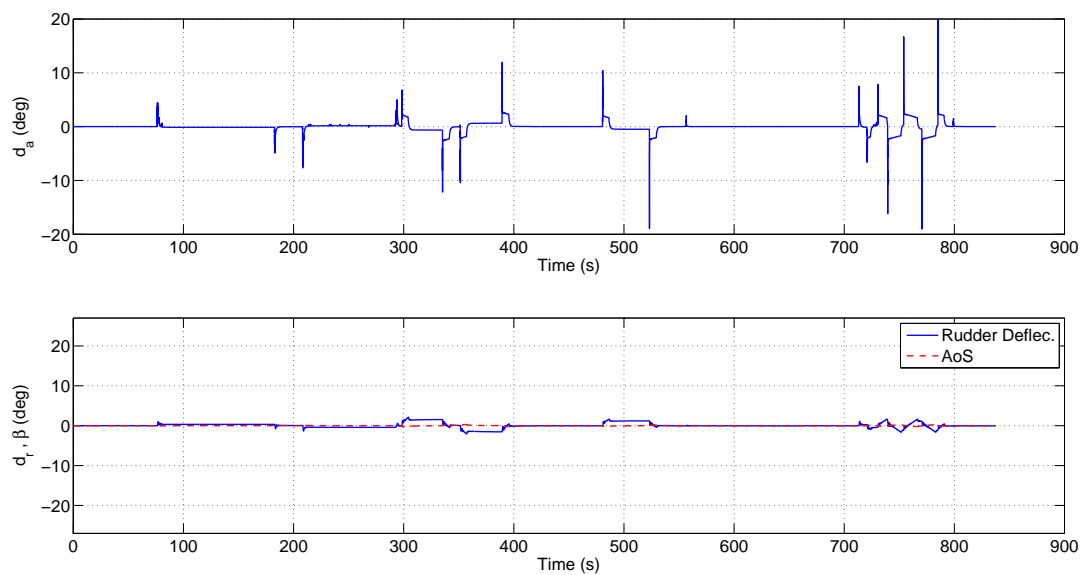
Figure B.44: Maneuvering in mode 4

Figure B.45: Maneuvering in mode 4

B.5   Descend Mode Simulation Data

The functional description of the Climb Mode serves as a satisfactory description of the Descend Mode.
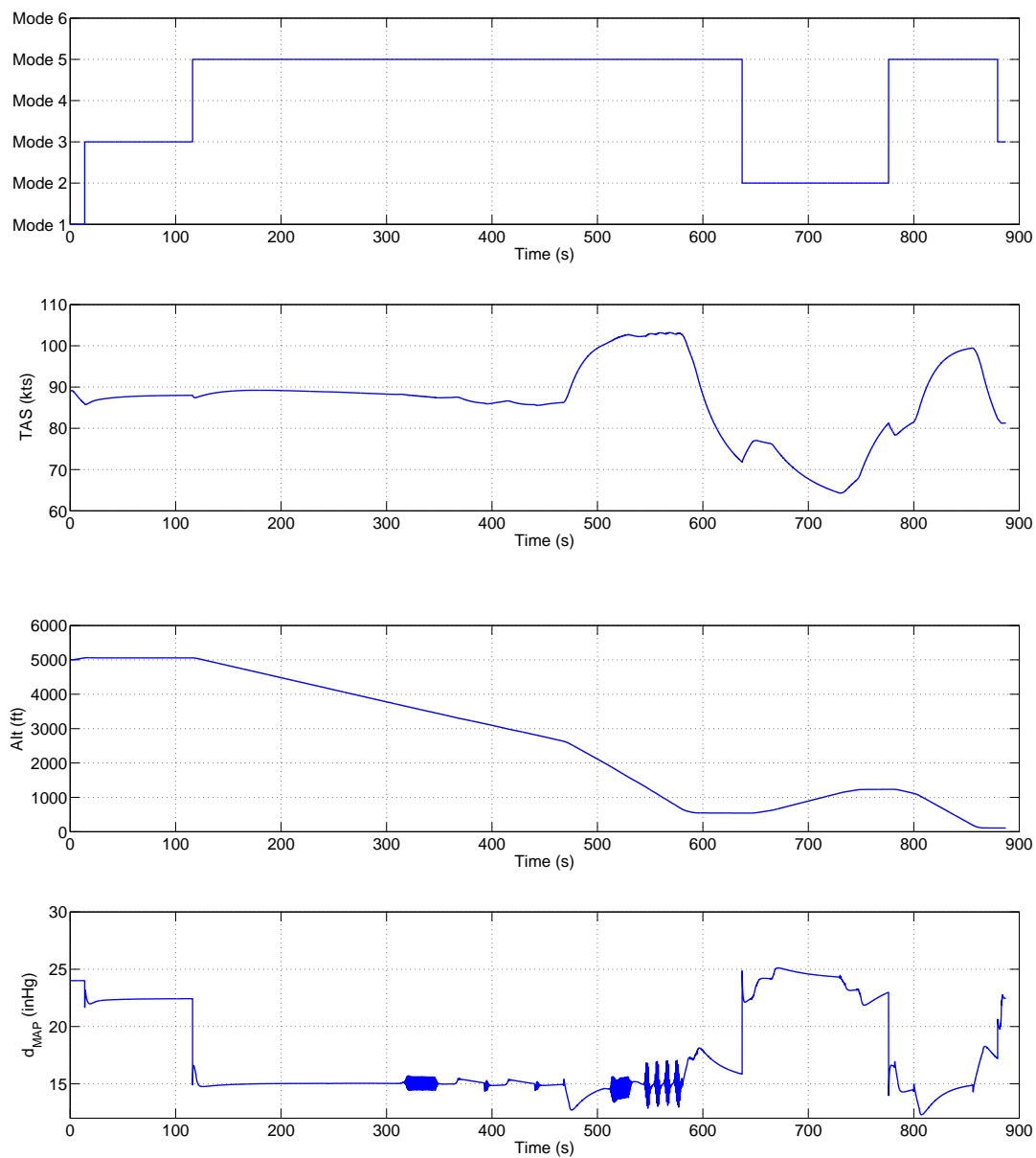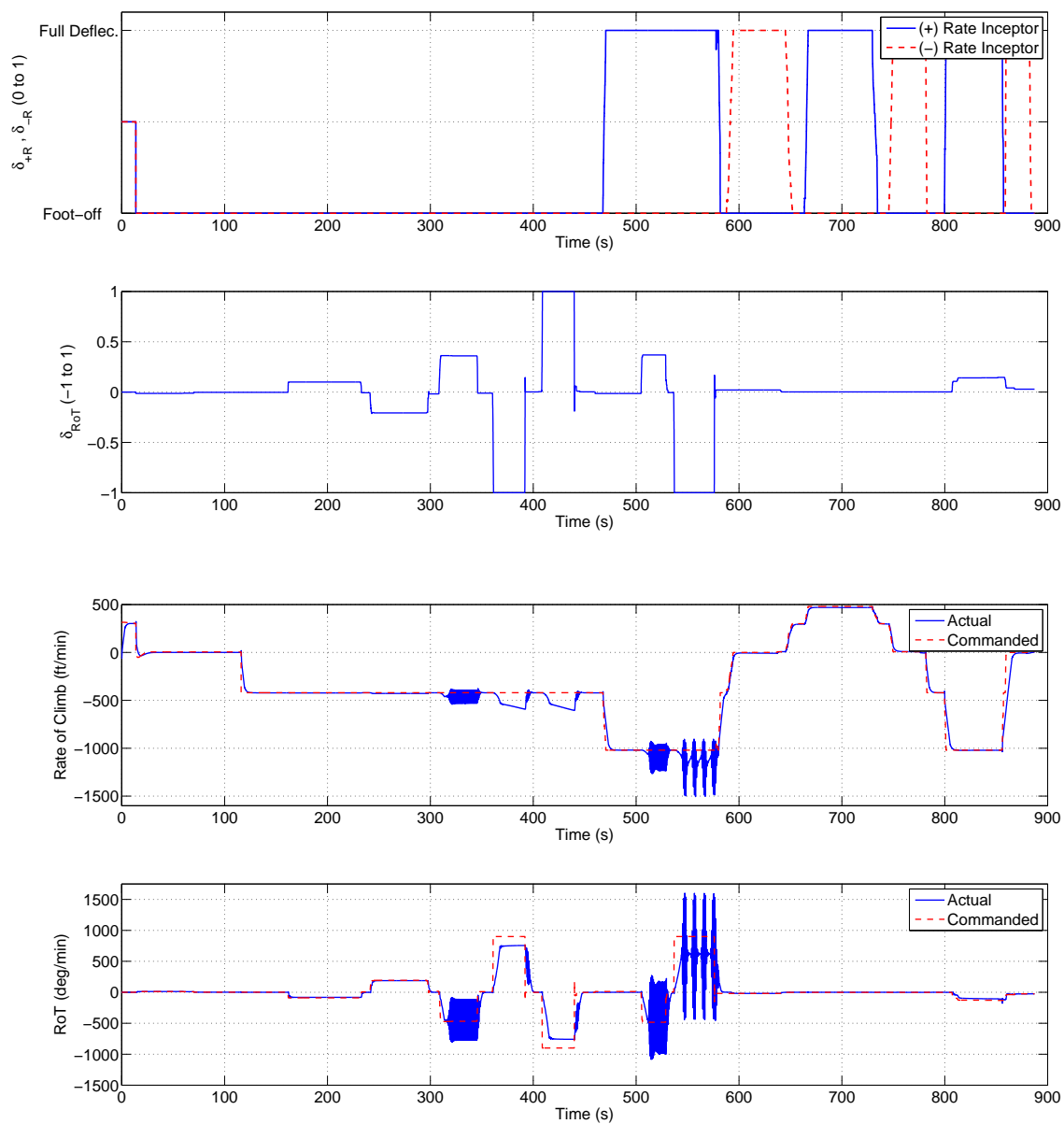
Figure B.46: Descending in mode 5

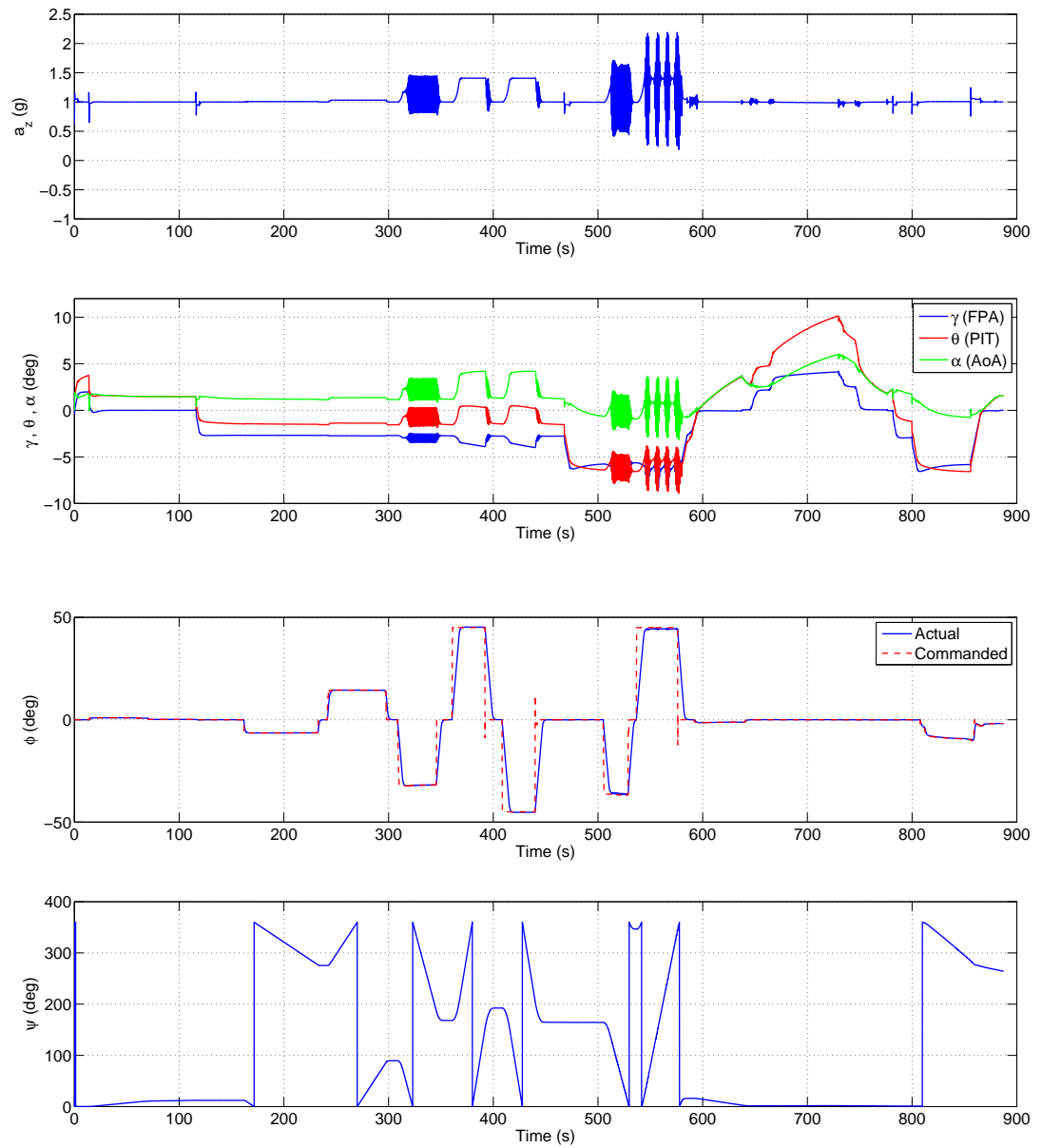Figure B.47: Descending in mode 5

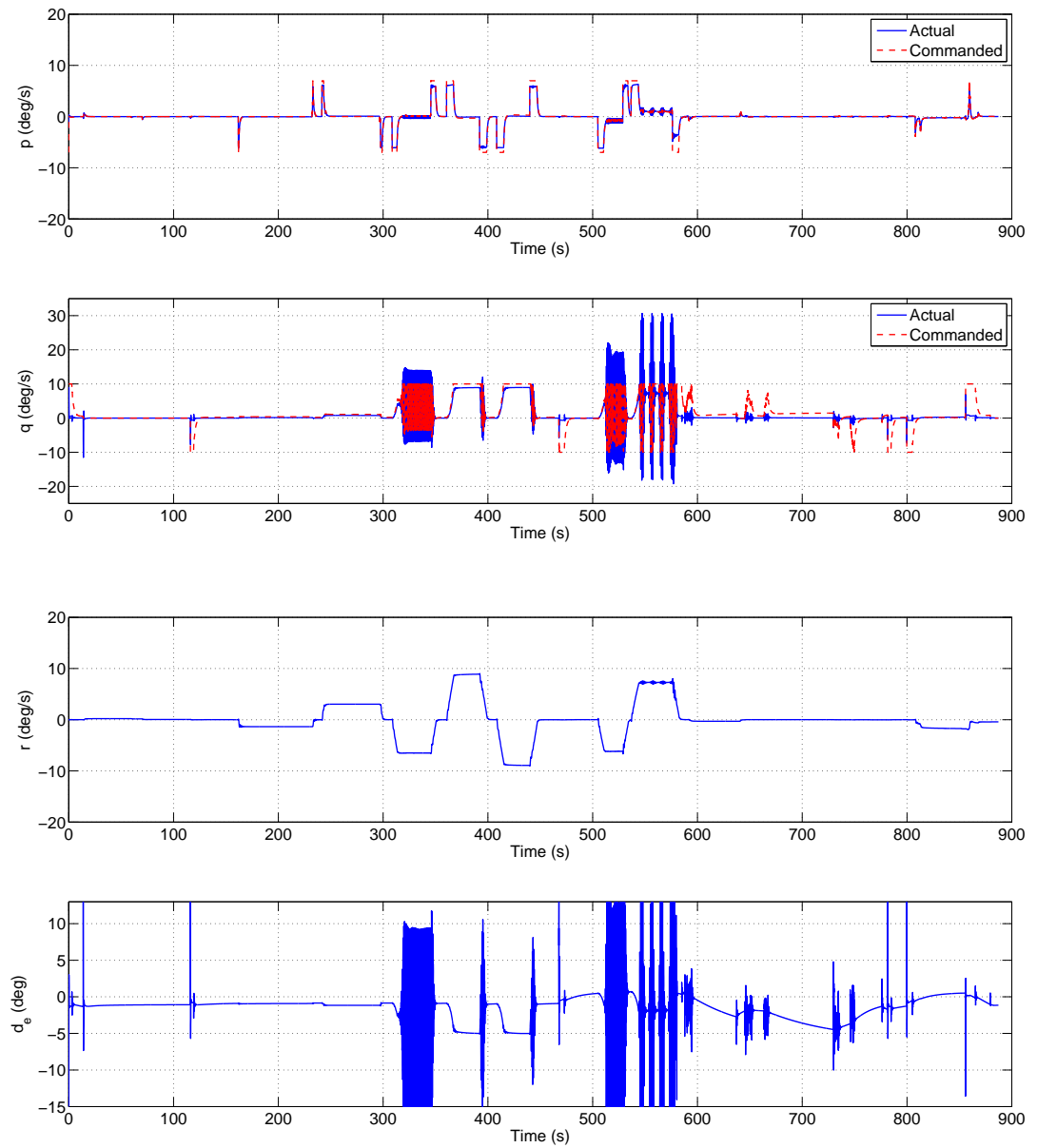Figure B.48: Descending in mode 5

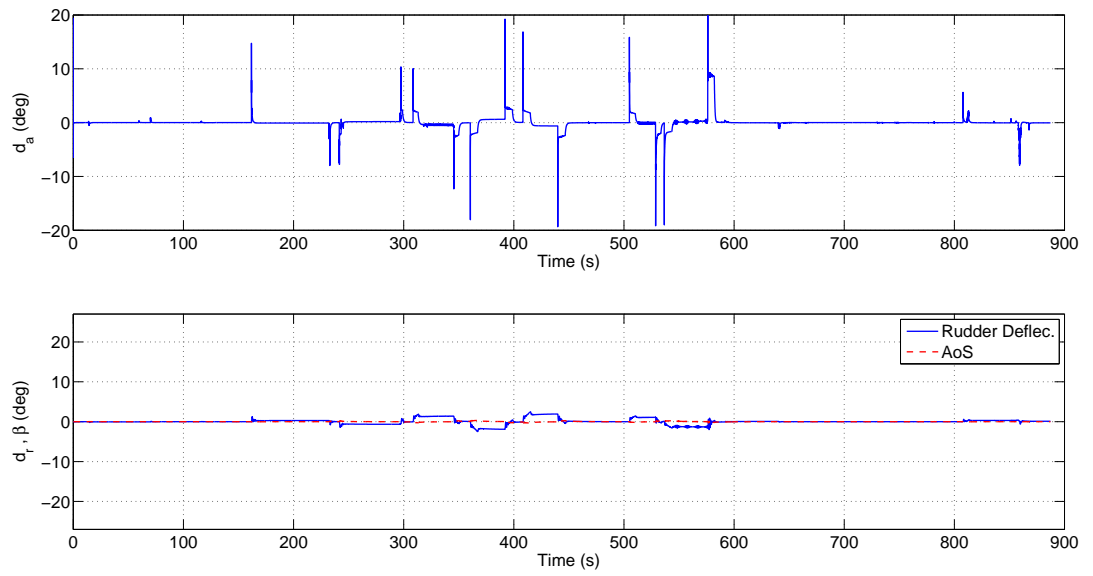Figure B.49: Descending in mode 5

Figure B.50: Descending in mode 5

B.6 Approach Mode Simulation Data

This section provides data from the approach phase of the run. The following plots show the aircraft transitioning from Mode 1 to 3 and finally to Mode 6 or the Approach Mode.

At approximately t=30s, Mode 6 is engaged and the $\dot{h} - q$ control law starts capturing the 3 degree glide slope. Pedal inceptor input enables the modulation of the aircraft flight path angle in order to provide a means to take corrective action if the pilot is above or below the glideslope. Subsequent inputs demonstrate the ability of the aircraft to maintain the desired flight path angle.
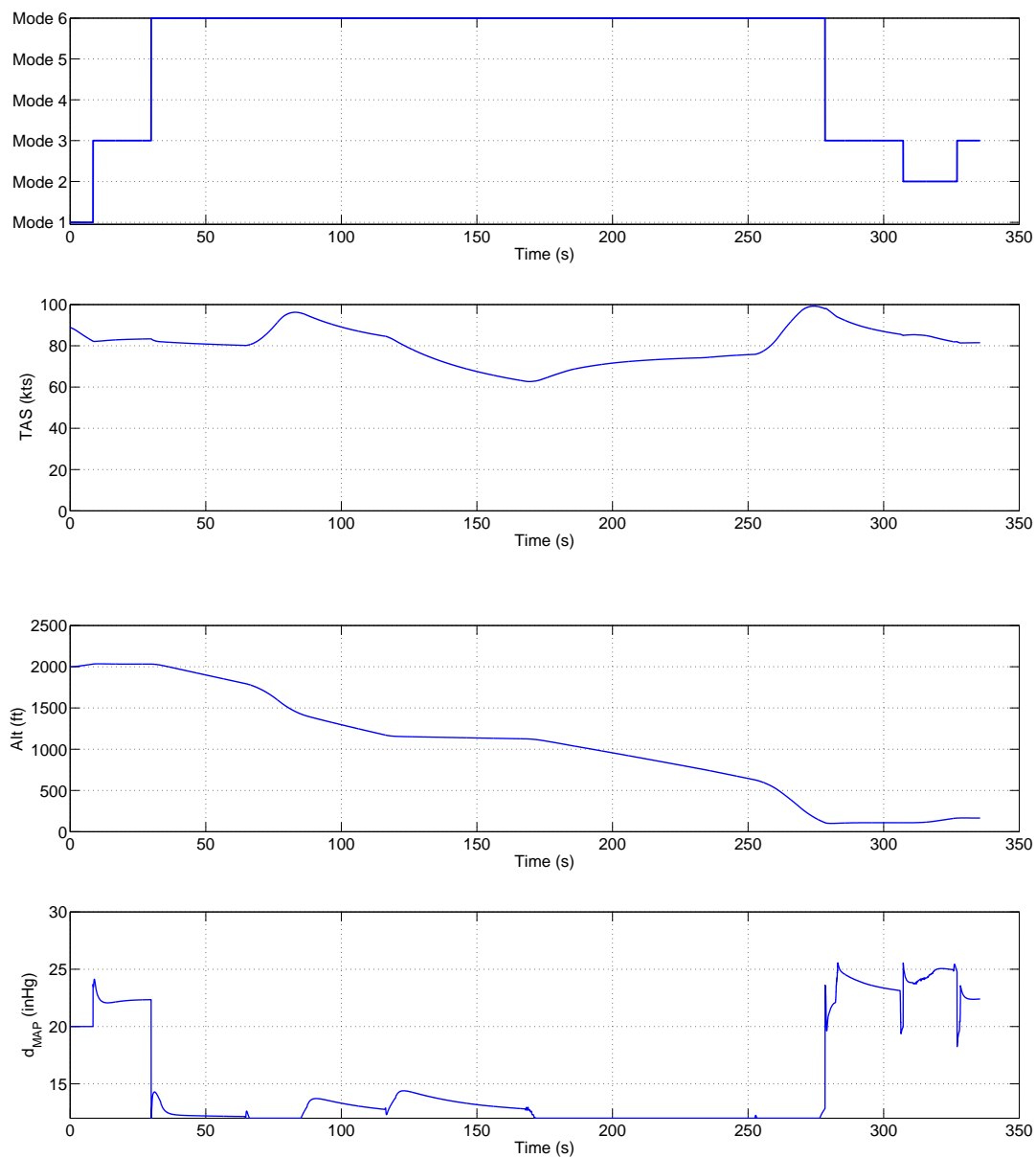
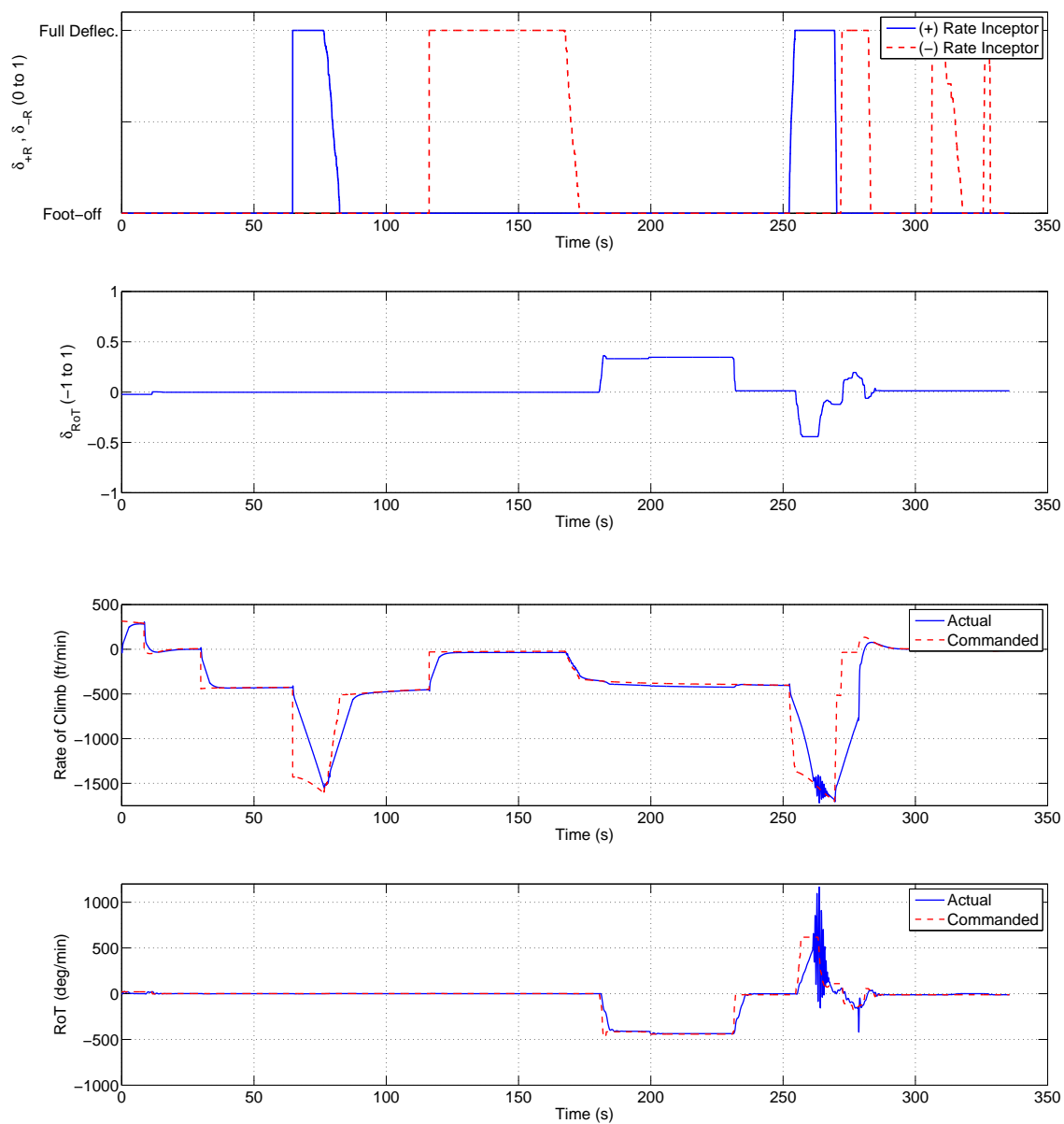Figure B.51: Glide slope capture in mode 6
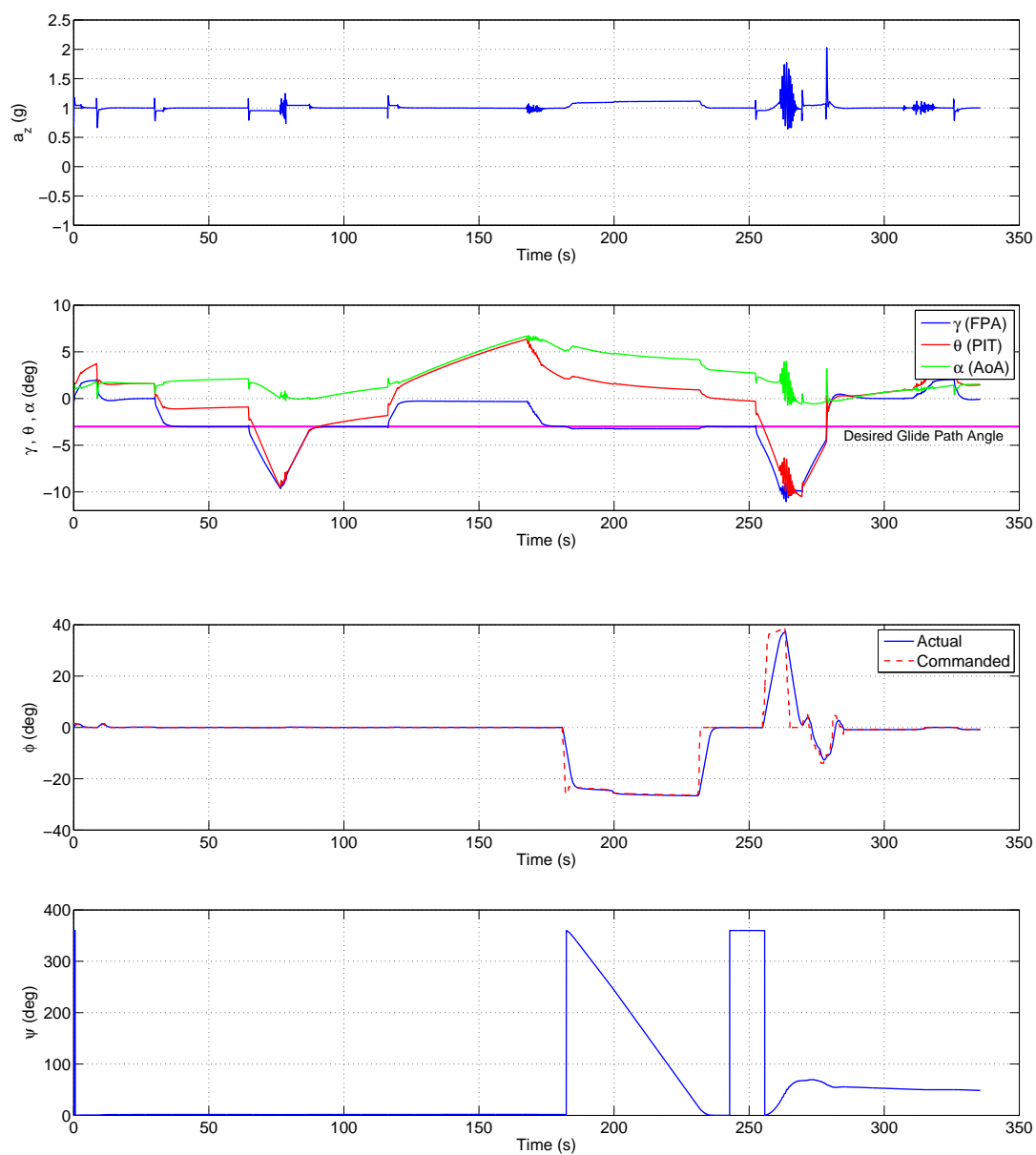
Figure B.52: Glide slope capture in mode 6
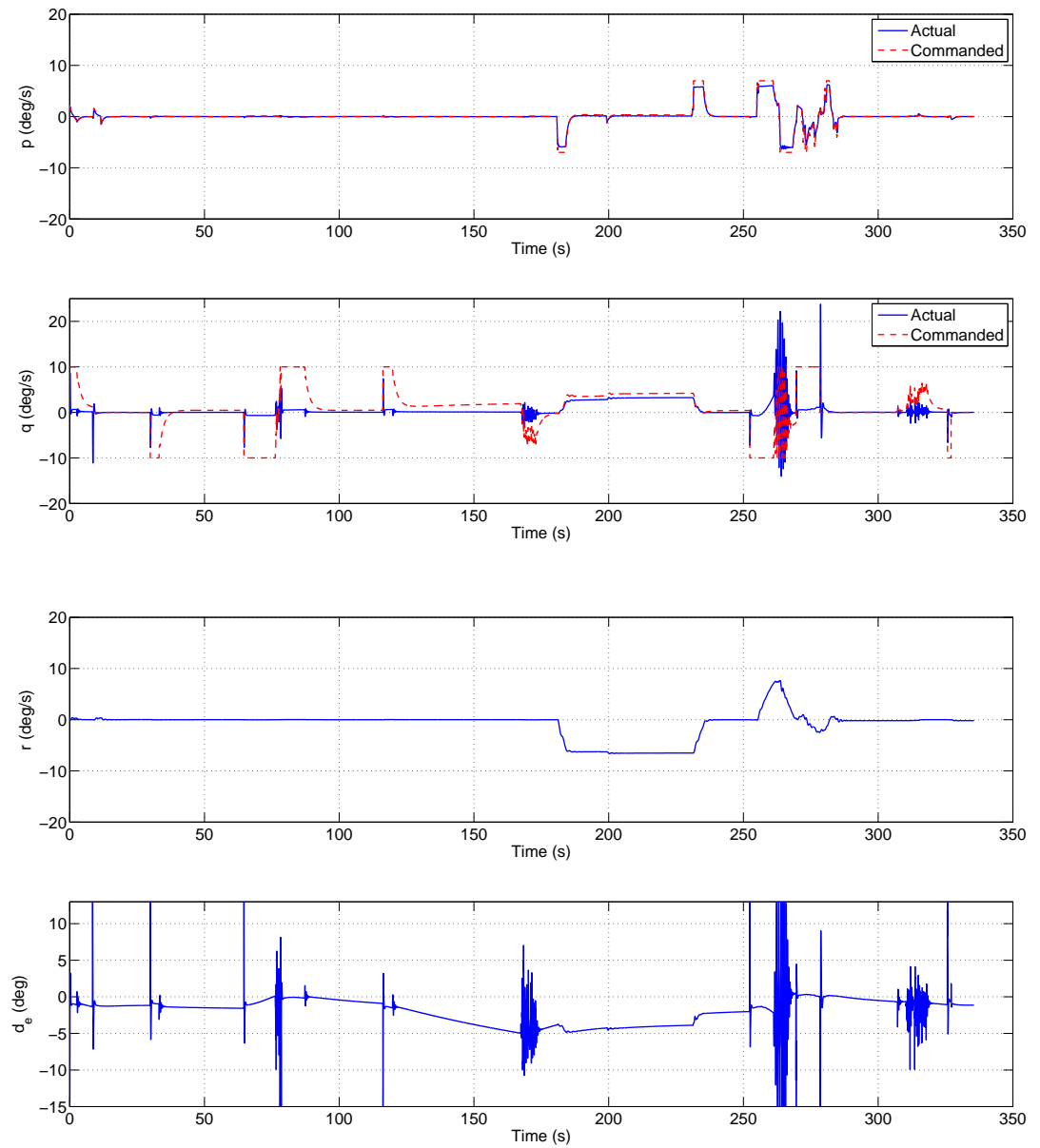
Figure B.53: Glide slope capture in mode 6
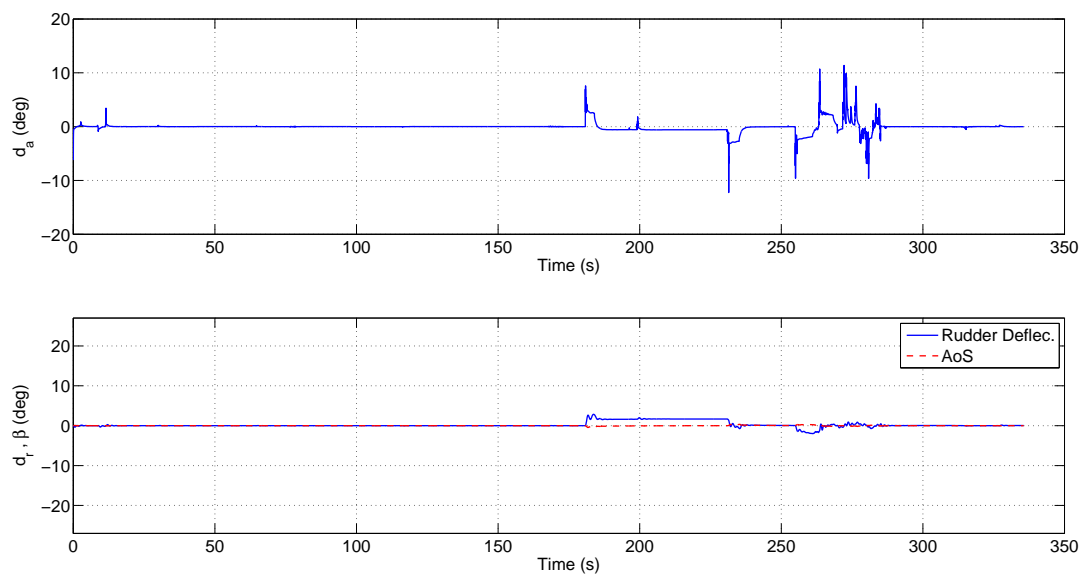
Figure B.54: Glide slope capture in mode 6

Figure B.55: Glide slope capture in mode 6

REFERENCES

Abzug, M. J., & Larrabee, E. E. (2005). *Airplane stability and control: A history of the technologies that made aviation possible.* Reading Massachusetts: Cambridge University Press.

Affordable alternative transportation agate – revitalizing general aviation [NASA Article]. (1996). Retrieved from https://www.nasa.gov/centers/langley/news/factsheets/AGATE.html

Bainbridge, L. (1983). Ironies of automation [Journal Paper]. *Automatica*, *19*(6), 775-779.

Bangor, A., Kortum, P., & Miller, J. (2009). Determining what individual sus scores mean: Adding an adjective rating scale [Journal Article]. *Journal of Usability Studies*(Vol.4, Issue 3).

Barber, M. R., Jones, C. K., Sisk, T. R., & Haise, F. W. (1966). *An evaluation of the handling qualities of seven general-aviation aircraft* (Technical Note No. TN D-3726). Flight Research Center.

Beringer, D. B. (2002). *Applying performance-controlled systems, fuzzy logic, and fly-by-wire controls to general aviation* (Report).

Borst, C., Mulder, M., van Paassen, M., & Mulder, J. (2006). Path-oriented control/display augmentation for perspective flight-path displays [Journal Article]. *Journal of Guidance, Control, and Dynamics*(Vol.29, No.4).

Campbell, J. P., Hunter, P. A., Hewes, D. E., & Whitten, J. B. (1952). *Flight investigation of the effect of control centering springs on the apparent spiral stability of a personal-owner airplane* (Report).

Carroll, T., & McAvoy, W. H. (1929). *Spiral tendency in blind flying* (Technical Note No. No. 314). Langley Memorial Aeronautical Laboratory.

Carvalho, C. G. (2013). *Mapping automotive like controls to a general aviation aircraft* (Masters Thesis). Embry-Riddle Aeronautical University.

Chambers, J. R. (2005). *Innovation in flight: Research of the langley research center on revolutionary advanced concepts for aeronautics.* Yorktown Virginia: NASA History Office.

Duerksen, N. (2003, July 14-17). Advanced flight controls and pilot displays for general aviation [Conference Paper]. *AIAA International Air and Space Symposium and Exposition: The Next 100 Years*(AIAA 2003-2647).

FAA. (2003). *General aviation controlled flight into terrain awareness* (Advisory Circular No. AC-61-134).

Falkena, W. (2012). *Investigation of practical flight control systems for small aircraft* (PhD Thesis). Technische Universiteit Delft.

Falkena, W., & Borst, C. (2010, December). Future avionics for small aircraft: Towards safer personalized air transportation [Magazine article].

Field, E. J., & Giese, S. E. D. (2005). *Appraisal of several pilot control activity measures* (Article No. AIAA 2005-6032). AIAA Atmospheric Flight Mechanics Conference and Exhibit.

Flemisch, F. O., Adams, C. A., Conway, S. R., Goodrich, K. H., Palmer, M. T., & Schutte, P. C. (2003). *The h-metaphor as a guideline for vehicle automation and interaction* (Technical Memorandum No. TM-2003-212672).

Goodrich, K., Schutte, P., & Williams, R. (2011, September 20-22). Haptic-multimodal flight control system update [Conference Paper]. *11th AIAA Aviation Technology, Integration, and Operations (ATIO) Conference*.

Hahn, A. S. (2006). *Next generation nasa ga advanced concept* (Conference Paper No. 2006-01-2430).

Hunter, P. A. (1948). *Flight measurements of the flying qualities of five light airplanes* (Technical Note No. 1573).

Lambregts, A., & Cannon, D. (1979). *Development of a control wheel steering mode and suitable displays that reduce pilot workload and improve efficiency and safety of operation in the terminal area and in windshear* (Article No. 79-1887). Guidance and Control Conference.

Loschke, P. C., Barber, M. R., Enevoldson, E. K., & McMurtry, T. C. (1974). *Flight evaluation of advanced control systems and displays on a general aviation airplane* (Technical Note No. TN D-7703). Flight Research Center.

Martin, D. M. (1990). Analysis and design of sidestick controller systems for general aviation aircraft [NASA Article]. *Journal of Guidance, Control, and Dynamics*(Vol.13, No.1).

Phillips, W. F. (2009). *Mechanics of flight.* Hoboken New Jersey: John Wiley 'I&' Sons, Inc.

Phillips, W. H., Kuehnel, H. A., & Whitten, J. B. (1956). *Flight investigation of the effectiveness of an automatic aileron trim control device for personal airplanes* (Report No. Report 1304).

Schutte, P., Goodrich, K., & Williams, R. (2012, July 20-25). Towards an improved pilot-vehicle interface for highly automated aircraft: Evaluation of the haptic flight control system [Conference Paper]. *4th AHFE International Conference on Applied Human Factors and Ergonomics*.

Sellon, A. (2004, April 20). The 1927 guggenheim safe aircraft competition [Article]. Retrieved from `http://www.aerofiles.com/guggen-sac.html`

Sixteenth annual report of the national advisory committee for aeronautics (Annual Report No. 16). (1930).

Stewart, E. (1994). *A piloted simulation study of advanced controls and displays for novice general aviation pilots* (Article No. AIAA 94-0276). 32nd Aerospace Sciences Meeting and Exhibit.